Structural Interpretation Methods
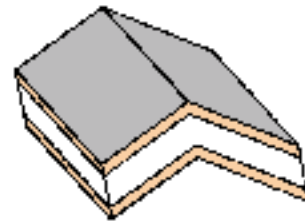
1A-1: Defining folds

Basic concepts

Folds are bends or flexures of layered rock that form in response to motion along faults, diapirism, compaction, and regional subsidence or uplift. Folds are expressed in seismic reflection profiles as one or more regions of dipping reflections (*dip domains*) that correspond to inclined stratigraphic contacts.
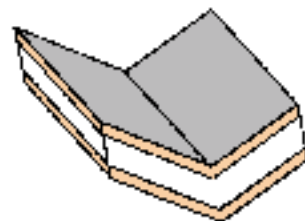
Folds come in three basic types:
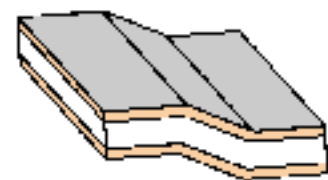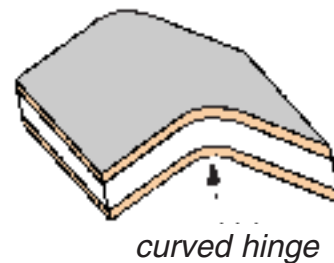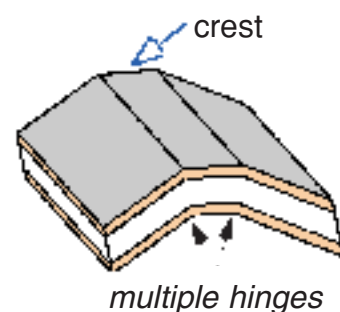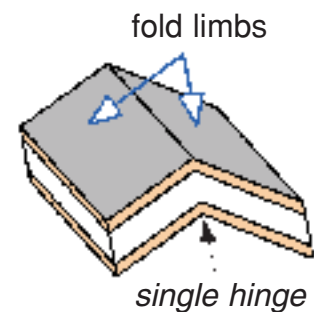
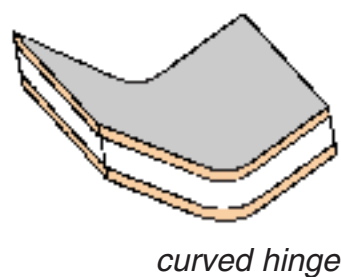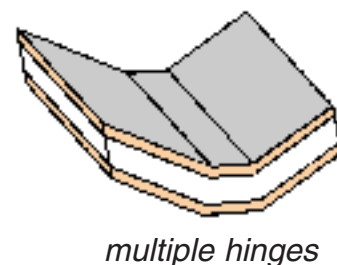**monoclines**   **anticlines**   **synclines**

Folds are composed of one or more dip domains, and may have angular or curved fold shapes:

anticlines

fold limbs   crest

single hinge   multiple hinges   curved hinge

synclines

single hinge   multiple hinges   curved hinge
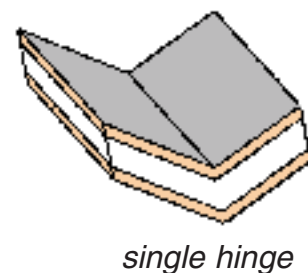
Dip domains are separated by **axial surfaces**; imaginary planes which, when viewed in two dimensions, form *axial traces*. *Anticlinal axial surfaces* occupy concave-downward fold hinges; *synclinal axial surfaces* occupy concave-upward fold hinges.

anticlinal axial surfaces

axial trace

angular hinge   multiple angular hinges   curved hinge

synclinal axial surfaces

single hinge   multiple angular hinges   curved hinge
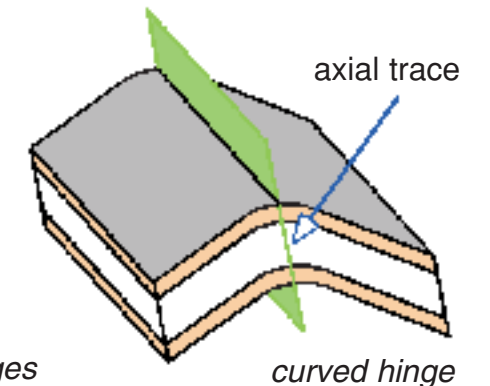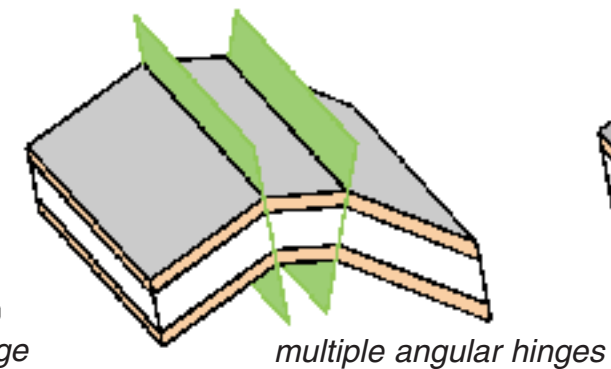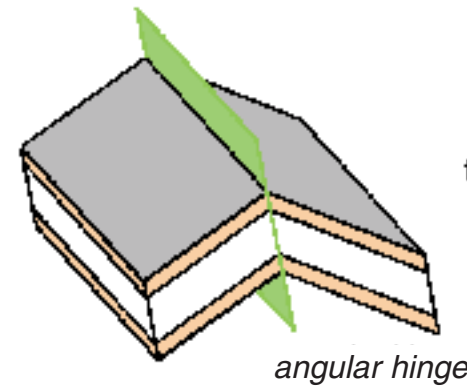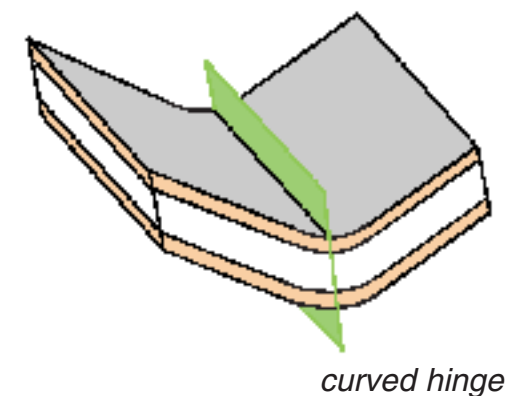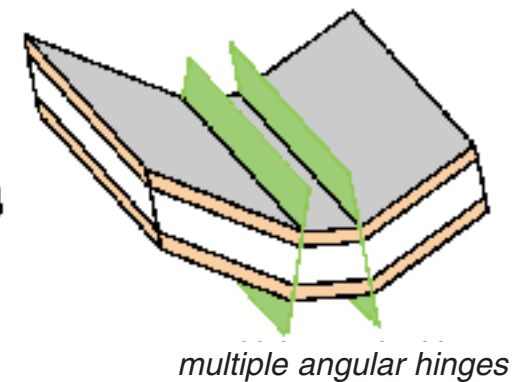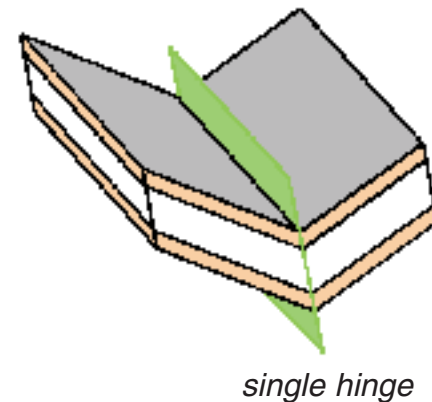
Axial surfaces often occur in pairs that bound fold limbs, which are also called *kink bands*:
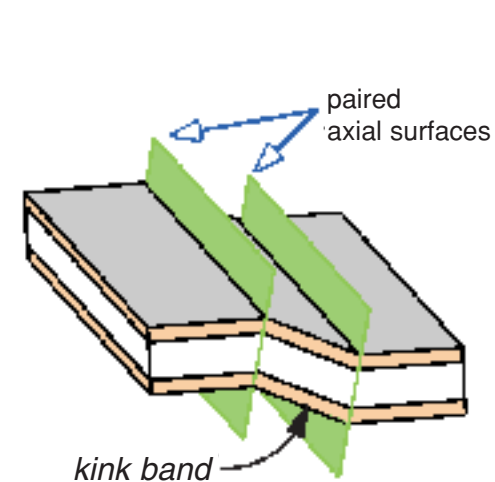
two sets of paired axial surfaces

paired axial surfaces

kink band

kink bands
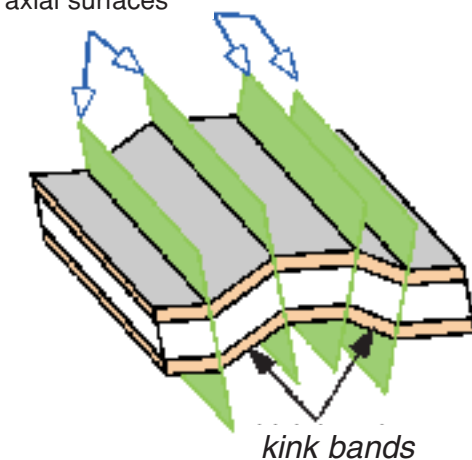
Folds in seismic sections

**Monocline,
San Joaquin
Valley,
California,
U.S.A.**
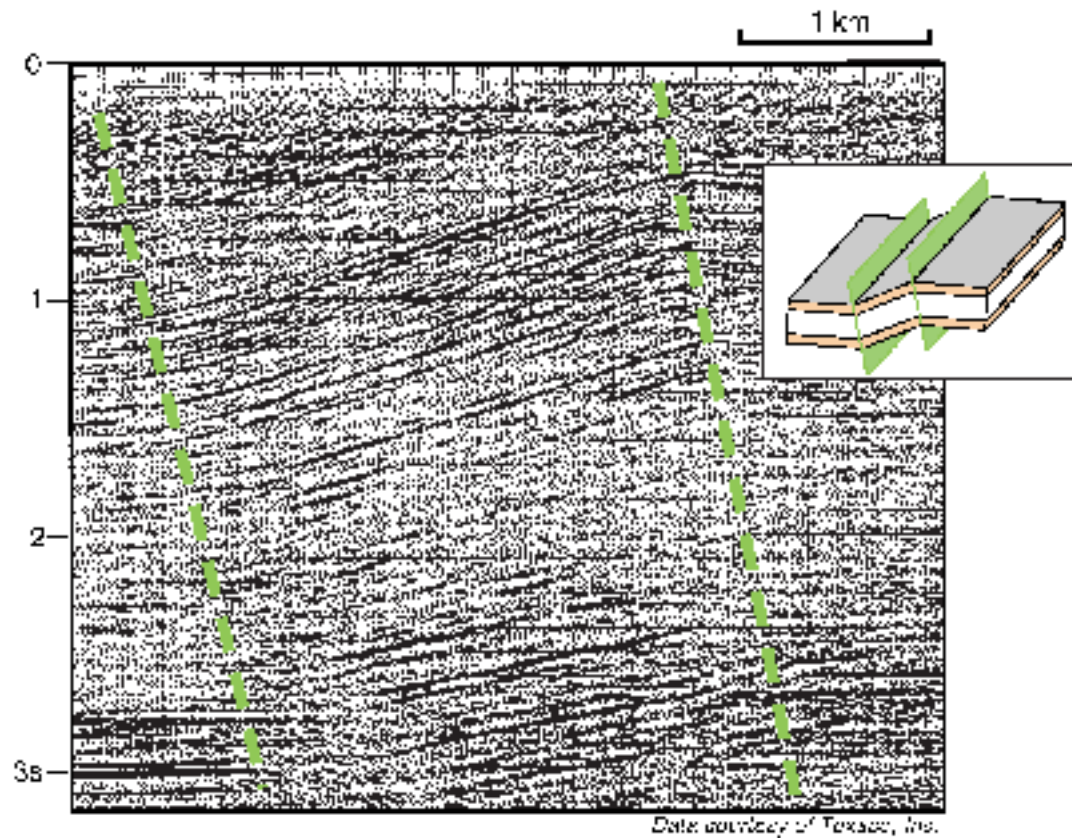
**Syncline,
Santa Barbara
Channel,
California,
U.S.A.**
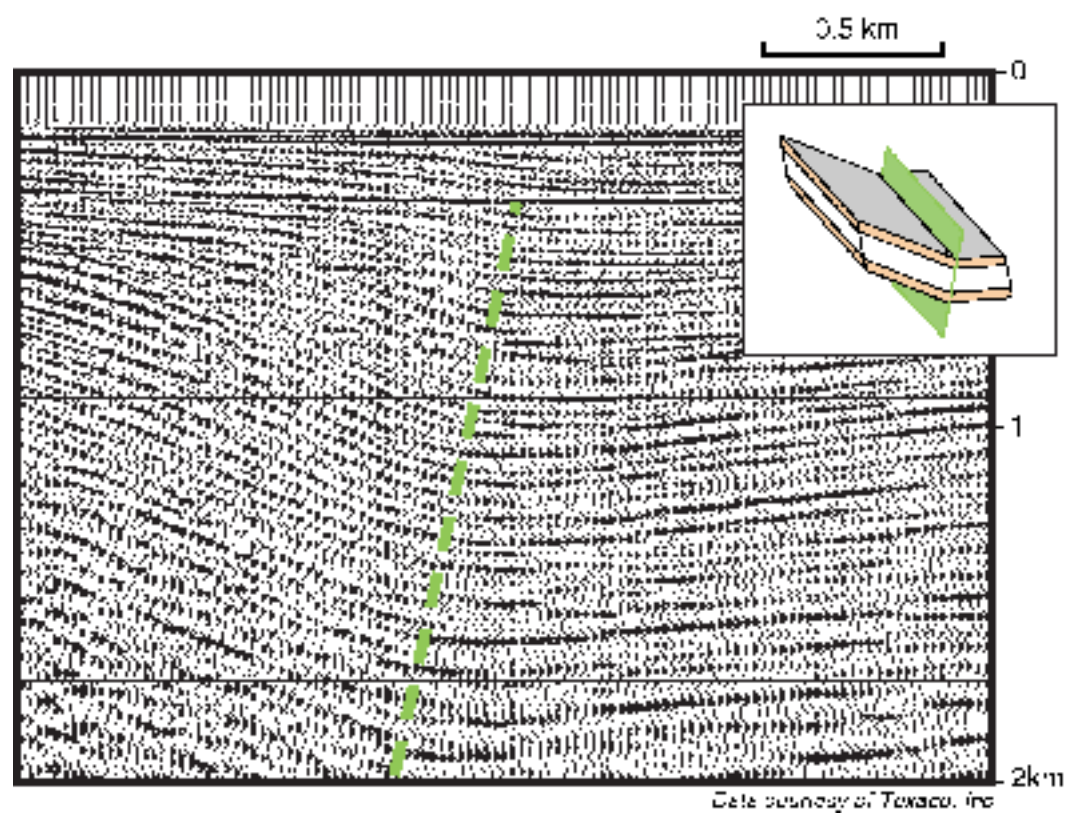
Single Hinge Anticline, Niger Delta, Nigeria

Multiple Hinge Anticline, Permian Basin, Texas, U.S.A.
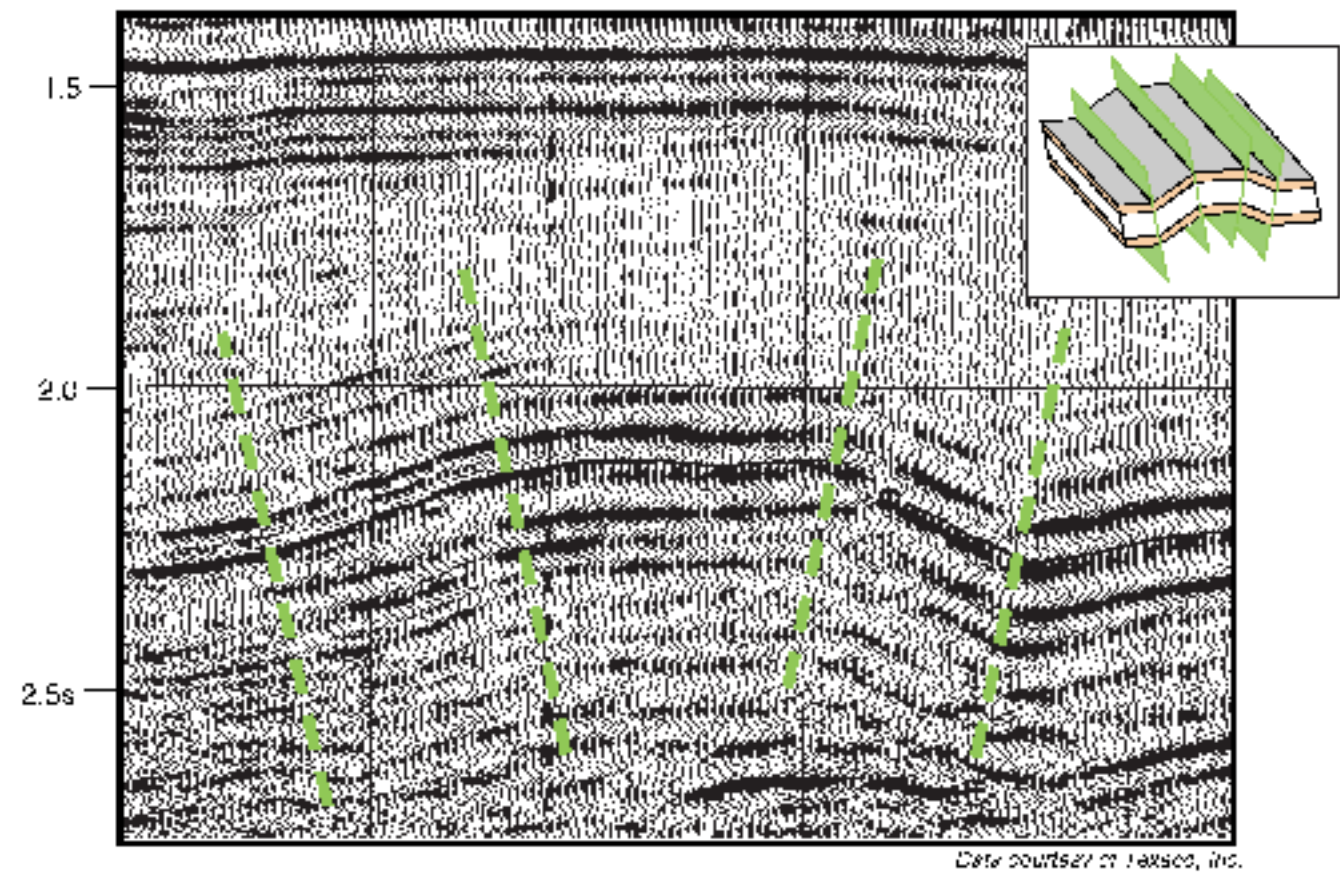
Folds and bedding thickness

Folds are classified based on whether or not the thickness of stratigraphic layers changes in dip domains or across axial surfaces.

Parallel folds preserve layer thickness, and are common in strata that deformed predominantly by *flexural slip* (see inset at right). Axial surfaces bisect inter-limb angles in parallel folds.

Parallel fold model
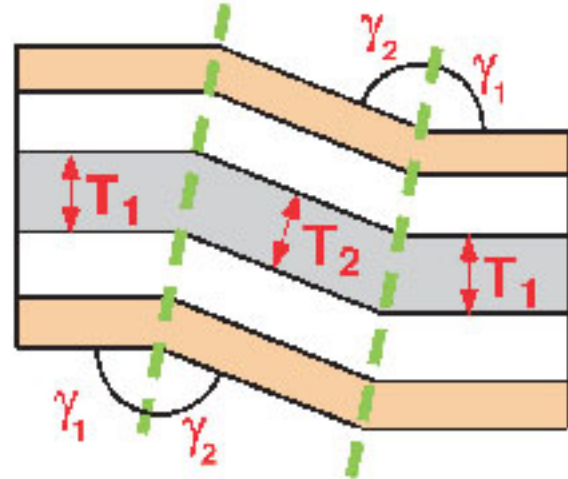
Layer thickness is conserved: Bed thickness T_1 equals bed thickness T_2.
Bisecting axial surfaces: Interlimb angle γ_1 equals interlimb angle γ_2.

Various types of folds exhibit non-parallel behavior, where the thickness of stratigraphic layers changes gradually in dip domains or abruptly across axial surfaces. These thickness changes may be caused by various deformation mechanisms, including *ductile flow* within incompetent beds. Alternatively, thickness changes may be depositional in origin. Axial surfaces do not bisect interlimb angles in non-parallel folds. Rather, axial surface orientations are governed by the magnitude of the change in bed thickness.

Non-parallel fold model

Parallel fold, synclinal axial surface

$$T_2 = T_1$$

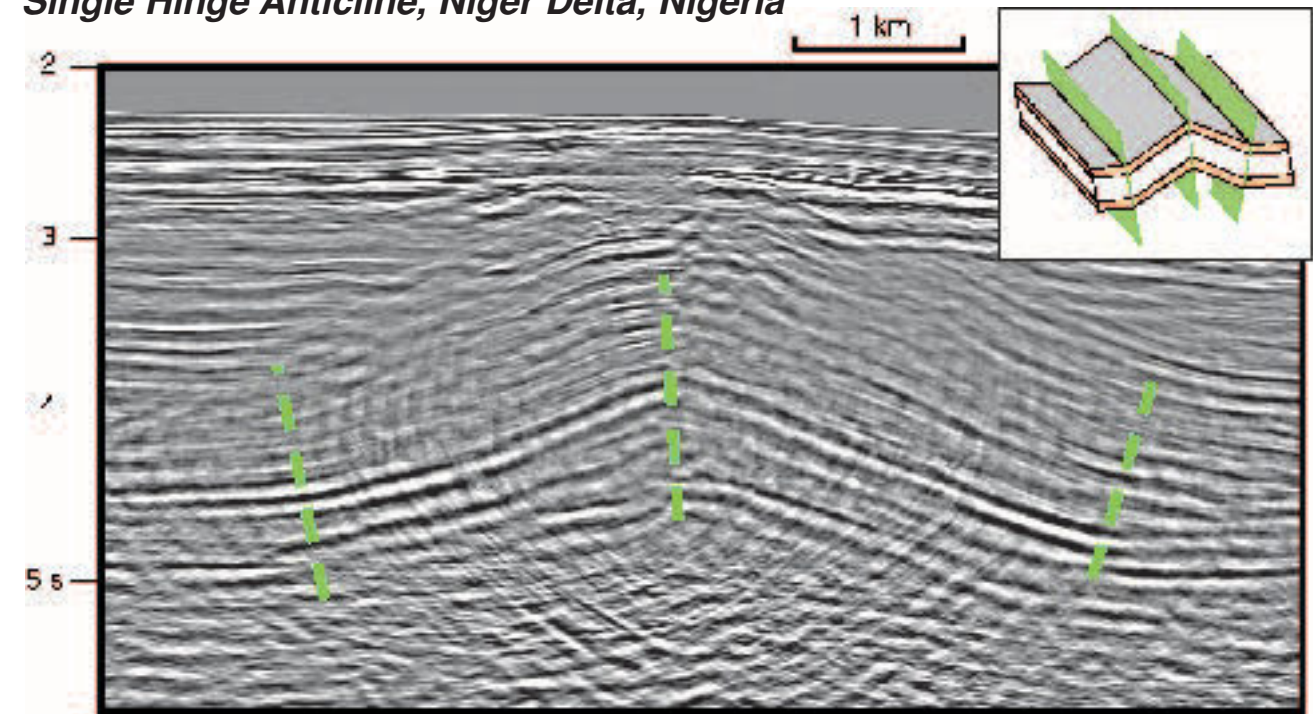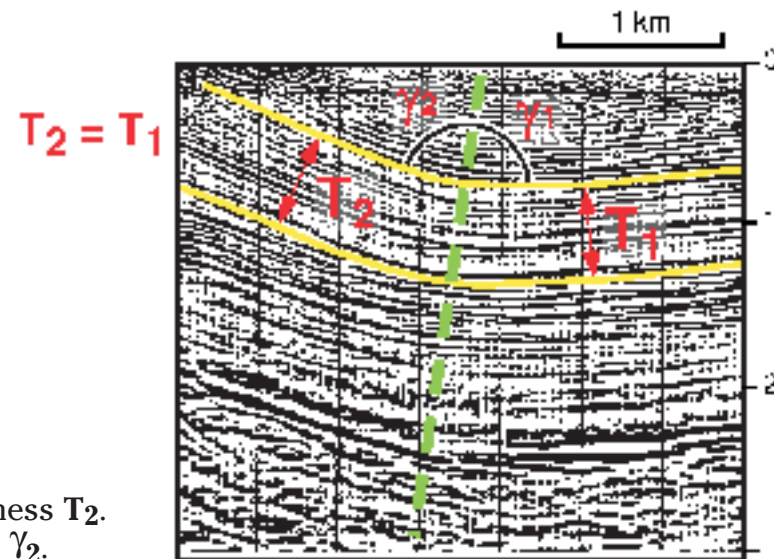### Non-Parallel fold, anticlinal axial surface

$$T_2 > T_1$$

general rule:

$$\frac{T_1}{T_2} = \frac{\sin \gamma_1}{\sin \gamma_2}$$
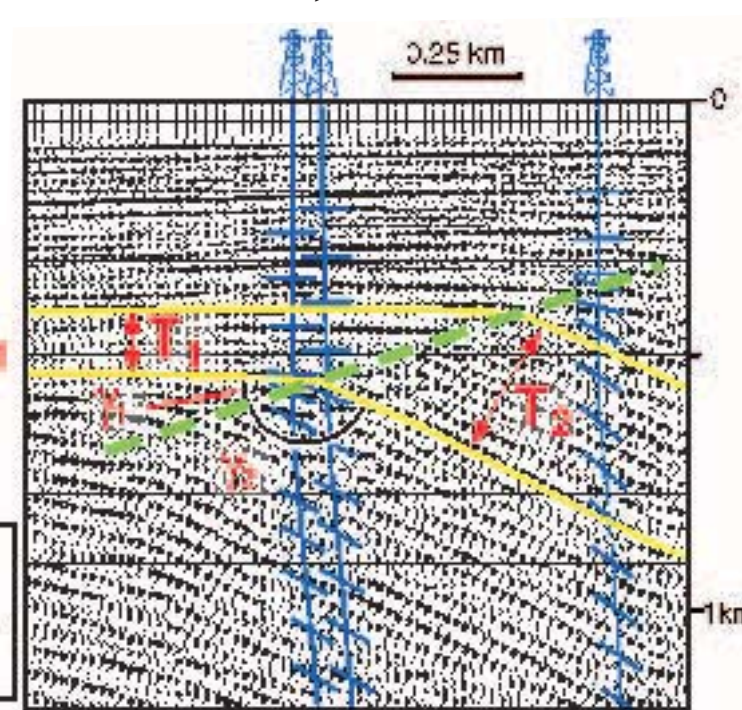
Parallel folds commonly form by a deformation mechanism called **flexural slip**, where folding is accommodated by motions on minor faults that occur along some mechanical layering — usually bedding. Flexural-slip surfaces, which can be observed in core or outcrop, may vary in spacing from a few millimeters to several tens of meters in spacing.

slip surfaces

The amount of offset on flexural-slip faults increases as the fold tightens (note slip increase from models 1 to 2), and is a function of the spacing of slip surfaces.

Slip changes instantaneously across axial surfaces in angular folds (models 1, 2); whereas, slip increases along bedding surfaces through the hinge in curved-hinge folds (model 3).
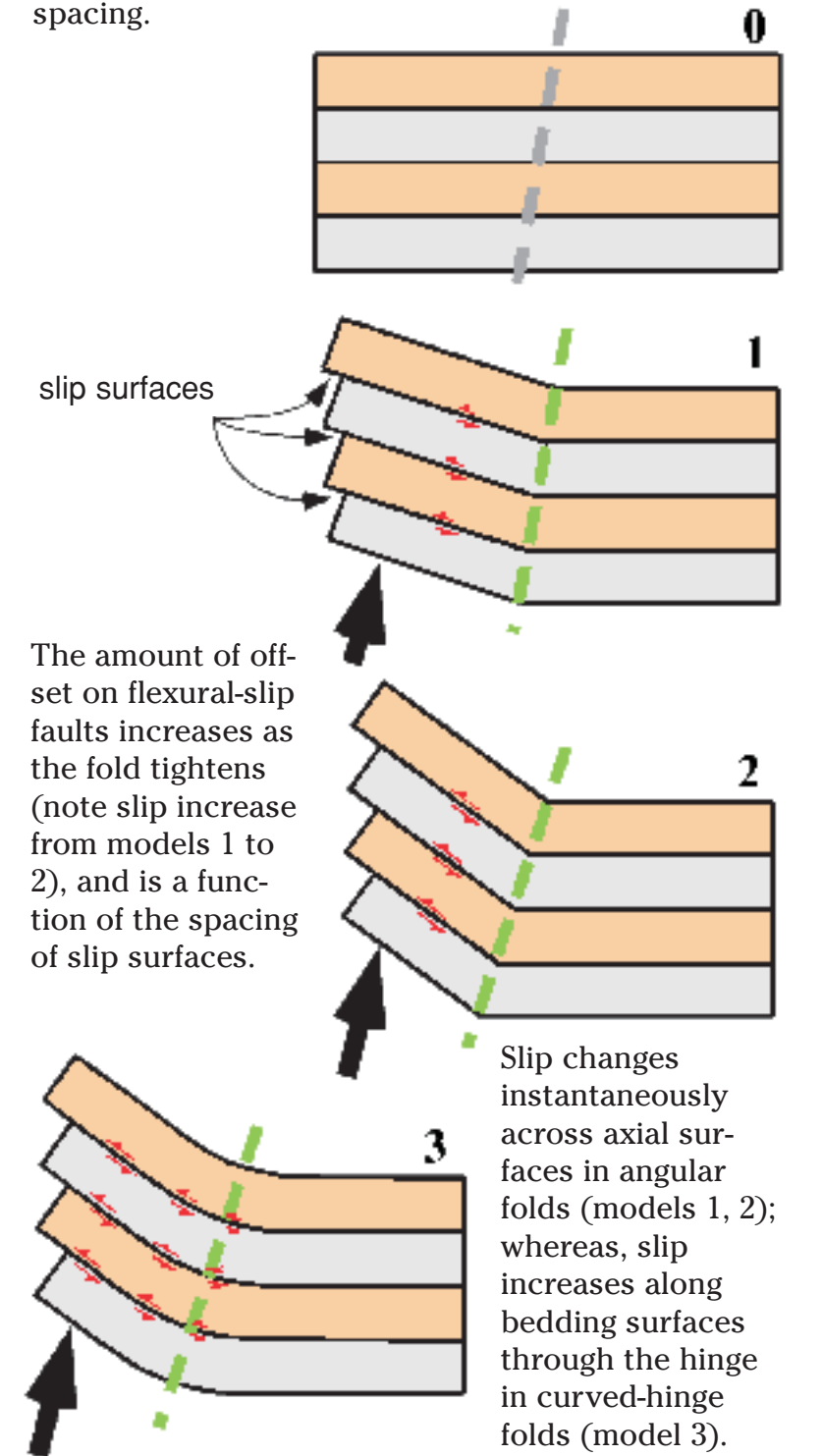
Shortcomings in seismic images of folds

Folds can be distorted or only partially imaged in seismic sections. Two common shortcomings are:

(1) **Overlapping reflections in non-migrated or under-migrated sections;** *and*

(2) **poor imaging of steeply dipping fold limbs.**

Balanced model
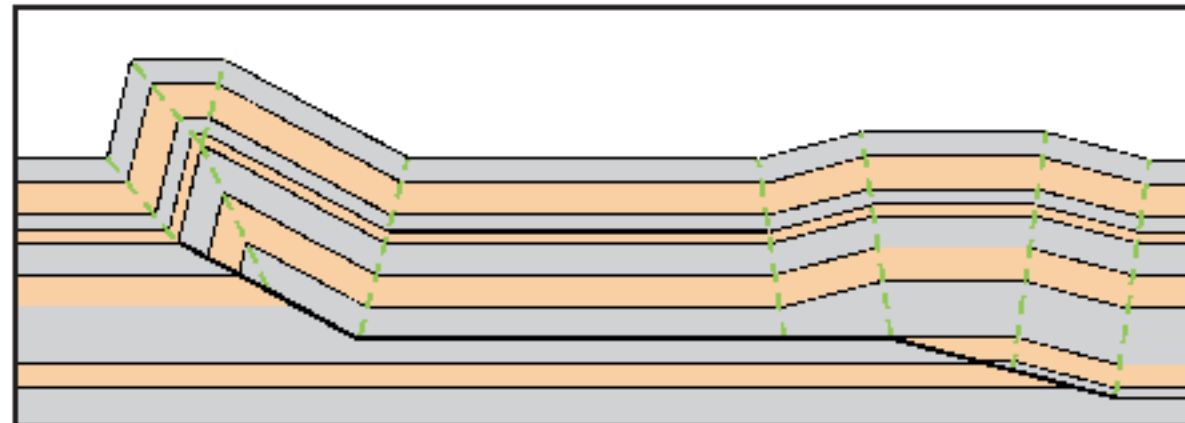
Overlapping reflections occur in synclines (1) on this stacked section; similar patterns persist in under-migrated sections. The steep limb is not imaged and diffractions are present (2).

Synthetic seismic

Stacked section
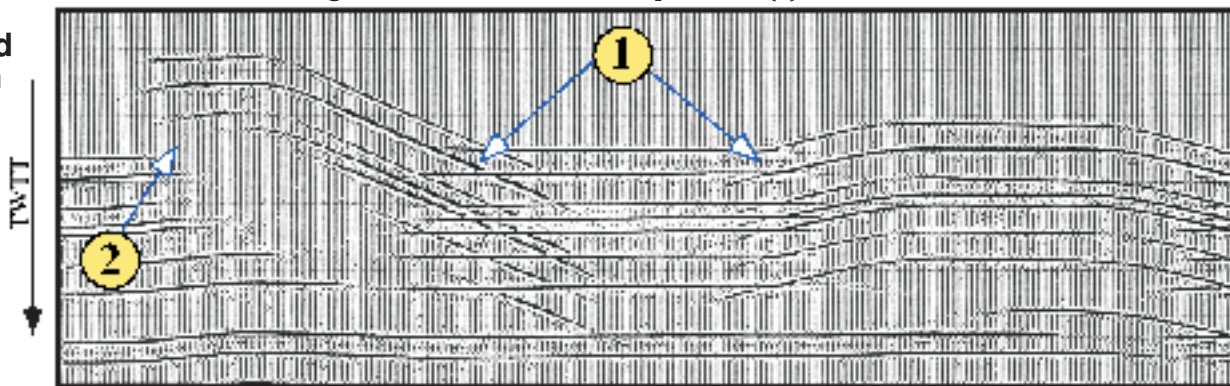
Proper migration removes overlapping reflections and collapses diffractions, but the steep limb remains un-imaged.

Migrated section
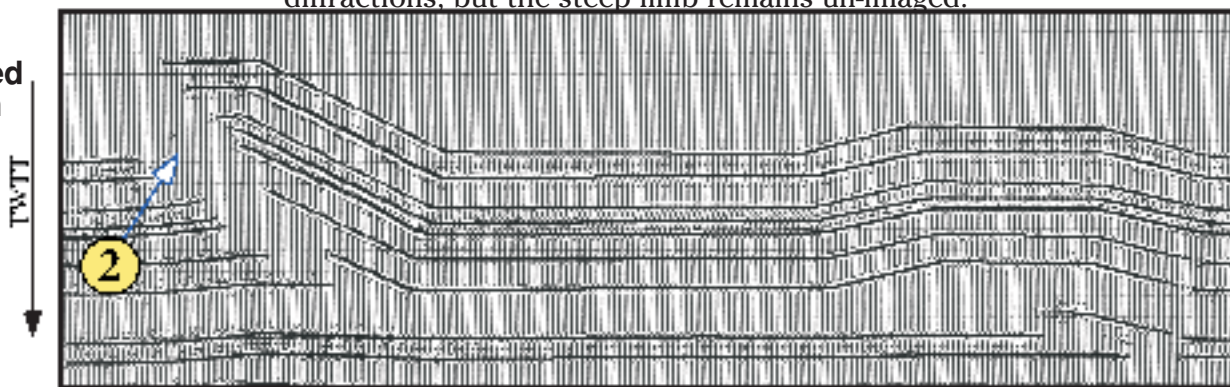
Locating axial surfaces in seismic sections

Migration moves dipping reflections upward and laterally to properly image the fold geometry, but reflections on non-migrated or under-migrated sections do not accurately represent fold shape. However, axial surfaces can be inferred on these sections by mapping the truncations of horizontal reflections.

Model

Stacked section (synthetic)

Step 1: Pinpoint truncations of horizontal reflections as they enter the poorly imaged zone. Note that diffractions, dipping toward the fold, may emanate from these truncations.

reflection truncations

diffractions
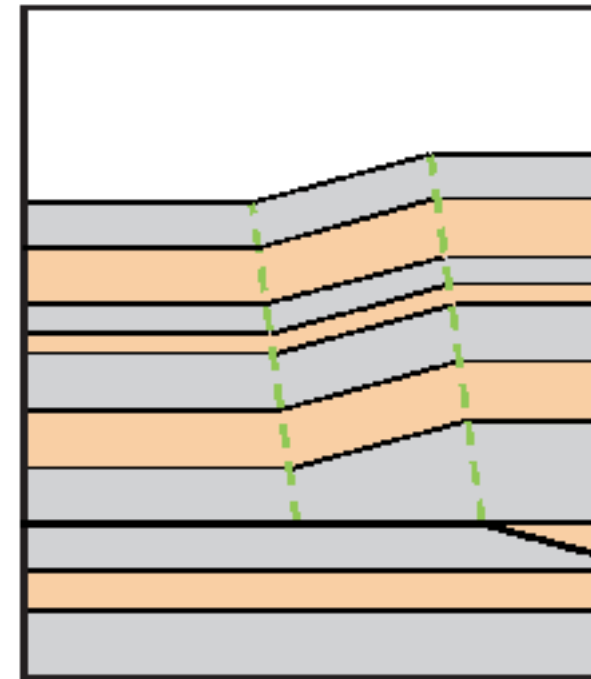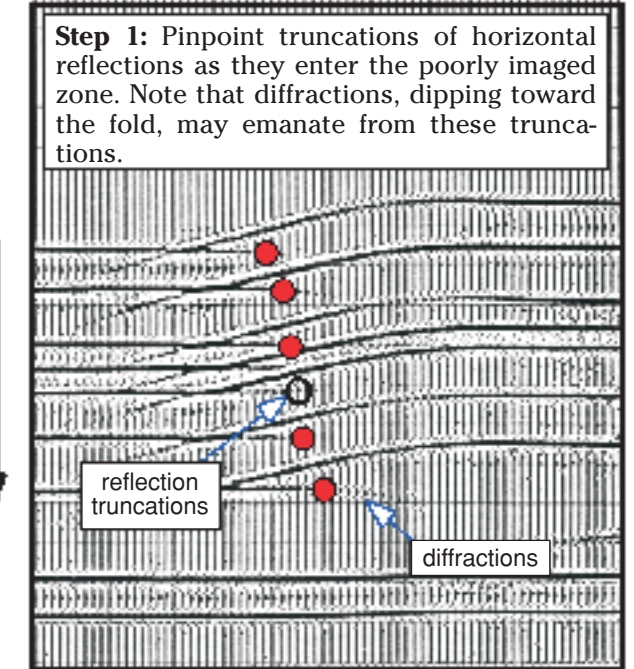
Migrated section (synthetic)

Stacked section (synthetic)

Step 2: Fit an axial surface that best matches the aligned truncations. Note that the interpreted axial surface matches closely with the axial surface defined in the migrated section (left).

axial surface
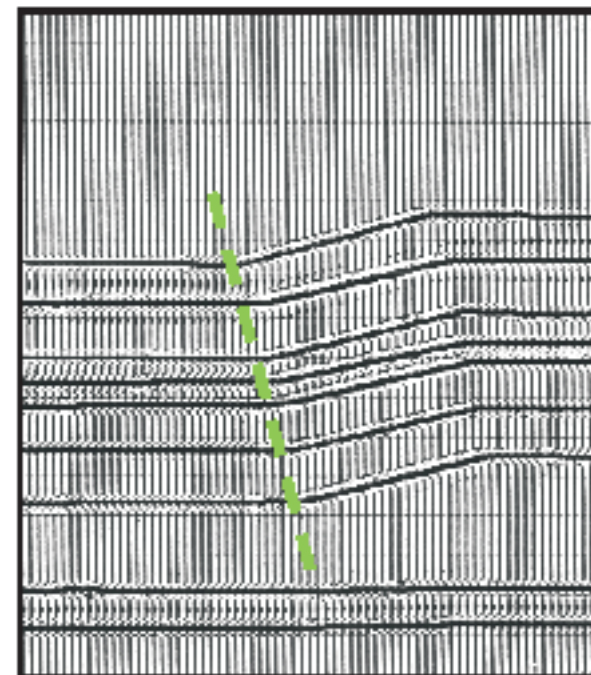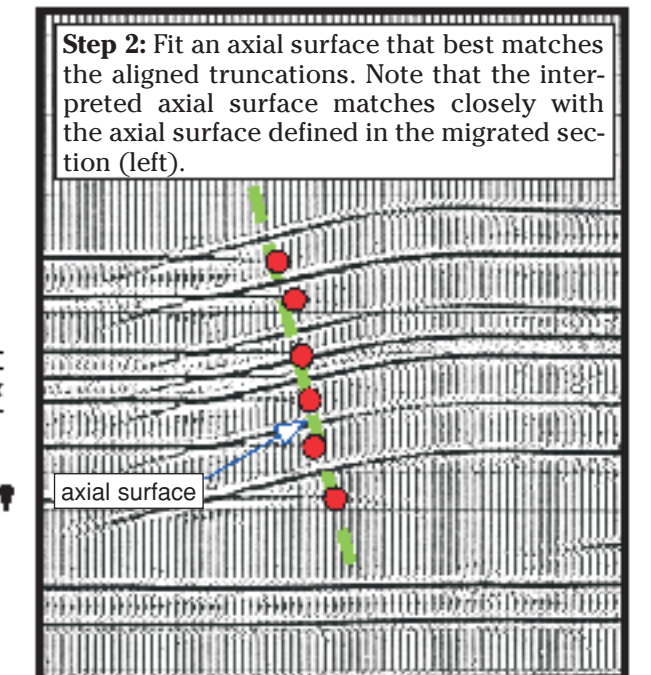
TWTT is two-way travel time.

Interpreting folds in poorly imaged zones

Poorly imaged zones on folds are commonly caused by, and interpreted as, faults or steep limbs. Both solutions are often permissible and should be evaluated. Here, we describe a method of interpreting parallel folds in poorly imaged zones.

A: Is the poorly imaged zone a fault or steep fold limb?

2-D, post-stack time migration displayed in depth

Data courtesy of Texaco, Inc.
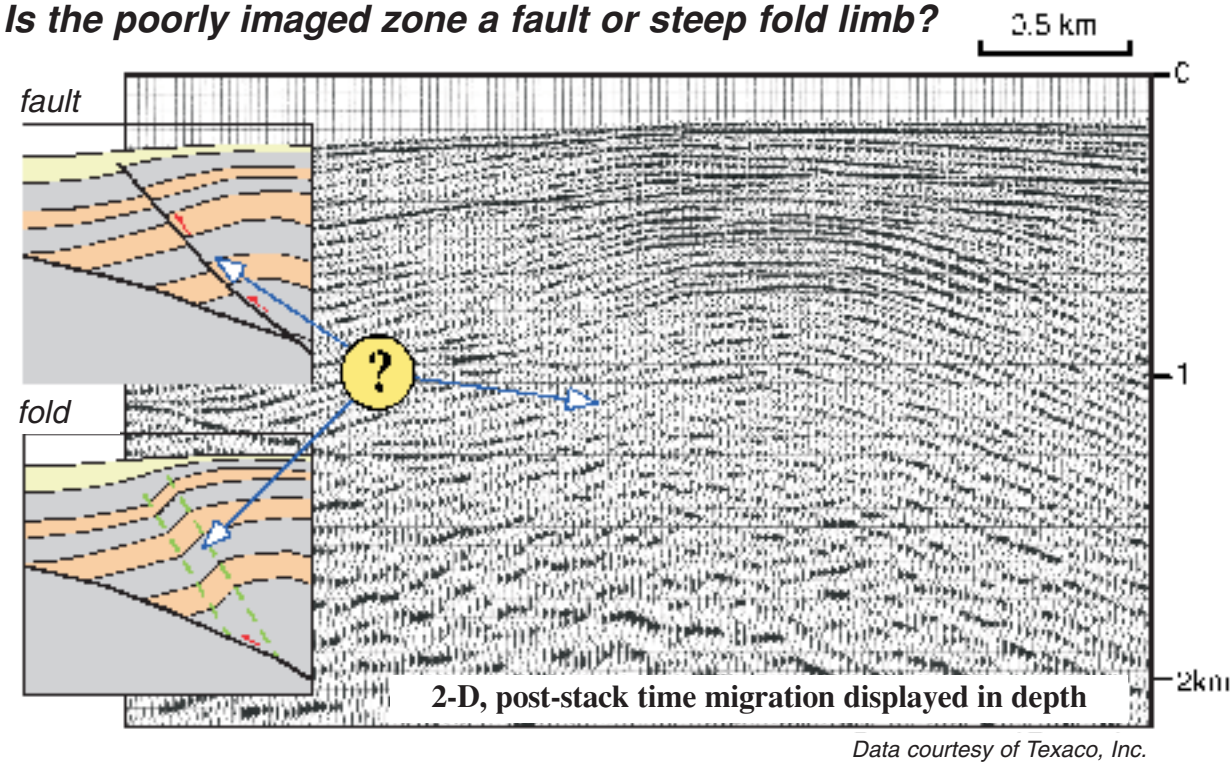
C: Interpretation using the parallel fold method
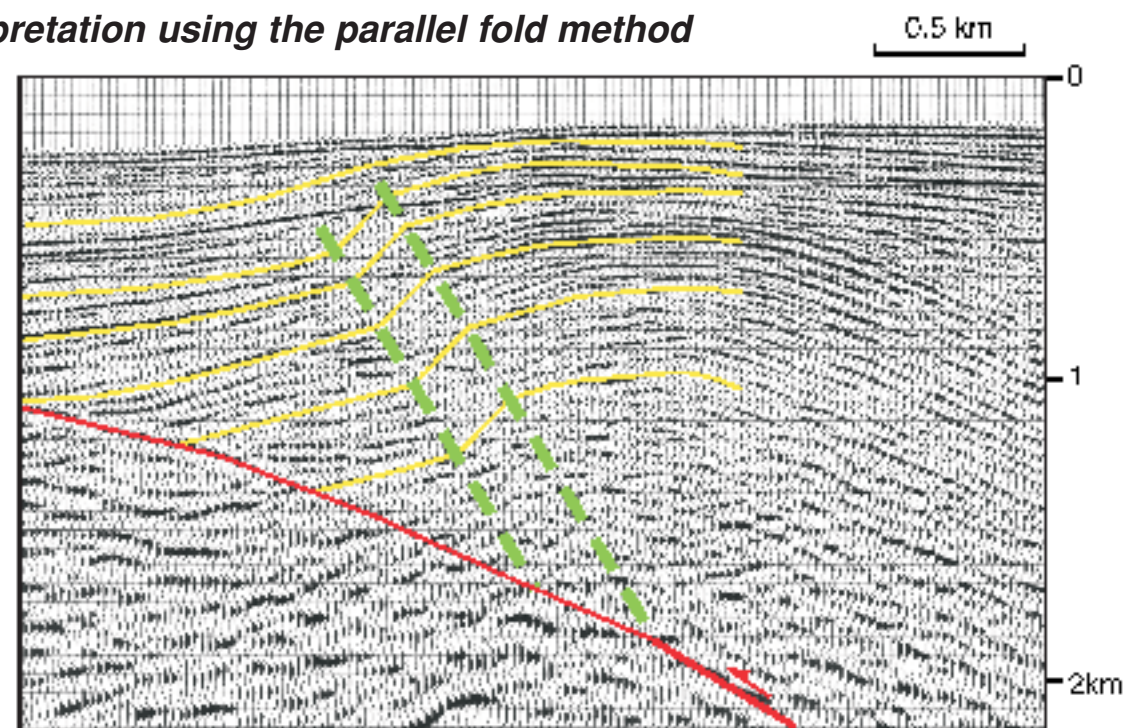
B: Method for interpreting parallel folds in poorly imaged zones

Step 1: Pinpoint truncations of reflections as they enter the poorly imaged zone.

Step 2: Fit parallel axial surfaces that best match the aligned truncations. Measure the average dip outside of the fold limb and measure γ_1.

Step 3: Define the dip of beds in the kink band by making γ_2 equal to γ_1.
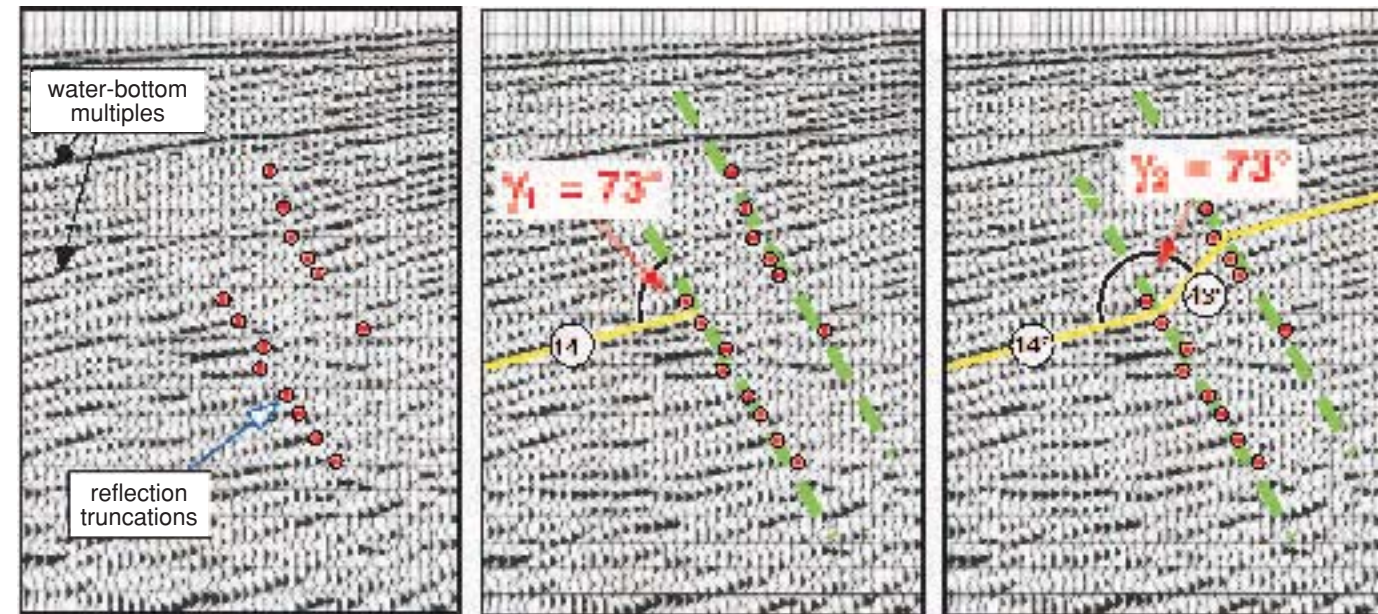
D: Confirmation of fold geometry with dipmeter log and 3-D seismic image

3-D, post-stack time migration displayed in depth

Data courtesy of Texaco, Inc.
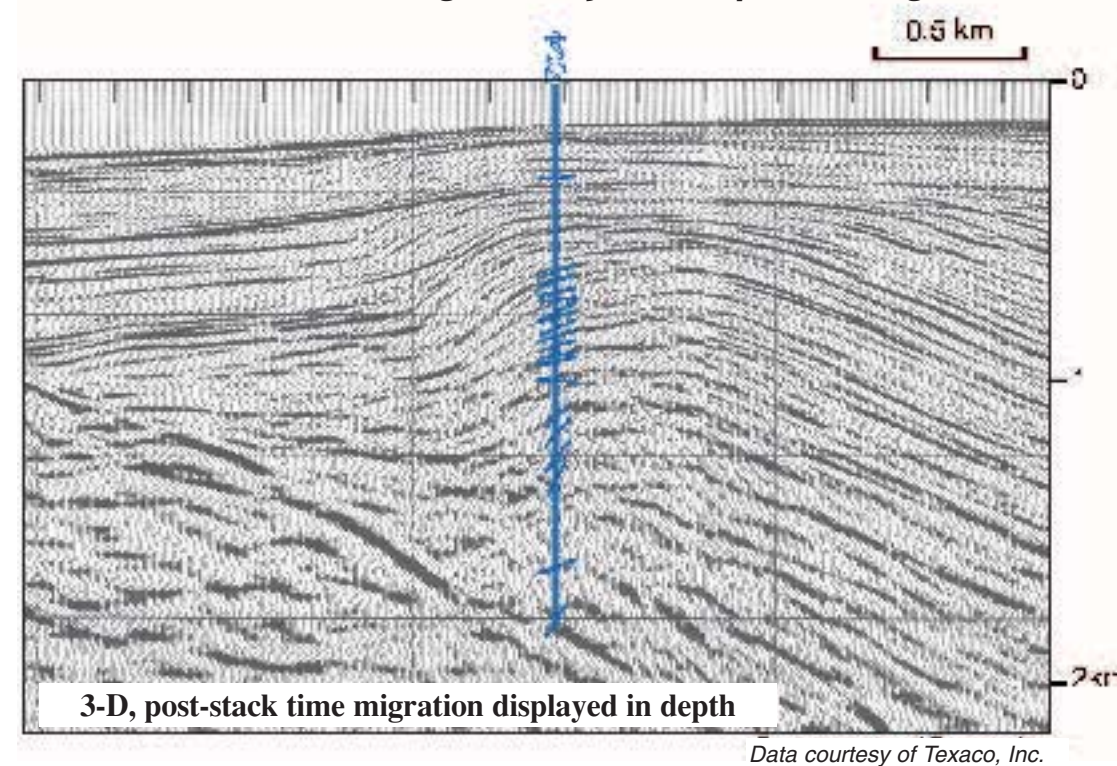
In this example, 3-D seismic data and a dipmeter log confirm the presence of steeply dipping beds in the poorly imaged zone. The primary test of the fold interpretation, however, is whether or not the horizons correlate properly across the poorly imaged zone. If they do, a parallel fold interpretation is permissible. If they do not, a non-parallel fold or fault likely occupies the poorly imaged zone.

1A-2: Recognizing thrust and reverse faults

Faults are identified in seismic reflection profiles through:

(1) fault cutoffs — terminations of reflections or abrupt changes of reflection attributes (e.g., amplitude, polarity) at fault surfaces;

(2) terminations of fold limbs or kink bands; and

(3) direct fault-plane reflections, produced by changes in velocity and density across or within fault zones.

Cutoffs and fault plane reflections (criteria 1 and 3) directly constrain fault positions. Thrust faults and their cutoffs, however, are generally difficult to image and identify, and thus the recognition of kink-band terminations (criterion 2) is a vital component of interpreting these faults. In this section, we describe how these criteria can be used together to identify and interpret thrust and reverse faults in seismic sections.

Fault cutoffs and kink-band terminations

balanced model

Incipient fault with markers along fault surface.

Fault with offset markers and cutoffs. Note that hanging wall kink bands terminate downward into the fault surface.
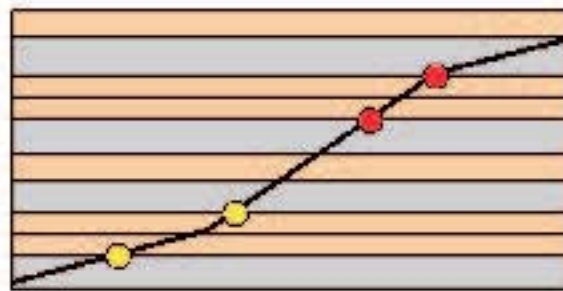
in outcrop

Fault cutoffs in outcrop, Mississippian Joana limestone, Nevada, U.S.A.

(Hook et al., 1997)
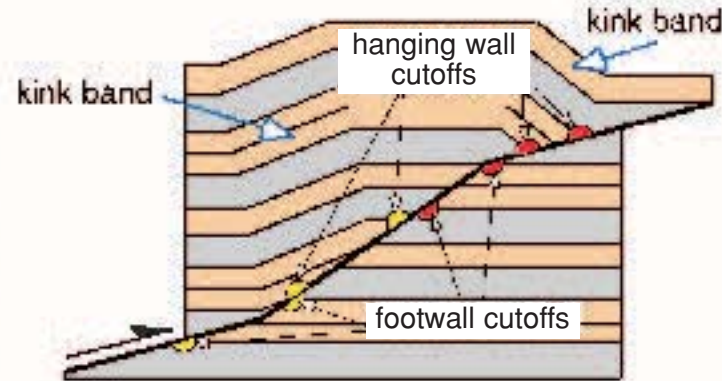
in synthetic seismic

Seismic forward model showing fault cutoffs (1) and downward terminating kink-bands (2).
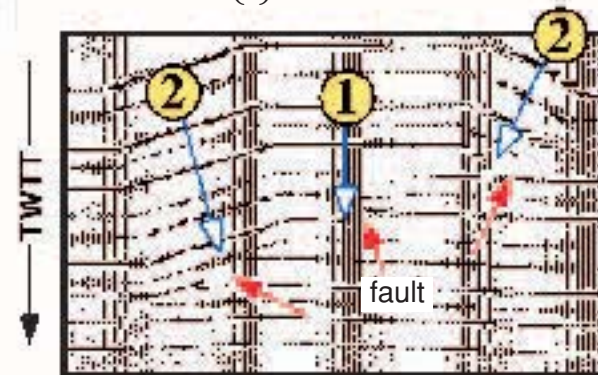
Recognizing and interpreting faults in seismic section
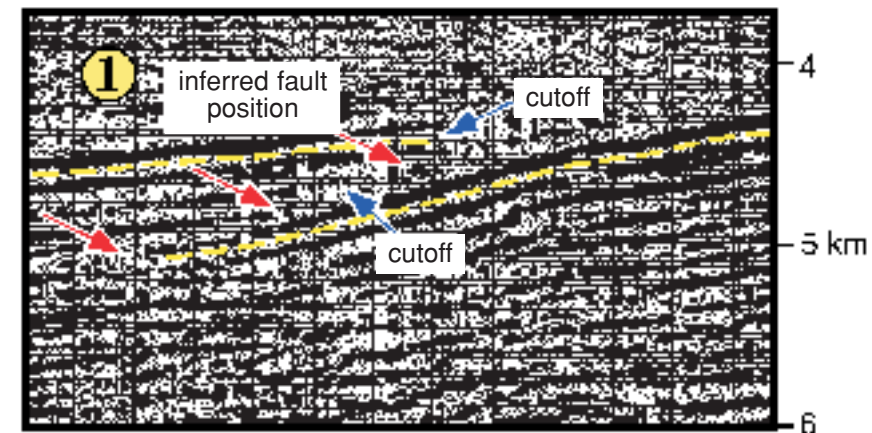
Data courtesy of Texaco, Inc.

fault cutoffs

Abrupt terminations (cutoffs) and duplications of prominent reflections constrain the position of a gently dipping thrust fault. (2-D seismic data, Permian basin, Texas, U.S.A.)

kink-band terminations

Thrust faults and bed-parallel detachments can be identified by the abrupt, downward terminations of kink bands. Terminations are generally marked by regions of dipping reflections above horizontal or more gently dipping reflections, and may contain fault cutoffs. Dipping reflections in kink bands represent strata folded in the hanging wall of a thrust/reverse fault or detachment; whereas, horizontal or more gently dipping reflections represent footwall strata below the fault or detachment. Thus faults and/or detachments should be interpreted at the transition between these two dip domains.
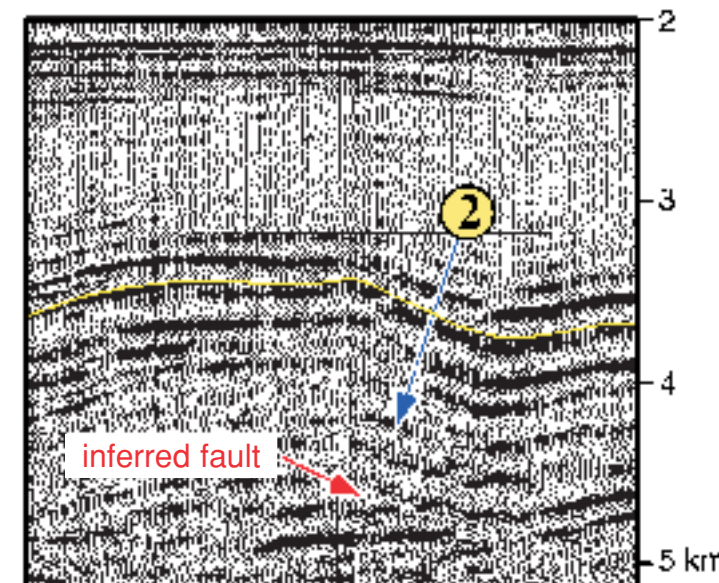
Data courtesy of Texaco, Inc.

Downward terminating kink band (2) defines the position of a gently dipping thrust. (3-D seismic data, Permian basin, Texas, U.S.A.).
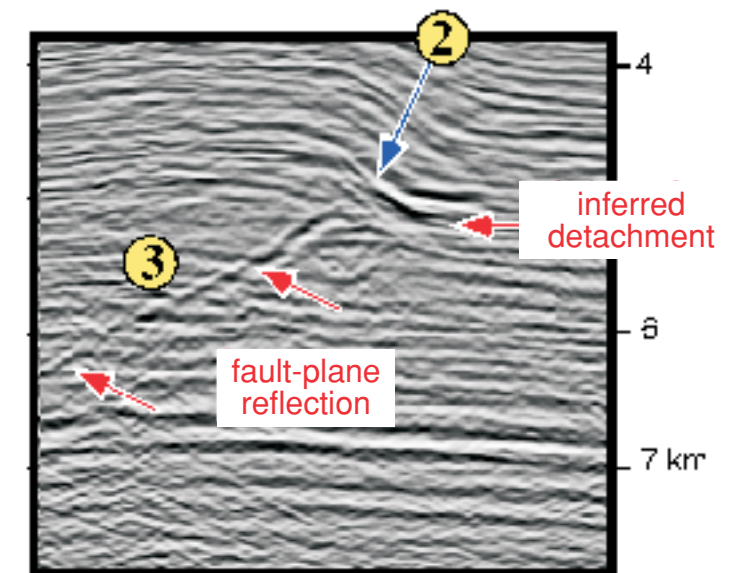
Data courtesy of Mabone, Ltd.

Downward terminating kink band (2) and fault-plane reflection (3) define the position of a thrust fault that shallows to an upper detachment. (3-D seismic data/Niger Delta).

Interpreting thrust ramps on seismic sections

Combinations of the three fault recognition criteria are employed to interpret thrust faults on the seismic section presented here.

This section images structures that involve two large thrust faults, which can be interpreted using the fault recognition criteria. The top panel is an uninterpreted section across a fold and thrust belt in the Andean foothills, Ucayali basin, Peru. Faults in the lower section are interpreted using: Cutoffs (1), kink-band terminations (2), and fault-plane reflections (3). Note how a series of cutoffs and kink-band terminations can corroborate, and be used to extrapolate beyond, the fault-plane reflections. (2-D seismic data, reprinted from Shaw et al., 1999, and published courtesy of Perupetro).

Seismic Example: Peruvian Andes

interpreted faults

dipping over horizontal reflections

dipping over horizontal reflections

VE of 1:1

5 km
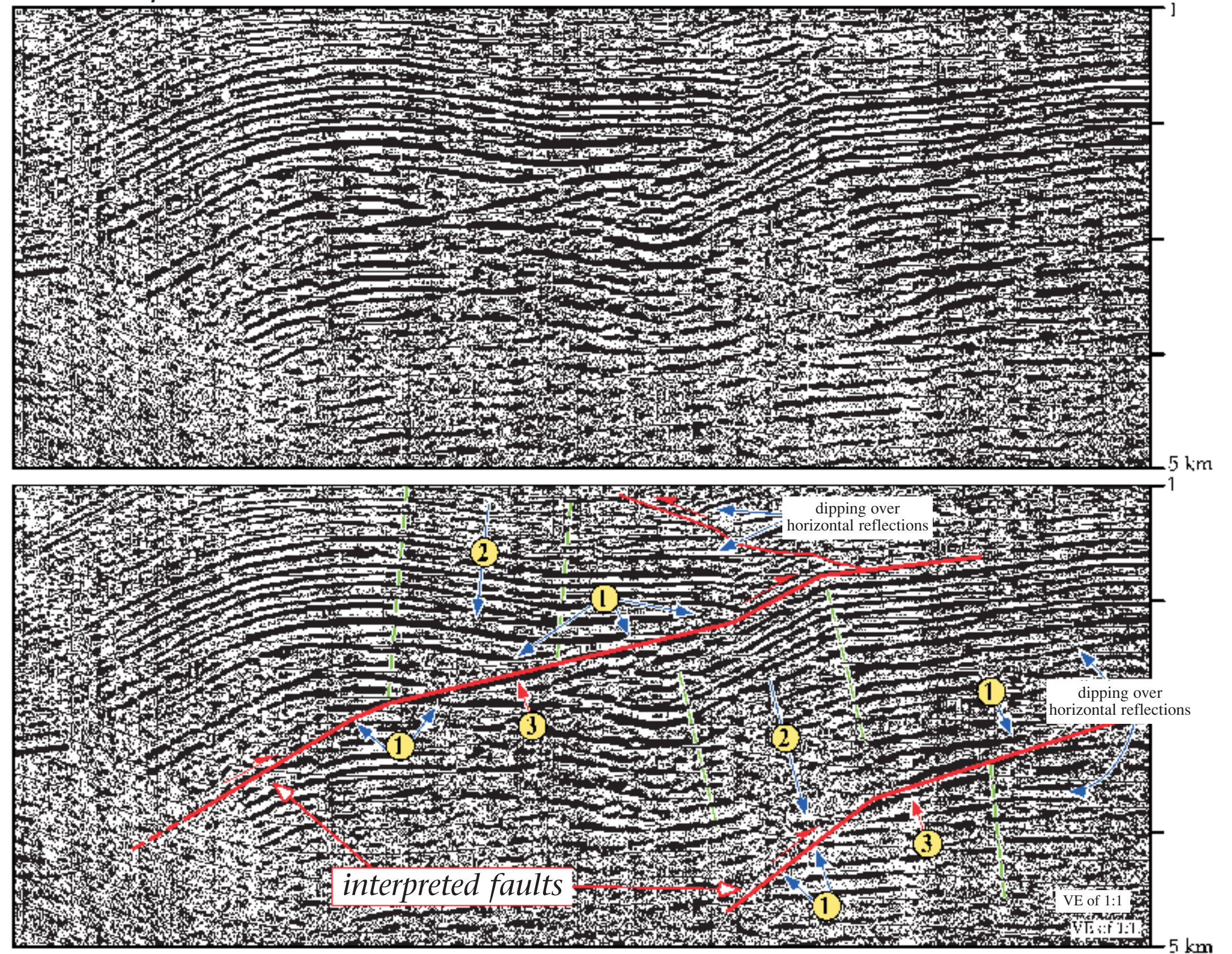
Recognizing detachments

Detachments are faults that run along bedding or other stratigraphic horizons, and thus generally are horizontal or dip at low angles. In fold and thrust belts, detachments are commonly referred to as **decollements**. Detachments are generally not imaged directly on seismic sections, but rather are interpreted at the base and/or top of thrust ramps. Basal detachments can be located in seismic sections by defining the downward terminations of kink bands, as described on the preceding pages.

These two seismic sections have prominent detachments. In the section at right, the detachment is located at the base of a single-thrust thrust ramp. The fold in the hanging wall of the thrust is produced by slip across the fault bend that is formed at the connection of the thrust ramp and detachment. This class of fault-bend fold is described in section 1B-1. In the section below, a regional detachment forms the base of several thrust ramps.

Seismic Example: Sichuan basin, China
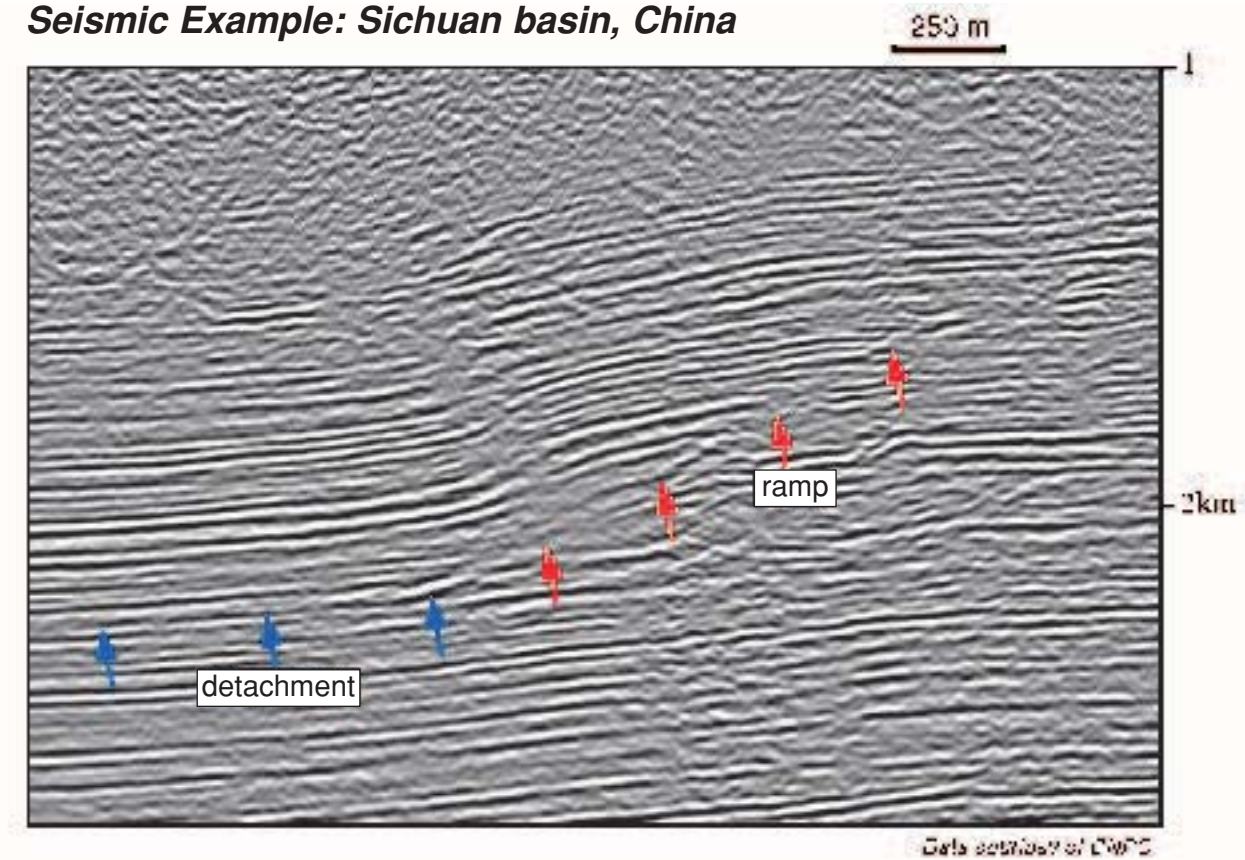
Seismic Example: Nankai Trough, Japan
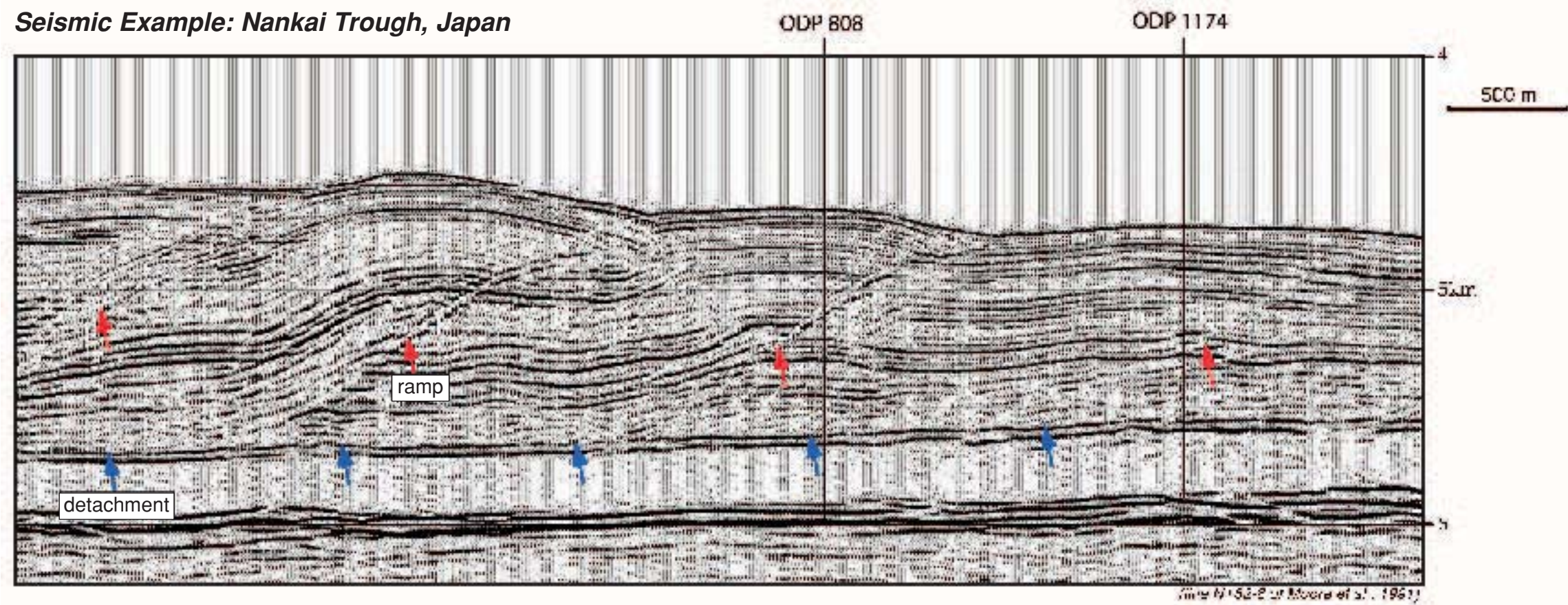
1A-3: Recognizing growth strata

Growth or **syntectonic strata** are stratigraphic intervals that were deposited during deformation. The ages of growth strata therefore define the timing of deformations. In contractional fault-related folds, growth strata typically thin across fold limbs toward structural highs. The geometries of growth structures are controlled primarily by the folding mechanism and the relative rates of sedimentation and uplift. Thus, growth fold patterns imaged in seismic data are often considered diagnostic of folding mechanism and sediment-to-uplift ratio. In this section, we describe common patterns of growth strata in fault-related folds that are imaged in seismic reflection data.

Growth strata in seismic section:
Sedimentation exceeds uplift

Data courtesy of Caltex and Texaco, Inc.
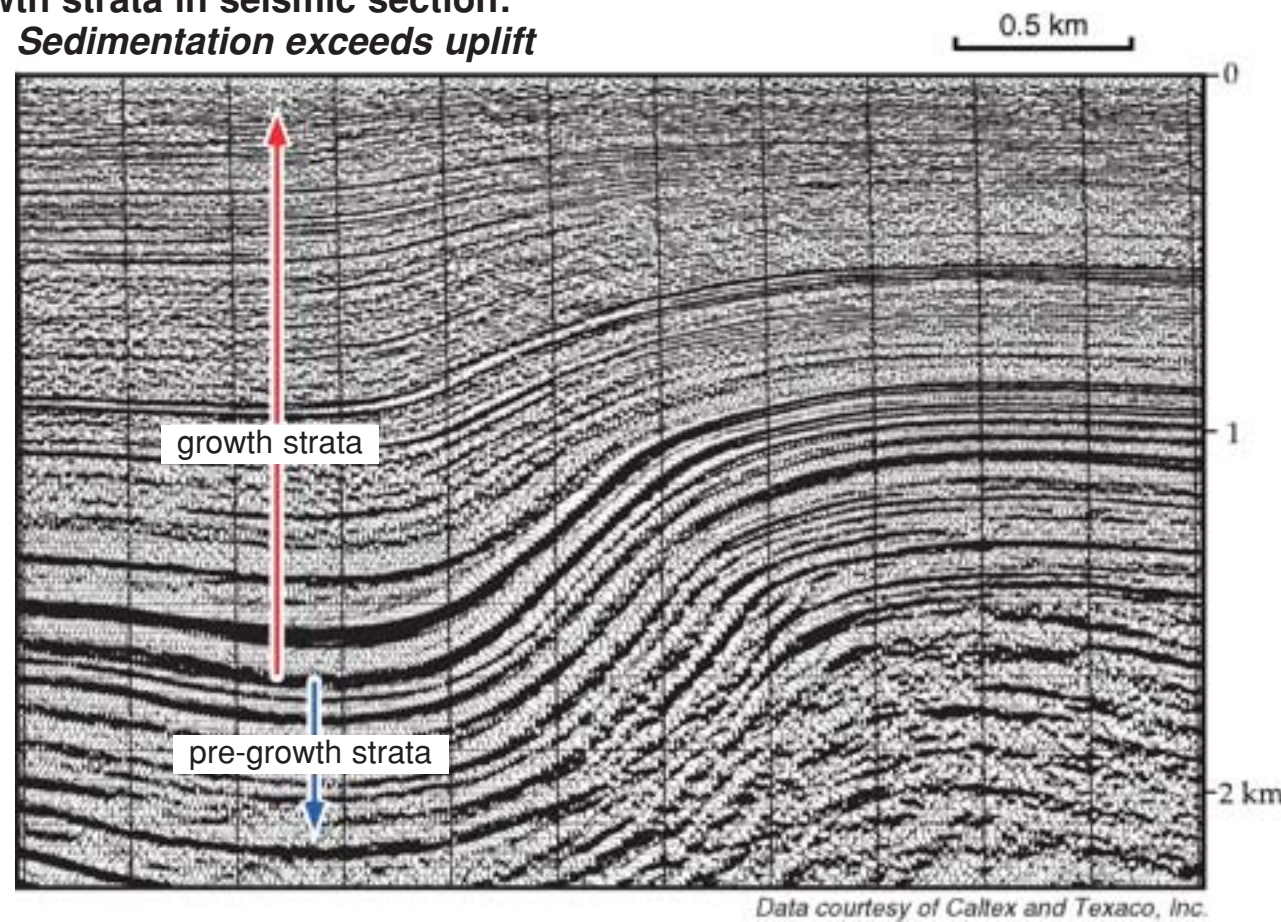
In cases where the sedimentation rate exceeds the uplift rate, growth strata are typically characterized as sequences, bounded by two or more seismic reflections, that thin toward the structural high. Growth strata are generally folded in one or more limbs of the structure. In this seismic section, growth strata thin onto the fold crest, with the lowermost growth units exhibiting the greatest thickness changes. (2-D seismic data, reprinted from Shaw et al., 1997).

Growth strata in seismic section:
Uplift exceeds sedimentation

Data courtesy of VERITAS DGC Limited
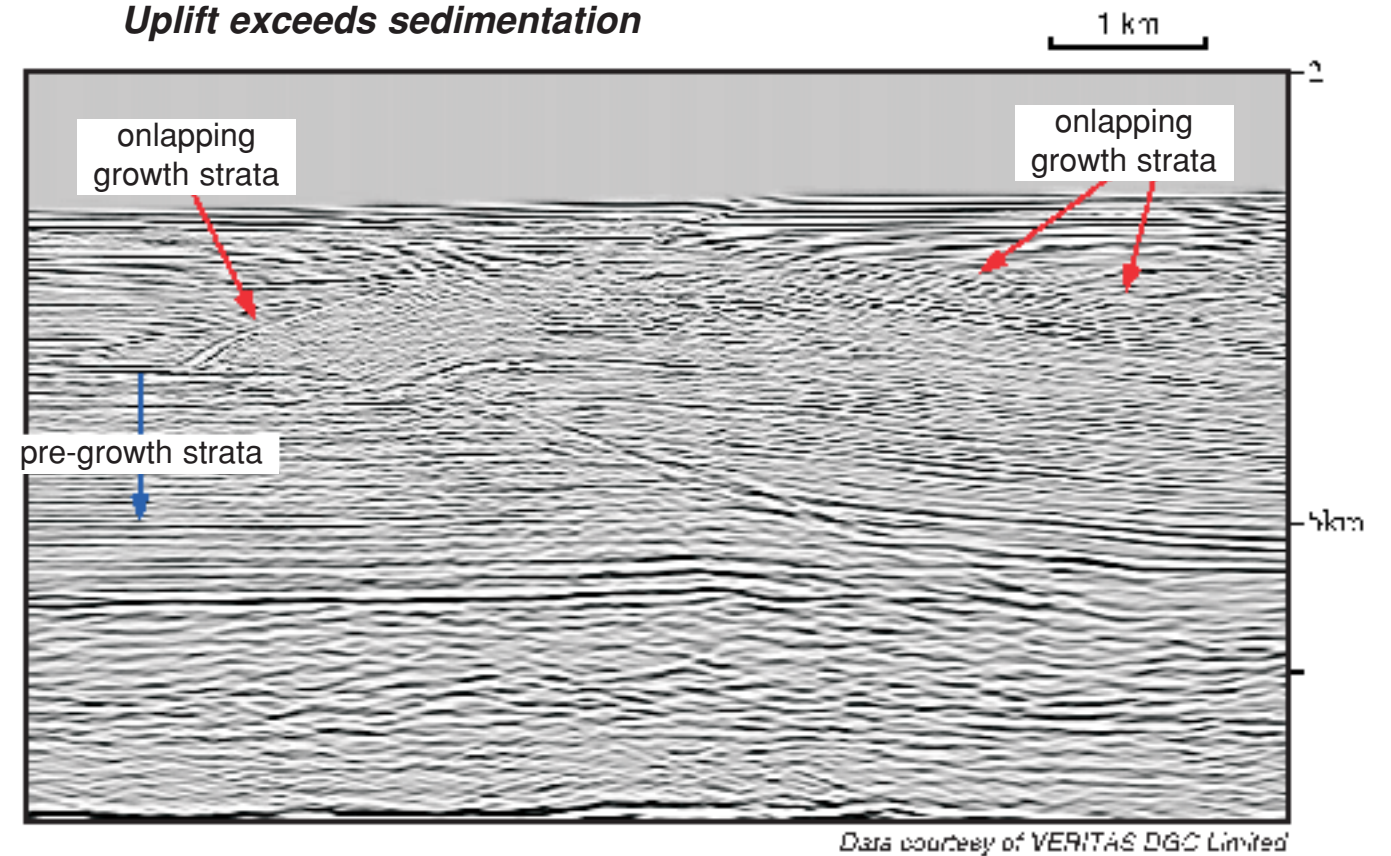
In cases where the uplift rate exceeds the sedimentation rate, growth strata typically thin toward, and onlap, the structural high. Growth strata are generally not present above the fold crest, but are folded in one or more limbs of the structure. In this seismic section, growth strata onlap the backlimb and forelimb of a fault-related fold. The growth strata are overlain by post-tectonic strata, which are described later in this section. (This structure is interpreted more completely in sections 1B-1 and 1B-4).

Growth strata as records of fold kinematics

Two folding mechanisms — ***kink-band migration*** and ***limb rotation*** — are commonly ascribed to contractional fault-related folds. These folding mechanisms typically yield distinctive patterns of deformed growth strata above fold limbs. Thus, seismic images of growth folds can be used to identify the folding mechanisms, which in turn can dictate the kinematic theory (e.g., fault-bend folding or detachment folding) that is most appropriate to guide the structural interpretation of the seismic data.

Folding by kink-band migration

pre-growth strata only   **sedimentation > uplift**   **sedimentation < uplift**

Folding by progressive limb rotation

pre-growth strata only   **sedimentation > uplift**   **sedimentation < uplift**
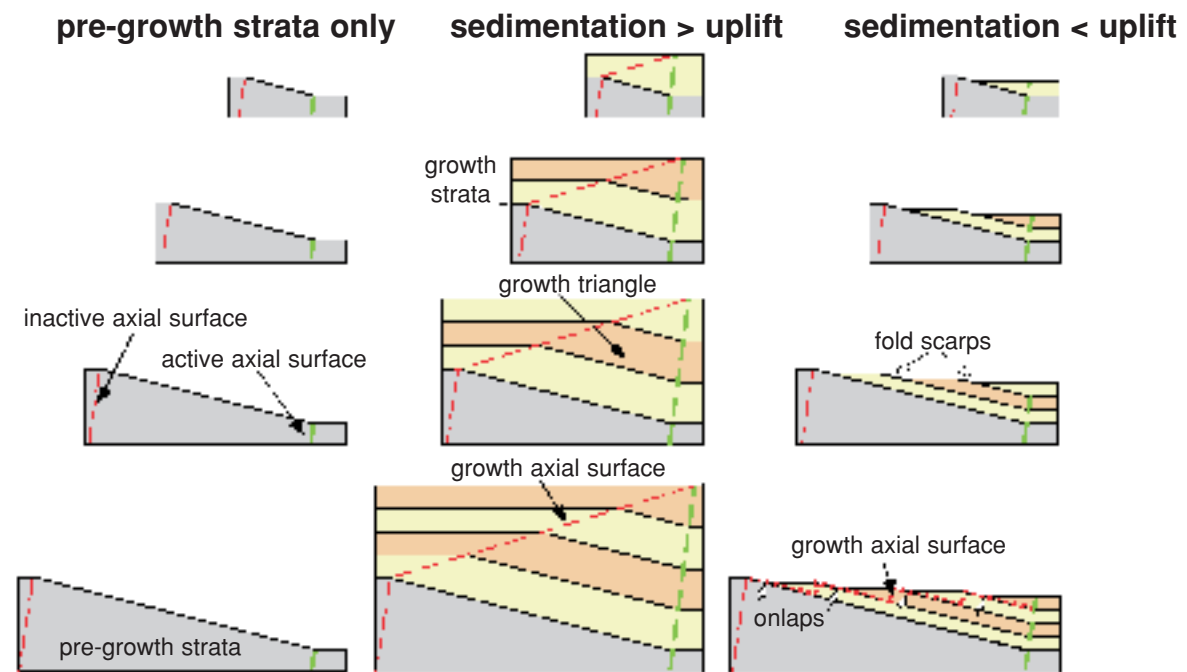
In fault-related folds that develop purely by kink-band migration, fold limbs widen through time while maintaining a fixed dip (Suppe et al., 1992), as illustrated in the sequential model involving pre-growth strata only *(above left)*. Material is incorporated into the fold limb by passing through an active axial surface, which at depth is generally pinned to a bend or tip of a fault (Suppe, 1983; Suppe and Medwedeff, 1990). The fold limb in growth strata is bounded by the active axial surface and the *growth axial surface,* an inactive axial surface that defines the locus of particles originally deposited along the active axial surface. In these sequential models, the synclinal axial surface is active, and the anticlinal axial surface is inactive.

In the case where sedimentation rate exceeds uplift rate *(above center)*, strata are folded through the synclinal axis and incorporated into the widening fold limb. The dip of folded growth strata is equal to dip of the fold limb in pre-growth strata. The width of the dip panel for each growth horizon corresponds to the amount of fold growth that occurred subsequent to the deposition of that marker. As a result, younger horizons have narrower fold limbs than do older horizons, forming narrowing upward fold limbs or kink bands in growth strata *(growth triangles)*. In the case where uplift rate exceeds sedimentation rate *(above right)*, each increment of folding produces a discrete fold scarp located where the active axial surface projects to the Earth's surface (Shaw et al., 2004). Subsequent deposits onlap the fold scarp, producing stratigraphic pinchouts above the fold limb. Fold scarps and stratigraphic pinch-outs are displaced laterally and folded as they are incorporated into widening limbs.

Contractional fault-related folding theories that exclusively invoke kink-band migration include fault-bend folding (Suppe, 1983), constant-thickness and fixed axis fault-propagation folding (Suppe and Medwedeff, 1983), and basement-involved (triple junction) folding (Narr and Suppe, 1994).

In fault-related folds that develop purely by limb rotation with fixed hinges (i.e., inactive axial surfaces), the dip of the fold limb increases with each increment of folding as illustrated in the sequential model involving pre-growth strata only *(left)*. In the case where sedimentation rate exceeds uplift rate *(center)*, strata are progressively rotated with each increment of folding. Thus, older growth horizons dip more steeply than do younger horizons, yielding a pronounced fannin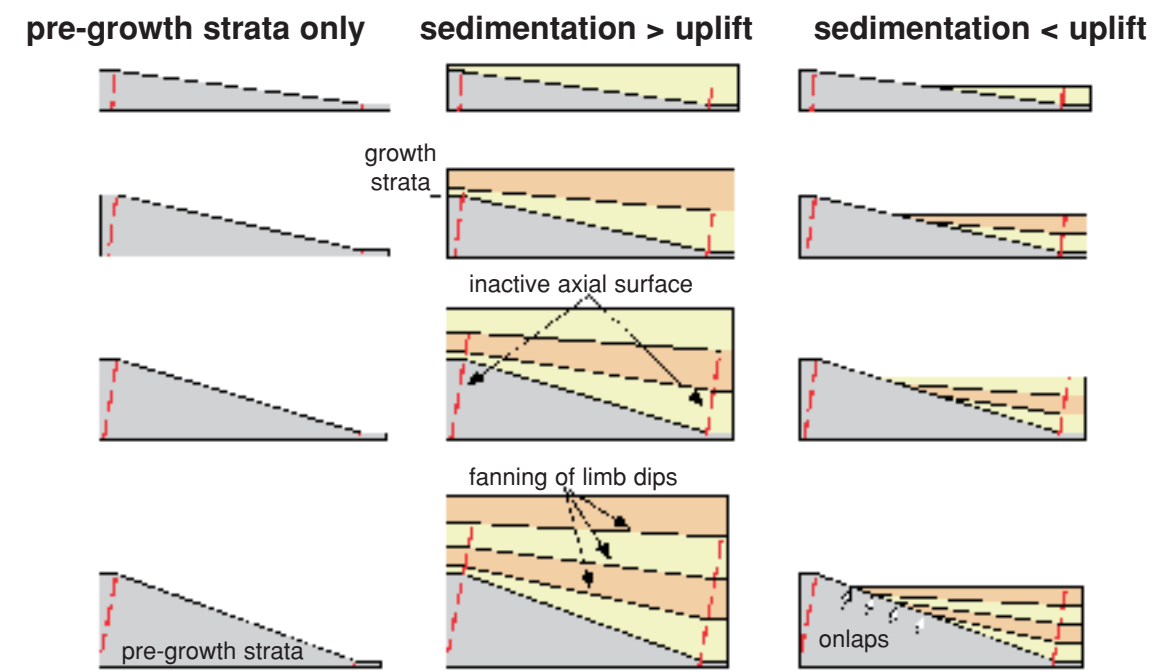g of limb dips in growth strata. Fold limb width, however, remains constant. In the case where uplift rate exceeds sedimentation rate, growth strata also exhibit a fanning of limb dips. However, growth strata typically onlap the fold limb.

Contractional fault-related folding theories that exclusively invoke limb rotation include certain classes of detachment folds (Dahlstrom, 1990; Hardy and Poblet, 1994).

Growth structures in seismic data

Growth structures imaged in seismic sections commonly exhibit patterns that are similar to the kink-band migration or limb-rotation models that were described on the previous page. In other cases, folds may develop by a combination of kink-band migration and limb rotation, resulting in hybrid patterns of growth structure. This section presents three seismic profiles as examples of kink-band migration, limb rotation, and hybrid growth structures.

Folding by kink-band migration

Seismic Example: Santa Barbara Channel, California, U.S.A.

(from: Shaw et al. 2004) Data courtesy of Texaco, Inc.
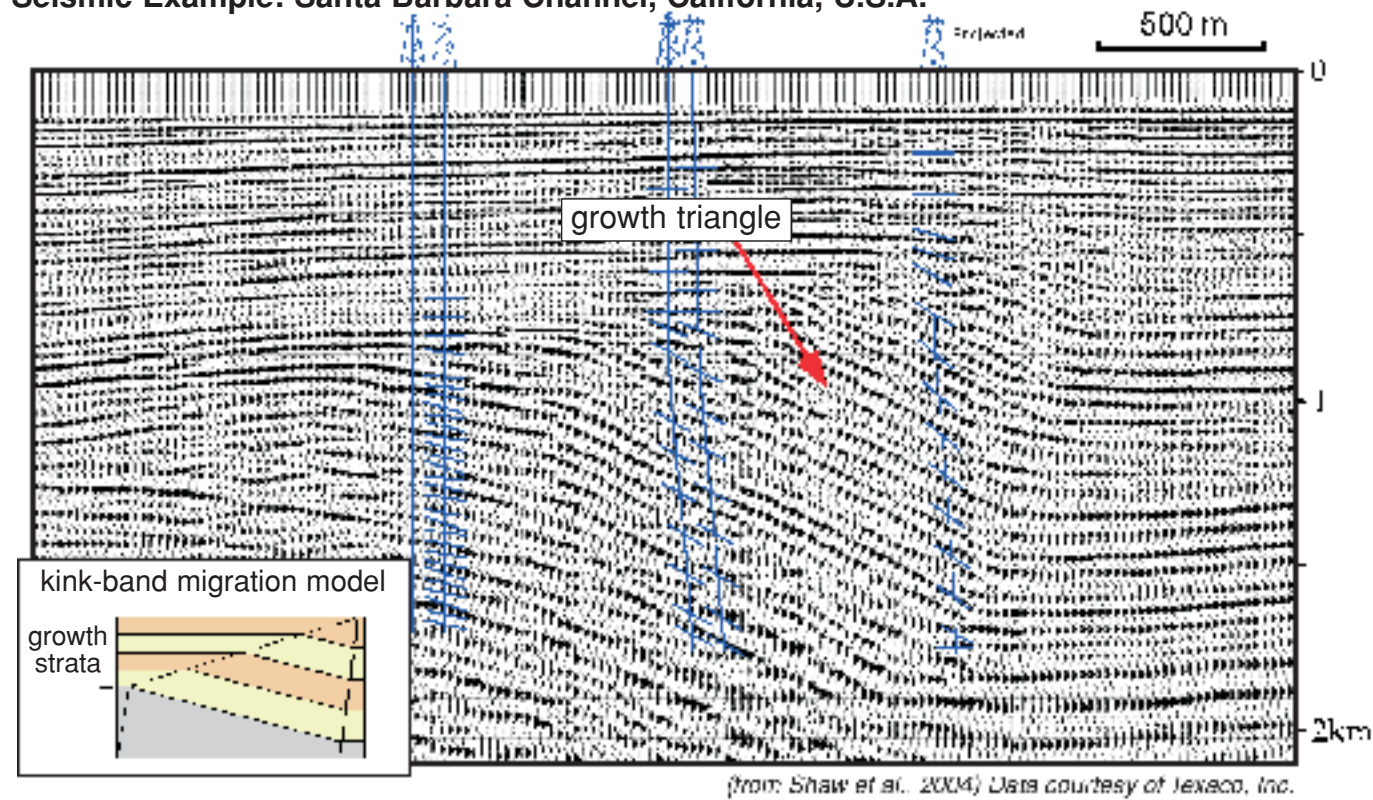
(top) The seismic section above shows a narrowing upward fold limb, or growth triangle, where bed dips within the fold limb generally do not shallow upward, consistent with folding by kink-band migration. Dipmeter data in the wells corroborates the reflector dips. *(upper right)* In this section, a fanning and upward shallowing of limb dips within growth strata are consistent with folding by progressive limb rotation. The core of the anticline is filled with salt, which presumably thickened during deformation, leading to progressive rotation of the overlying fold limbs. *(lower right)* The growth structure in this section contains both a growth triangle and a fanning of limb dips, suggesting folding by a combination of kink-band migration and limb rotation mechanisms. Kinematic theories that employ hybrid folding mechanisms include shear fault-bend folds (Suppe et al., 2004; see section 1A-4), certain classes of detachment folds (Dahlstrom, 1990; Hardy and Poblet, 1994; see section 1B-3), and trishear fault-propagation folds (Erslev, 1991; Hardy and Ford, 1997; Allmendinger, 1998; see section 1B-2).

Folding by progressive limb rotation

Seismic Example: offshore Angola
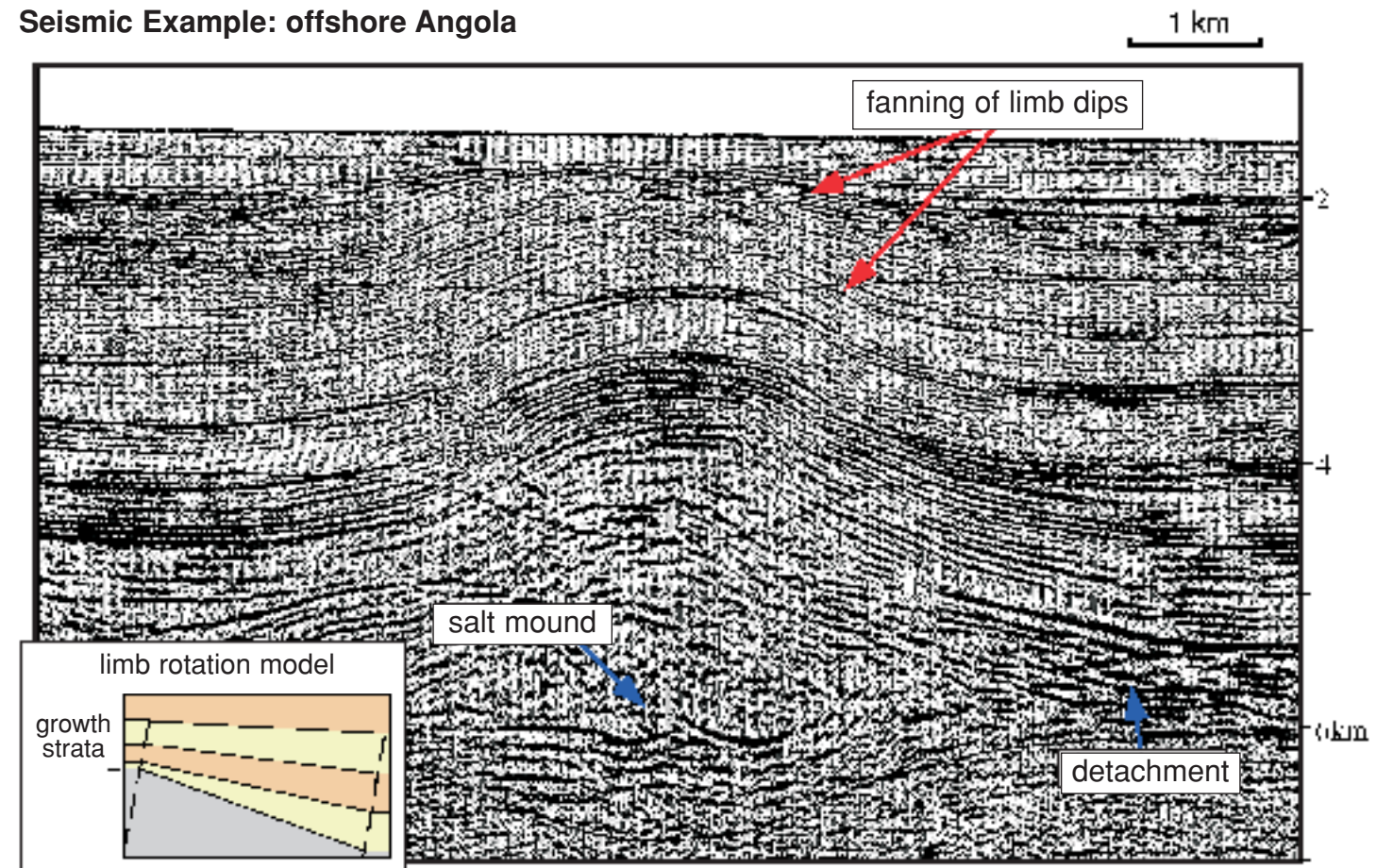
Folding by both kink-band migration and limb rotation

Seismic Example: San Joaquin basin, California, U.S.A.

(from Medwedeff, 1989; Suppe et al. 2004)
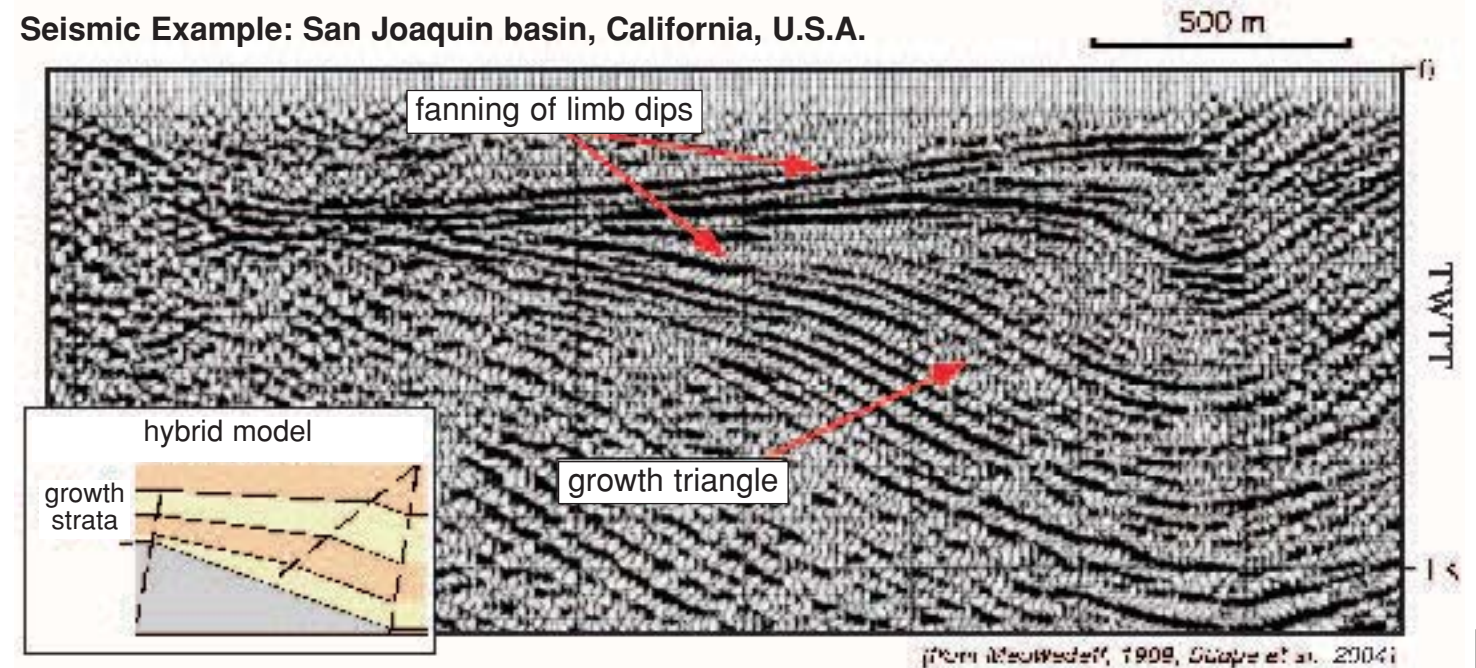
Distinguishing drape from growth strata

Sedimentary drape sequences are stratigraphic intervals that were deposited above a structure after deformation ceased, yet they are warped due to primary sedimentary dip and/or compaction. Drape sequences exhibit a wide range of patterns depending on the sedimentary environment and facies. In some cases, drape sequences have patterns that are similar to those of growth strata deformed by limb rotation. In this section, we illustrate the potential similarity of drape and growth patterns, and show an example of a drape sequence in a seismic section.

Kinematic models

Drape sequence
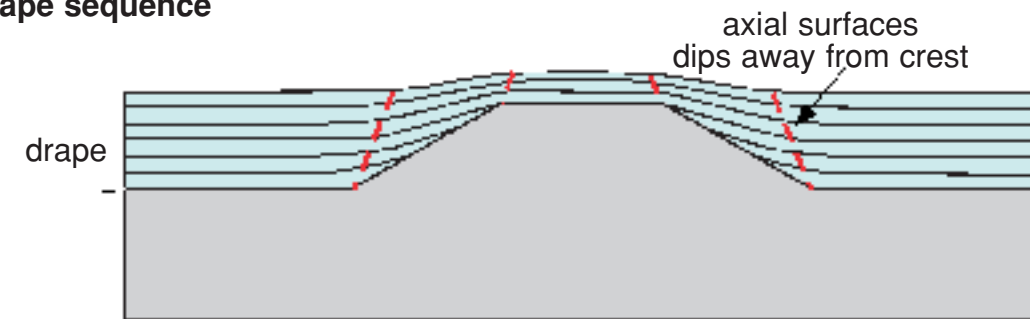
Growth fold
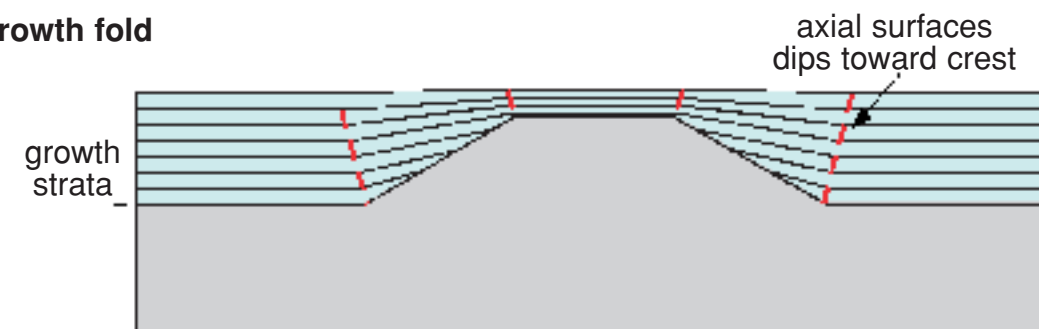
The top model shows a post-tectonic drape sequence above a rigid basement high. The drape sequence thins toward the crest of the structure, with younger strata having less relief than older units. The lower model shows growth strata above a fold developed by progressive limb rotation. The two stratigraphic patterns are similar, and in some cases difficult to distinguish. Incorrect interpretations of drape and growth sequences can lead to flawed estimates of structural timing and kinematics. Thus, care should be taken in trying to distinguish between drape and growth sequences.

One common difference between drape and growth sequences is the orientation of axial surfaces. Axial surfaces in drape sequences often are vertical or dip away from the structural crest, reflecting a state of tension and due, in some cases, to compaction (Laubach et al., 2000). In contrast, axial surfaces in contractional folds generally dip toward the structural crest, reflecting a state of compression. Thus, careful interpretation of axial surfaces, along with consideration of regional tectonic history, can, in some cases, help to distinguish between drape and growth sequences.

Drape folding

Seismic Example: offshore California Borderlands, U.S.A.
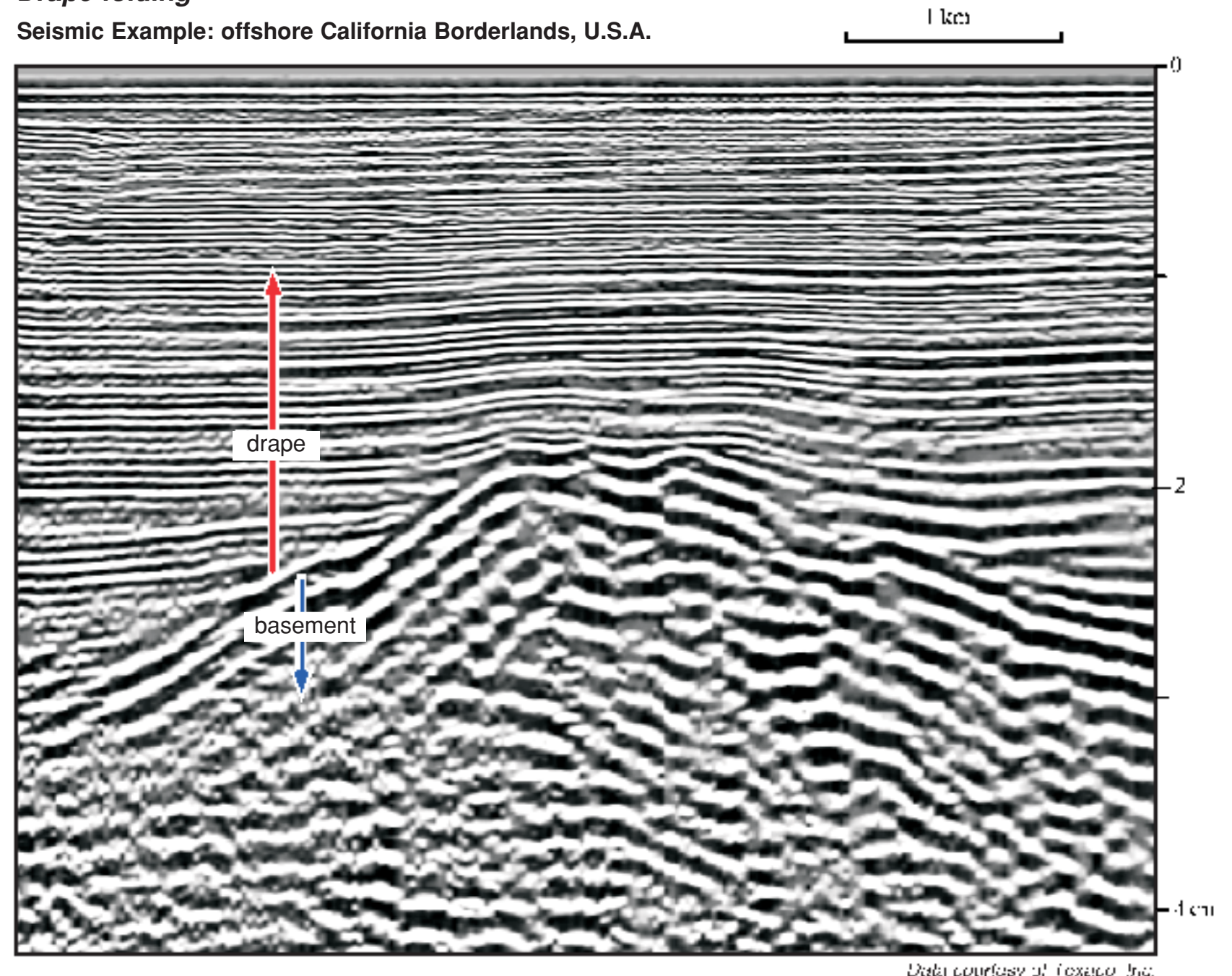
This seismic section images a siliciclastic drape sequence that onlaps and overlies a ridge of metamorphic basement rocks.

1B-1: Fault-bend folds

Basic concept

Fault-bend folds form as hanging wall-rocks move over bends in an underlying fault. This section describes the geometry and kinematics of fault-bend folding after Suppe (1983) and introduces basic techniques for interpreting these structures in seismic data.

To describe the basic concept of fault-bend folding, we will consider the hypothetical case of a fault in cross section with one bend joining upper and lower segments. *Rigid-block translation* of the hanging wall parallel to the upper fault segment produces a void between the fault blocks; whereas, translation of the hanging wall parallel to the lower fault segment produces an "overlap." Both of these cases are unreasonable.

Rigid-Block Translation
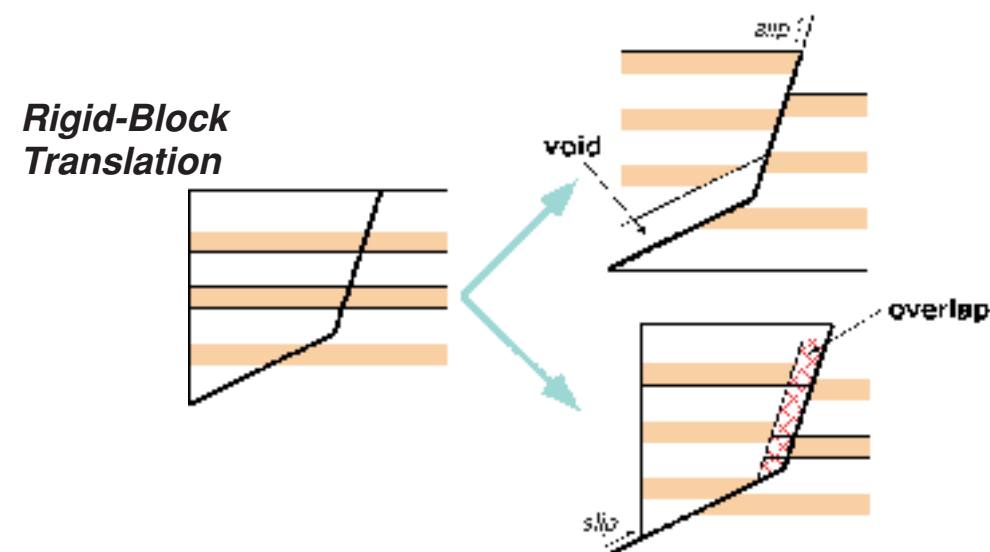
In contrast, folding of the hanging wall block through the development of a kink band accommodates fault slip without generating an unreasonable overlap or void. This fault-bend folding (Suppe, 1983) is localized along an *active axial surface*, which is fixed with respect to the fault bend. After strata are folded at the active axial surface, they are translated above the upper fault segment. The *inactive axial surface* marks the locus of particles that were located along the active axial surface at the initiation of fault slip. The inactive axial surface moves away from the active axial surface with progressive fault slip, and thus the width of the intervening kink band is proportional to the amount of fault slip.
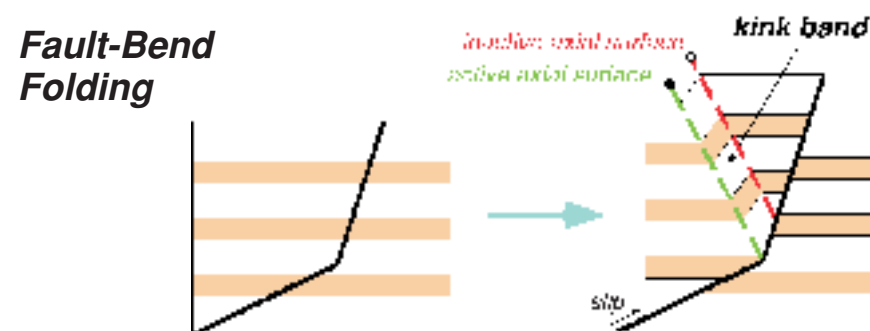
Fault-Bend Folding

Synclinal fault-bend folds

Synclinal fault-bend folds form at concave-upward fault bends. Synclinal axial surfaces are pinned to the fault bend and are generally active; whereas anticlinal axial surfaces are inactive and move with the hanging wall block. Figures below show a kinematic model, a field example, and a seismic example of synclinal fault-bend folds.

Kinematic Model

Field Example

Kicking Horse Canyon, Alberta, Canada. (JHS/FDB)
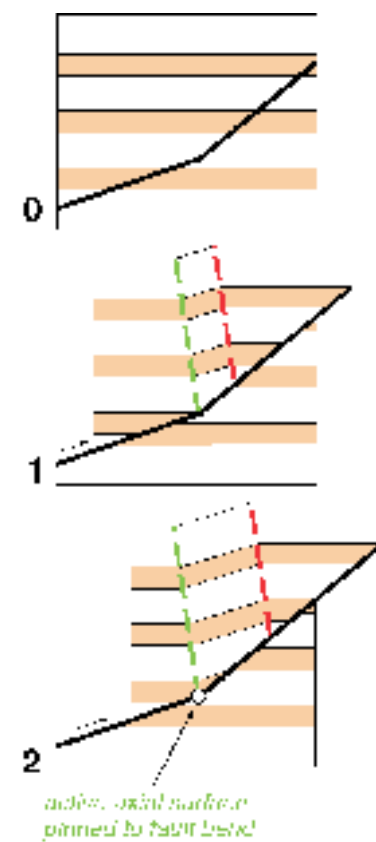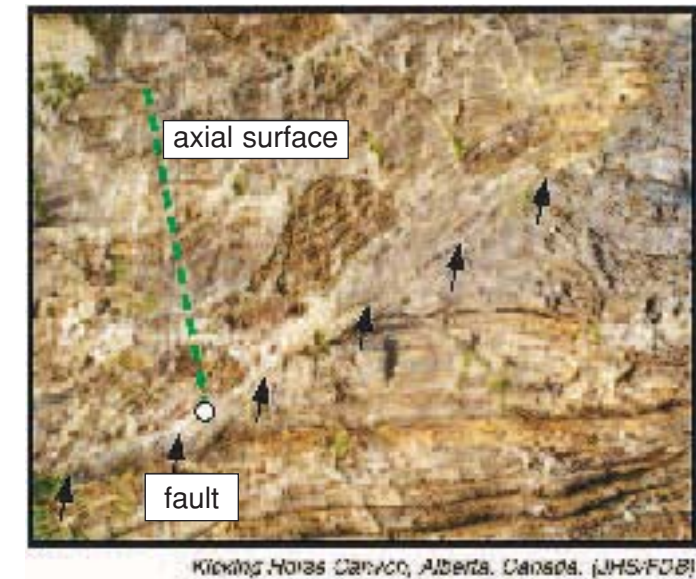
Seismic Example: Argentina
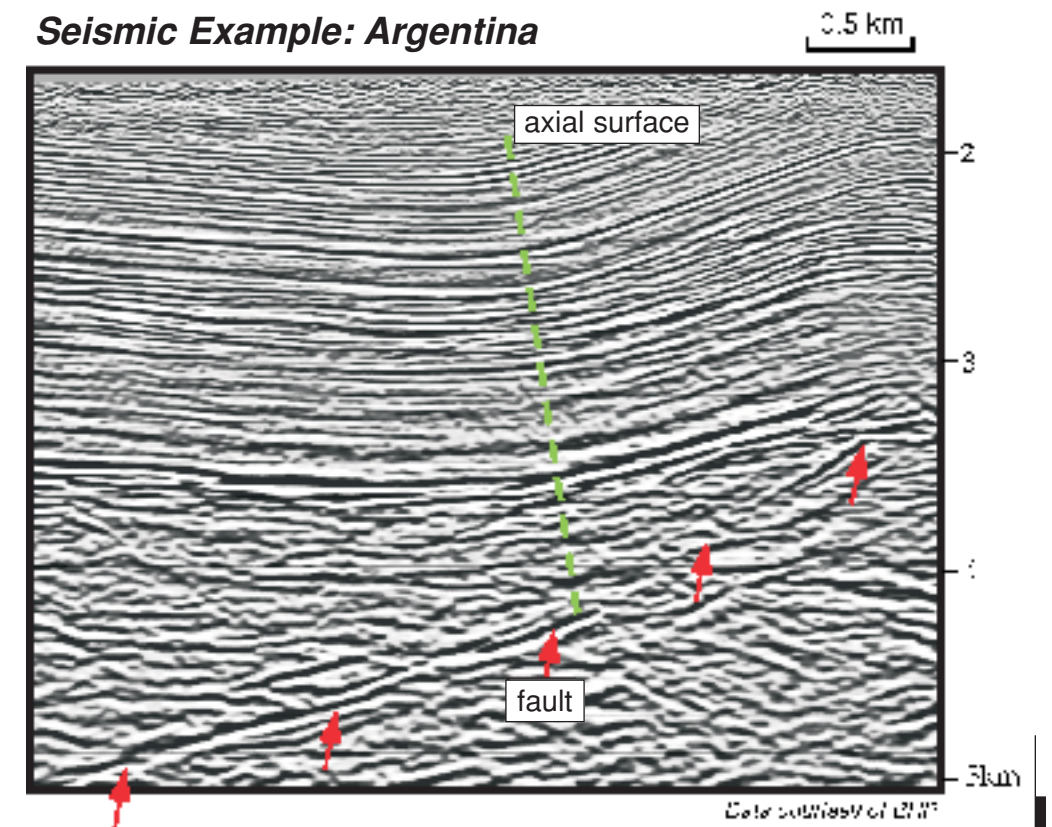
Anticlinal fault-bend folds

Anticlinal fault-bend folds form at concave-downward fault bends. Anticlinal axial surfaces are pinned to the fault bend and are generally active; whereas, synclinal axial surfaces are inactive and move with the hanging wall block. Figures below show a kinematic model, a field example, and seismic examples of anticlinal fault-bend folds.
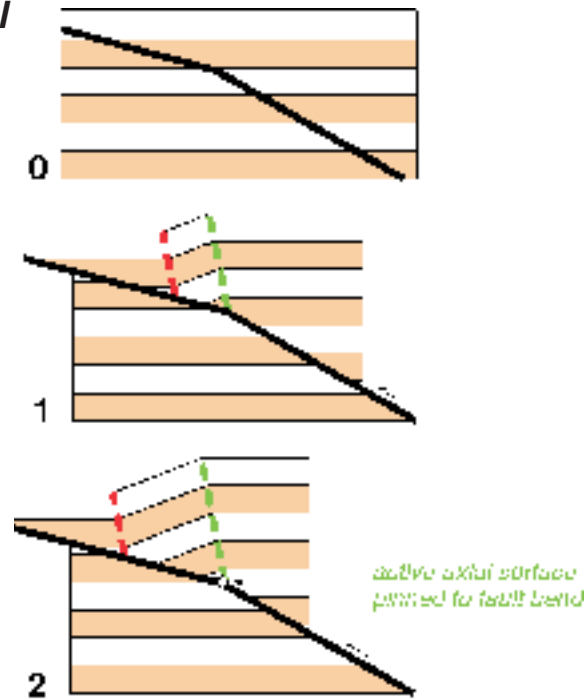
Kinematic Model

active axial surface
pinned to fault bend

Field Example

axial surface

fault

Crows Nest Pass, Alberta, Canada. (USFCO)

Seismic Example: Niger Delta

0.5 km

axial surface

fault

Data courtesy of Mobil Limited

Seismic Example: Permian basin, U.S.A.

1 km

axial surface

fault

Data courtesy of Texaco, Inc
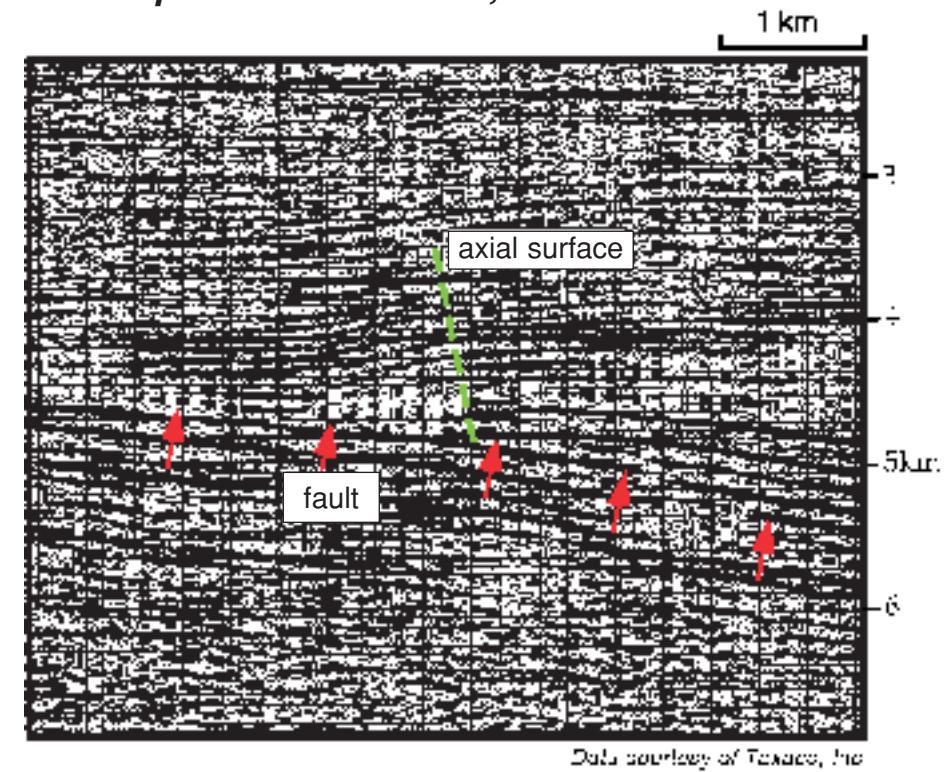
Quantitative fault-bend folding

Based on assumptions of conservation of bed length and thickness during folding, the shape of a fault-bend fold is related to the shape of the fault by:

$$\phi = \tan^{-1}\left\{\frac{-\sin(\gamma-\theta)\,[\sin(2\gamma-\theta)-\sin\theta]}{\cos(\gamma-\theta)\,[\sin(2\gamma-\theta)-\sin\theta]-\sin\gamma}\right\}$$

$$\beta = \theta - \phi + (180 - 2\gamma) \quad \text{Suppe (1983)}$$

Where θ is the hanging wall cutoff angle before the fault bend; φ is the change in fault dip; β is the hanging wall cutoff after the fault bend, and; γ is one half of the interlimb angle, such that the axial surfaces bisect the interlimb angles and bed thicknesses are preserved. If two of these values are known, the remaining two values can be determined.

The fault-bend fold relations are displayed in the graph below. The left side of the graph describes *anticlinal fault-bend folds*, where the fold is concave toward the fault; the right side of the graph describes *synclinal fault-bend folds*, where the fold is convex toward the fault.

When interpreting seismic sections, typically the interlimb angle (γ) can be observed (see section 1A-2) and one of the hanging wall cutoff angles (θ or β) can be specified. Using the graph, the change in fault dip (φ) and the remaining cutoff angle can be determined.

For anticlinal fault-bend folds there are two fold solutions for each θ and φ value; *first mode solutions* produce open folds that have been shown to effectively describe many observed fold geometries; whereas, *second mode solutions* are geometrically valid but have not been shown to effectively describe natural fold shapes.

Anticlinal fault-bend folds   Synclinal fault-bend folds
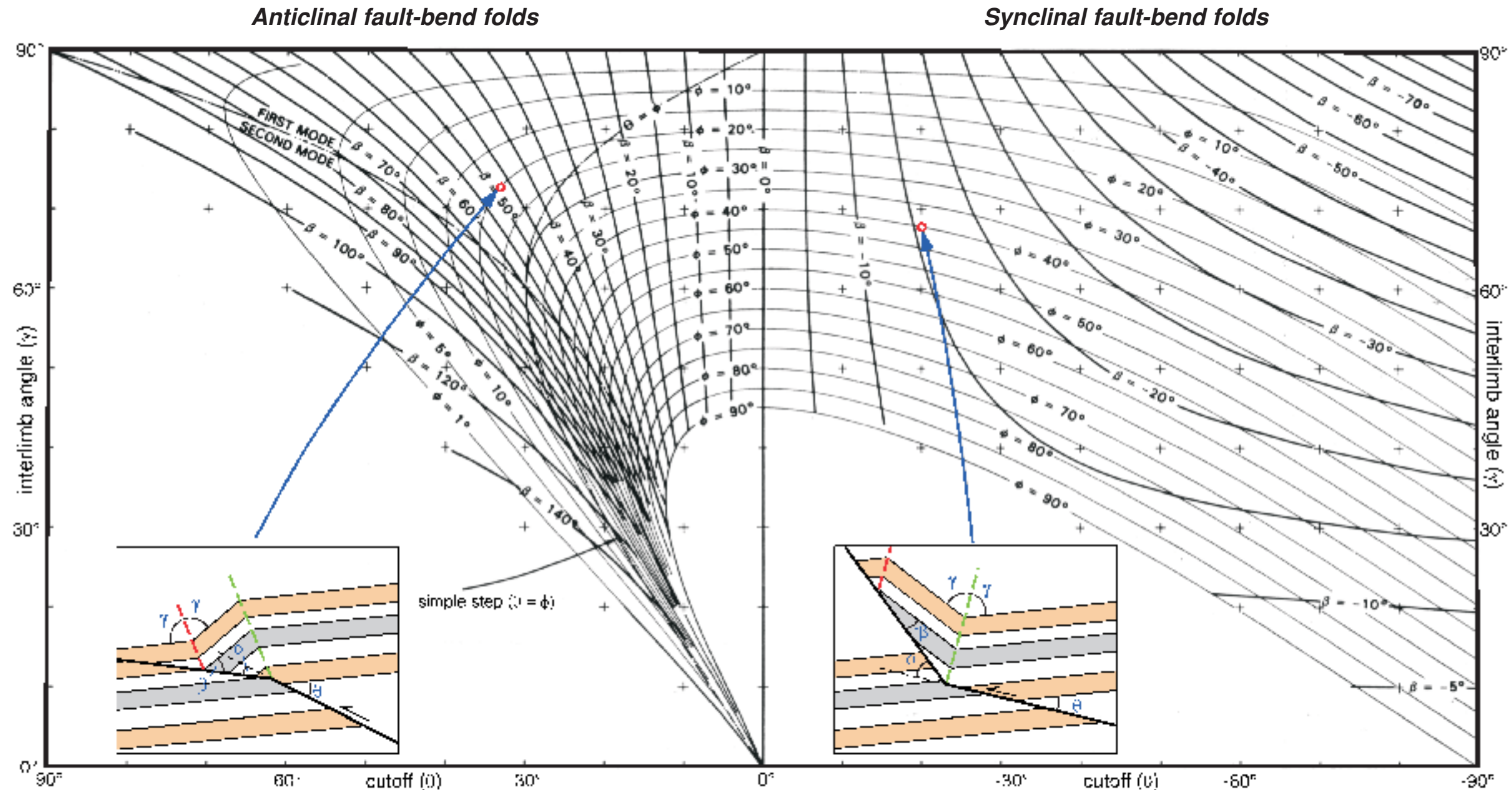
Fault slip and fault-bend folds

The magnitude of fault slip can change across fault bends, as slip is consumed or produced by fault-bend folding. In cases where the initial cutoff angle is not equal to zero ($\theta \neq 0$), anticlinal fault-bend folds consume fault slip and synclinal fault-bend folds produce fault slip. The change in fault slip is described by the parameter R, which is the ratio of slip magnitude beyond (S_1) and before (S_0) the fault bend.

$$R = S_1/S_0$$

In cases where the initial cut-off angle (θ) equals zero, then R equals one (R=1). When the initial cut-off angle (θ) does not equal zero, R can be determined if any two of the four geometric parameters (θ, ϕ, β, γ) are specified using fault-bend fold theory (Suppe, 1983). The graph below plots R as a function of initial cut-off angle (θ), interlimb angle (γ), and change in fault dip (ϕ), and is of the same format used to describe fault-bend fold geometry.

R varies greatly as a function of the tightness of the fold, which is reflected in part by the interlimb angle (γ). Tight (perhaps with steep limbs) anticlinal folds generally consume larger amounts of slip (hence they have lower R values) than do gentle anticlinal folds. Tight synclinal folds generally produce larger amounts of slip (hence they have higher R values) than do gentle anticlinal folds.

In both synclinal and anticlinal fault-bend folds with a single fault bend, the width of the fold limb measured along the fault equals the slip (S_1).
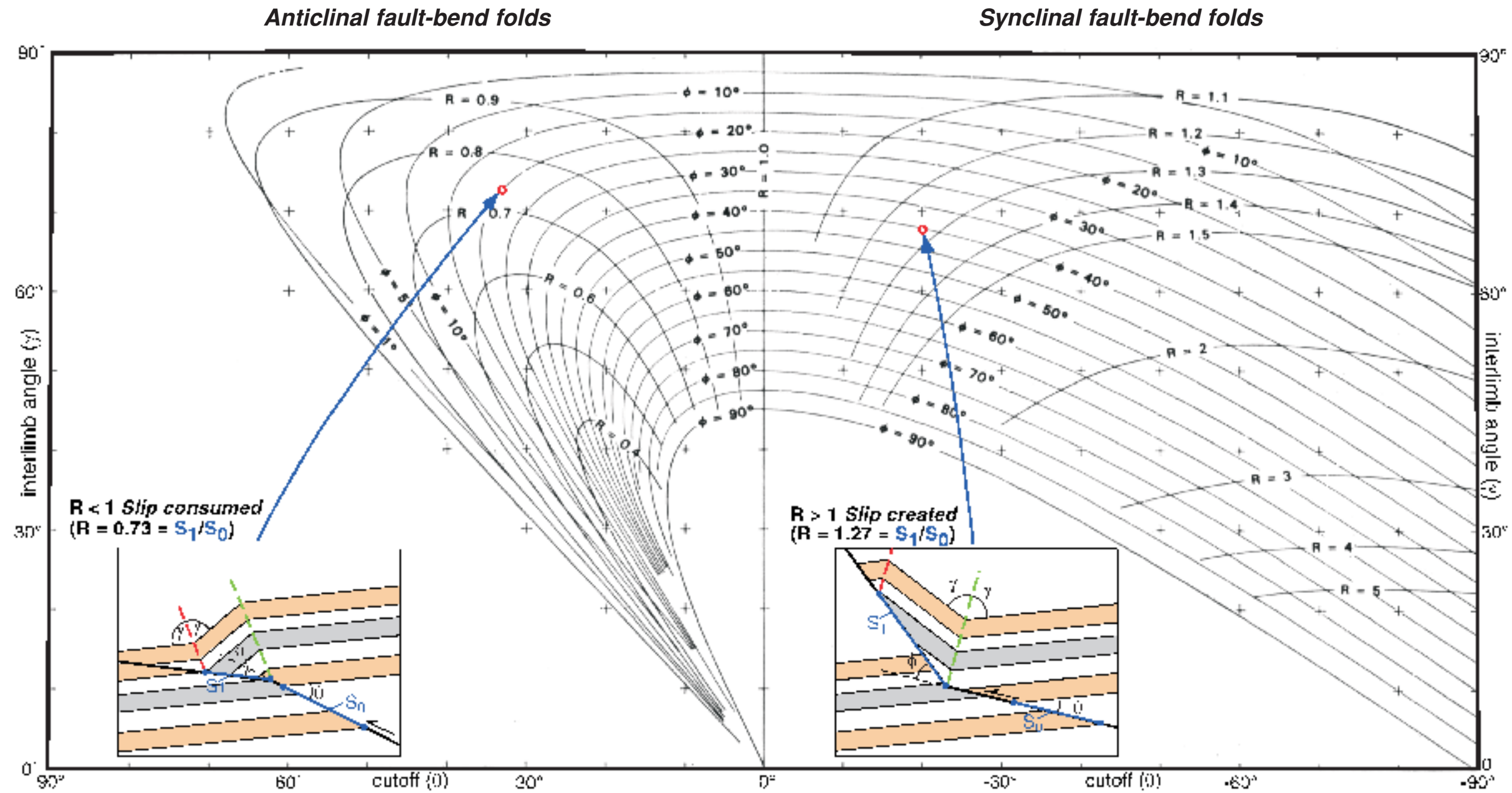
Anticlinal fault-bend folds Synclinal fault-bend folds

Seismic interpretation of a synclinal fault-bend fold

This section describes the interpretation of a synclinal fault-bend fold imaged in seismic reflection data. The lower portion of the fault and the syncline are well imaged, and fault-bend folding theory is used to predict the orientation of the upper portion of the fault.

In Figure 1, fault-plane reflections define the position of a thrust ramp located beneath a syncline. Based on the imaged fold shape and fault ramp, the initial cutoff angle (θ) and interlimb angle (γ) can be measured as:

$$\theta = 15°; \gamma = 82°$$

Using the synclinal fault bend fold graph (Figure 2), γ and θ are used to determine the change in fault dip (ϕ) and the hanging wall cutoff after the fault bend (β):

$$\phi = 15°; \beta = 14°$$

ϕ and β values are used to model the structure in Figure 3. Note that the predicted upper fault segment agrees closely with the fault position as constrained by reflection terminations and potential fault-plane reflections.

Synclinal fault-bend fold, Argentina

1. Observations/Initial Interpretation
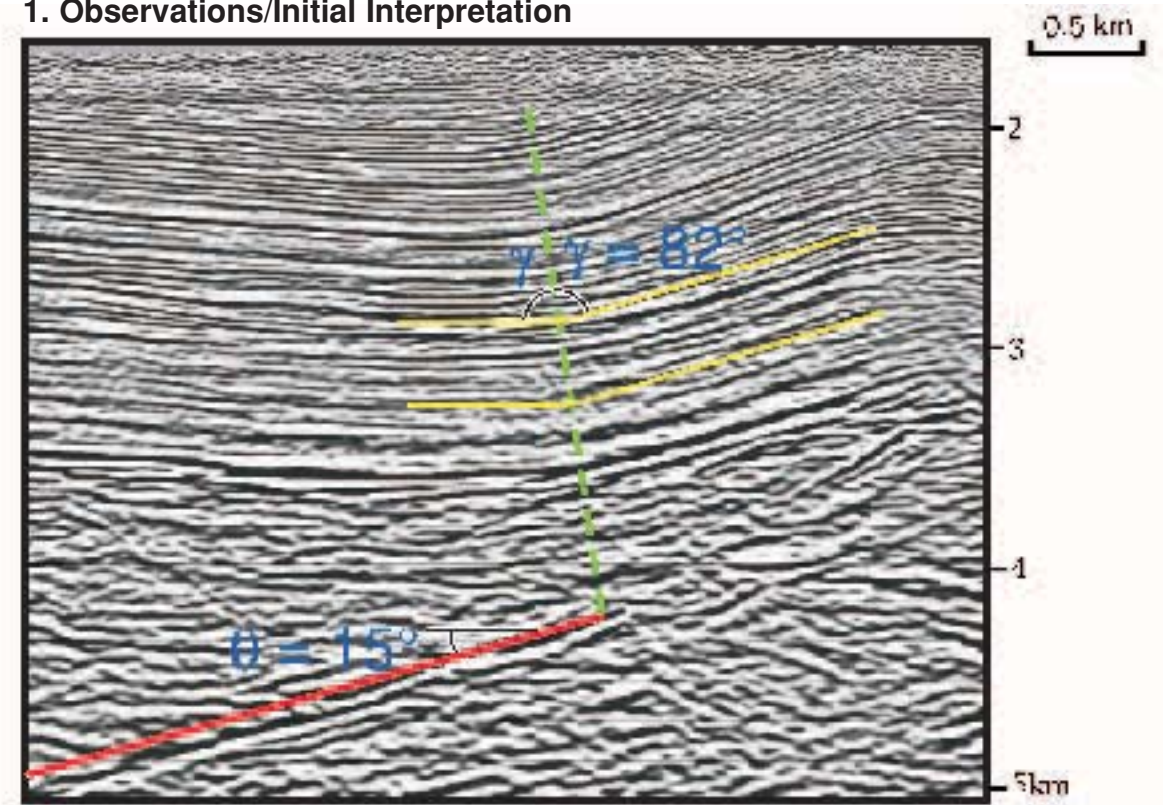
2. Synclinal fault-bend fold graph
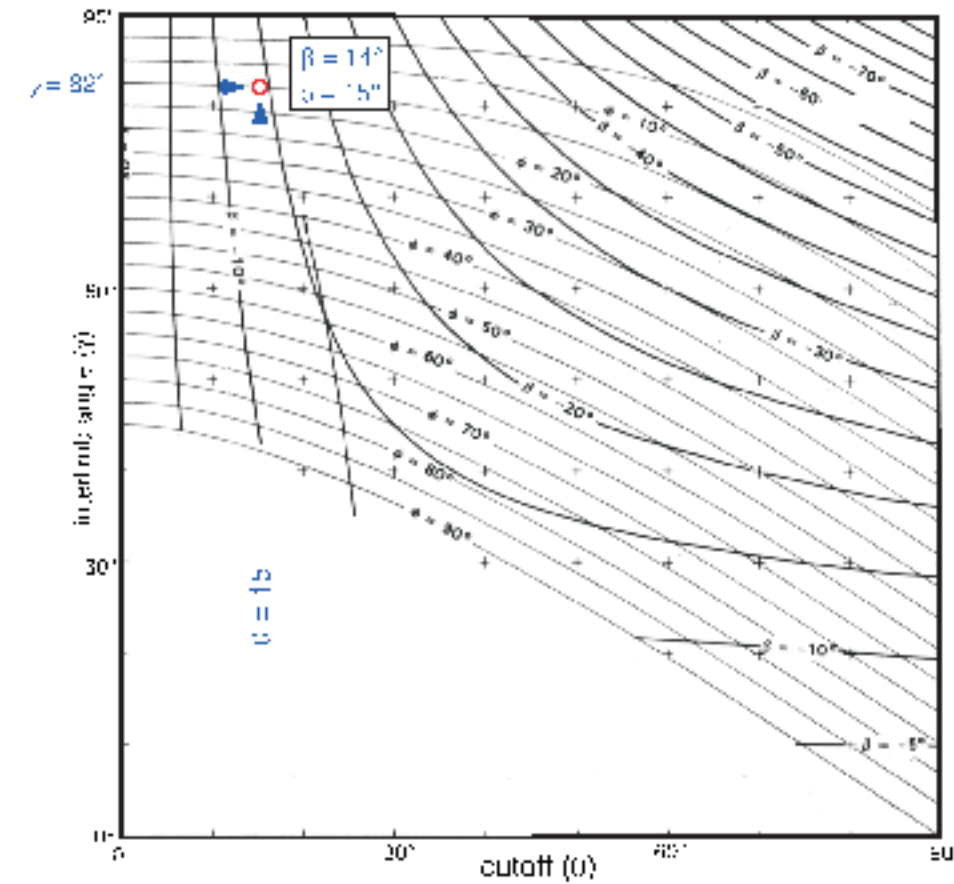
3. Prediction
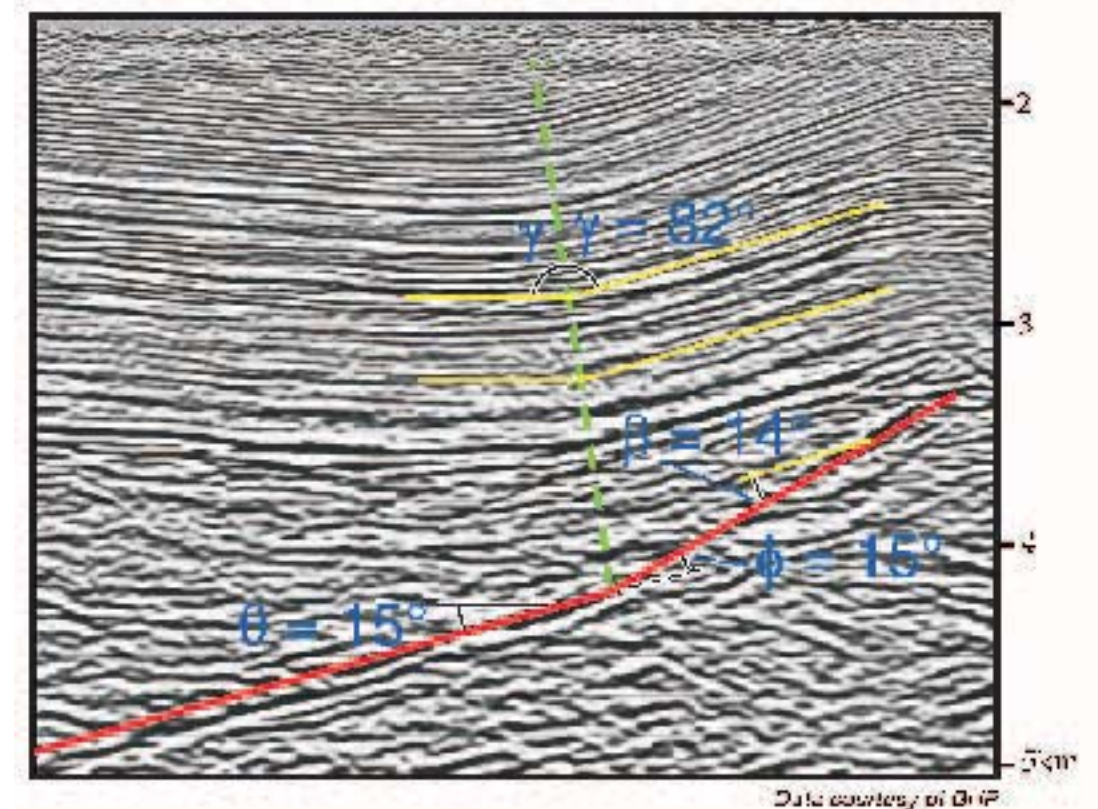
Data courtesy of BHP

Seismic interpretation of an anticlinal fault-bend fold

This section describes the interpretation of an anticlinal fault-bend fold imaged in seismic reflection data.

In Figure 1, fault-plane reflections and reflection truncations define the position of a thrust ramp located beneath an anticline. Based on the imaged fold shape and fault ramp, the initial cut-off angle (θ) and interlimb angle (γ) can be defined as:

$$\theta = 24°; \gamma = 80°$$

Using the anticlinal fault bend fold graph (Figure 2), γ and θ are used to determine the change in fault dip (ϕ) and the hanging wall cutoff after the fault bend (β):

$$\phi = 16°; \beta = 28$$

ϕ and β values are used to model the structure in Figure 3. Note that the predicted upper fault segment agrees closely with the fault position as constrained by reflection terminations and the downward termination of the forelimb.

In this example, slip below the fault bend (S_0) is also interpreted based on offset reflections. Based on the slip ratio R predicted for this fault-bend fold (obtained using the graph presented in the previous section), the slip above the fault bend (S_1) is calculated as follows:

$$R = (S_0/S_1) = 0.87; \text{ given } S_0 = 1.7 \text{ km, then } S_1 = 1.5 \text{ km}$$

2. Anticlinal fault-bend fold graph

Anticlinal fault-bend fold, Niger Delta

1. Observations / Initial Interpretation

3. Prediction
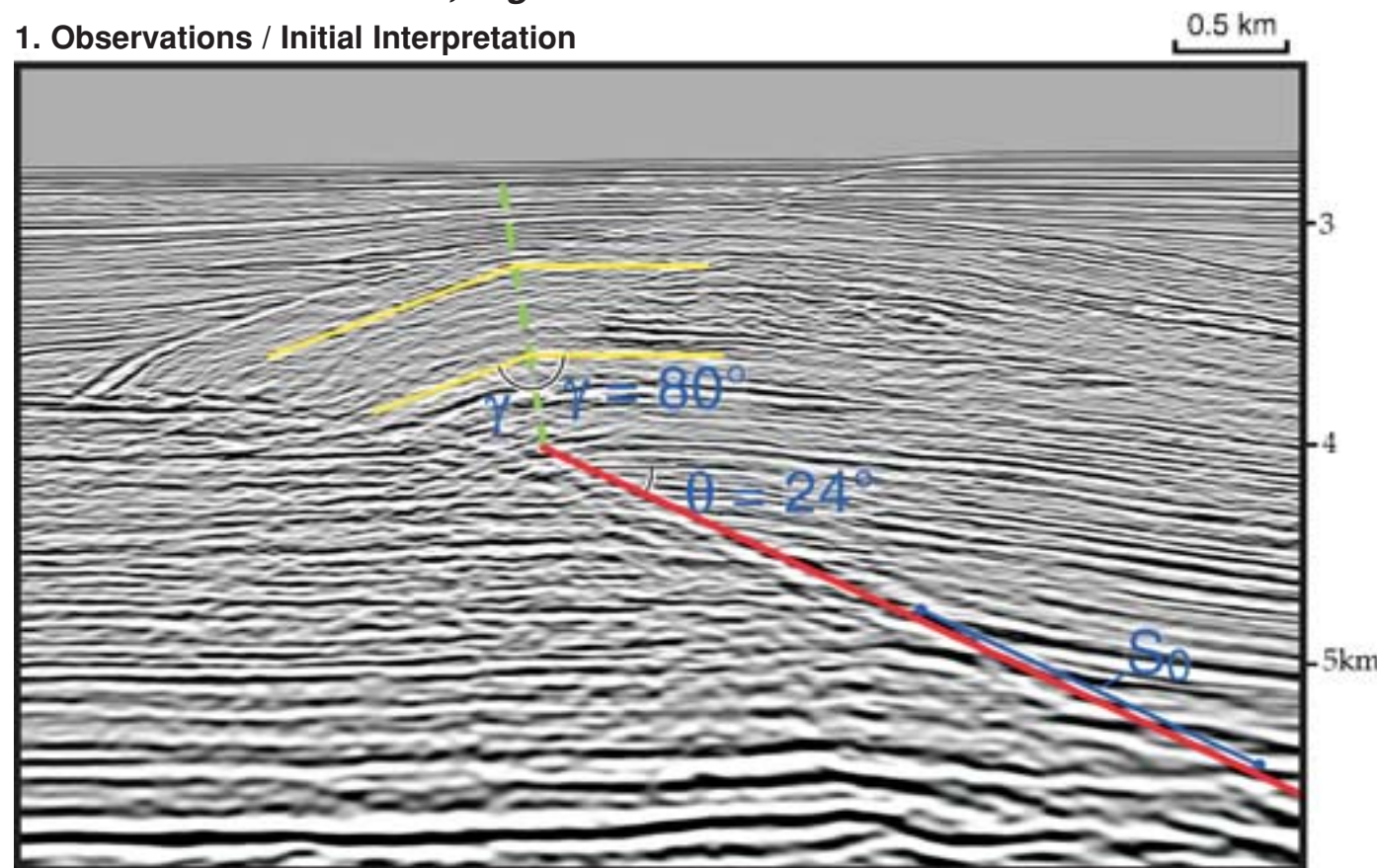
Composite fault-bend folds: Ramp anticlines

The most common representation of a fault-bend fold involves deformation above a thrust ramp connecting upper and lower detachments, often referred to as a ramp anticline. In fact, this structure consists of two fault-bend folds — one related to each fault bend — and thus is part of a class of "composite" fault-bend folds. This section describes the kinematic evolution of a simple ramp anticline after Suppe (1983), the geometry of which is governed by the quantitative fault-bend folding theories described in the preceding pages.

Kinematic development of a composite fault-bend fold

0: An incipient thrust fault and axial surfaces in undeformed strata.
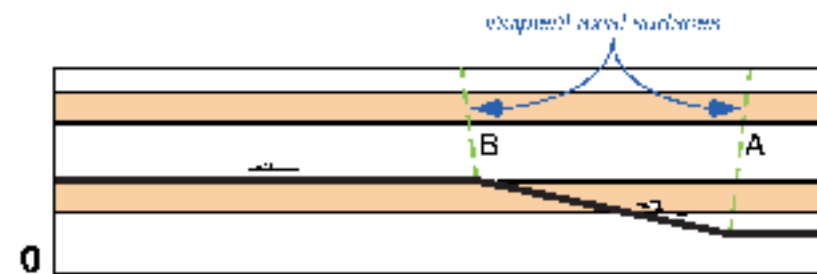
1: Fault slip causes folding of the hanging wall block along active axial surfaces A and B that are pinned to the two fault bends. Inactive axial surfaces A′ and B′ form at fault bends and are passively translated away from active axial surfaces by slip. Kink-band width A-A′ or B-B′ measured along bedding equals slip on the underlying fault segment. The difference in kink-band width between back and front limbs reflects slip consumed in folding.
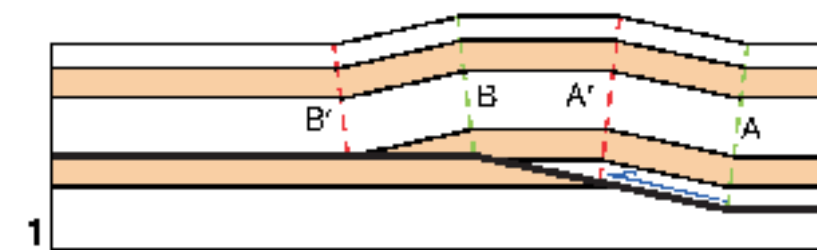
2: Progressive fault slip widens both kink bands. Models 1 and 2 are in the *crestal uplift stage* because the fold crest elevates with increasing fault slip.
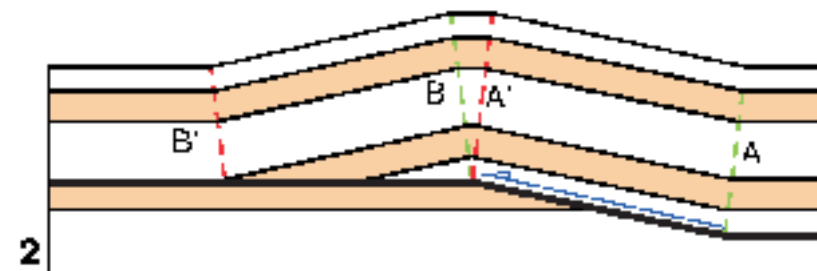
3: When the axial surface A′ reaches the upper fault bend, material from the back limb is refolded onto the crest and the front limb kink-band B-B′ is translated along the upper detachment. In model 3, A and A″ are active axial surfaces; B and B′ are inactive axial surfaces. Model 3 is in the crestal broadening stage because the fold crest widens without producing additional structural relief with increasing fault slip. In the *crestal broadening stage,* slip exceeds the width of the fold limbs, and is equal to the distance between axial surfaces A-A′ measured along the fault.
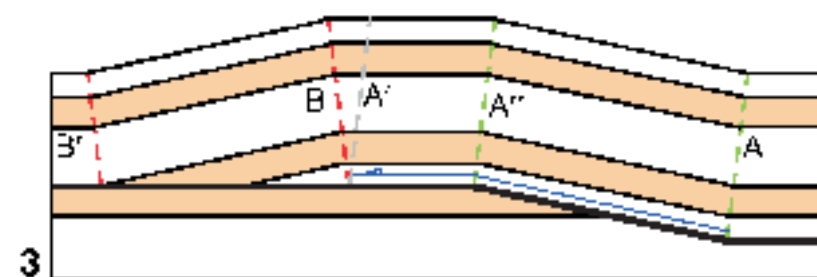
Seismic Example: Pitas Point, Santa Barbara Channel, California, U.S.A.

Uninterpreted section
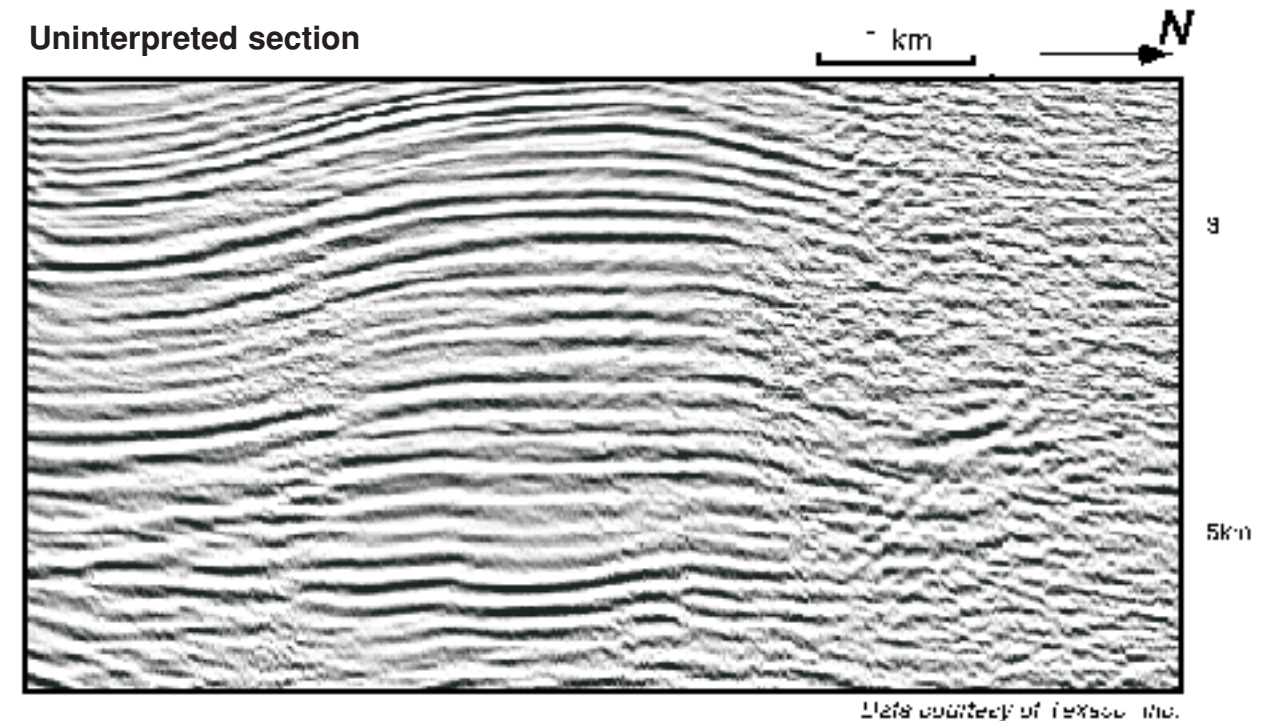
Interpreted section
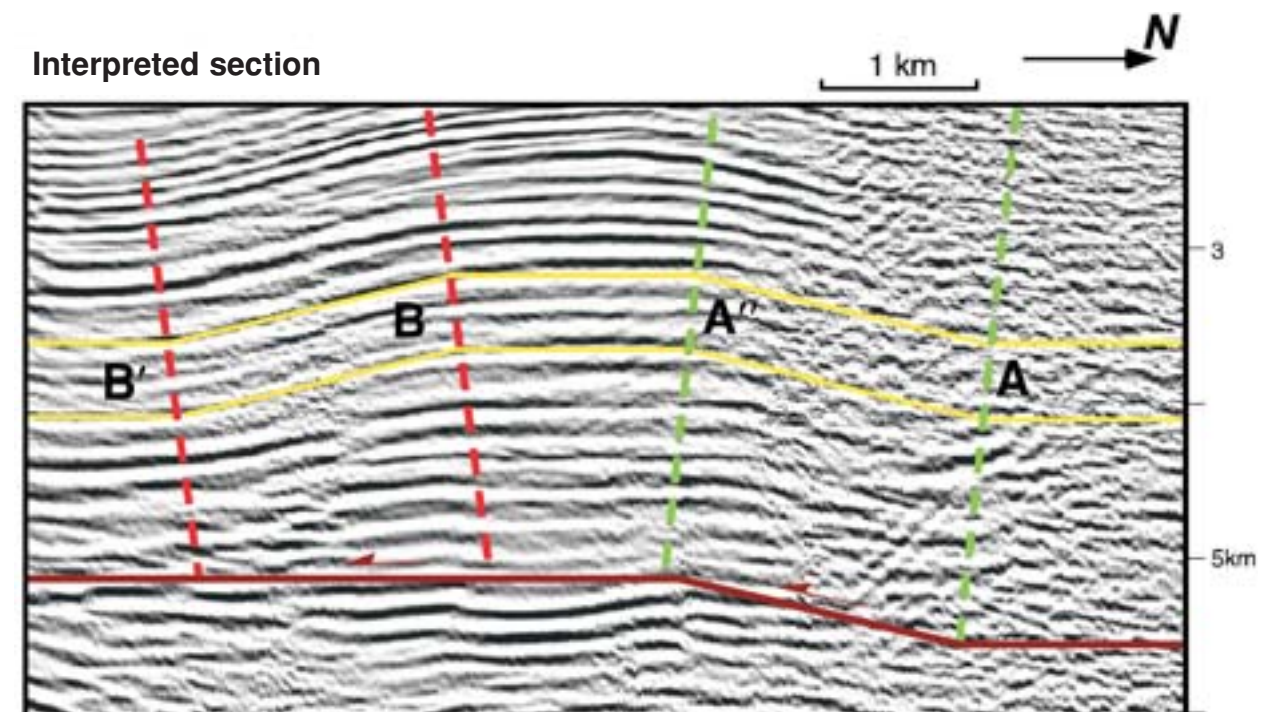
"Multi-bend" fault-bend folds

In addition to simple ramp anticlines, composite structures include multi-bend fault bend folds (Medwedeff and Suppe, 1997), which contain two or more bends of similar concavity or convexity. Initially, slip across each bend produces a distinct kink band; however, with progressive fault slip, kink bands merge and interact. These interactions can be highly complex, spawning many new axial surfaces and dip domains. Thus, multi-bend fault-bend folds are generally characterized by the presence of multiple dip domains in backlimbs and forelimbs. Figures below show kinematic models of multibend fault-bend folds and a seismic example.

Kinematic development of multi-bend fault-bend folds

Convex upward (anticlinal) bends

Concave upward (synclinal) bends

Seismic Example: Niger Delta

Multi-bend fault

Interpreted section

0: Incipient fault with two convex upward bends. **1:** Slip yields two kink bands associated with the two fault bends. **2:** Kink bands widen with progressive slip. **3:** Portions of kink bands are refolded, yielding a steeply dipping fold panel.

0: Incipient fault with two concave upward bends. **1:** Slip yields two kink bands associated with the two fault bends. **2:** Kink bands widen with progressive slip. **3:** A portion of the lower kink band is refolded as it moves onto the upper fault ramp.

Modeling curved fold hinges

Folds generally exhibit some curvature in their hinges. Most fault-related fold analysis techniques approximate these curved hinge zones as perfectly angular folds or as multi-bend folds composed of two or more planar hinge segments (Medwedeff and Suppe, 1997). In many cases, these approximations adequately describe large folds, with small zones of hinge curvature separating long, planar fold limbs of the scale typically imaged in seismic data. Moreover, these approximations are useful because they allow for rigorous area and line length balancing. In some cases, however, it may be necessary to more accurately describe curved hinge zones. Here we introduce a curved-hinge fault-bend fold model after Suppe et al. (1997), which obeys fault-bend folding relations but imparts fault curvature on the fold shape using the concept of entry and exit axial surfaces. Other techniques of modeling curved fold hinges (e.g., trishear folding — Erslev, 1991) are described in later sections.

Synclinal fault-bend folds
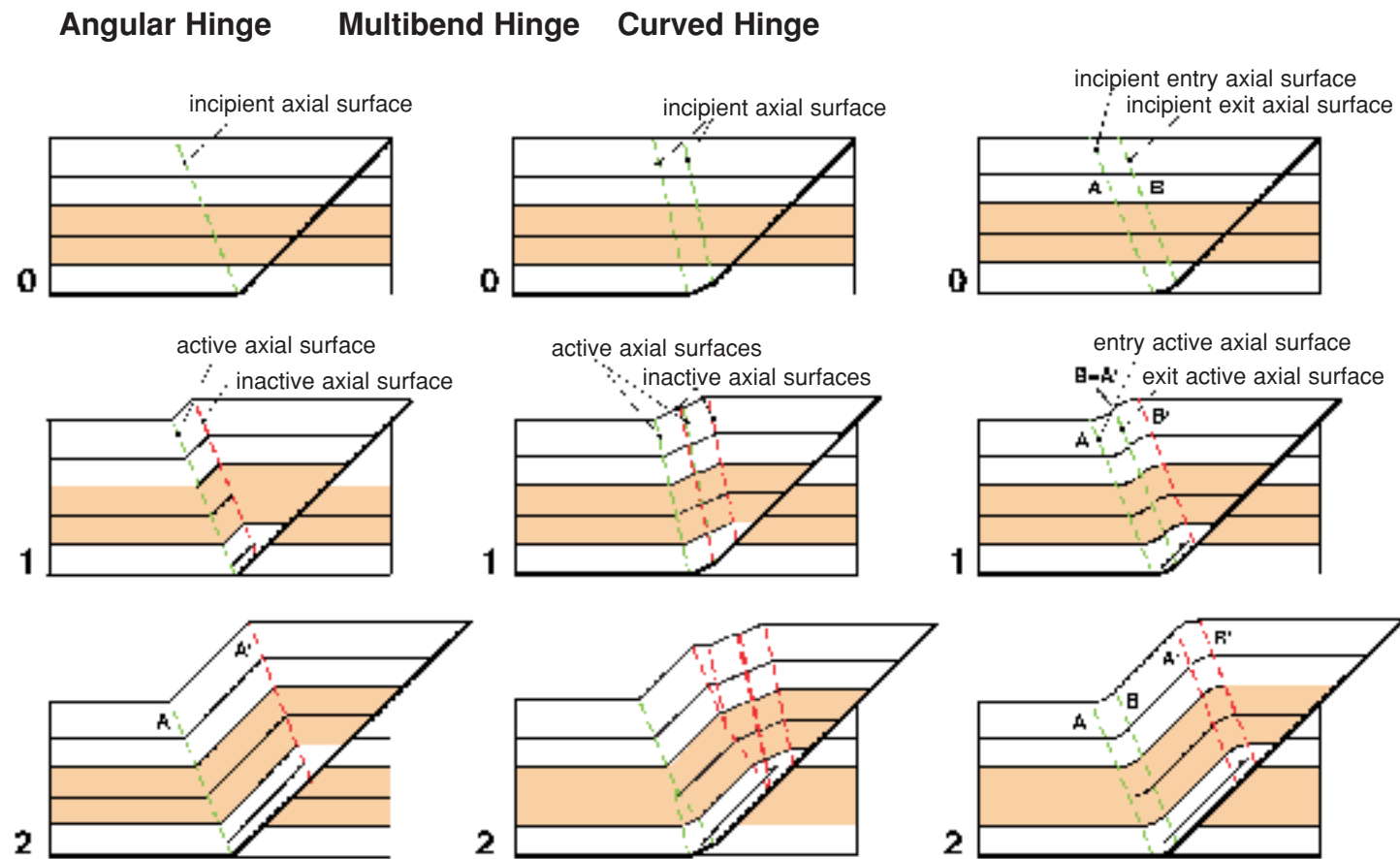
Sequential models of a synclinal fault-bend fold with an angular hinge.

Sequential models of a multibend synclinal fault-bend fold with two fault ramp segments.

Sequential models of a curved hinge synclinal fault-bend fold. **0:** Two incipient active axial surfaces bound the zone of curvature on the fault. **1:** Slip causes folding of the hanging wall rocks. Folding begins as rocks pass through the entry active axial surface (A), and ceases as rocks pass through the exit active axial surface (B). **2:** Progressive slip widens the kink band, as inactive axial surfaces (A′ and B′) are passively translated up the fault ramp.

Seismic Example: Sichuan basin, China

Uninterpreted section

Interpreted section
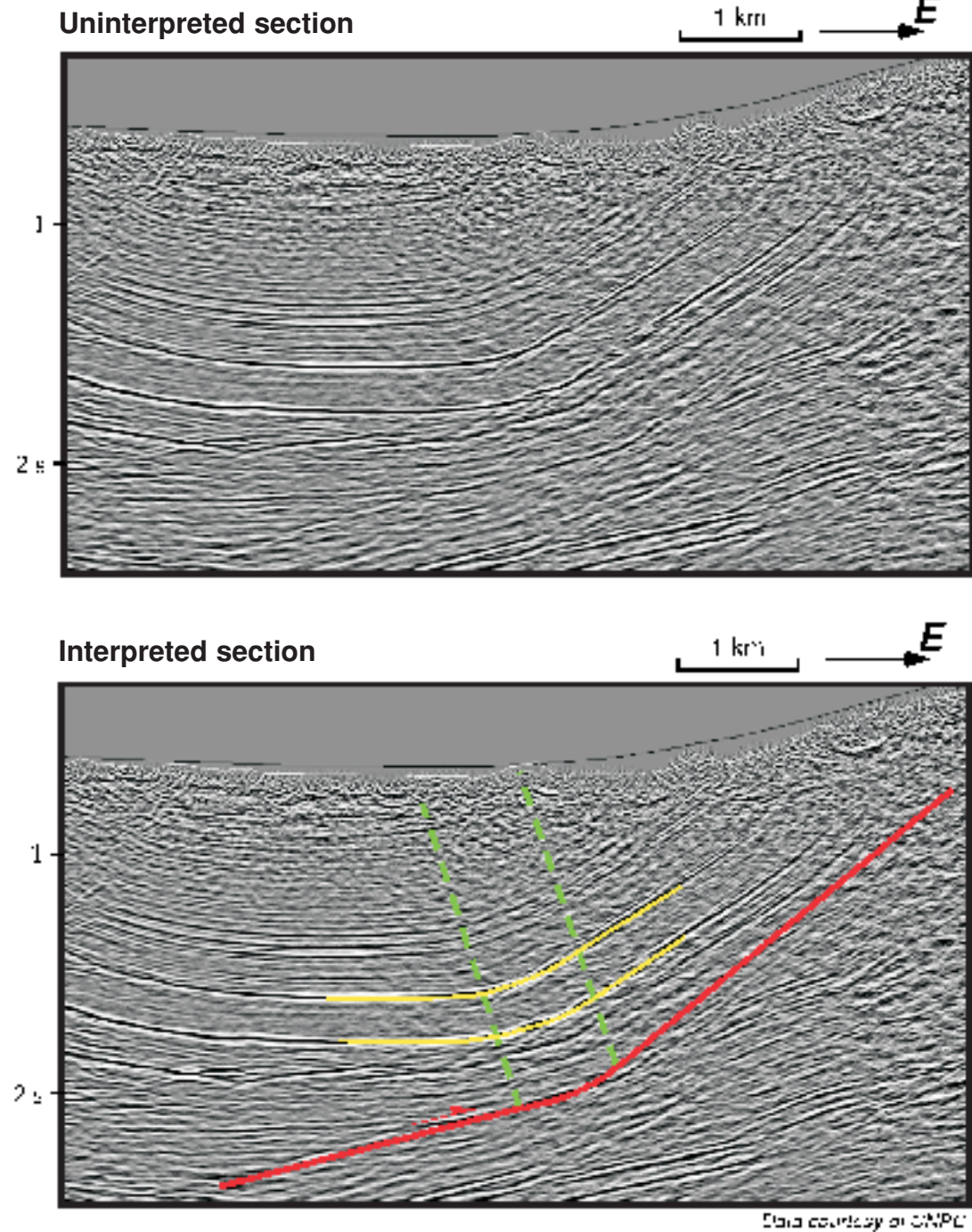
Growth fault-bend folds — high sedimentation rates

Fault-bend folds develop by kink-band migration, where fold limbs maintain a constant dip but generally widen as fault slip increases. When sedimentation rate exceeds uplift rate, folds that develop by kink-band migration have syntectonic (growth) strata that form narrowing upward dip domains, or growth triangles, above fold limbs (see section 1A-3). Below, we use kinematic models to describe how these growth structures develop in a composite fault-bend fold, and show examples of growth structures in seismic sections.

Fault-bend fold with growth strata
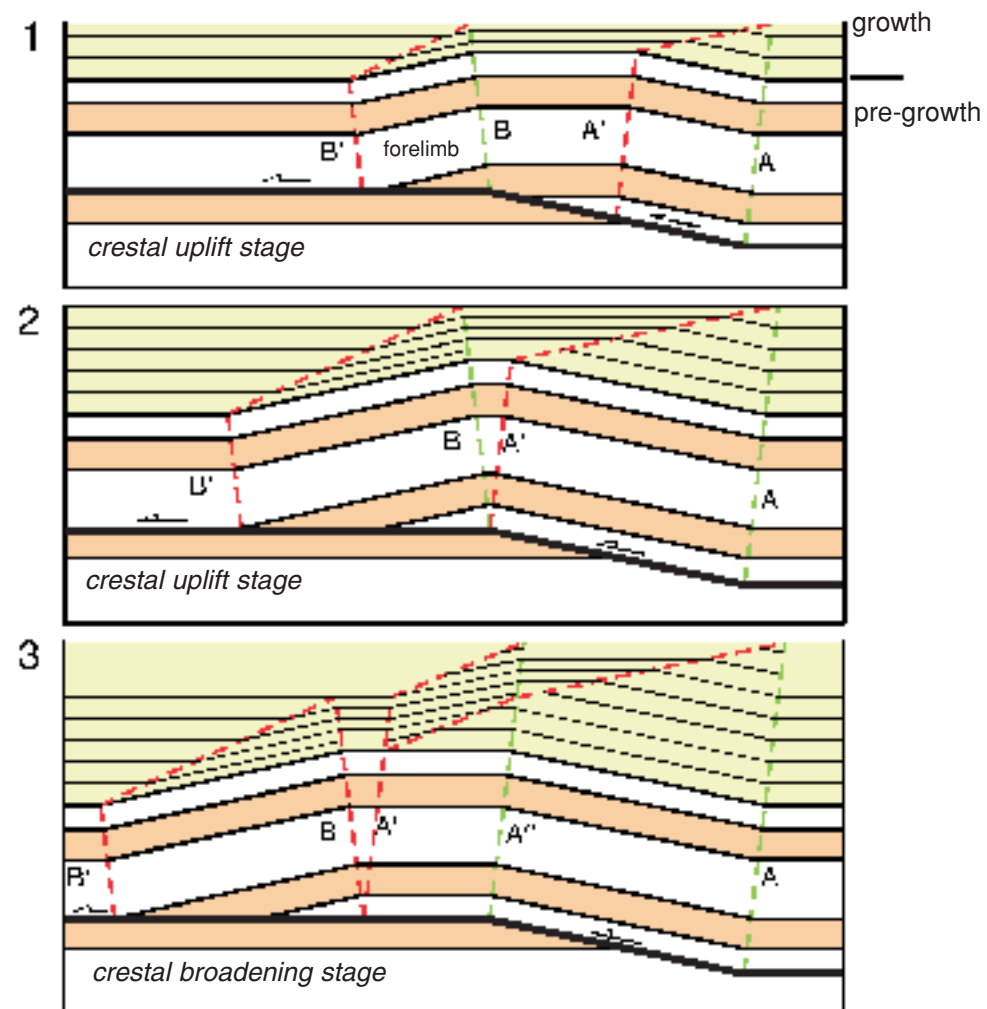
Sequential model of a growth fault-bend fold (Suppe et al., 1992; Shaw et al., 1996) with sedimentation rate > uplift rate. Model 1 consists of a composite fault-bend fold developed above a ramp between detachments. The fold is in the crestal uplift stage of growth (Shaw et al., 1994b), as fault slip is less than ramp width. In Model 2, additional slip widens the kink bands, which narrow upward in the growth section (see section 1A-4). In Model 3, fault slip is greater than ramp width. Thus, strata are refolded from the back limb (A-A″) onto the crest of the structure, which widens with fault slip (crestal broadening stage, Shaw et al., 1994b). Growth strata are also folded above the crest, as they pass through active axial surface A″. Forelimb axial surfaces (B-B′) are released from the fault bend and passively translated above the upper detachment, and thus do not deform young growth strata.

Seismic Example: Santa Barbara Channel, California, U.S.A.

Active synclinal axial surface — backlimb FBF
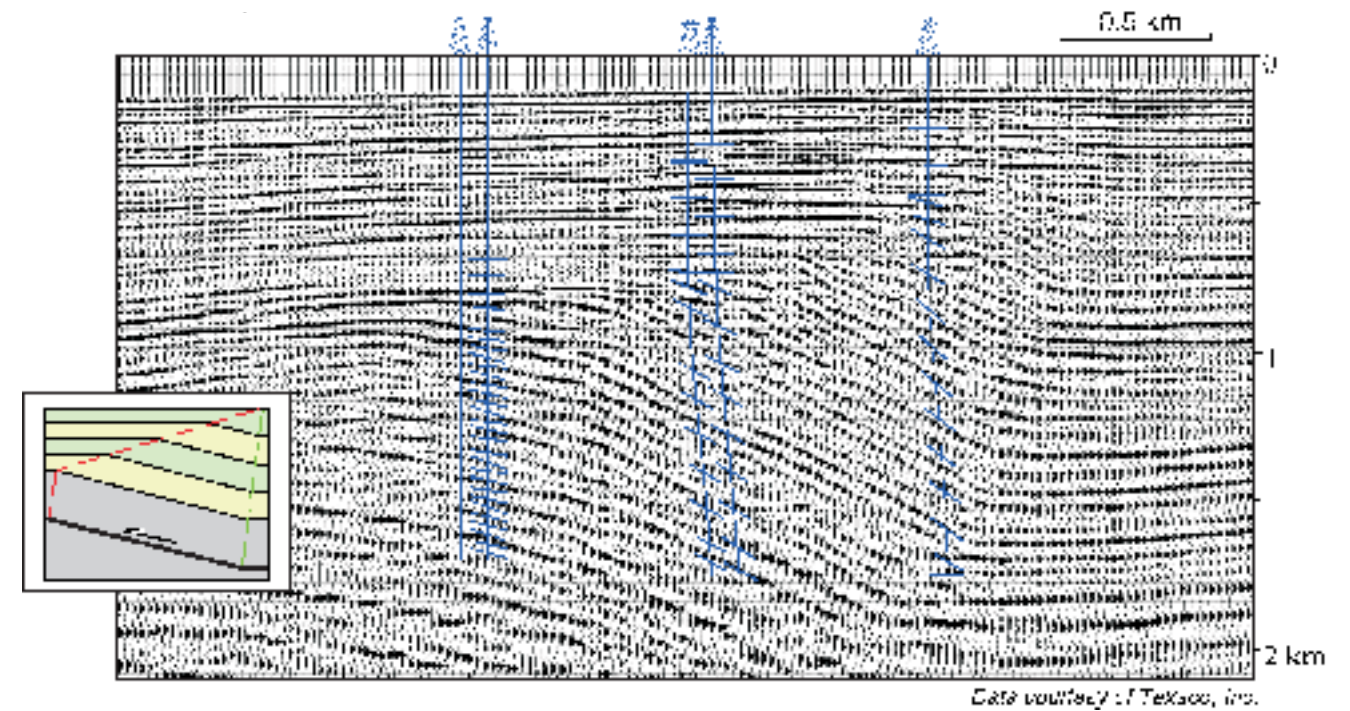
Seismic Example: Los Angeles basin, California, U.S.A.

Active anticlinal axial surface — forelimb FBF
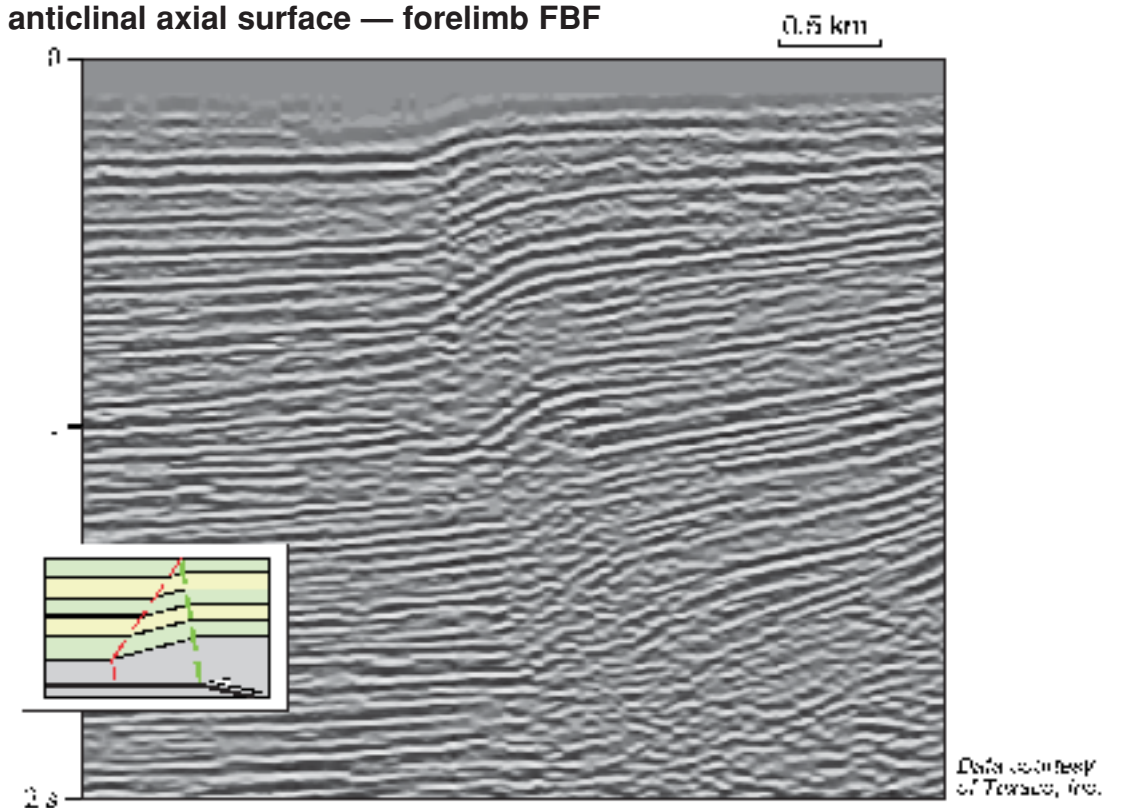
Growth Fault-Bend Folds — low sedimentation rates

In cases where sedimentation rate is less than or equal to the uplift rate, fault-bend folds develop patterns in growth strata that are distinct from growth triangles (see section 1A-3). In limbs with active synclinal axial surfaces, growth strata are folded concordantly with the underlying kink band; whereas, in limbs with inactive synclinal axial surfaces growth strata simply onlap kink bands. Below we describe how these growth patterns are expressed in a composite fault-bend fold after Medwedeff (1989) and Suppe et al. (1992).
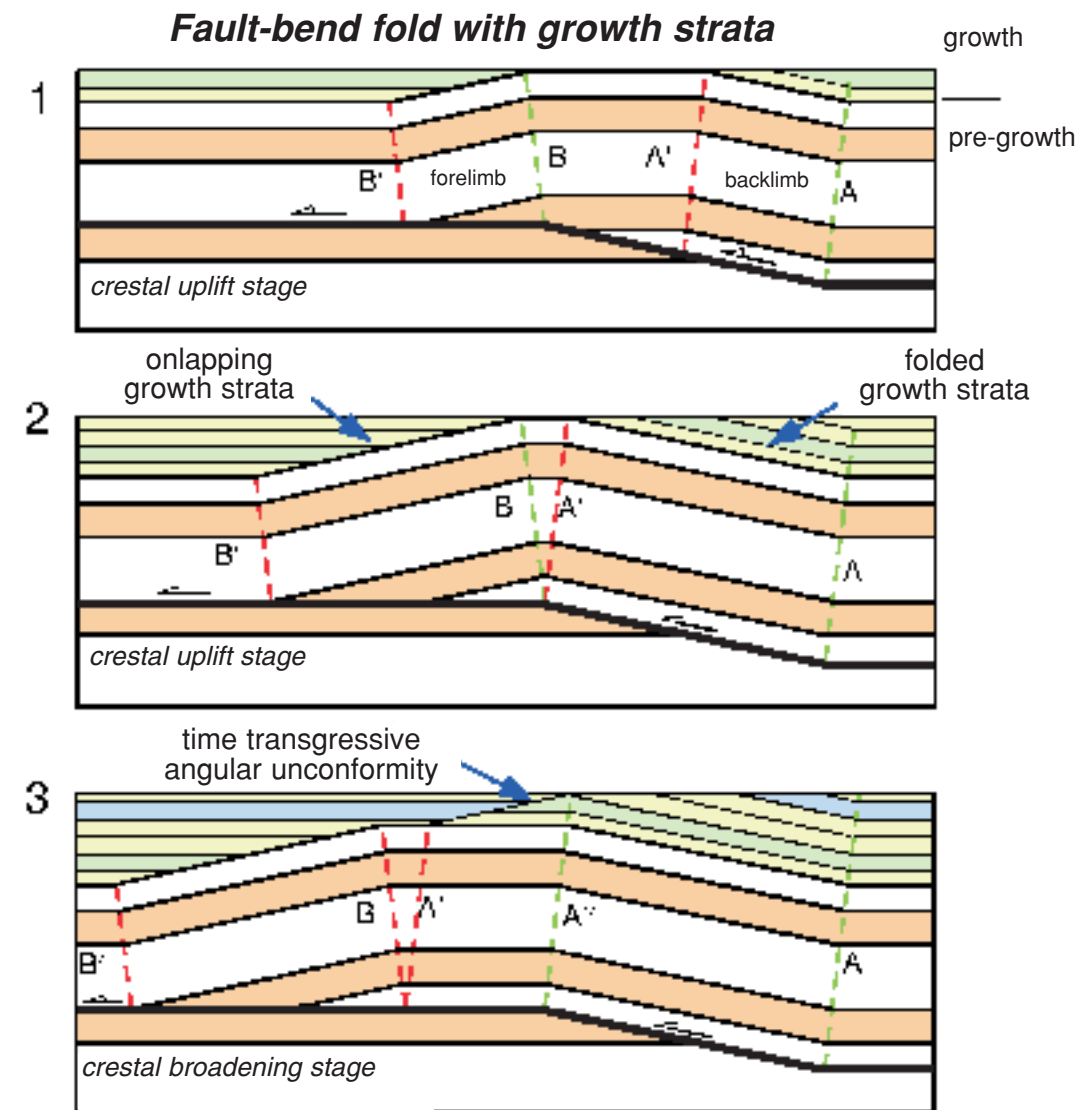
Sequential model of a growth fault-bend fold (Medwedeff, 1989; Suppe et al., 1992) with a sedimentation rate equal to the uplift rate. Model 1 consists of a composite fault-bend fold developed above a ramp between detachments. Growth strata in the backlimb are folded concordantly with the underlying kink band. In contrast, undeformed growth strata onlap the forelimb. In Model 2, additional slip widens kink bands and the growth pattern is maintained. In Model 3, fault slip is greater than ramp width. Thus, strata are refolded from the back limb (A-A″) onto the crest of the structure, which widens with fault slip. Growth strata are also re-folded above the crest, as they pass through active axial surface A″. Formerly inclined growth strata from the backlimb become horizontal. Coeval deposition above the fold crest forms a time trangressive angular unconformity. In Model 3, the sedimentation rate is held constant and equal to the uplift rate of particles within the back limb.
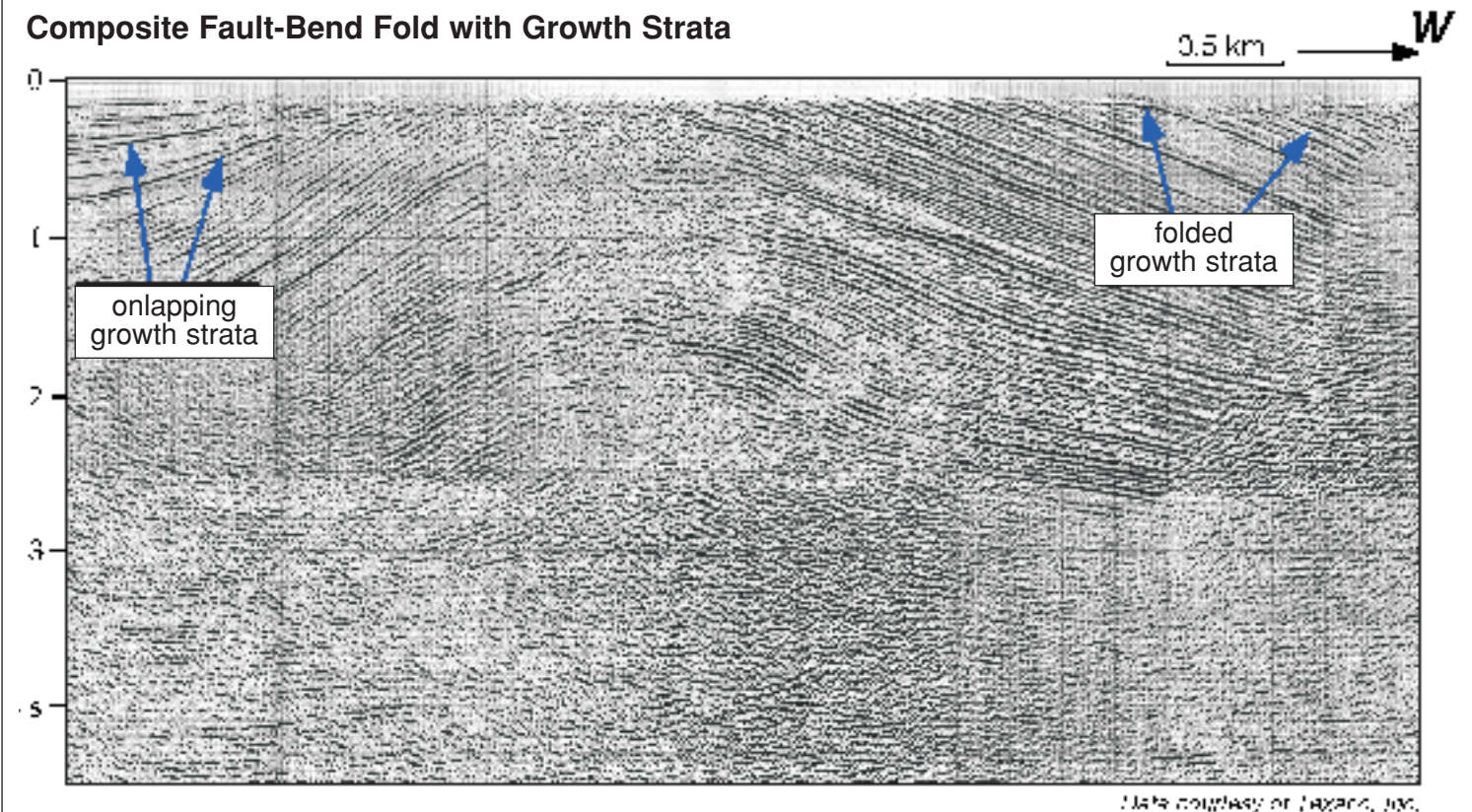
Seismic reflection profile across the Western San Joaquin basin (Lost Hills anticline) showing contrasting patterns of growth strata between backlimb (west) and forelimb (east) that are consistent with fault-bend folding where sedimentation rate is less than or equal to uplift rate (see model 2, left). The fanning of limb dips above the front limb may be due to sedimentary drape and compaction, or may reflect a component of limb rotation in fold growth (see section 1A-3).

1B-2: Fault-propagation folds

Basic concept

Fault-propagation folds form at the tips of faults and consume slip. These folds are generally asymmetric, with forelimbs that are much steeper and narrower than their corresponding backlimbs. Several modes of folding at fault tips have been described to explain these structures, including: constant thickness and fixed axis fault propagation folding (Suppe and Medwedeff, 1990); trishear folding (Erslev, 1991; Hardy and Ford, 1997; Allmendinger, 1998); and basement-involved (triple junction) folding (Narr and Suppe, 1994). In this section, we describe these kinematic theories, emphasizing their common characteristics, and introduce basic techniques for interpreting fault-propagation folds in seismic data.

To describe the basic concept of fault-propagation folding, we will consider the hypothetical case of a fault ramp in cross section that propagates upward from a detachment (note that fault-propagation folds may originate from faults with or without detachments). As the fault ramp propagates upward in sequential models 0 to 2, an asymmetric fold develops in the hanging wall with vergence in the transport direction. The fold consumes slip on the ramp, with slip being greatest at the ramp base and zero at the fault tip. As slip increases, the fault tip advances and the fold grows larger while maintaining the same basic geometry.
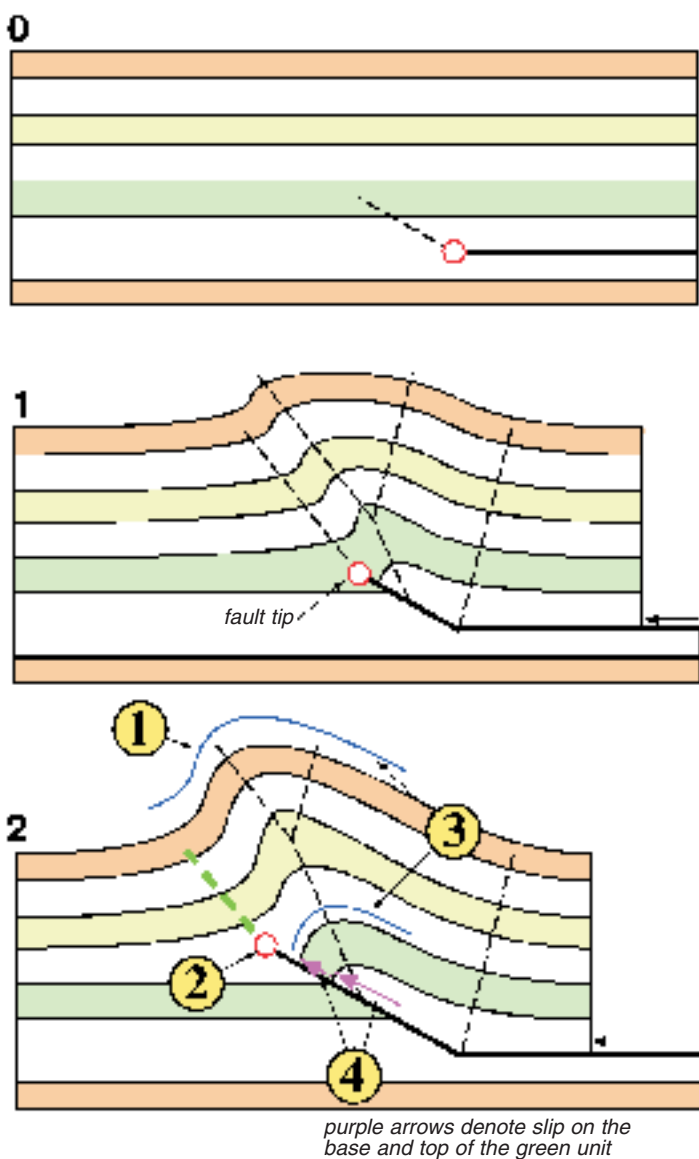
Common characteristics

Although fault-propagation folds exhibit a wide range of geometries, several characteristics are common to most structures, including:

1) folds are asymmetric, with forelimbs that are generally much steeper and more narrow than their corresponding backlimbs;

2) synclines are pinned to the fault tips;

3) folds tighten with depth; and

4) slip on the fault decreases upward, terminating within the fold.

Schematic fault-propagation fold model

purple arrows denote slip on the base and top of the green unit

Examples

Fault-propagation folds are common in outcrop and at scales typically imaged by seismic reflection data. This field example *(right)* has several characteristics of fault-propagation folds, including asymmetry, the presence of a narrow, steeply dipping forelimb, and the downward increasing tightness of the fold.

The seismic example is a fault-propagation fold at the southern margin of the Tanan Uplift in the southern Tarim basin. In this example, a thrust ramp delineated by fault-plane reflections terminates upward into the forelimb of an asymmetric fault-propagation fold.

Field Example

Professor Bill Brown highlighting a fault-propagation fold in Cambrian Fort Sills limestone, Arbuckle Mountains, OK, U.S.A. (S.C. Hook)

Seismic Example: Tarim basin, China
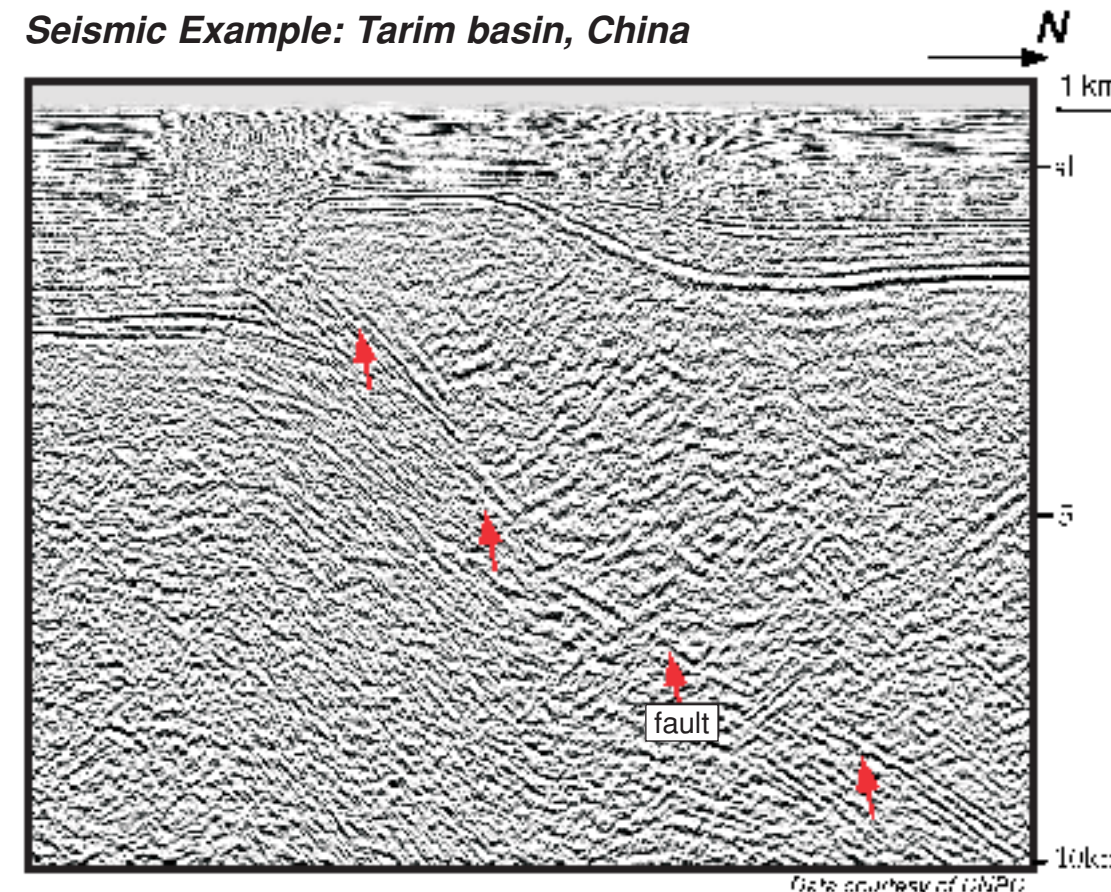
Constant thickness fault-propagation folds

Suppe and Medwedeff (1990) present a general relationship between fold shape and fault shape for parallel (constant thickness) fault propagation folds assuming angular fold hinges and conservation of bed length. This section describes the kinematic development of a constant-thickness fault-propagation fold, and the quantitative relations that can be used to model or interpret these structures.

Constant thickness fault-propagation folds develop as a fault propagates upward from a bend. An active, synclinal axial surface is pinned to the fault tip. As strata pass through this axial surface, they are folded into the forelimb. Depending on the fault geometry, strata may also pass through the anticlinal axial surface into the forelimb, or from the forelimb onto the fold crest. The backlimb develops much like a fault-bend fold, although the limb width is typically greater than fault slip.

Fault-propagation folds have several geometric relations that are useful in constructing models and interpreting structures, including:

1) The distance between the fault bend and the point where the anticlinal axial surface meets the fault equals the fault dip-slip at the bend.

2) The bifurcation point of the anticlinal axial surface occurs along the same bedding horizon as the fault tip.

Kinematic Model
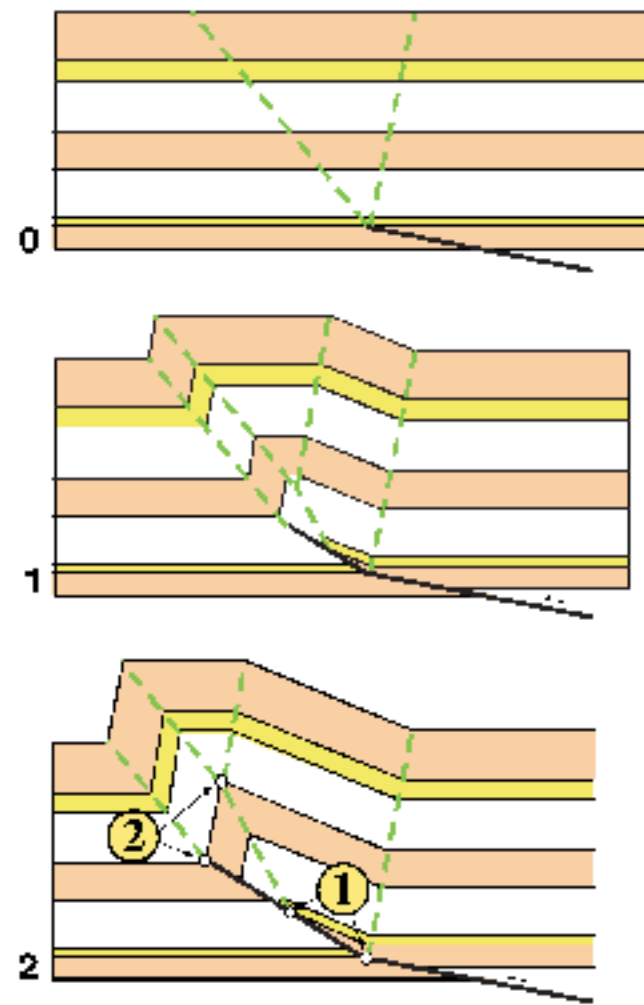
FPF terminology

The following terms are used in the derivation and graphs that describe fault-propagation folds.

θ_1 = hanging wall cut-off (lower fault segment)
θ_2 = footwall cut-off (upper fault segment)
ϕ = change in fault dip
γ = forelimb syncline interlimb angle
γ^* = anticlinal interlimb angle
δ_b = backlimb dip
δ_f = forelimb dip
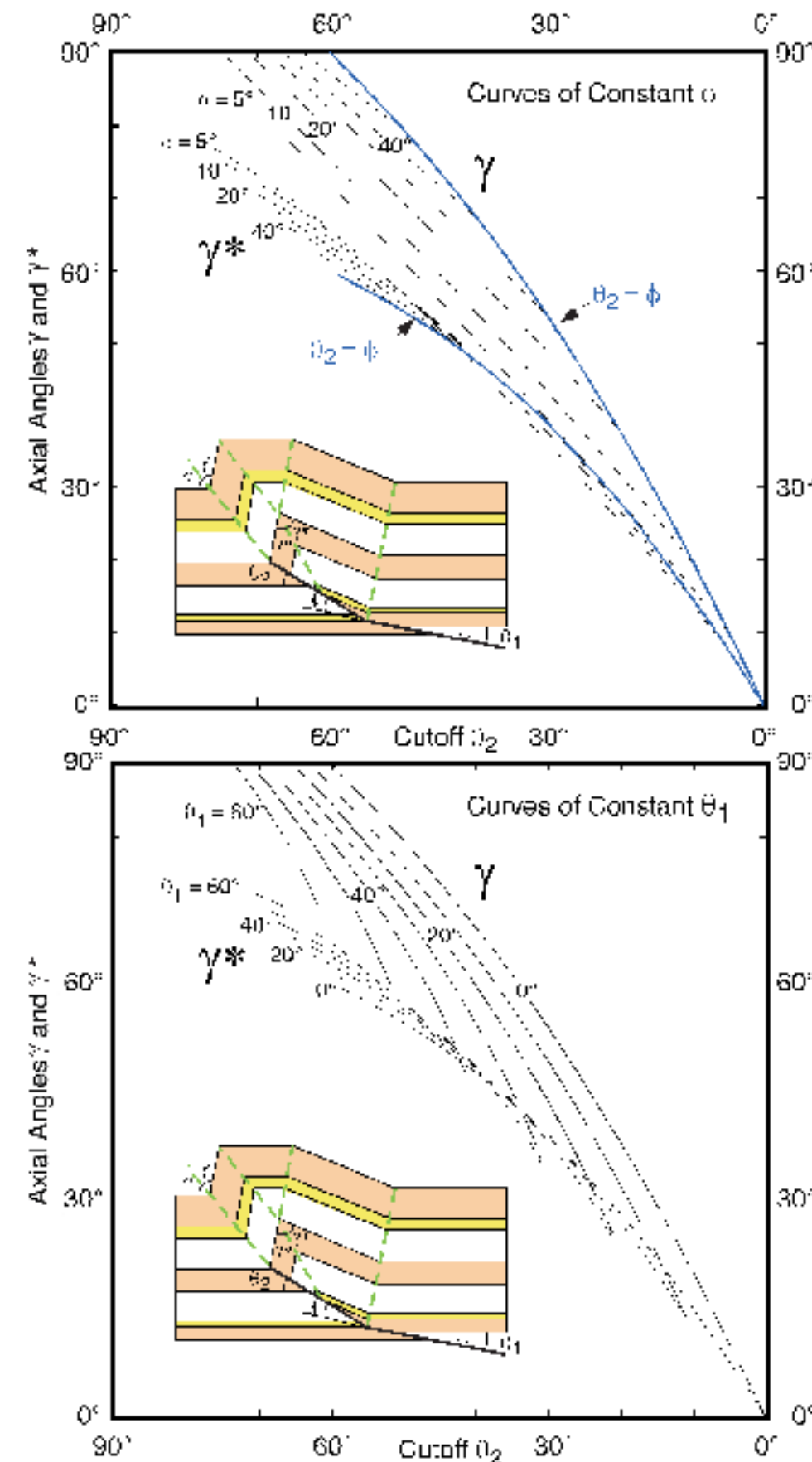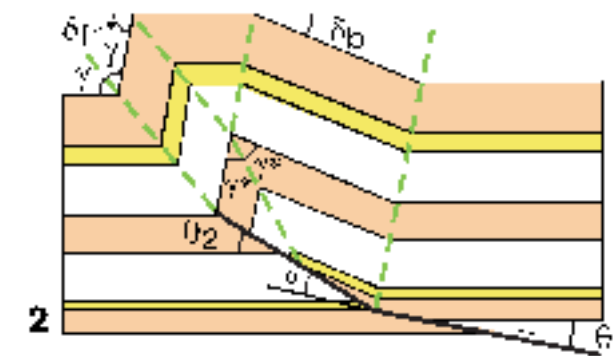
These graphs show the relationships between fault shape (θ_2) and fold shape (γ and γ^*) for constant thickness fault-propagations folds. The special case of ramping from a detachment is shown as the lines $\theta_2 = \phi$. These relations will be used to interpret a fault-propagation fold imaged in a seismic profile later in this section.

Fixed-axis fault-propagation folds

Suppe and Medwedeff (1990) present a second, general relationship between fold shape and fault shape called *fixed-axis fault-propagation fold theory*. This theory is similar to the constant thickness theory, except that it allows for bed thinning or thickening in the forelimb (see also Jamison, 1987). These thickness changes are induced because the forelimb anticlinal axial surface is fixed, meaning that material does not pass through it. The style and magnitude of bed thickness changes are dictated by the initial fault shape and cut-off angles. This section describes the kinematic development of a fixed-axis fault-propagation fold, and the quantitative relations that can be used to model and interpret these structures.

These sequential models (0–2) illustrate that fixed-axis fault propagation folds develop in a similar manner to constant-thickness fault-propagation folds. However, the anticlinal axial surfaces are fixed (inactive), causing forelimb thickening or thinning. Folds with low cut-off angles generally exhibit forelimb thickening, whereas, folds with high cutoff angles generally exhibit forelimb thinning.

Kinematic Models

with forelimb thickening

with forelimb thinning
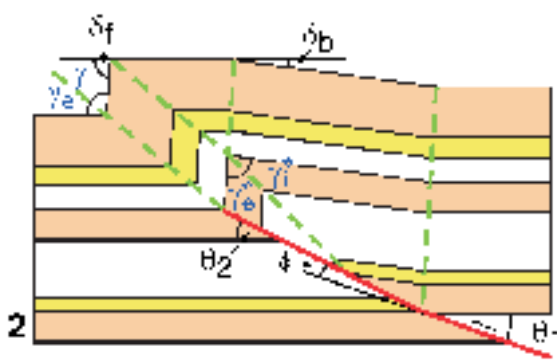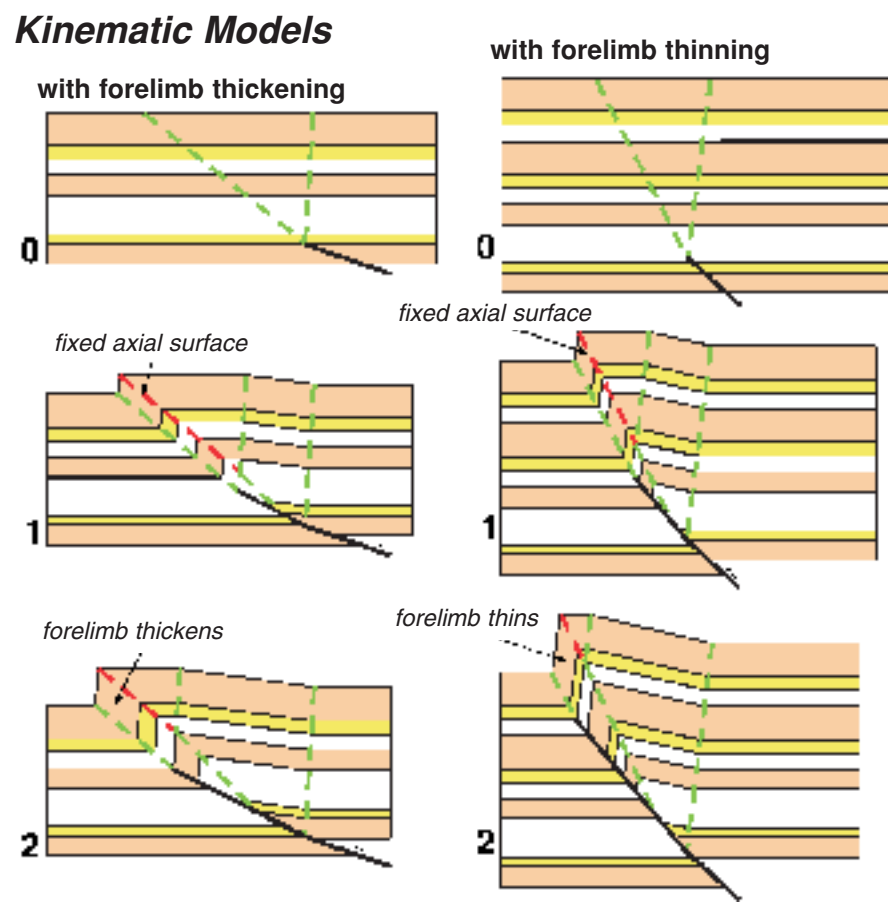
FPF terminology

Fixed-axis theory redefines the axial angles (γ values) associated with a fault-propagation fold. The remaining parameters (θ, ϕ, δ_b, and δ_f) are the same as in constant thickness fault-propagation folds.

γ_e = forelimb syncline exterior axial angle
γ_i = forelimb syncline interior axial angle
γ_e^* = anticlinal exterior axial angle
γ_i^* = anticlinal exterior axial angle

These graphs show the relationships between fault shape (θ_2) and fold shape (γ_e, γ_e^*, γ_i, and γ_i^*) for fixed-axis fault-propagations folds. The special case of ramping from a detachment is shown on the two graphs at left as the lines $\theta_2 = \phi$. Note that separate graphs must be used to define the interior (γ_i, and γ_i^*) and exterior (γ_e and γ_e^*) axial angles.

Seismic interpretation using fault-propagation fold theory

This section presents an interpretation of a structure imaged in seismic reflection data as a fault-propagation fold as described by Suppe and Medwedeff (1990). The seismic profile shows a highly asymmetric fold, with a poorly imaged forelimb, which are characteristics of many seismic images of fault-propagation folds.

The seismic section shown below is interpreted in five steps on this and the following page. To help distinguish between the two alternative theories, the graph below (from Suppe and Medwedeff, 1990) shows the relationship of forelimb to backlimb dips for both constant thickness and fixed axis fault propagation folds. Pairs of limb dips that plot along the "Fixed-Axis Theory" curve indicate that the structure may be interpreted using this theory. Limb dips that plot along, or to the left of, the $\phi = \theta_2$ curve may be interpreted using constant-thickness theory. The two theories are coincident along the portion of the "Fixed-Axis Theory" curve that lies on, or to the left of, the $\phi = \theta_2$ curve.

Limb dips estimated from seismic profile

Step 1: Limb dips are estimated in the seismic profile by interpretation of the reflector dips on the backlimb, and by correlation of horizons 1 and 2 across the poorly imaged forelimb.

Limb dips in fault-propagation folds

Step 2: Based on the forelimb (δ_f = 58°) and backlimb (δ_b = 11°) dips estimated on the seismic profile, the fold is inconsistent with fixed-axis theory. However, the structure may be interpreted as a constant thickness fault-propagation fold with a change in fault dip (ϕ) of 7° and an initial cutoff angle (θ_1) of 42°. On the following page, these values are used to predict the fold shape (γ and γ^*) and cutoff (θ_2) angles, and to generate an interpretation of the structure.

Seismic Interpretation of Contractional Fault-Related Folds

Step 3: To interpret the structure using constant-thickness fault propagation fold theory, the upper portion of the fold is interpreted using the kink method, where axial surfaces bisect the interlimb angles (see section 1A-1). This interpretation yields a forelimb interlimb angle (γ) of 61°.

The tip of the fault is located by projecting the axial surfaces that bound the fold crest to their point of intersection. From this intersection point, follow bedding along the forelimb (as defined by δ_f) until it intersects the forelimb synclinal axial surface. This intersection defines the tip of the fault.

Initial Interpretation

Step 4: The remaining fault-propagation fold parameters (θ_2 and γ^*) are then determined from one of the two constant thickness fault-propagation fold graphs. Given a γ value of 61° and a change in fault dip (ϕ) of 7° (from preceding page), the theory predicts an interlimb angle (γ^*) of 55.5° and a cut-off angle (θ_2) of 49°. These values are used to complete the interpretation.

Complete Interpretation
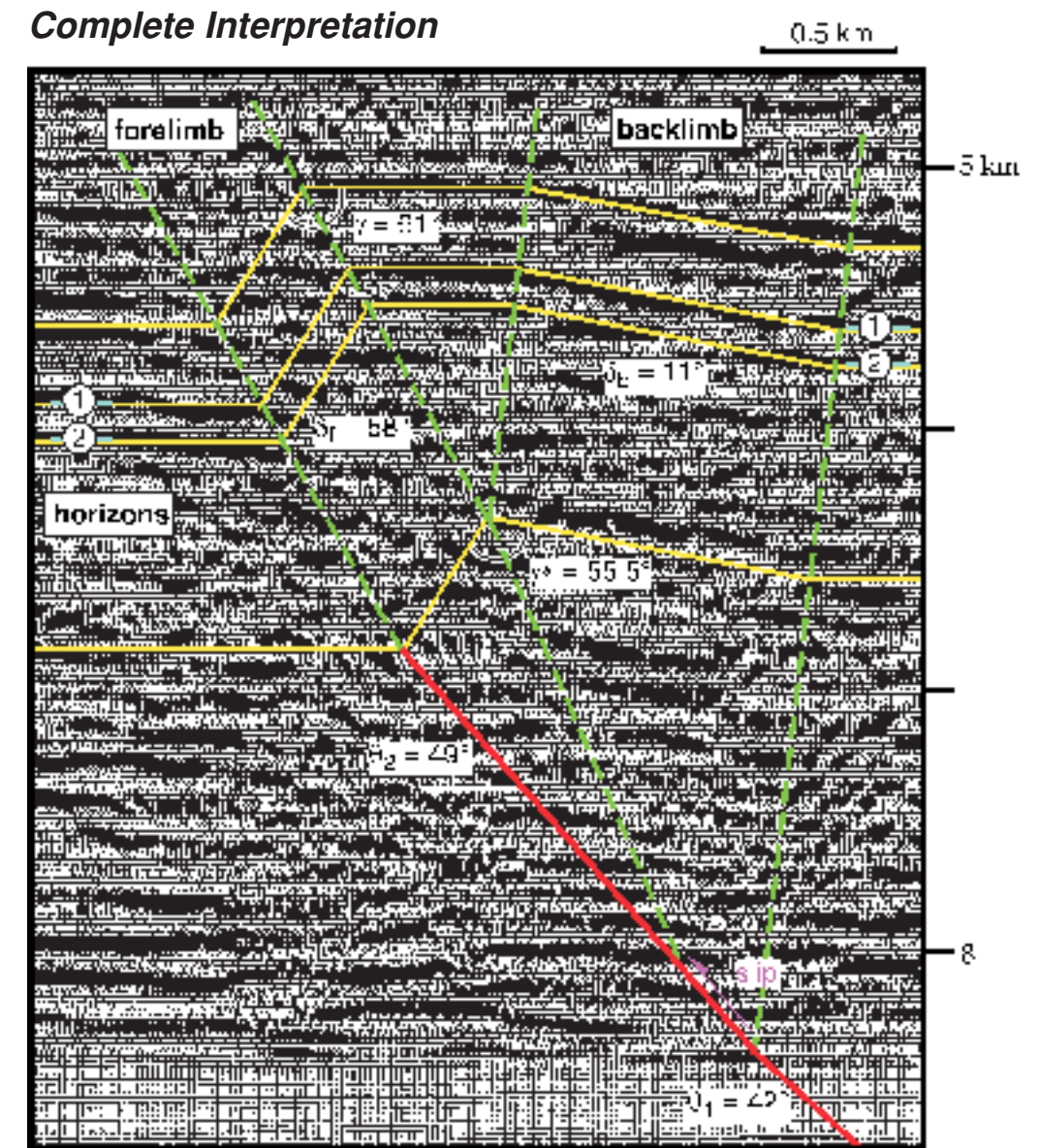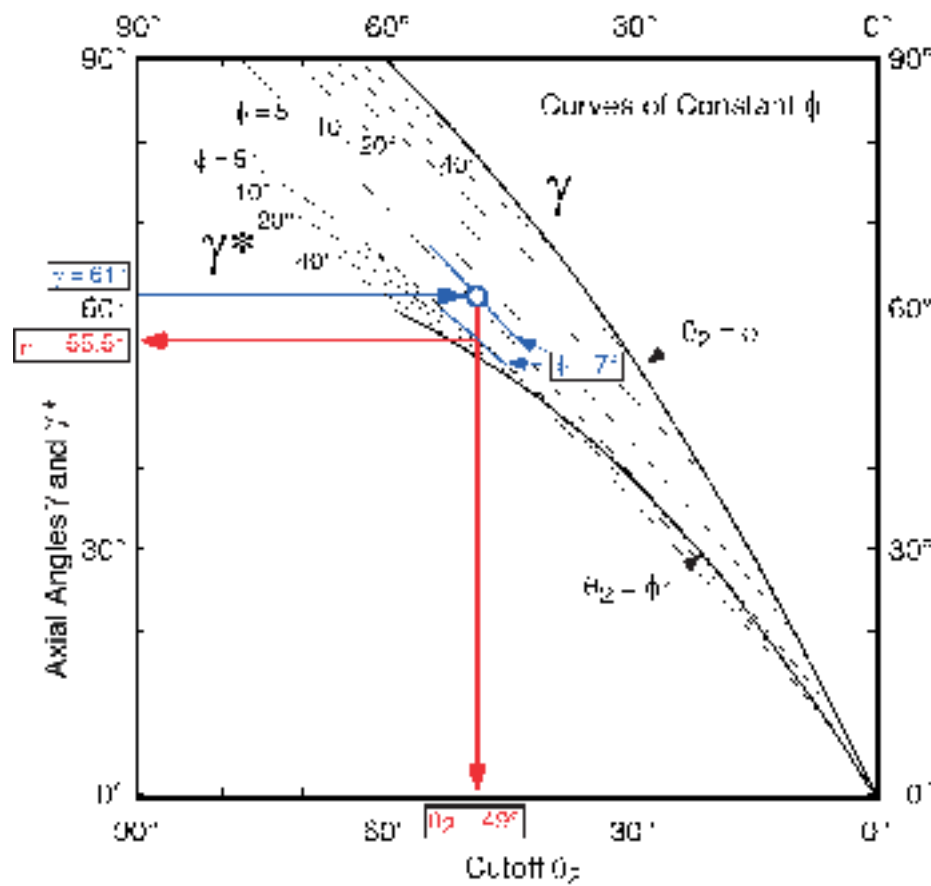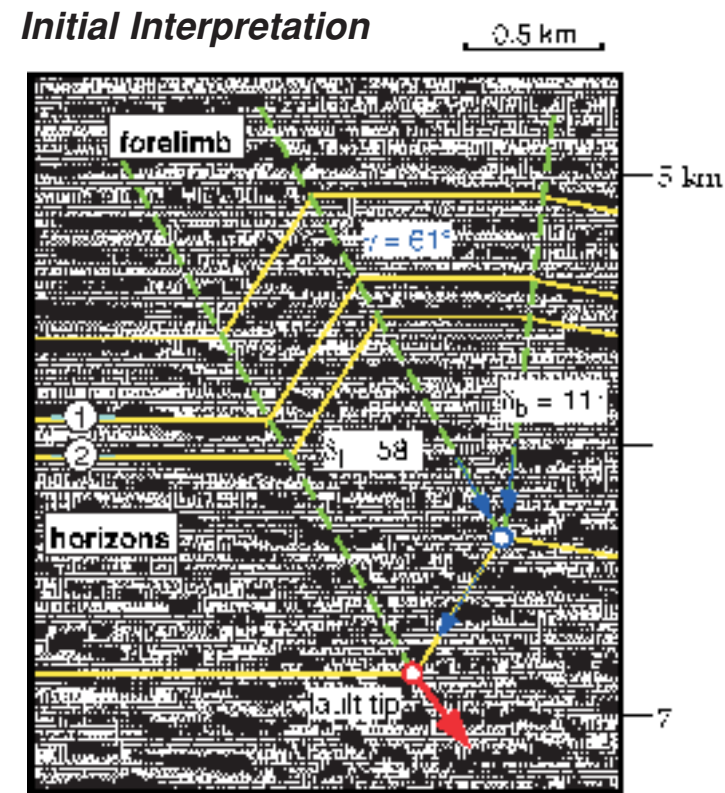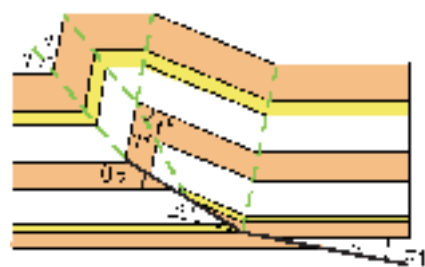
**Step 5:** The interpretation is completed by extending the fault down from its tip at an angle of 49° (based on θ_2) to the point where it intersects the backlimb synclinal axial surface. At this point, the fault shallows by 7° (based on ϕ) to a dip of 42°. The interior anticlinal axial surface bisects the interlimb angle between the forelimb and backlimb, and extends down to the fault. The distance between the point where this axial surface intersects the fault and the fault bend equals the fault slip at the bend.

In summary, this model-based interpretation provides an internally consistent, area balanced description of the structure that honors the seismic data. In general, constant-thickness and fixed-axis fault-propagation fold theories are most applicable to structures with pairs of discrete, parallel axial surfaces bounding fold limbs with roughly constant bed dips. Bed thickness changes in the forelimb, relative to other parts of the structure, are best explained with fixed-axis theory. Comparisons of the forelimb and backlimb dips can also be used to distinguish between these two alternative theories. On the following pages, we describe other modes of folding that may better describe structures with broadly curved fold hinges, variable forelimb dips, non-parallel axial surfaces, and/or substantial footwall deformation.
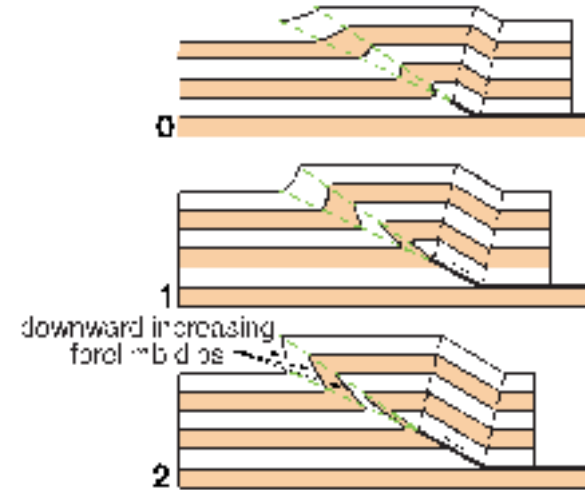
Trishear fault-propagation folds

Erslev (1991) proposed an another mode of fault-propagation folding, known as *trishear*. Trishear folds form by distributed shear within a triangular (trishear) zone that expands outward from a fault tip. Folds develop in the trishear zone and cross sectional area, but not bed thickness or length, and are preserved through deformation. The displacement field, and thus fold shape, is straightforward to calculate. However, it must be done iteratively. Hence, the method cannot be applied graphically or analytically (Allmendinger, 1998). Here, we describe some of the basic characteristics of trishear folds, and use the theory as implemented by Hardy and Ford (1997) and Allmendinger (1998) to model and interpret these structures.

Theory
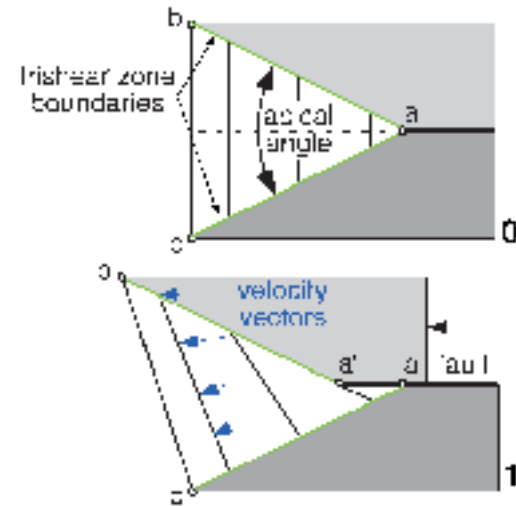
The trishear zone (a-b-c) is bound by two surfaces that define an intervening apical angle. The surfaces may or may not be symmetric with respect to the fault (Zehnder and Allmendinger, 2000). To preserve cross sectional area (a-b-c = a-a'-b-c) during deformation, there must be a component of displacement toward the footwall, as reflected by the velocity vectors. To model a trishear fold, the apical angle, the fault dip, and the propagation to slip ratio (P/S) of the fault are specified. (after Erslev, 1991; and Allmendinger, 1998).

Kinematic model

This sequential model (0 - 2) shows the development of a trishear fault-propagation fold at the tip of a thrust ramp that steps upward from a detachment. The backlimb of the structure is a simple fault-bend fold. The geometry of the forelimb is a function of the apical angle, the fault dip, and the P/S ratio. Small apical angles generally yield tight, highly strained forelimbs, whereas large apical angles generally yield broad, gently strained forelimbs. At a given apical angle, the steepness of the forelimb increases with progressive slip. The steepness of the forelimb also increases downward. This pattern is characteristic of trishear folds, and contrasts with the constant forelimb dips exhibited by constant-thickness and fixed-axis fault-propagation folds.

Propagation to slip ratio
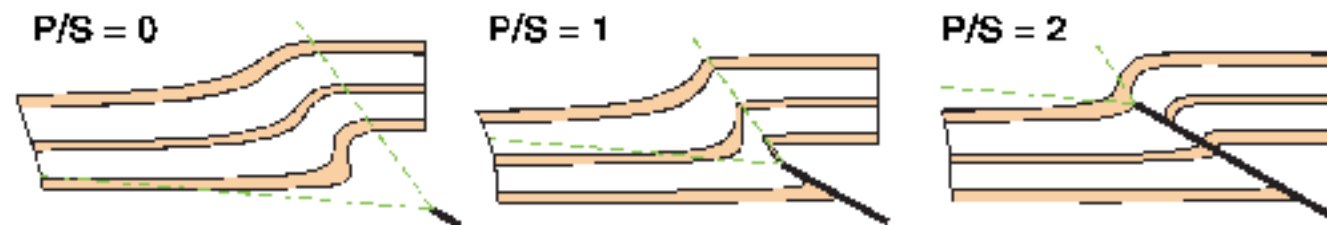
Fault propagation to slip ratio (P/S) has an important influence on fold shape. Low P/S ratios generally yield steep, tightly folded forelimbs with pronounced bed thickening. High P/S ratios generally yield shallow, gently folded forelimbs with less bed thickening (from Allmendinger, 1998).

Seismic section
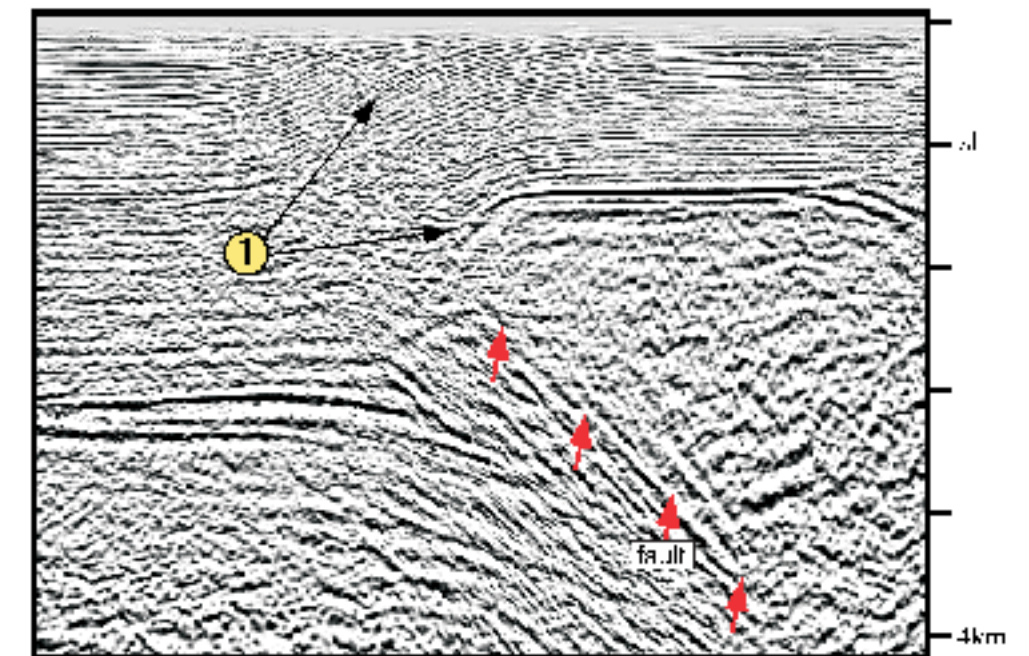
Trishear interpretation
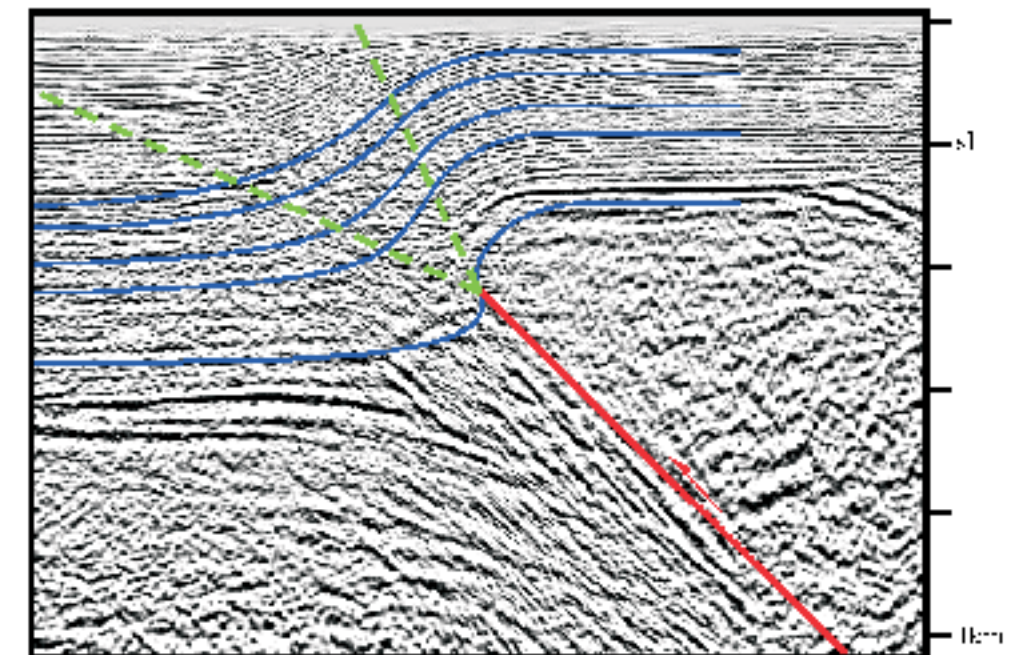
The fault-propagation fold in this seismic section has a broadening upward zone of folding and a fanning of forelimb dips (1). These patterns are forward modeled using trishear, based on parameters derived through an inversion method (Allmendinger, 1998). The best fitting model is displayed on the seismic section in the lower panel.

In summary, trishear folds are easily distinguished from constant-thickness and fixed-axis fault-propagation folds, in that they display an upward-widening, curved fold limb ahead of the fault tip, which leads to an upward decrease in limb dip.

Basement-involved (drape) folding with migrating triple junctions

Fault-propagation folds that involve basement (crystalline) rock are commonplace, and tend to have shapes that differ from those described by constant-thickness and fixed axis fault-propagation fold models (Suppe and Medwedeff, 1990). Several geometric and kinematic theories have been developed to explain these structures, including models with forelimb shear distributed in triangular zones, such as the trishear model described in the preceding section (Erslev, 1991; Mitra and Mount, 1998). This section describes another kinematic theory proposed by Narr and Suppe (1994), in which fold growth is governed by the migration of a fault-fault-fold triple junction. The theory is then applied to interpret a fault-propagation fold in seismic data.

Kinematic model
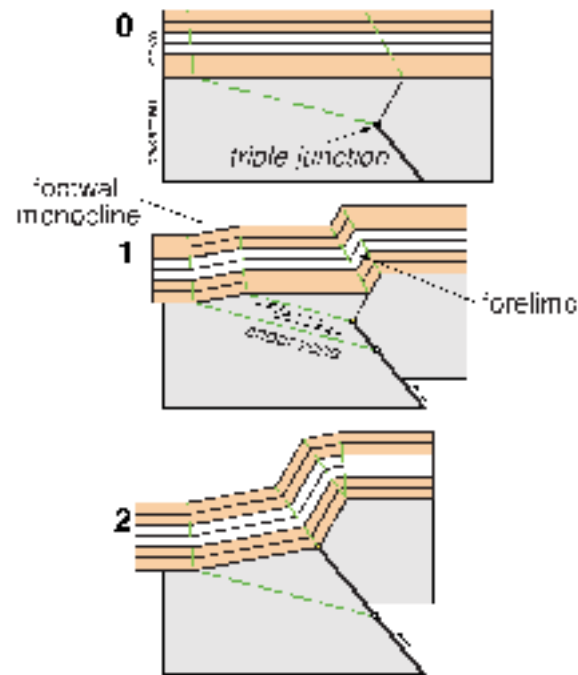
In the Narr and Suppe (1994) basement-involved model, folding is driven by the migration of a fault-fault-fold (axial surface) *triple junction*. The triple junction moves upward with progressive fault slip, causing shear of the footwall that forms a monocline. Uplift of the hanging wall also induces folding of the sedimentary cover, producing a forelimb with bed dips that are parallel to the dip of the upper fault segment. Stages 0–2 show progress development of a migrating triple junction fold model.
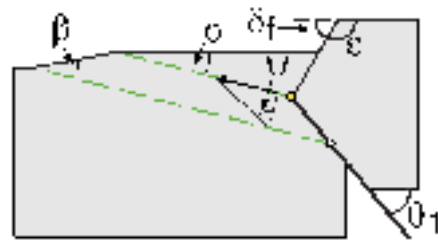

Fold and fault shape
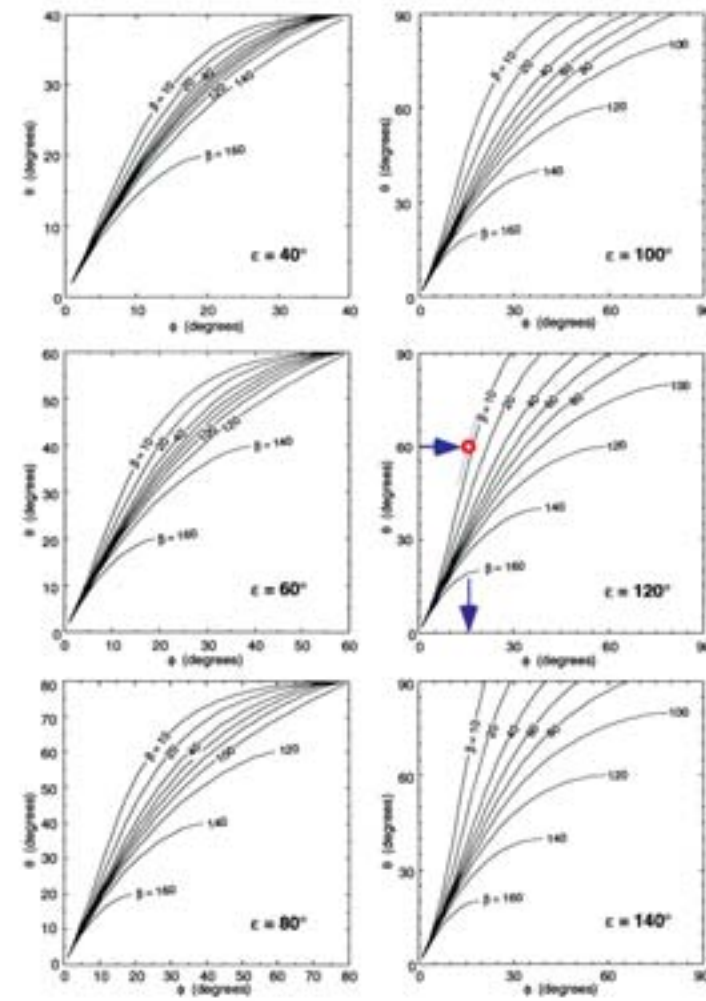
These graphs describe relations among the five parameters that describe triple-junction folds. Each graph is for a specific ε value. When modeling structures imaged in seismic sections, ε is generally selected by interpreting the forelimb dip value (δ_f). The dip of the footwall monocline is also commonly resolved on seismic sections, leaving one additional parameter to be determined (ϕ or θ) before a unique solution can be obtained. From Narr and Suppe (1994).

Triple junction fold terminology

Five parameters describe basement-involved triple junction folds, three of which must be specified to derive the remaining two values:

- θ_1 = hanging wall cutoff of lower fault segment
- ε = dip of upper fault segment (generally = $180° - \delta_f$)
- β = dip of footwall monocline
- ϕ = dip of footwall shear orientation
- ψ = footwall angular shear

Seismic Example: Orito Field, Putamayo basin, Colombia
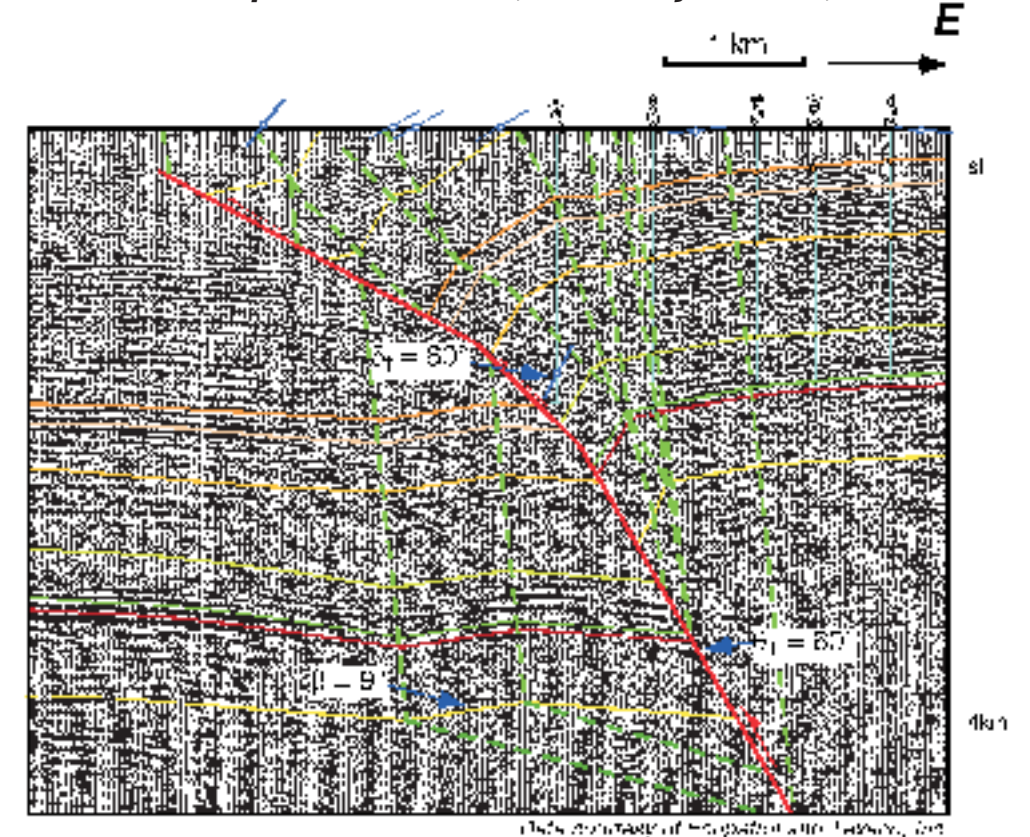
Seismic profile of a basement-involved fault propagation. The footwall monocline and steep (poorly imaged) forelimb are characteristic of triple junction fault-propagation fold models. In the interpretation, the shear orientation (ϕ) and angle (ψ) were estimated from the graph at left using: 1) the maximum forelimb dip value (δ_f), estimated from oriented well core and surface dips, to define ε (120°); 2) the reflection truncations to estimate the fault dip (θ = 60°), and; 3) the dip of the footwall monocline (β = 9°). The interpreted section involves additional deformation induced by a breakthrough of the main fault, a process which is described later in this section, but nevertheless the structure maintains the basic geometry described by the migrating triple junction theory of Narr and Suppe (1994).

Growth fault-propagation folding

Syntectonic (growth) strata are folded in distinctive patterns above fault-propagation folds. Forelimb growth structures, in particular, vary among the different fault-propagation fold models and thus can be diagnostic of the folding mechanism. In this section, we contrast growth patterns developed above fault propagation folds as described by Suppe and Medwedeff (1990) and trishear folds (Erslev, 1993), using kinematic models and examples imaged in seismic sections.
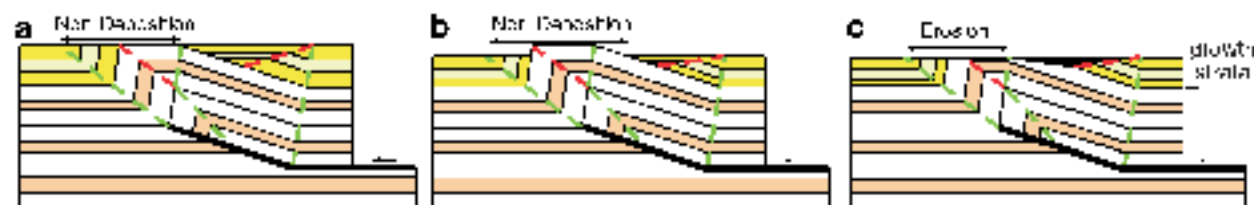
Growth fault-propagation fold

Growth trishear fold
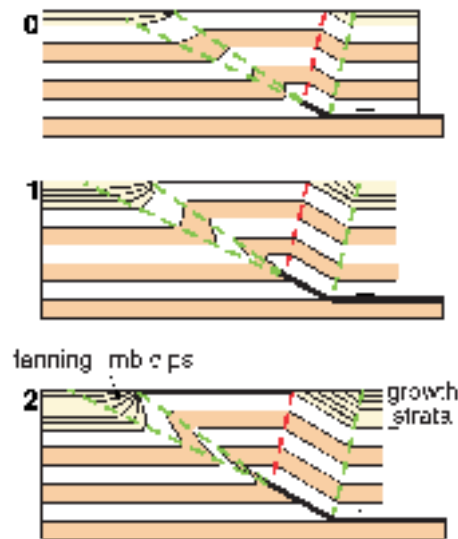

Kinematic models
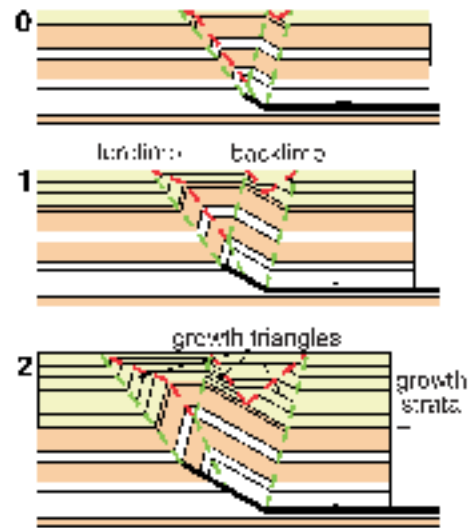
Fault-propagation folds of Suppe and Medwedeff, (1990) grow by kink-band migration, with two active axial surfaces bounding the backlimb, and one or two active axial surfaces bounding the forelimb. Syntectonic strata above the fold limbs form growth triangles. When sedimentation rate exceeds uplift rate, as in this model, two growth triangles develop on the backlimb. Fixed-axis fault-propagation folds have a single forelimb growth triangle, whereas, constant thickness fault-propagation folds may have one or two forelimb growth triangles depending on the fault geometry. This sequential model (0–2), with a 29° fault ramp and a decollement, is a case where both constant-thickness and fixed axis theory converge to yield the same geometry.

Trishear folds (Erslev, 1993) generally develop by a combination of kink-band migration and limb rotation mechanisms, and these fold kinematics are reflected in growth strata. Progressive forelimb rotation during the formation of trishear folds generally yields an upward shallowing of bed dips in growth strata. This fanning of limb dips in trishear growth folds contrasts markedly with the growth triangles predicted by the constant-thickness and fixed axis theories. This sequential model (0–2) (after Hardy and Ford, 1997) has a sedimentation rate that slightly exceeds the uplift rate. The backlimb of this model forms by fault-bend folding, yielding a single backlimb growth triangle.
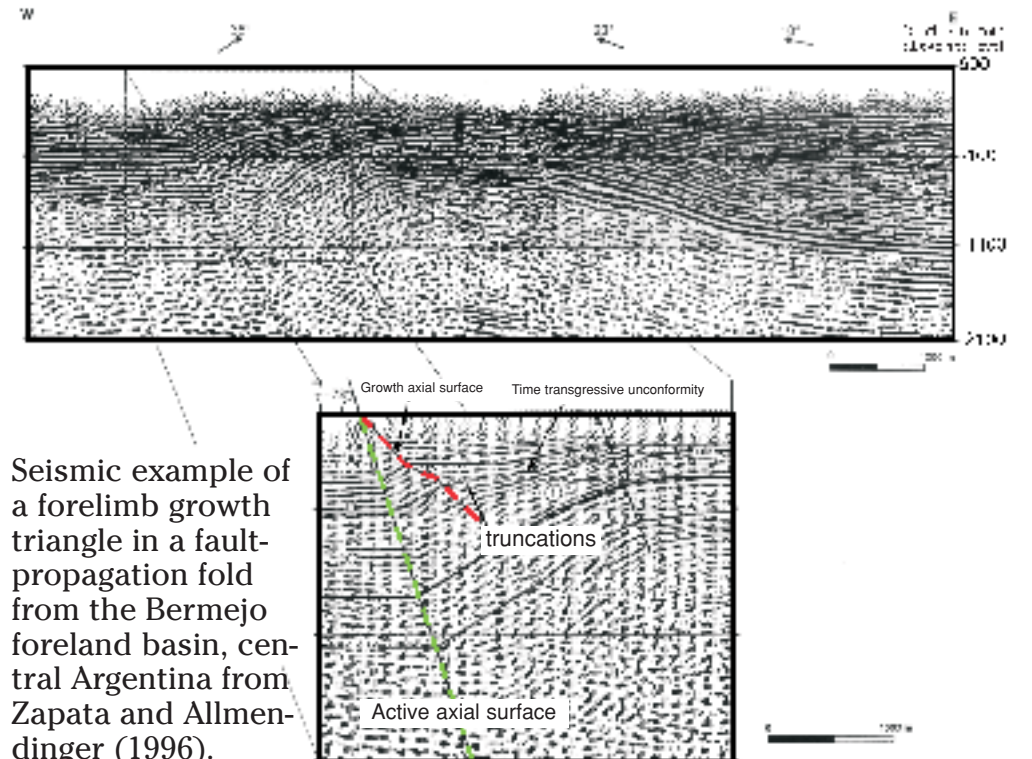
Effects of low sedimentation rates

Sedimentation rate relative to uplift rate can have a pronounced impact on resultant growth geometries. These three examples (a-c) show the effects of local non-deposition and erosion on growth structures in fault-propagation folds (after Suppe et al., 1992).

Seismic Example: Bermejo anticline, Argentina

Seismic example of a forelimb growth triangle in a fault-propagation fold from the Bermejo foreland basin, central Argentina from Zapata and Allmendinger (1996). Reproduced courtesy of the American Geophysical Union.

Seismic Example: Tarim basin, China
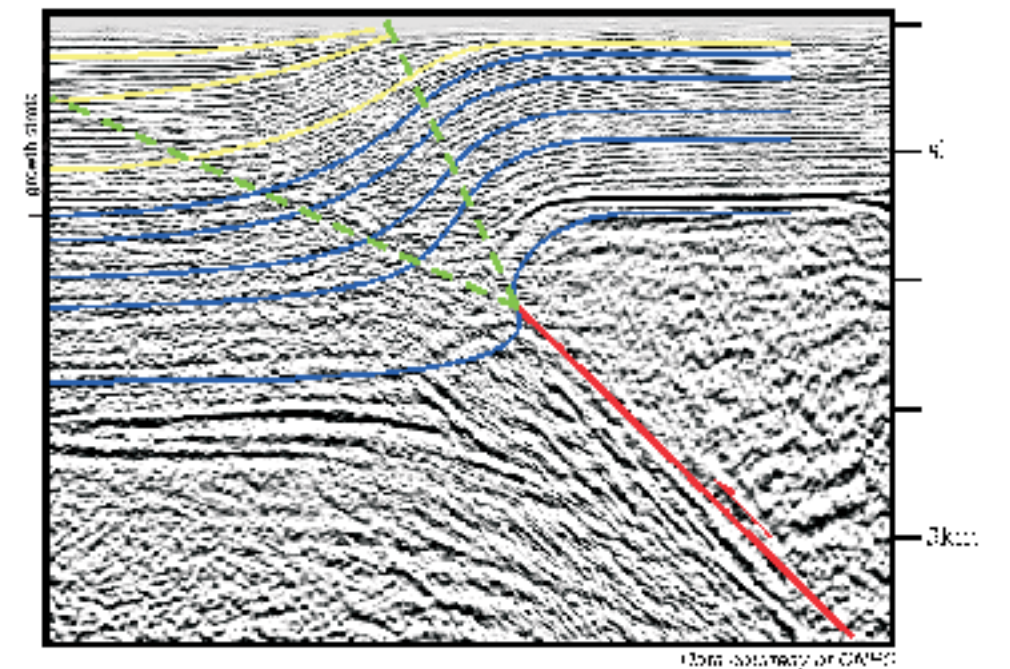
Seismic example of fanning forelimb dips in growth strata from the Tanan Uplift, Tarim basin, China. Section is overlain by a modeled trishear fold, described in the *trishear folding section*, that includes modeled growth horizons (yellow).

Breakthrough fault-propagation folds

At any stage of fold growth, faults may cut through fault-propagation folds, altering the geometries of these structures. The shapes of these "breakthrough" structures are influenced by the path of the fault, which often breaks through the forelimb or shallows to an upper detachment, as well as the folding mechanism. In cases where the slip on the breakthrough fault is substantial and/or structures are deeply eroded, only remnants of the original fault-propagation fold geometries may remain. In this section, we use several kinematic models to describe styles of breakthrough fault propagation folding, and show an example of this type of structure in a seismic section.

Forelimb breakthrough

Kinematic models
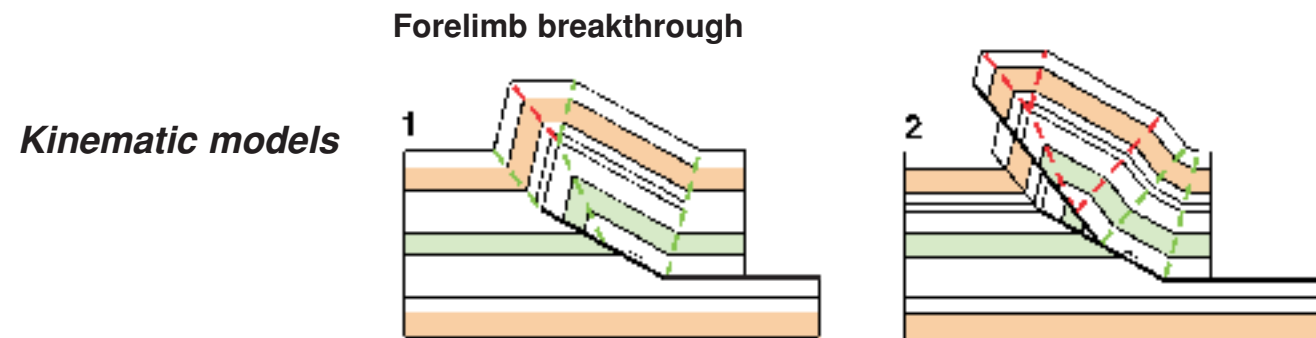
This sequential model (1–2) shows a constant-thickness fault propagation fold (1) where the fault breaks through the middle of the forelimb (2). The fault modifies the original fold geometry by offsetting the hanging wall portion of the forelimb, and producing an additional kink band within the backlimb that develops by fault-bend folding.

Breakthrough styles
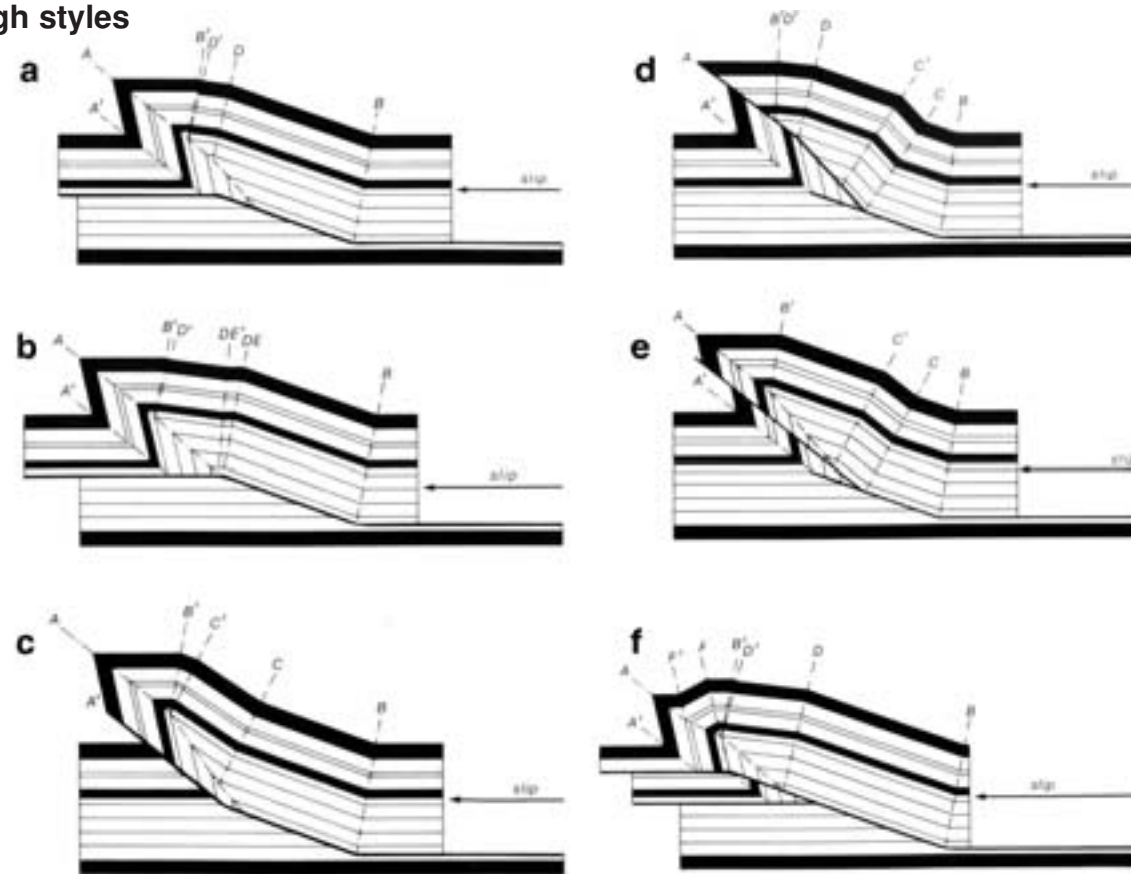
Models showing possible types of breakthrough structures after Suppe and Medwedeff (1990). a and b) decollement breakthroughs; c) synclinal breakthrough; d) anticlinal breakthrough; e) high-angle (forelimb) breakthrough; and f) low-angle breakthrough.

Trishear fold breakthrough   **Triple junction fold breakthrough**
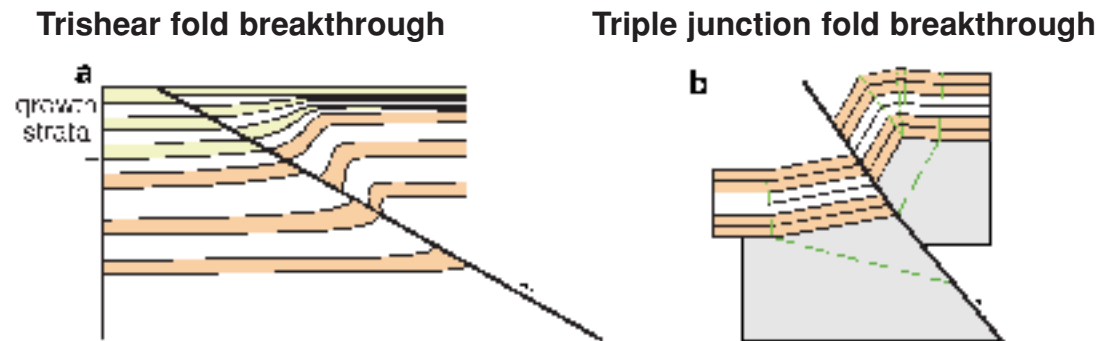
Faults in trishear and triple-junction fault-propagation folds may also breakthrough at any stage of fold growth. These models are examples of synclinal fault breakthroughs in: a) trishear fold after Allmendinger (1998); and b) a triple junction model after Narr and Suppe (1994). The geometries of breakthrough structures in all classes of fault-propagation folds vary substantially based on the fault path and, if the fault is non-planar, on folding kinematics after breakthrough.

Seismic Example: Argentina
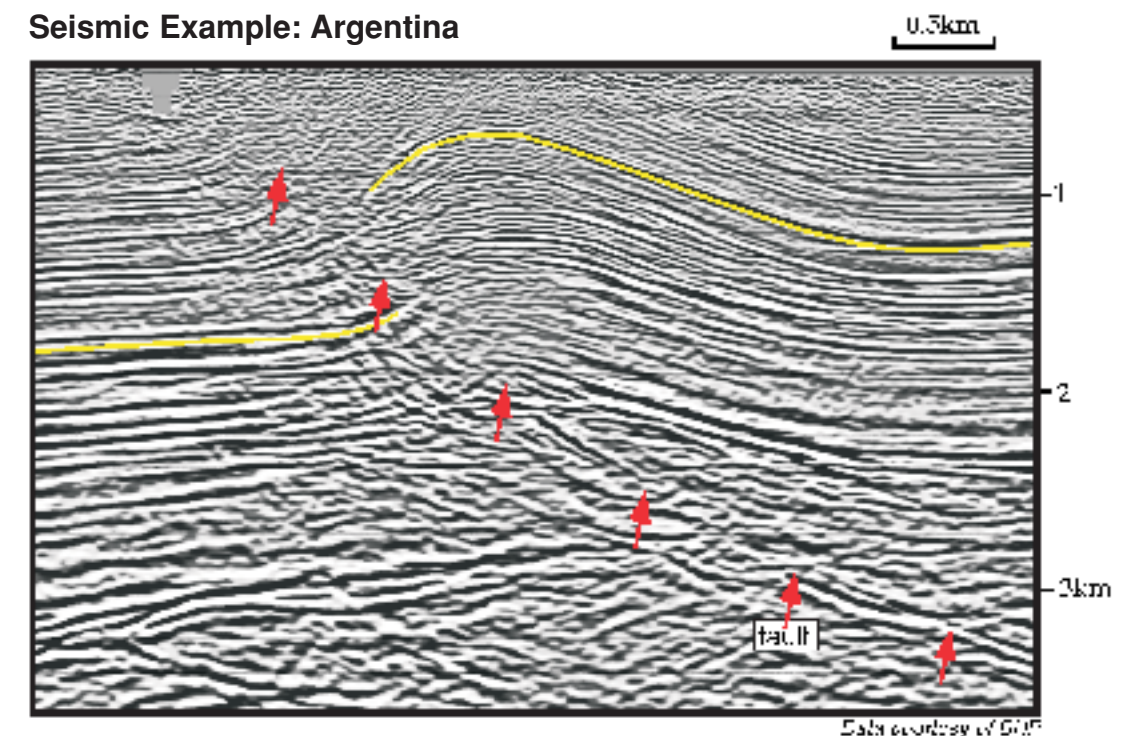
This seismic section illustrates a common forelimb breakthrough pattern. Although the forelimb is poorly imaged, reflection truncations and the hanging wall and footwall positions of the correlated horizon suggest that the fault extends through the structure. Nevertheless, the basic geometry of the fold is consistent with a fault-propagation folding mechanism, implying that this is a breakthrough structure.

1B-3: Detachment folds

Basic Concept

Detachment folds form as displacement along a bedding-parallel fault is transferred into folding of the hanging wall layers. Although detachment folds may share some geometric similarities with fault-bend and fault-propagation folds, they differ from these structures because they are not directly related to thrust ramps but rather to distributed deformation above detachments. In this section, we describe basic aspects of the geometry and kinematics of detachment folds. These insights are used to guide the interpretation detachment folds in seismic images.

Styles of Detachment Folds

Detachment folds form at a variety of scales, as isolated structures or in long fold trains, and many names are used to describe them. The term detachment fold is commonly applied to symmetric or asymmetric folds that develop above a relatively thick ductile unit and basal detachment. If folds are symmetric, have steep limbs, and develop above a relatively thin ductile unit, they are often called pop-up or lift-off folds (Mitra and Namson, 1989; Mount, 1990). Lift-off folds develop by isoclinal folding of the detachment in the core of the anticline, and when they have flat crests they are referred to as box folds.

Kinematic models of detachment folds
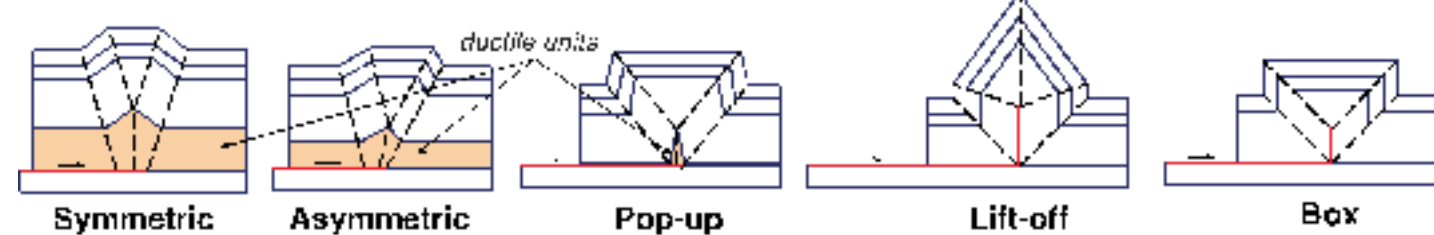
Common characteristics

Detachment folds generally share the following characteristics:
1) An incompetent, ductile basal unit thickened in core of fold, with no visible thrust ramp.

2) A detachment that defines the downward termination of the fold.

3) Competent pregrowth units that, if present, generally maintain layer thickness.

4) Growth units, if present, that thin onto the fold crest and exhibit a fanning of limb dips.
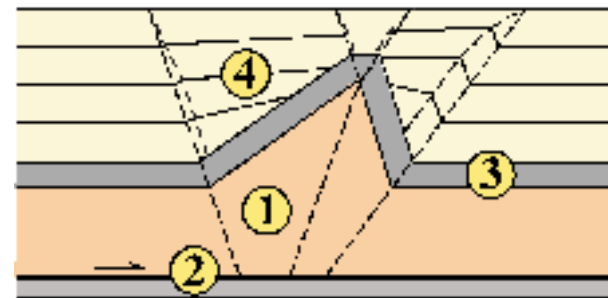
Examples

Detachment folds are common in outcrop and at scales typically imaged by seismic reflection data. They have been documented in the foreland of fold and thrust belts such as the Jura, Appalachian Plateau (Wiltschko and Chapple, 1977), and Tian Shan (Ferrari et al., section 2-14, this volume). Detachment folds are also common in passive margin fold belts, such as the Mississippi Fan (Rowan, 1997) and Perdido Fold Belts (Carmilo et al., section 2-24, this volume) in the Gulf of Mexico, and in the Campos Basin, Brazil, (Demercian et al., 1993), and the Niger Delta (Bilotti et al., section 2-12, this volume).

Field Example: Canadian Rockies
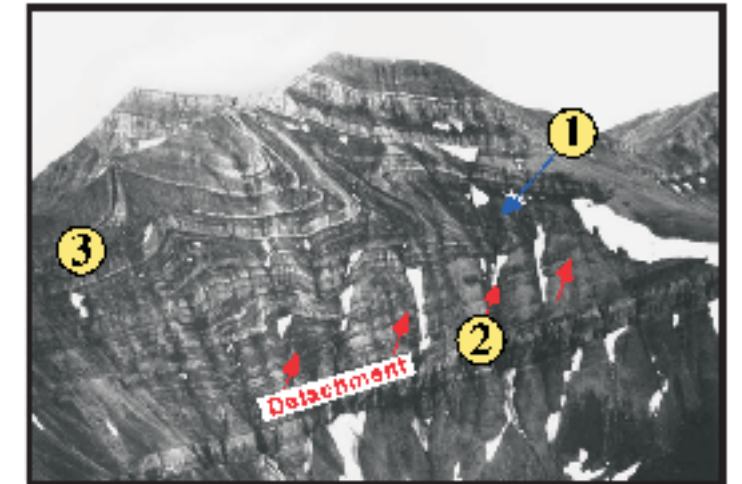
The field and seismic examples shown here have many of the common characteristics of detachment folds described at lower left.

modified from Fiebel and McClay (1990)

Seismic Example: Gulf of Mexico

modified from Rowan (1997)

Geometry and kinematics of detachment folds

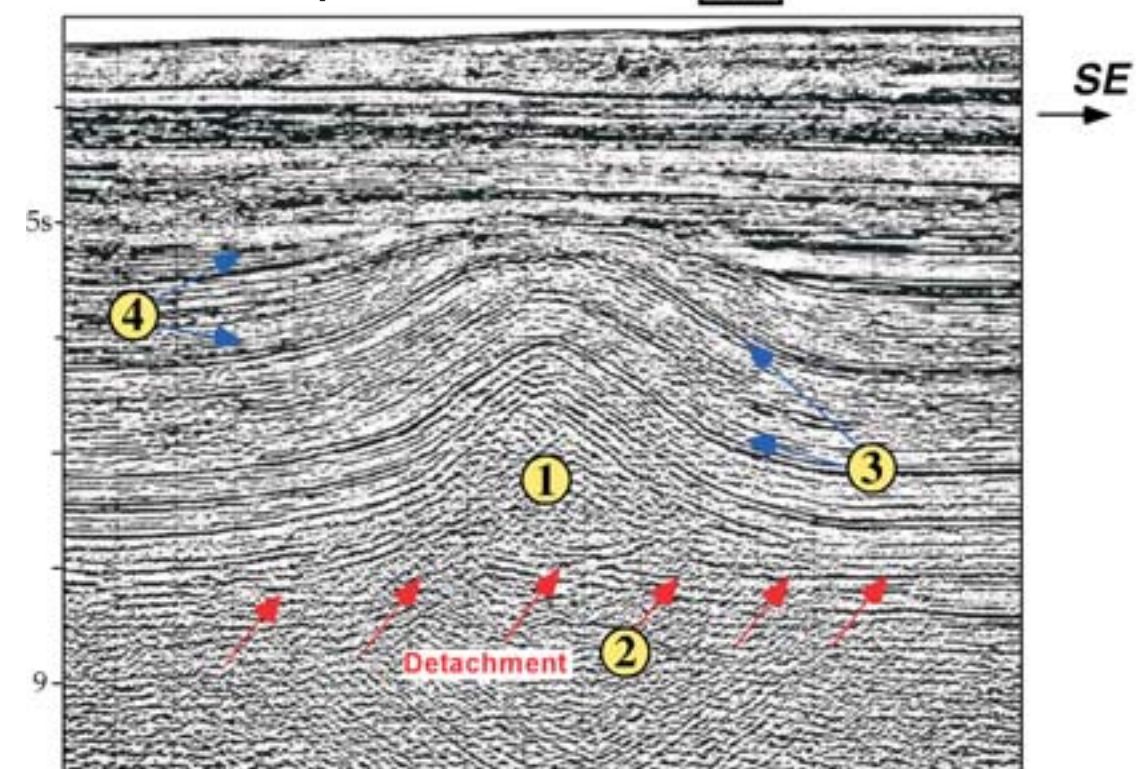There is no unique, quantitative relationship between fold shape and underlying fault shape for detachment folds, due in part to the ductile thicknening occurring in the fold core that generally does not preserve bed length or thickness. Thus, it is often difficult to uniquely constrain the geometry of these structures unless they are completely imaged. Nevertheless, several geometric and kinematic models have been developed (Dahlstrom, 1990; Ephard and Groshong, 1995; Homza and Wallace, 1995; Poblet and McClay, 1996) that can serve as guides for interpreting detachment folds in seismic images.

In this section, we present a geometric and kinematic model of detachment folding developed by Poblet and McClay (1996) that is particularly useful when analyzing growth strata associated with detachment folding that involves a competent unit. These authors propose three distinct mechanisms by which a fold can develop above a propagating detachment. In each of the models, it is the geometry and kinematics of folding in the competent layer (in particular, limb lengths and limb dips) that controls the folding. The incompetent, or ductile layer, is able to flow into, or out of, the fold core as deformation progresses. Layer thickness, line length, and area are conserved in the competent layers. If the detachment level is allowed to change, or if differential shortening occurs in the incompetent unit, then area is conserved in the ductile layer as well.

Poblet and McClay (1996) present three modes of detachment fold growth that are illustrated in the figure to the upper right (models 1–3), and differentiated based on their folding mechanisms as follows:

1) **Primarily Limb Rotation.** In this model, the limb lengths remain constant but the limbs rotate to accommodate shortening. A small amount of material must move through the axial surfaces, inducing a minor component of kink-band migration, as folding progresses. The incompetent unit is area balanced only if the detachment level varies or differential shortening occurs in the incompetent unit.

2) **Kink-band Migration.** In this model, limb dips remain constant, but their lengths increase to accommodate shortening. Material moves through the synclinal axial surfaces as folding progresses. The incompetent unit is area balanced only if the detachment level varies or differential shortening occurs in the incompetent unit.

3) **Limb Rotation and Kink-band Migration.** In this model, limb dips vary, as do limb lengths, but the ratio of the limb lengths remains the same. Strata moves through axial surfaces (primarily the synclinal surfaces), and rotate to accommodate shortening. The incompetent unit area is balanced.
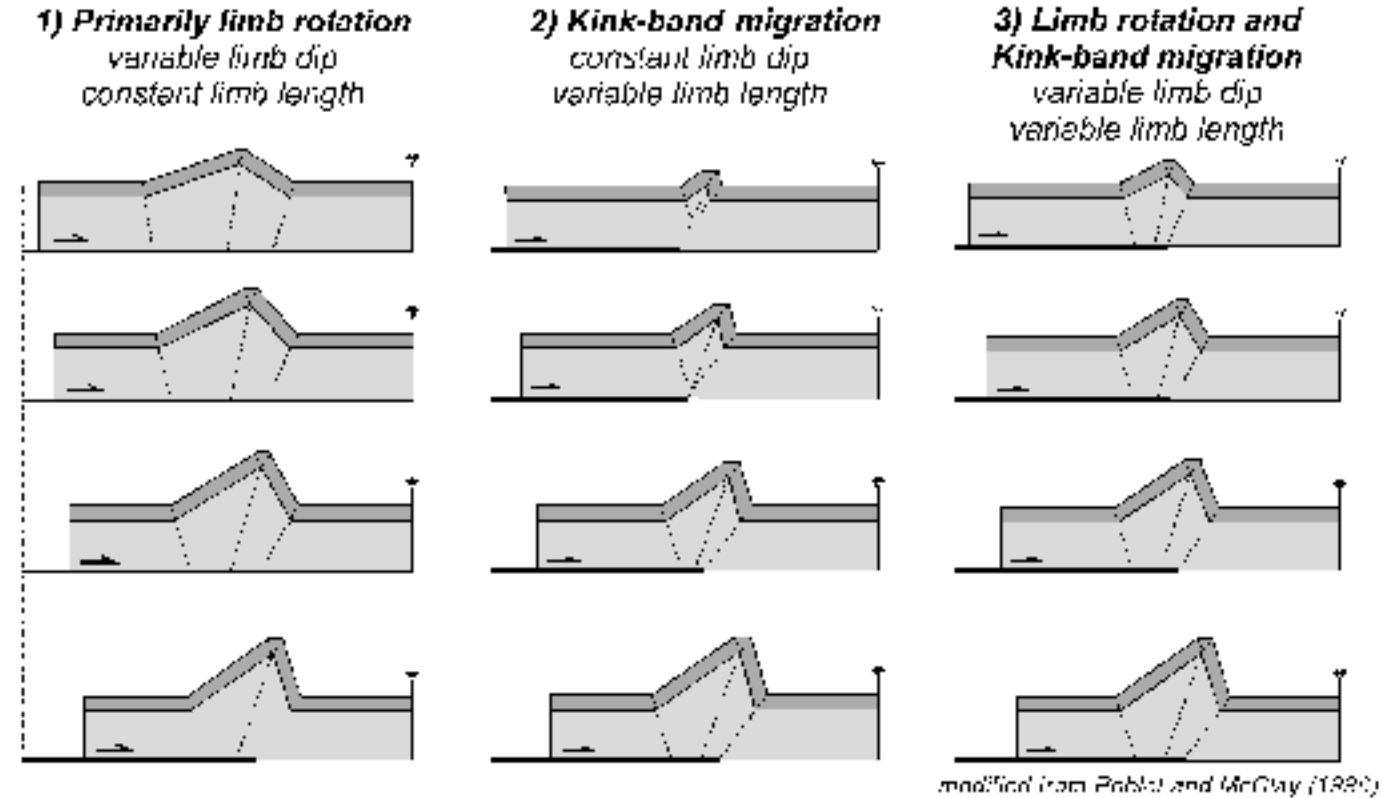
Two fundamental equations relate the shortening and uplift to the limb lengths and limb dips of these detachment folds: (equations)

$$S = L_b (1 - \cos \vartheta_b) + L_f (1 - \cos \vartheta_f + Lt \sin \vartheta_f)$$
$$u = L_b (\sin \vartheta_b) = L_f (\sin \vartheta_f)$$

based on the detachment fold terminology defined in the figure to the lower right.

Kinematic models of detachment folds

1) **Primarily limb rotation**
variable limb dip
constant limb length

2) **Kink-band migration**
constant limb dip
variable limb length

3) **Limb rotation and Kink-band migration**
variable limb dip
variable limb length

modified from Poblet and McClay (1996)

Detachment fold terminology

L_f = Front limb length

L_b = Back Limb length

S = Slip

ϑ_f = Front limb dip

ϑ_b = Back limb dip

u = Uplift

modified from Poblet and McClay (1996)
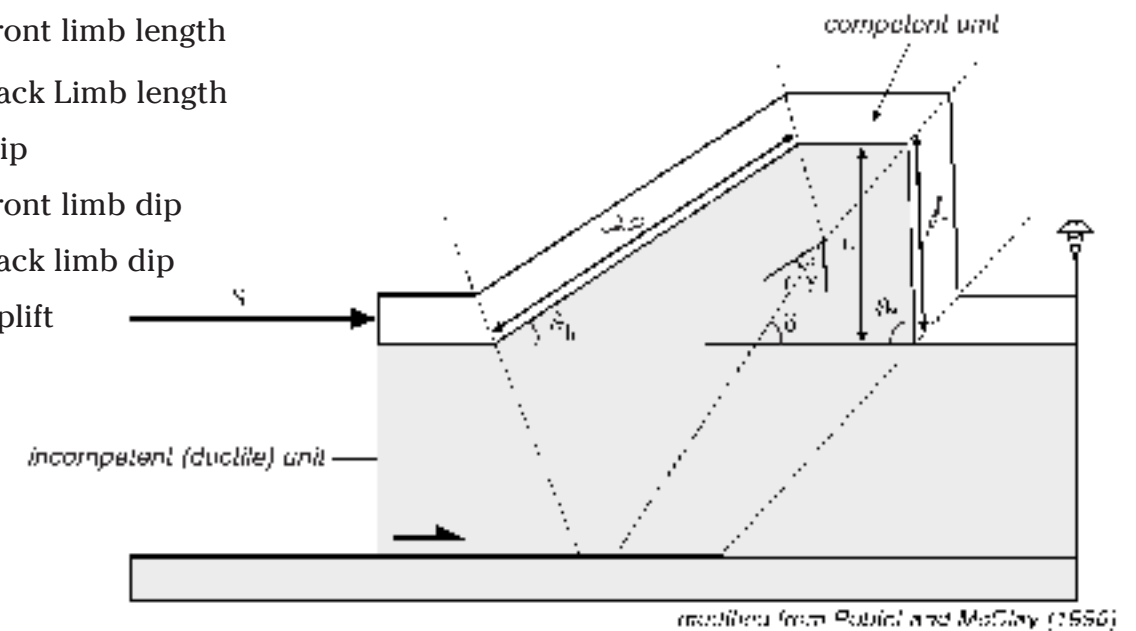
Growth strata associated with detachment folds

It is usually not possible to determine the folding mechanism of a detachment anticline from the geometry of pregrowth strata alone. For example, the three models on the previous page have identical final geometries, but the paths they took to get there (i.e., the fold kinematics), and the folding mechanisms, were quite different. Growth strata are, however, typically diagnostic of folding mechanism because they record the kinematic history of fold growth (see section 1A-3). Thus, growth strata can be used to distinguish between the modes of detachment folding described by Poblet and McClay (1996).

As illustrated in section 1A-3, kink-band migration causes growth strata to form narrowing-upward kink bands, or growth triangles, with bed dips that are parallel to those of the underlying pregrowth strata. Growth triangles are bounded by at least one active axial surface. In contrast, limb rotation causes progressive changes in limb dips that result in a fanning of limb dips in growth strata. In limb rotation structures, a minor amount of material may still move through axial surfaces that are continuously changing orientation, resulting in a minor amount of kink-band migration. Poblet and McClay (1996) refer to these as "limited-activity axial surfaces."

These models define the activity of axial surfaces that are involved in the three types of detachment folds defined by Poblet and McClay (1996):

Axial Surface Activity
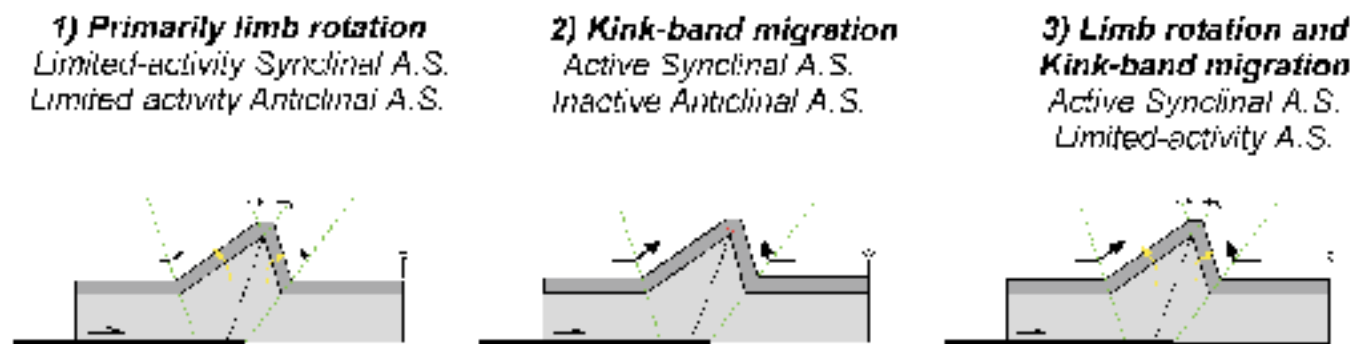
Based on these fold kinematics, growth strata have distinctive patterns in each type of detachment folds that are shown in the models (1–3) at upper right, which are described as follows:

1) Primarily Limb Rotation. In this model, growth strata predominantly display fanning of dips, recording the progressive rotation of the fold limbs. Small growth triangles form that define growth strata which migrated through the limited-activity axial surfaces.
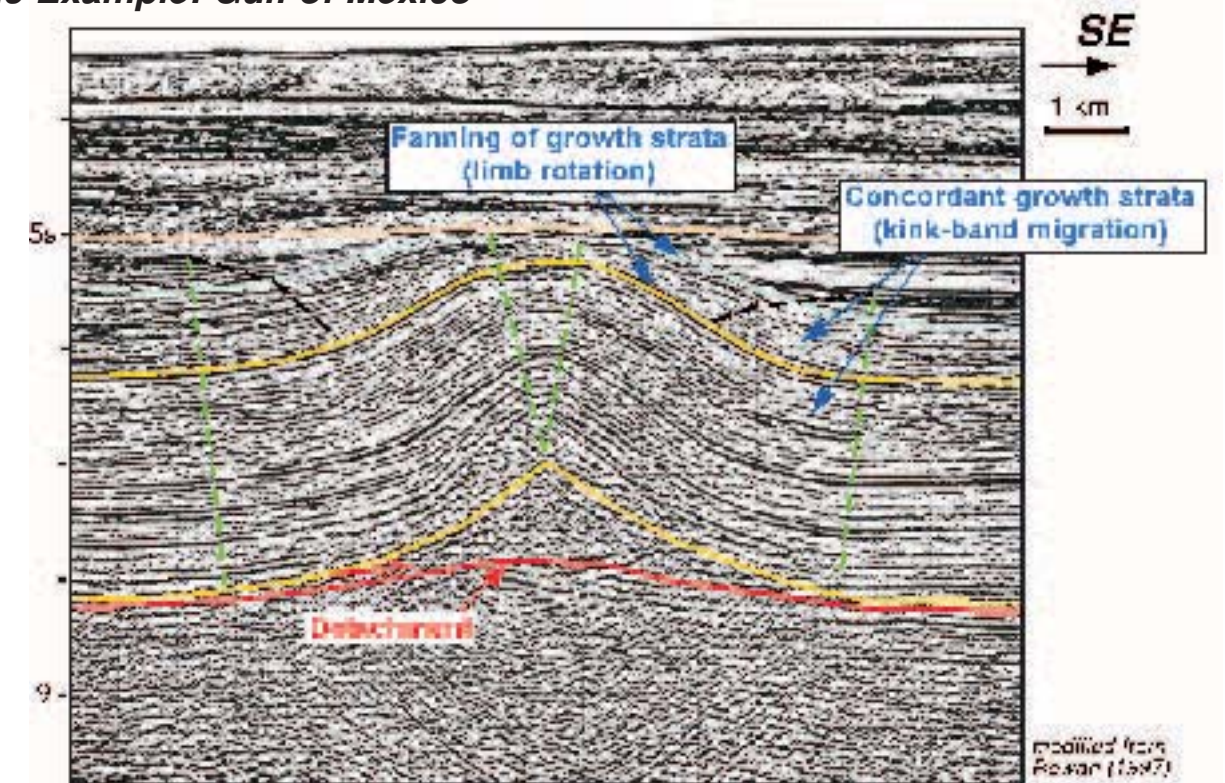
2) Kink-band Migration. In this model, growth strata form growth triangles because strata have migrated through the active synclinal axial surfaces.

3) Limb Rotation and Kink-band Migration. In this model, growth strata display some fanning of dip due to rotation of the fold limbs as well as growth triangles that record the migration of strata through the active synclinal axial surfaces.

Kinematic models of growth detachment folds
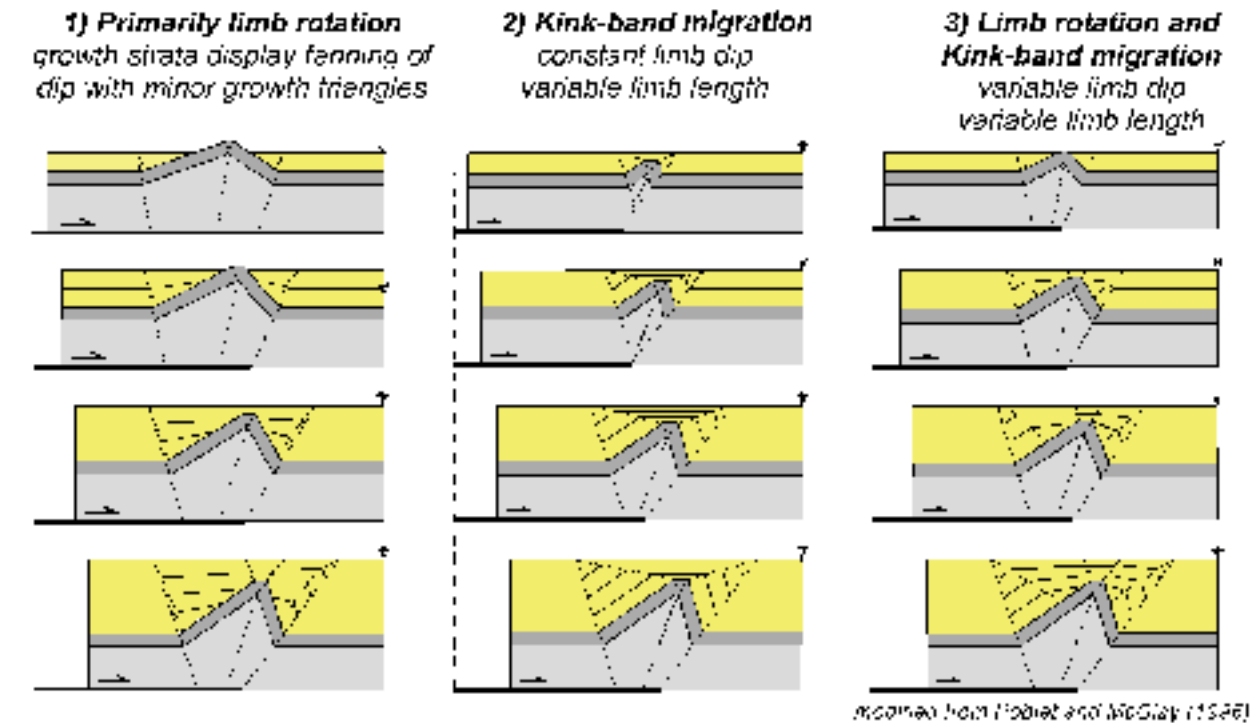
Seismic Example: Gulf of Mexico

This seismic line images a detachment anticline with patterns of growth strata that reflect folding by both limb rotation and kink-band migration, suggesting that the structure is compatible with model 3 shown above.

Seismic interpretation of a detachment fold: Angola continental slope

In this section, we describe the interpretation of a detachment fold imaged in a seismic reflection profile based on the fold models presented on the preceding pages.

Initial Observations. The fold from offshore west Africa shown at right is symmetric, with units that conserve layer thickness (3) and other units that clearly do not (1, 4). There is no obvious thrust ramp present, although reflectors underlying the fold are essentially flat suggesting the presence of a detachment (2).

Structural Interpretation. Based on the initial observations, this structure is interpreted as a detachment fold in the section at lower right. The detachment is interpreted to separate folded layers above from undeformed strata below. Above the detachment, a poorly imaged stratigraphic interval is thickened in the core of the fold (1). This incompetent unit represents an Aptian salt bed. The units directly above the salt broadly conserve layer thickness (3), indicating these strata have acted competently during deformation, probably deforming by flexural slip (see section 1A-2). The constant thickness of the units also indicates that they were deposited prior to folding. Above these units, layers that thin onto the crest of the fold (4) are growth strata. The growth strata generally fan above the fold limbs, with only small panels in the limbs having the same stratigraphic thickness that they do in the synclines. Thus, the fold grew mostly by limb rotation with only minor kink-band migration, similar to the model 1 detachment fold of Poblet and McClay (1996).


Initial observations
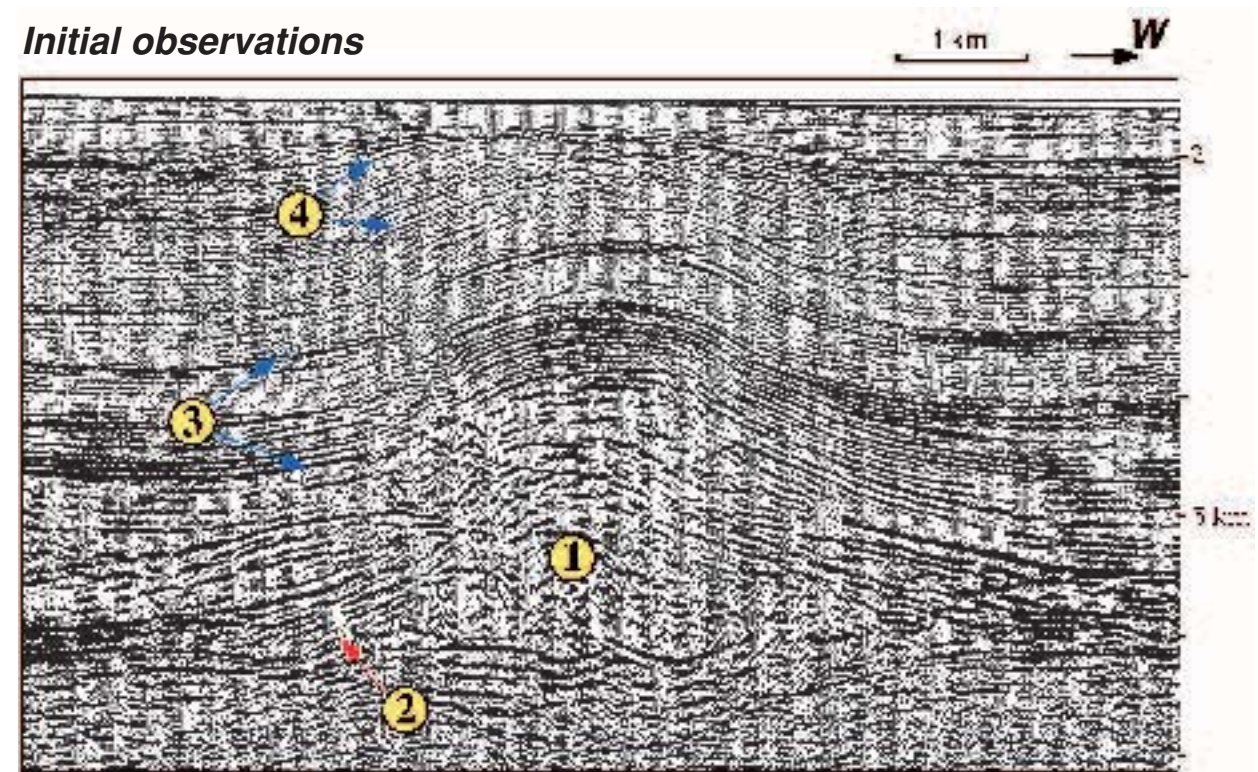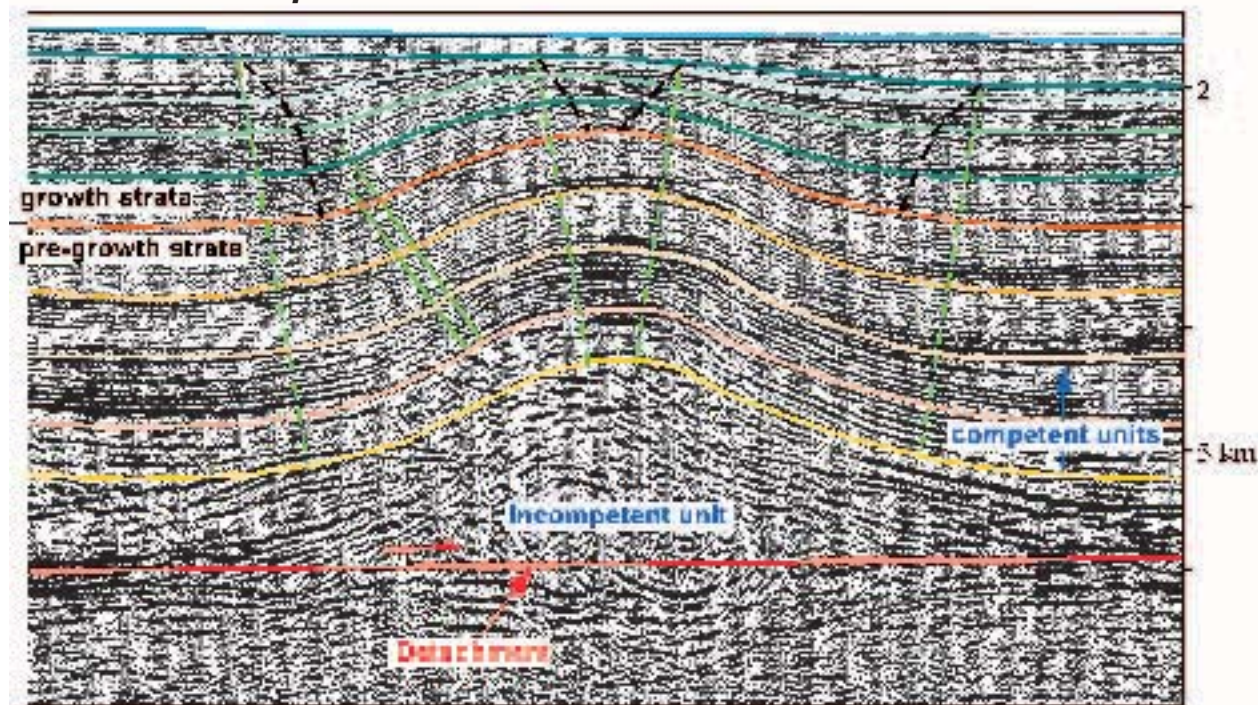
Calculating detachment depth: Why doesn't it always work?

Several techniques (e.g., Chamberlin, 1910; Epard and Groshong, 1993; Homza and Wallace, 1995) have been developed to determine the depth-to-detachment beneath anticlines based upon balancing the area uplifted in the fold with the displaced area as shown below in model A. In cases where the detachment depth is know independently, several authors have pointed out that the predicted and observed detachment depths do not always match (Wiltschko and Chapple, 1977; Jones, 1987; Dahlstrom, 1990; Groshong and Epard, 1994; Homza and Wallace, 1995; Poblet and Hardy, 1995). (In the case of the Angolan detachment fold interpreted in this section, the predicted depth-to-detachment is greater than 15 km!). These discrepancies arise because balancing the uplifted area with displaced area has two implicit assumptions, namely that: 1) The thickness of the ductile unit outside of the fold is maintained, and; 2) All of the material in the thickened zone comes from within the plane of the section. One or both of these assumptions may be invalid for detachment anticlines as well as other types of fault-related folds, as shown below in model B. In particular, detachment folds with highly ductile cores involving salt or over-pressured muds often show withdrawal of material in the synclines (and away from fold), causing local thinning of the ductile interval and subsidence of overlying strata. Withdrawn material is presumably moved into the core of the fold. Alternatively, or in addition, material in the thickened core of the fold may be derived from out of the plane of section. Both processes invalidate the assumptions of classic depth-to-detachment calculations, leading to predicted detachment depths that are generally far too deep. Thus, care should be taken to avoid applying these methods of calculating depth-to-detachment in detachment folds with ductile cores.

Depth-to-detachment calculations
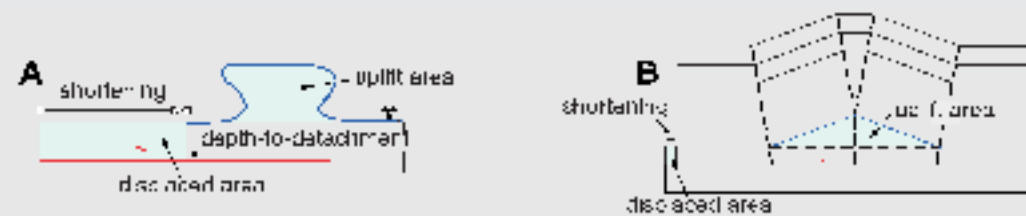
Model A shows the classic method of calculating the depth to detachment, based on the assumption that the uplift area is equal to the displaced area. The shortening, which is typically determined by unfolding a layer while conserving line length, and the uplift area are used to calculate the detachment depth by:

depth-to-detachment = displaced area / shortening

Model B shows a typical detachment fold where the uplift area greatly exceeds the displaced area. In these cases, standard depth-to-detachment calculations inaccurately predict detachment depths.
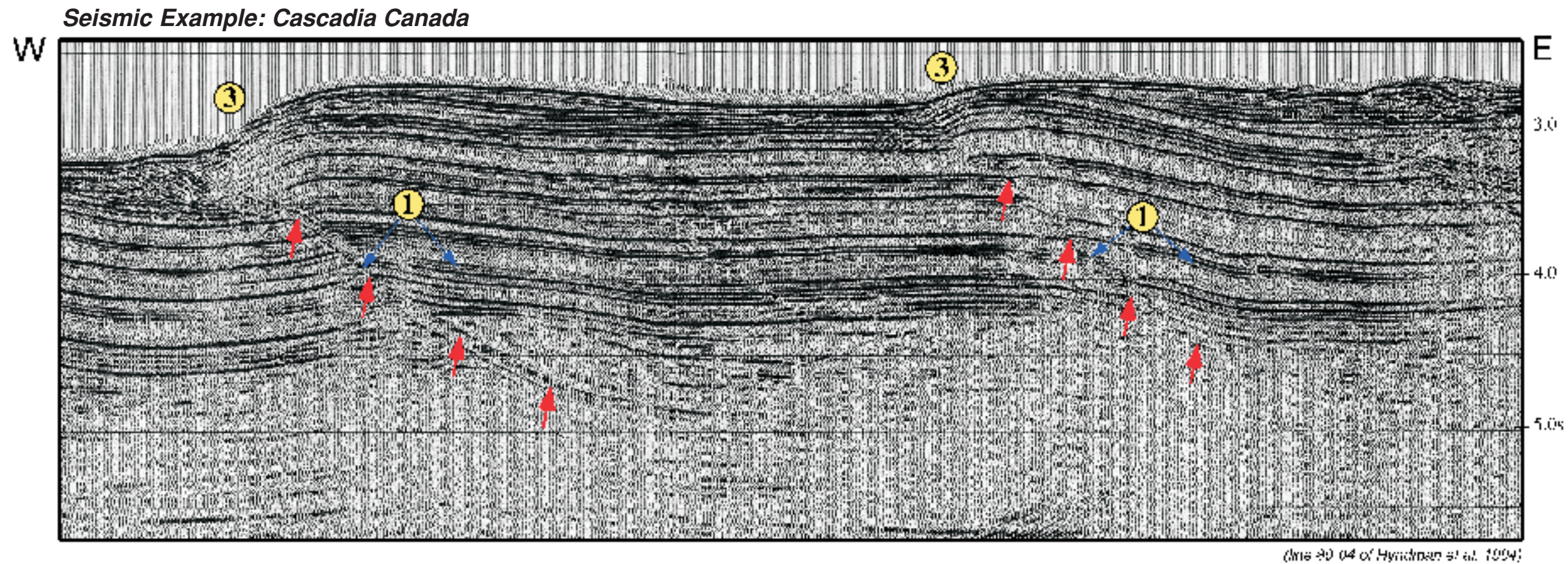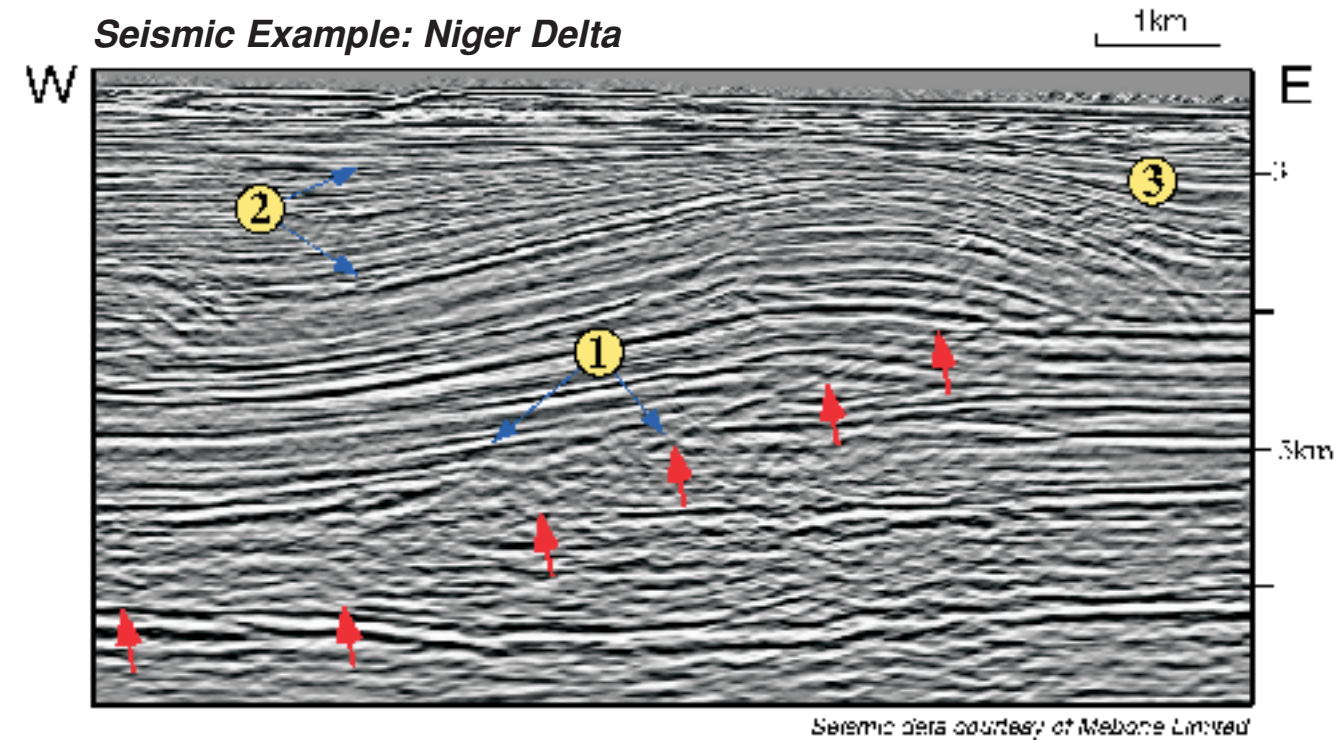

Structural interpretation

1B-4: Shear fault-bend folds

Basic concept

Shear fault-bend folding produces ramp anticlines with very distinctive shapes that reflect a significant non-flexural-slip component to the deformation. The structural style typically shows long back-limbs that dip less than the fault ramp, in contrast with classical fault-bend folding. This section describes the geometry and kinematics of shear fault-bend folding after Suppe, Connors, and Zhang (2004) and introduces basic techniques for recognizing and interpreting these structures in seismic images.

Recognizing the structural style

The typical structural style for ramp anticlines produced by shear fault-bend folding has back limbs that dip less — in many cases very much less — than the fault-ramp (1). If a significant stratigraphic section is deposited over the back limb during fold growth it typically shows evidence of limb rotation (2). These ramp anticlines also commonly show front limbs (3) that are quite narrow relative to their long back limbs.

Seismic Example: Niger Delta

Seismic data courtesy of Melbone Limited

Seismic Example: Cascadia Canada

(line 90-04 of Hyndman et al. 1994)

Shear is the essence

Classical fault-bend folds (section 1B-1) deform by flexural slip of the beds as they slide over fault bends (A), conserving layer thickness. In contrast, shear fault-bend folds undergo additional distortion of the hanging wall or footwall, that is they undergo additional *shear*. This additional shear usually is concentrated in a weak detachment interval such as shale or evaporite that deforms by bedding-parallel *simple shear* — like the geometric model below (B). Alternatively, shear may be more distributed as in the analog model from David Elliott (1976) based on sheets of paper (C) or it may involve a bedding-parallel shortening and thickening, which is called pure shear. Shear fault-bend folds can also form by some combination of pure and simple shear or by more heterogeneous deformation as shown below in the distinct-element mechanical simulation by Luther Strayer (D).

Models
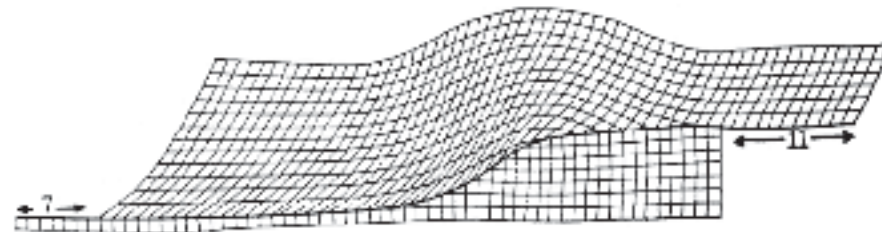
A: Classic fault-bend fold   **B: Shear fault-bend fold**

C: Analog model of shear fault-bend fold

D: Mechanical model of shear fault-bend fold

## Shear in a seismic example: Cascadia Canada

Flexural-slip unfolding of a shear fault-bend fold yields a hanging wall shape that doesn't match the footwall because there has been deformation in addition to flexural slip. In this example from the Cascadia accretionary wedge, offshore western Canada, the hanging-wall fault shape is determined by unfolding the layers while conserving line length. The difference between the unfolded hanging-wall fault shape and the actual fault shape yields the *shear profile*, showing that there has been layer-parallel simple shear. The shear is concentrated in the yellow and red basal layers.

**Interpreted section**
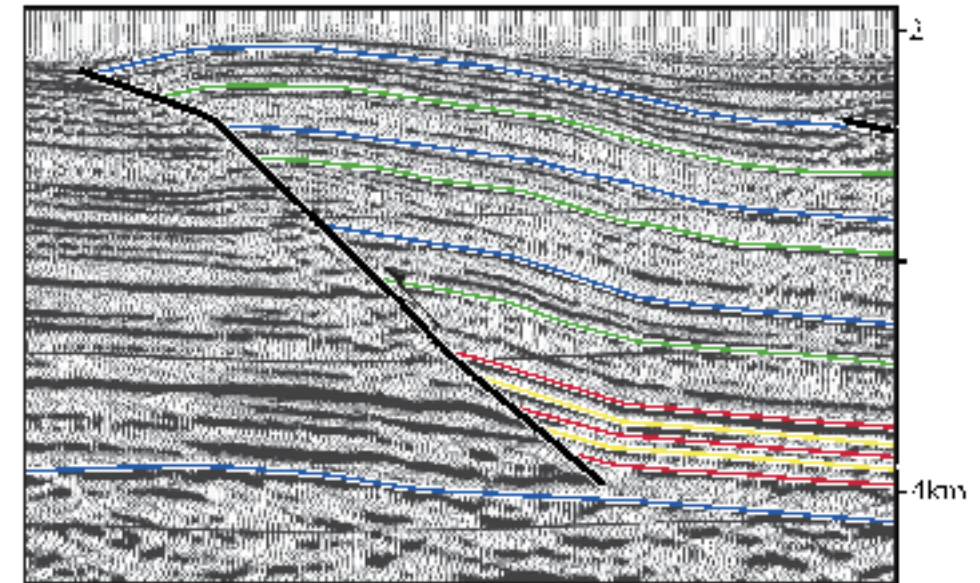
Flexural-slip unfolding gives the shear profile
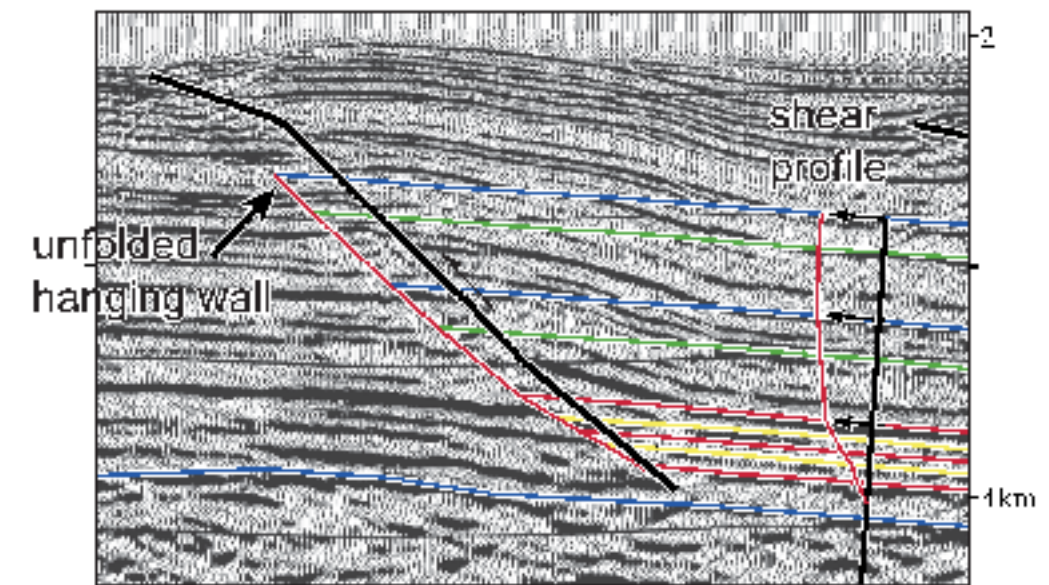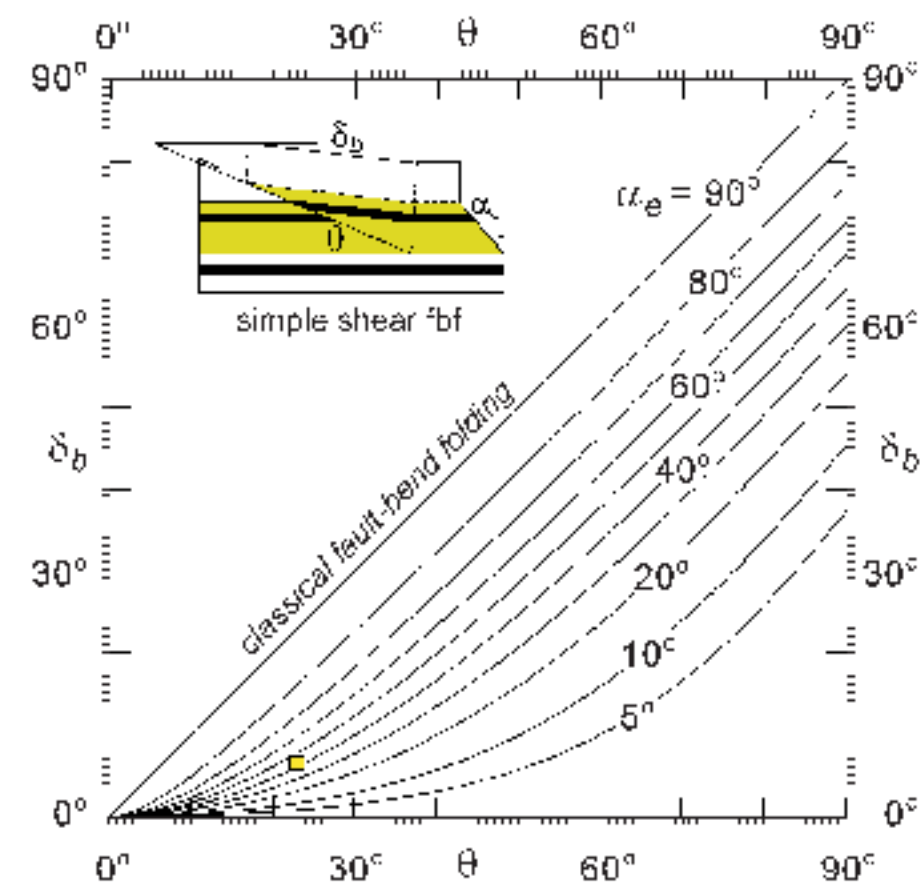
End-member shear fault-bend folding

End-member shear fault-bend folding. We can understand the fundamentals of shear fault-bend folding and quantitatively check our seismic interpretations by using two simple end-member theories, both involving a weak basal decollement layer of thickness h (shown in yellow). In the *simple-shear end member*, the decollement layer undergoes bedding-parallel simple shear with no actual basal fault, just a distributed zone of shear. In the *pure-shear end member*, the decollement layer slides above a basal fault and shortens and thickens in a triangular area above the ramp. Mixtures between these end members are possible, as shown at right, but many actual folds are close to the end members. *Classical fault-bend folding* is also an end member, with a basal layer of zero thickness (h = 0).

The shape of the fold shows us which stratigraphic interval is the decollement layer. The anticlinal axial surface terminates at the top of the decollement interval at (A). The synclinal axial surface terminates at the bottom (B). Also, if there is pure shear, the synclinal axial surface (C) doesn't bisect within the decollement layer because the latter is thickened above the ramp. These properties are useful in seismic interpretation.
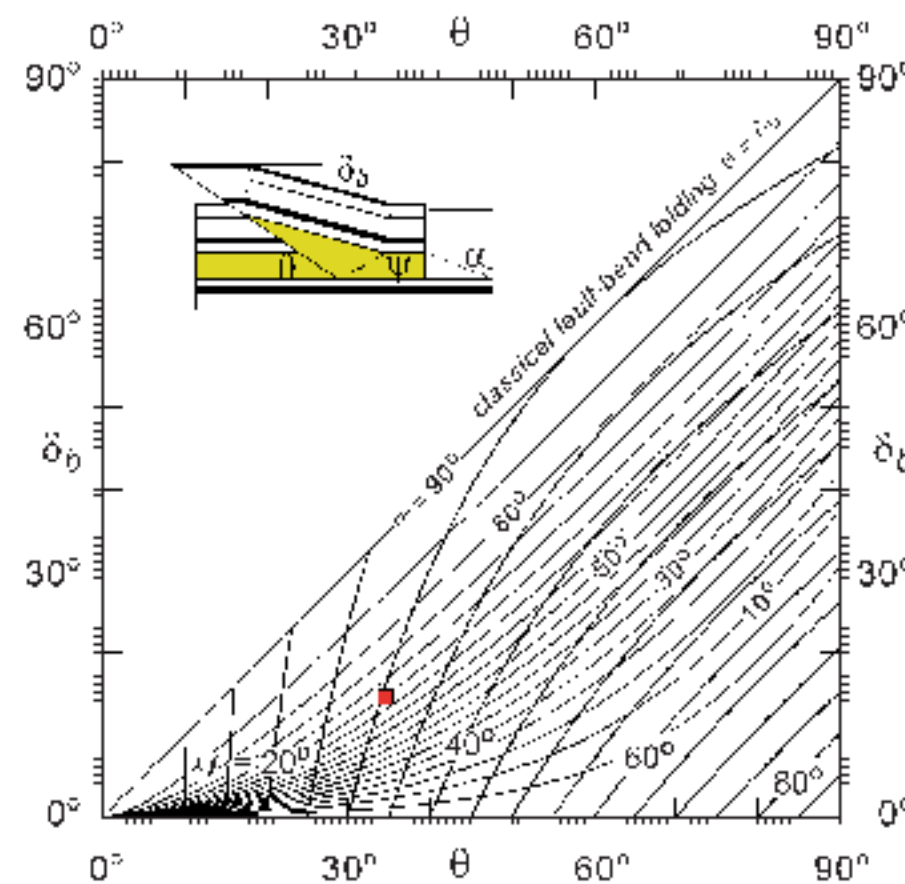
Fold types

Simple-shear fbf

Pure-shear fbf

Mixed-shear fbf

Classical fbf
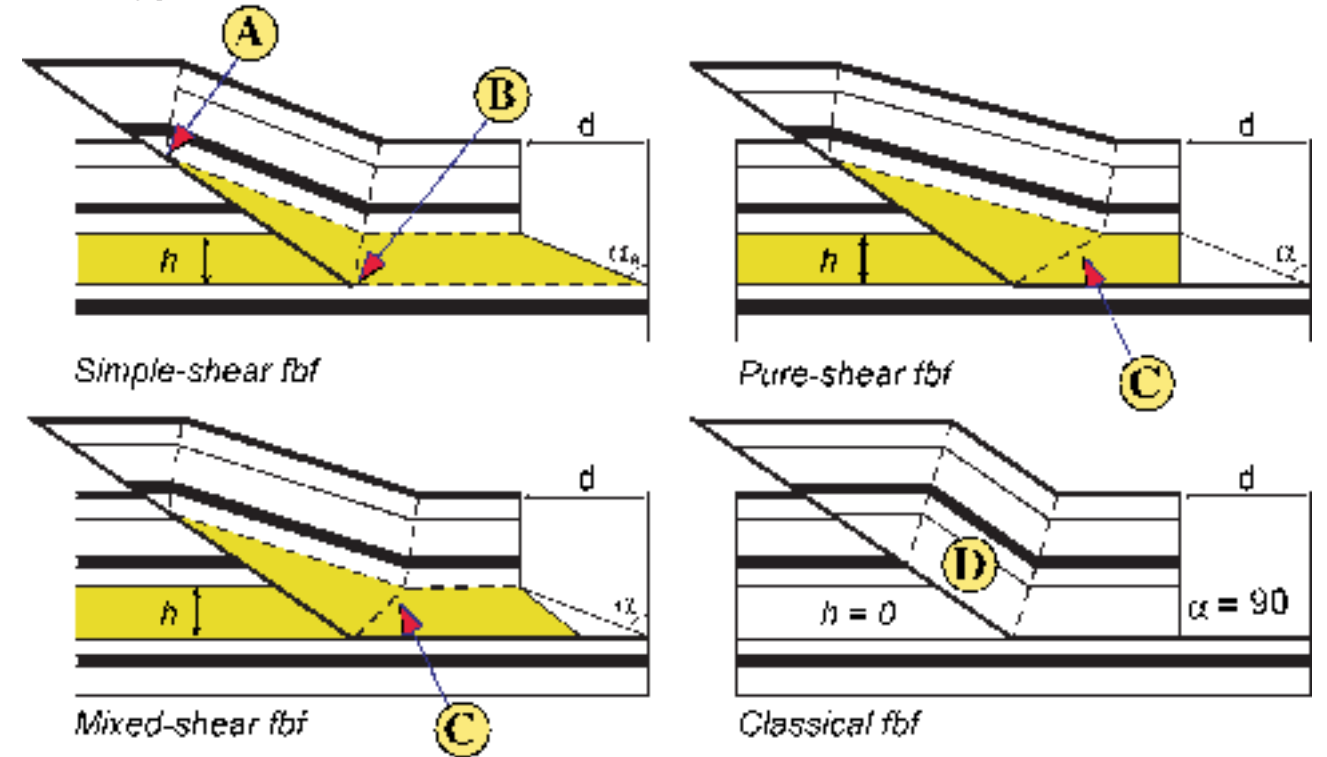
Simple-shear end-member

Pure-shear end member

Graphs of end-member theory. These end-member shear fault-bend fold graphs give the balanced relationship between ramp dip θ, back limb dip δ_β, and shear (α_e or α) across the basal layer. The shear is tan d/h, where d is the displacement at the top of the basal layer and h is its thickness. The dip of the back syncline in the basal layer (ψ) is useful in the pure-shear and mixed cases.

The inset drawing of the simple-shear graph shows a model shear fault-bend fold that corresponds to the yellow square (θ = 23°, δ_b = 6.5°, and α_e = 42°). The drawing of the pure-shear graph corresponds to the angles shown by the red square (θ = 34°, δ_b = 15.5°, α = 68°, and ψ = 30°).

Curiously, these shear fault-bend fold graphs also encompass classical no-shear fault-bend folding, which is reached in the limit of zero thickness h to the basal layer. Shear (d/h) becomes infinite (α_e or α = 90°) and the limb dip becomes parallel the fault (θ = δ_b) (D).

Seismic interpretation of a simple shear fault-bend fold: Cascadia, Canada

Initial assessment. The structure imaged in this seismic section from offshore western Canada (Hyndman et al., 1994) shows the characteristics of a shear fault-bend fold, especially the steepness of the fault dip (35-40°) relative to the back limb dip (5-13°). A front limb much narrower than the back (1) is also typical of shear fault-bend folds.

Interpreting the ramp geometry. The fault picks (shown below in red) constrain the fault geometry and rule out strongly listric fault interpretations. Also, note that there is a downward dying out of the fault throw (2), with throw going to zero at the base of the ramp (3). This is characteristic of shear fault-bend folds, in contrast with classical fault-bend folds.

Significance of synclinal geometry. The back syncline is planar, bisects the inter-limb angle (4), and terminates at the base of the fault ramp (3), indicating a simple-shear rather than a pure-shear fault-bend fold (see models previous page).

Fault picks
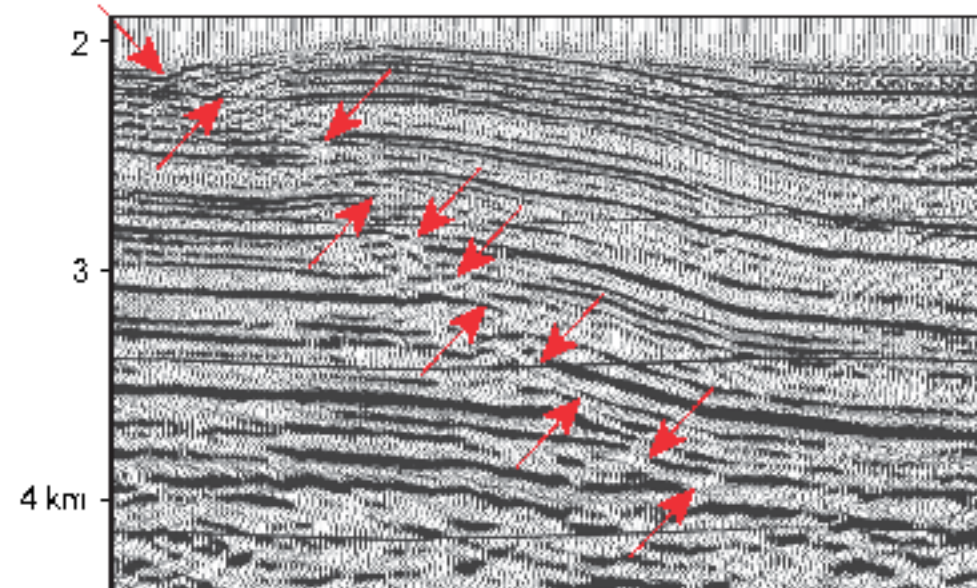
Timing of growth. Onlapping shallow reflectors (5) show that 120 m of growth strata have accumulated. Deformation began soon after termination of slip on the shallow hinterland thrust to the east, as defined by a seismic horizon (6) that is folded in the backlimb of the shear fault-bend fold but is undeformed above the thrust tip in the hinterland structure. Thickness and dip variations in growth strata record deformation by limb rotation and kink-band migration (5), consistent with shear fault-bend folding.
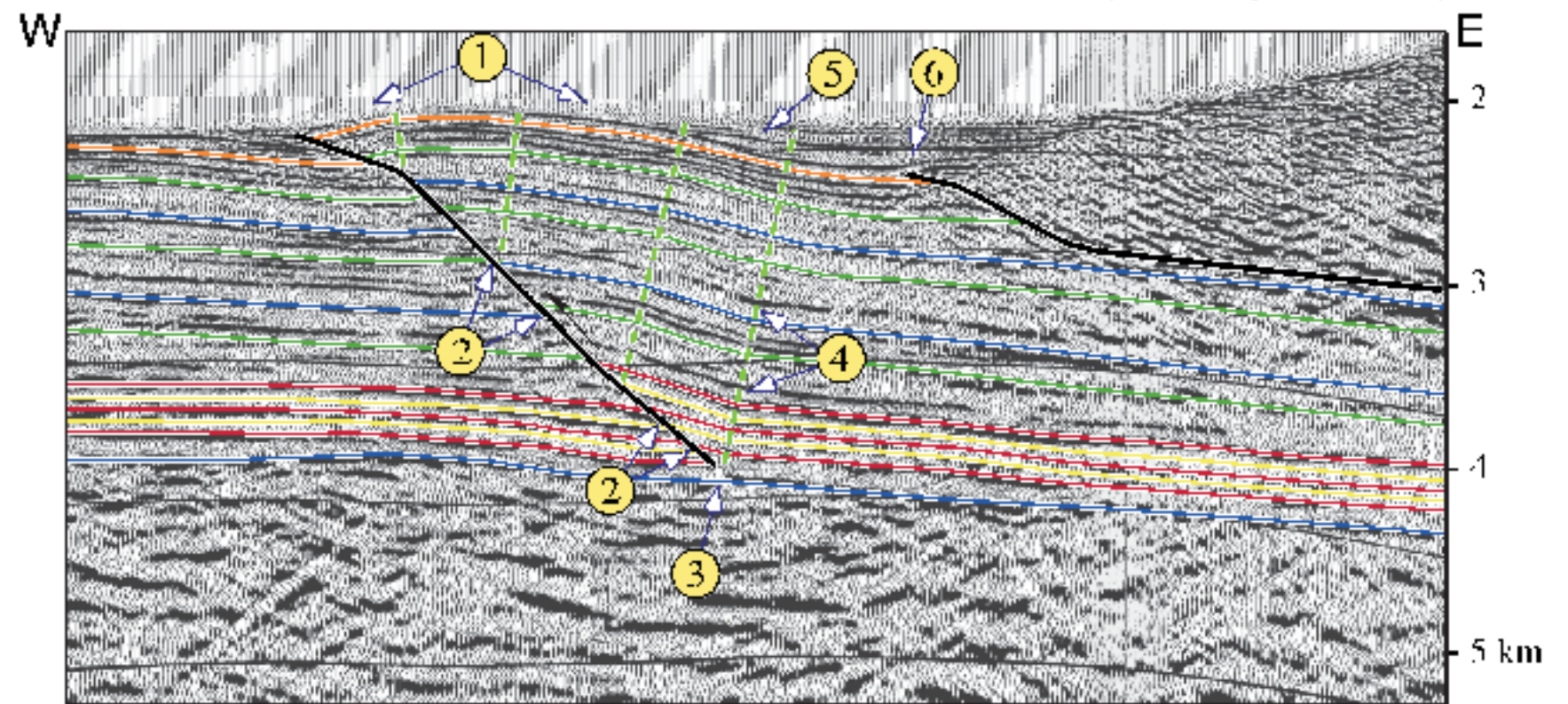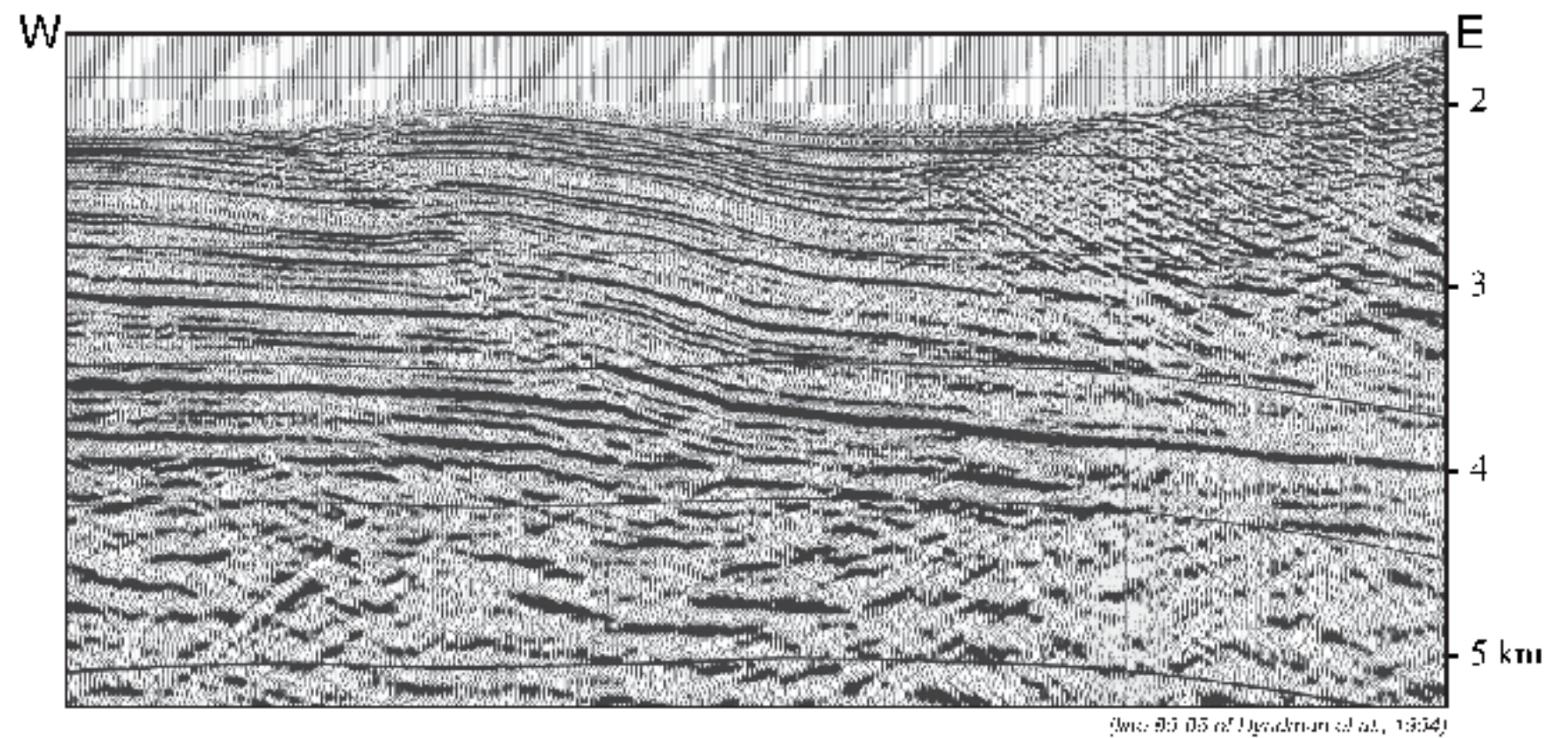
Refining and testing the seismic interpretation: Cascadia, Canada

Refining the interpretation. This structure is more complex than the simple models shown previously because the fault ramp is not straight but composed of two segments dipping 35° and 40°. Furthermore the backlimb has two kink bands *ab* and *bc* of different dips (1 and 2).

Testing the interpretation. Let us begin by treating each kink band of the backlimb (1 and 2) separately, predicting two shear amounts from the two limb dips. Then we will compare the predicted shear with the shear determined from unfolding the hanging wall to see if our interpretation is consistent.

Applying the simple-shear graph (shown at far right), we find that a backlimb dip δ_b of 11-12° within the lower kink band *ab* and a lower ramp dip θ of 35° predict an external simple shear α_e of 31-32° (1'). This agrees with the shear α_e of 31° determined by unfolding the hanging wall while conserving bed length as shown below (1''). The backlimb dip δ_b of 5° within the upper kink band *bc* and an upper ramp dip θ of 40° predict an external simple shear a_e of about 8° (2'), which also agrees with shear determined by the unfolding (2''). These quantitative tests give us more confidence that our seismic interpretation of this ramp anticline as a shear fault-bend fold is reasonable.
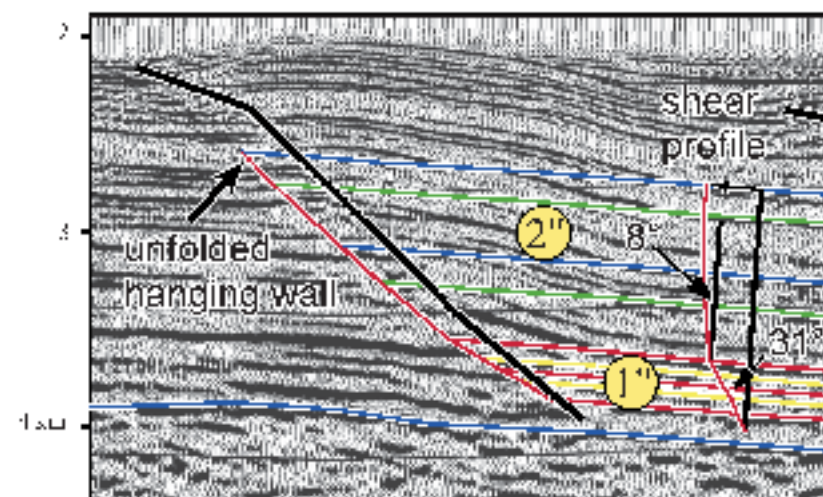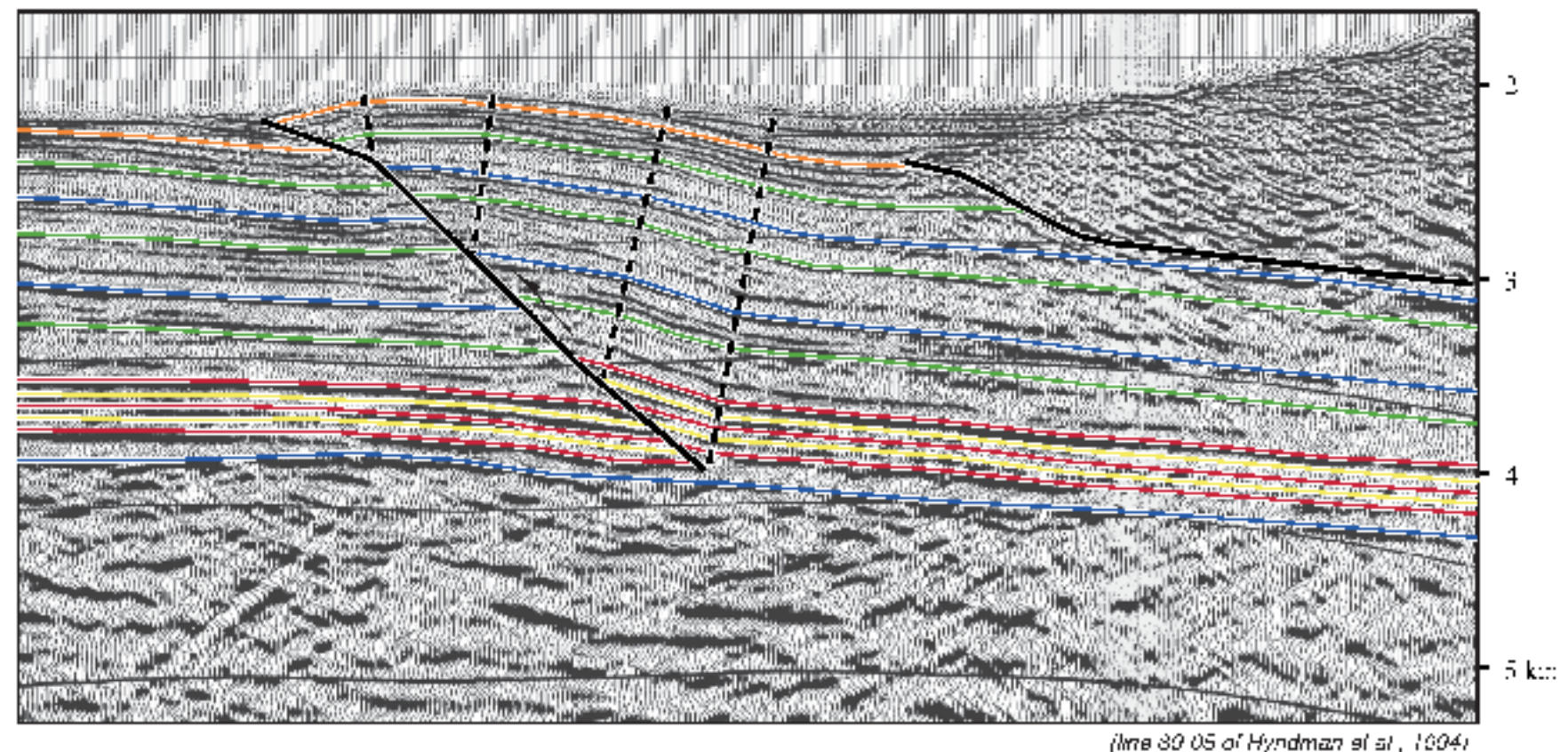
Two segments of the back limb

Interpreted depth section

(line 89 05 of Hyndman et al., 1994)

Two intervals of shear
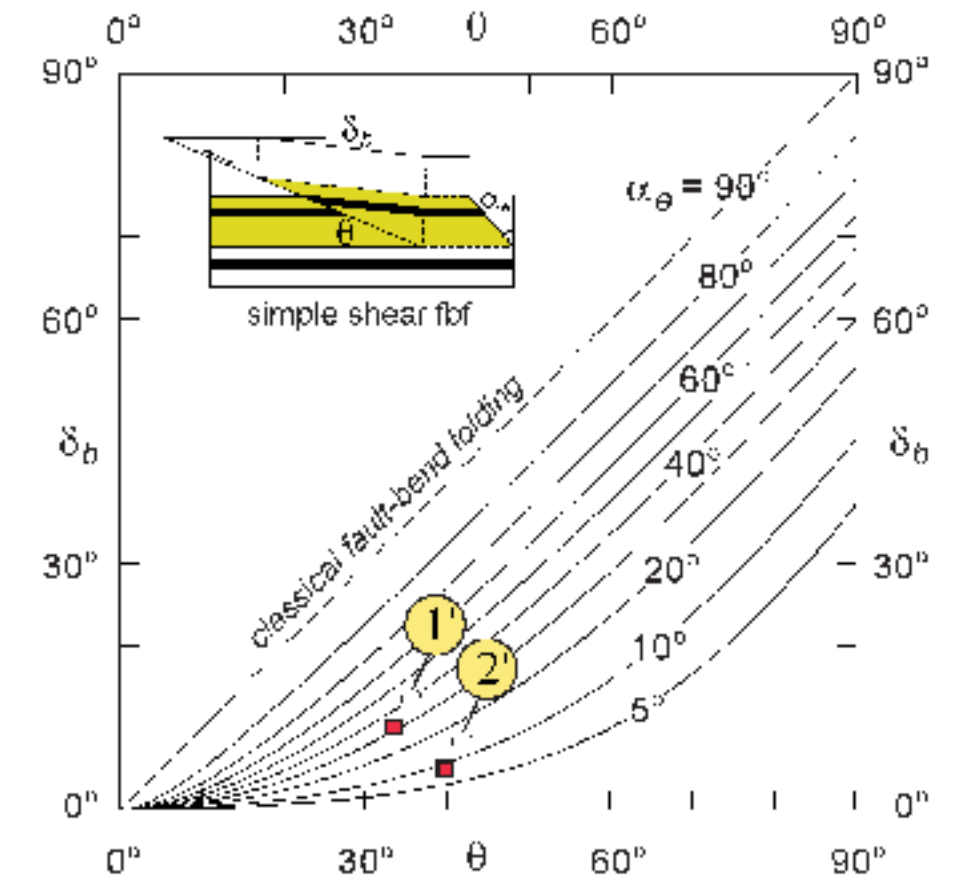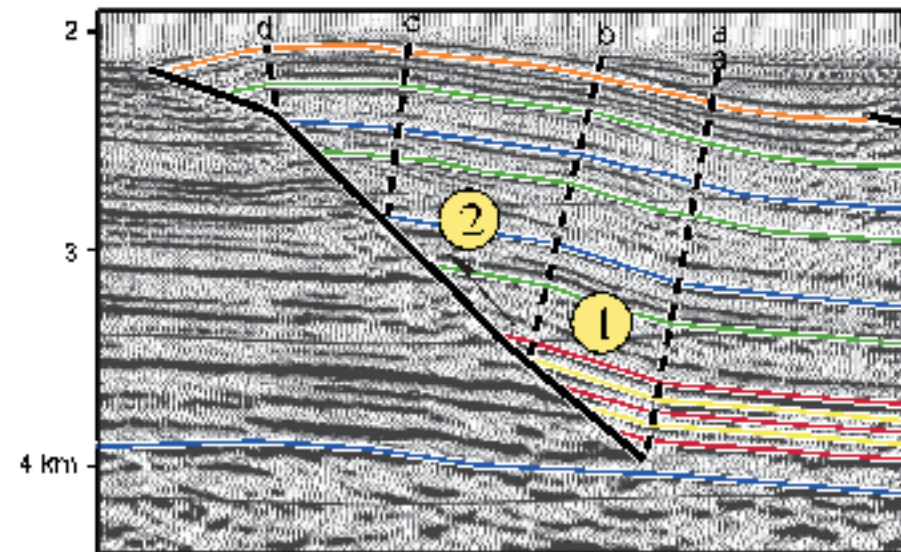
Evolution of shear fault-bend folds

Kinematic evolution. Both simple- and pure-shear fault-bend folds develop by combinations of limb lengthening (kink-band migration) and limb rotation. The graphs at right show the relationship between limb dip and shear for both fold types. In the limit of large shear (i.e., displacement), the fold geometry in pre-growth strata approaches the geometry of classical fault-bend folding, with a back-limb dip that approaches the ramp dip (θ approaches δ_b). However, even in these cases folds will grow with a component of limb rotation, recording their shear fault-bend fold heritage.

Heterogeneous simple shear
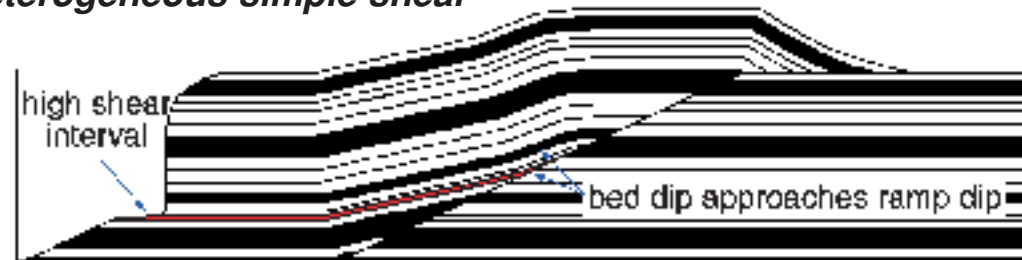
Note that in this heterogeneous simple-shear fold that the highest shear interval defines the base of the backlimb panel that most closely approaches the ramp dip.

Growth strata. The combination of limb rotation and limb lengthening that occurs in shear fault-bend folding is recorded by growth strata, as illustrated in the sequential kinematic models (A1-A3) shown below. Fanning of dips recording limb rotation (1) and growth triangles recording kink-band migration (2) (see section 1A-4). Growth strata in the example from the Niger delta at right show evidence of limb rotation.

As mentioned above, the fold geometry in pre-growth strata approaches the geometry of classical fault-bend folding, with bed dips (3) approaching the ramp dip, in the limit of large shear (i.e., displacement). The sequential large shear model at right (B1–B2), however, demonstrates that the component of limb rotation is recorded in growth strata (4), and thus can be used to distinguish large shear fault-bend folds from classical fault-bend folds.

Limb rotation plus kink-band migration
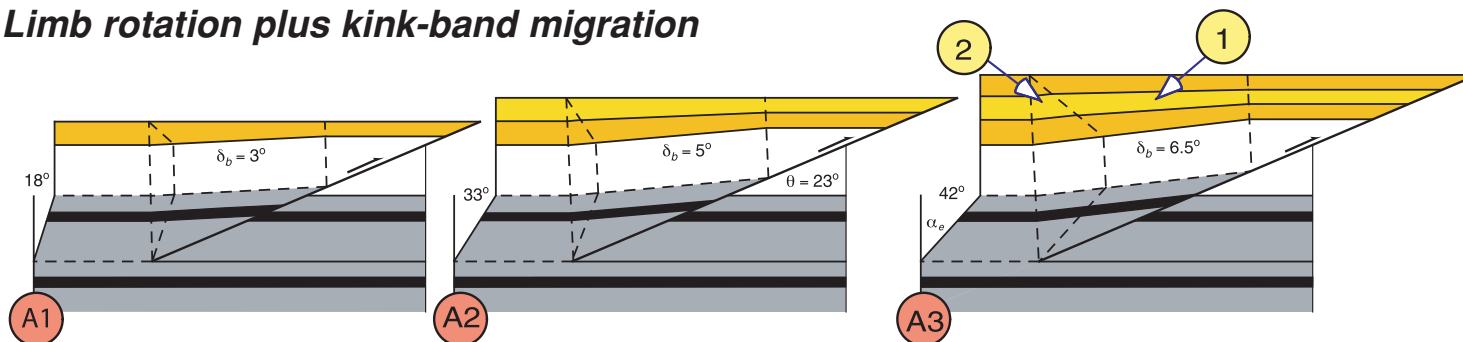
Relationships of backlimb dip (δ_b) to shear (α_e and a)
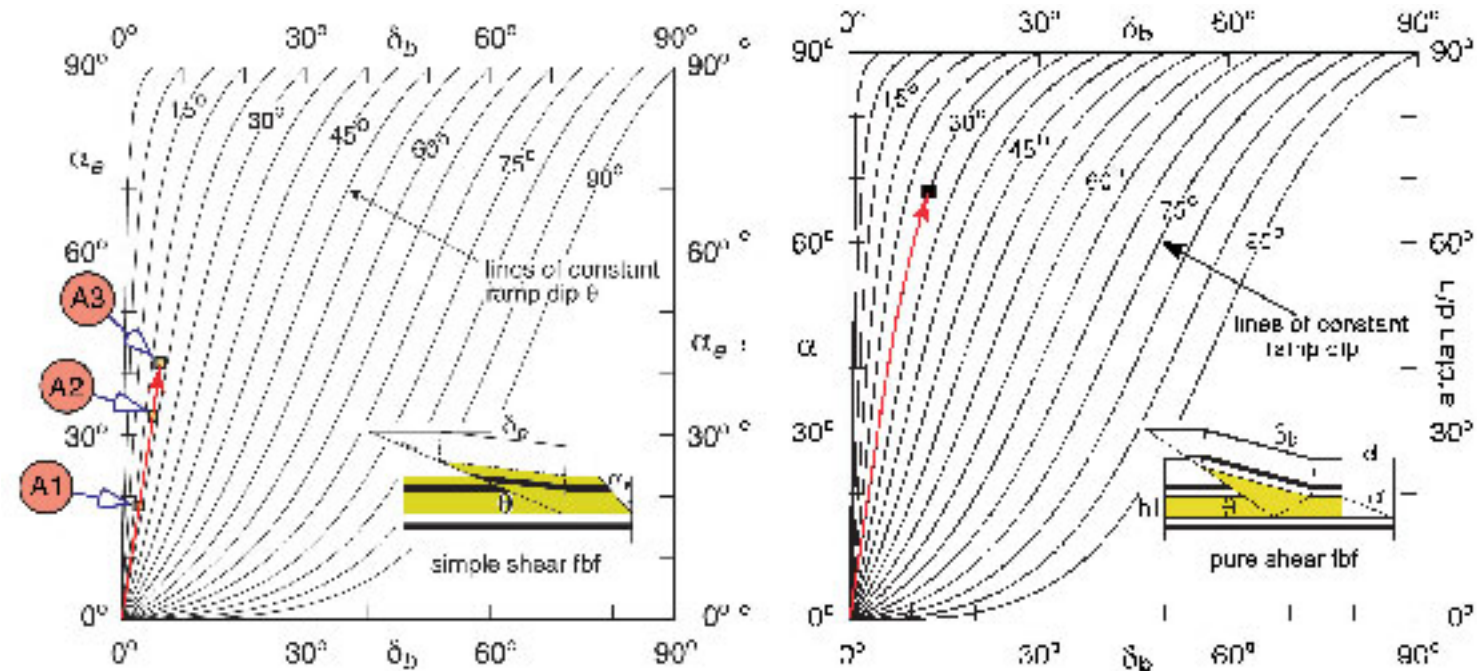
Given a constant ramp dip, the backlimb dip (δ_b) steepens as shear (α_e and α) increases. Points A1 to A3 correspond to models presented at lower left.

## *Large shear (displacement) fault-bend folds*
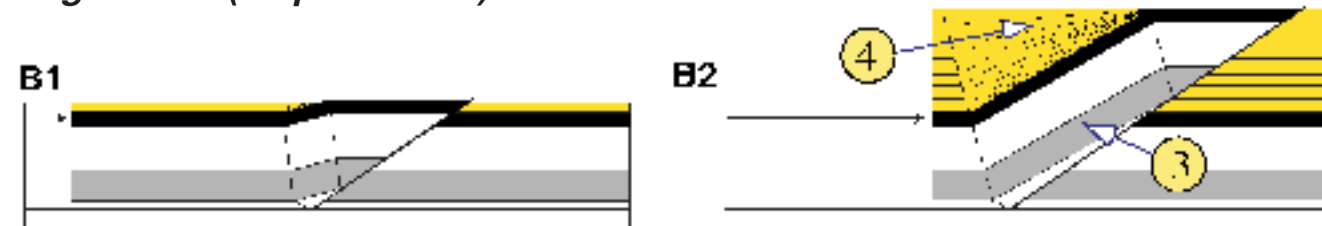
Niger delta limb rotation
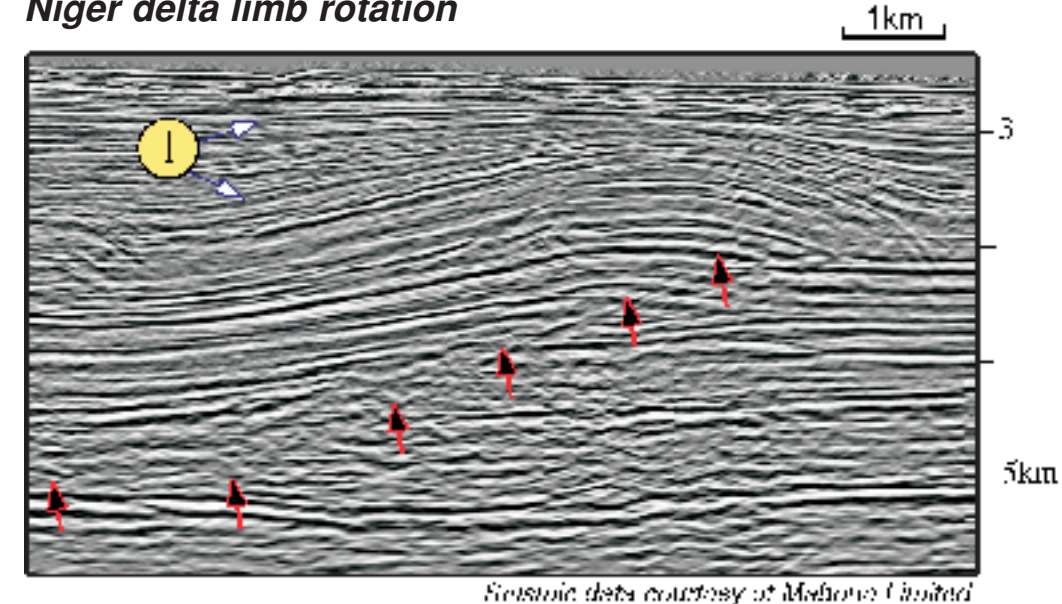
Seismic interpretation of pure-shear fault-bend folds: Nankai trough, Japan

Initial assessment. This line shows ramp anticlines developed in overpressured Shikoku basin turbidites above the master detachment (D) of the Nankai trough accretionary wedge. Note that the degree of shortening in the structures increases from south to north. Notice the qualitative characteristics of shear fault-bend folds, including backlimb dips that are less than ramp dip (A). Nevertheless these structures are more complex than the end-member models because of superposed low-amplitude detachment folding and secondary deformation, seen in both footwalls and hanging walls (B).

This depth-migrated dip line passes through Ocean Drilling Project holes ODP-808 and ODP-1174, which reach to the top of oceanic crust (C) (line NT62-8 Moore et al., 1990, 1991, 2002). The 19-meter-thick master detachment was cored in ODP-808 just above transparent pelagic sediments of the Shikoku basin (D).
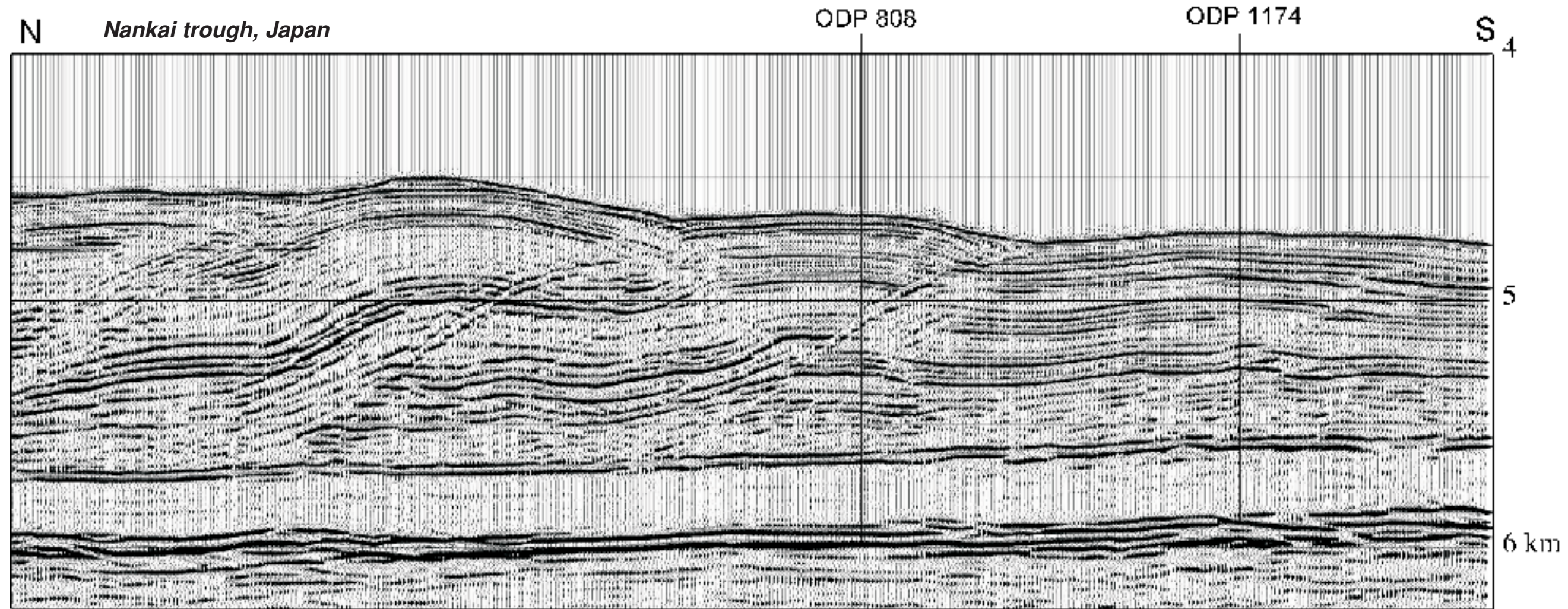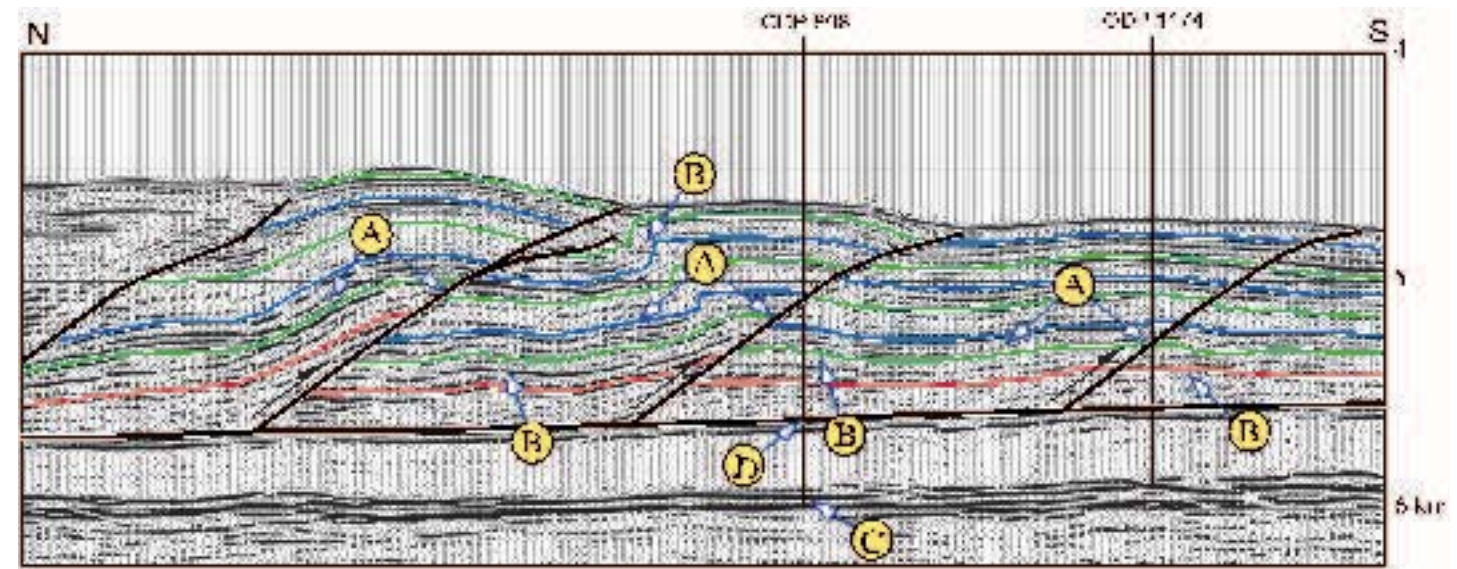
(line NT62-8 of Moore et al. 1990)

# Refining the seismic interpretation: Nankai trough, Japan

Strategy. We can test our qualitative interpretation by comparing the seismic geometry with the end-member theories.

Fault and limb geometry. In the seismic section shown at upper right, the fault-ramp is located based on reflector terminations shown as red arrows and by core from the ODP-808 hole (1). This gives a remarkably straight ramp, dipping at $\theta = 35°$, which is much greater than the average dip of the irregular backlimb ($\delta_b = 11$-$13°$), suggesting that this is a shear fault-bend fold. The back syncline in the strong reflectors (2) is displaced substantially to the hinterland of the base of the ramp, which favors pure-shear or mixed-shear models that we now test.

Comparing with the end-member theory. Plotting the backlimb dip $\delta_b = 13°$ and ramp dip $\theta = 35°$ on the pure-shear graph at far right (3) predicts a back synclinal dip $\psi = 31°$ in the basal decollement layer, which quantitatively agrees with the seismic image at right. In theory, the location of the top of the decollement layer (in orange) is at the inflection in the back syncline, which agrees with the location indicated independently by the fault cutoff of the back anticline (4) — supporting our pure-shear fault-bend fold interpretation. A complete interpretation is shown on the seismic image at lower right (see also Suppe et al., 2004).

Fault slip. The back-dip and ramp angles plotted on the graph (3) also give us the shear $\alpha = 69°$ of the basal layer. From this we can calculate the fault slip $d = 390$ m, based on a basal layer thickness h of about 230 m ($\tan \alpha = d/h = 1.7$).

Picking the fault
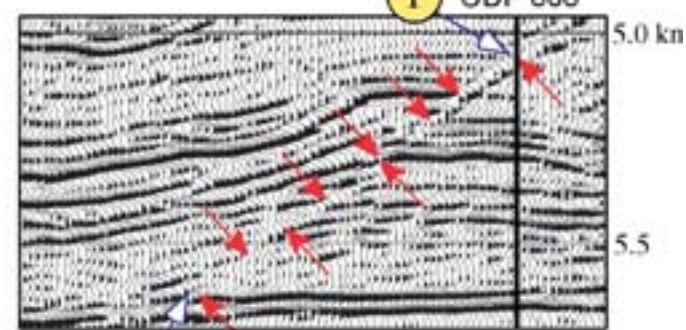
base of ramp is constrained by termination of horizontal reflector, plus overlying dipping reflectors

Comparing the seismic with an end-member model
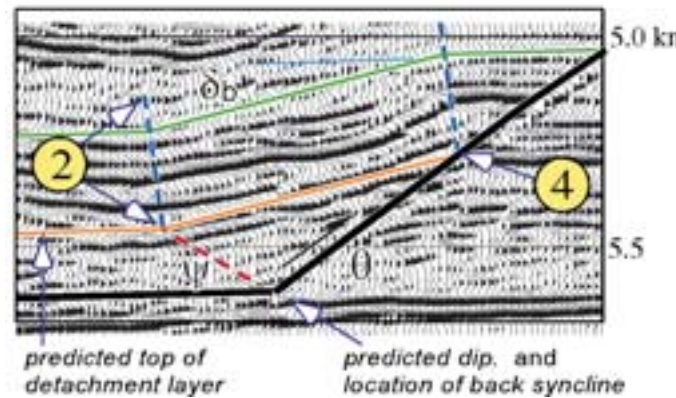
predicted top of detachment layer

predicted dip. and location of back syncline

Pure-shear end member

Depth section

(line NT62-8 of Moore et al., 1991)

Interpreted depth section

1B-5: Imbricate fault-bend folds

Basic concept

Imbricate structures form by the stacking of two or more thrust sheets and are common in fold and thrust belts worldwide. Imbricate structures can form by *break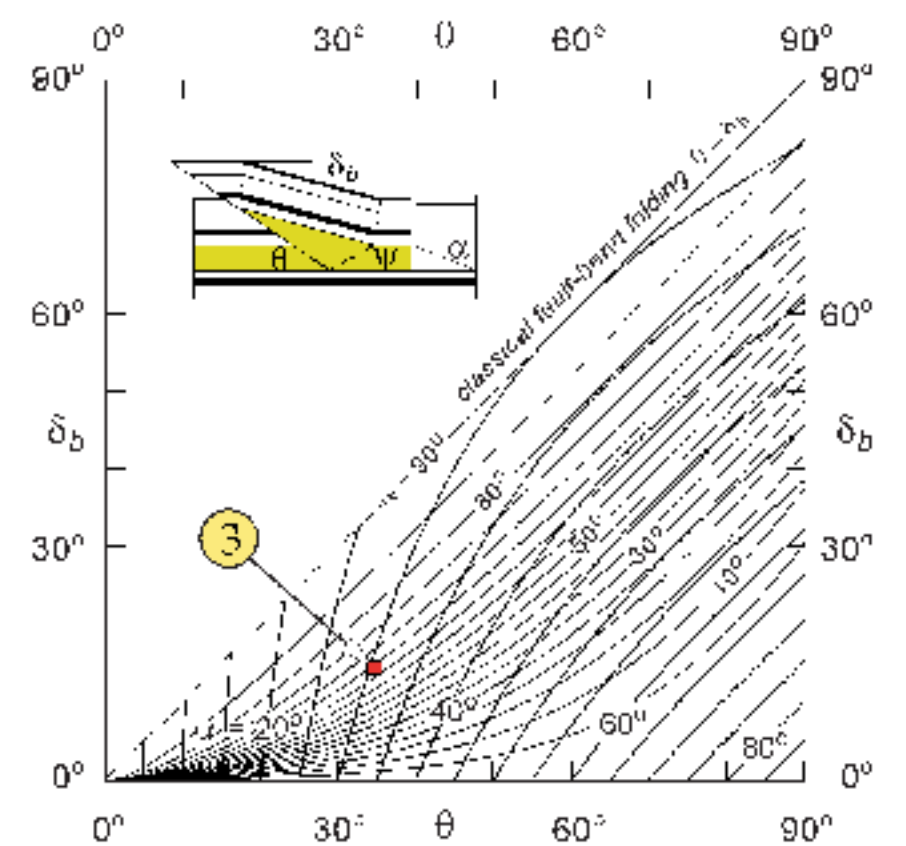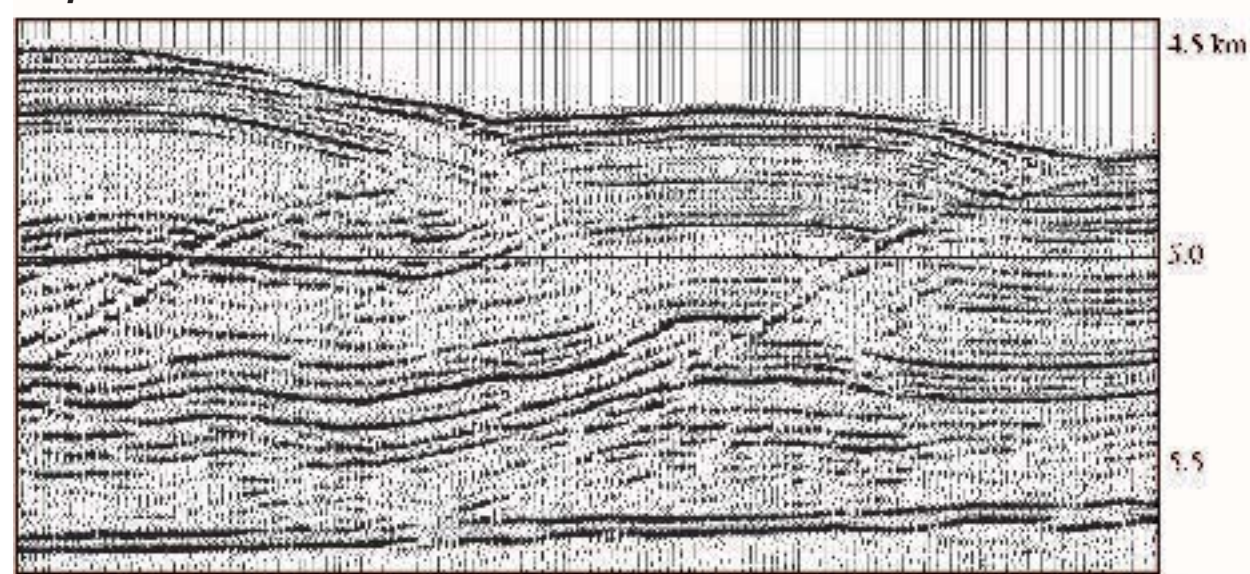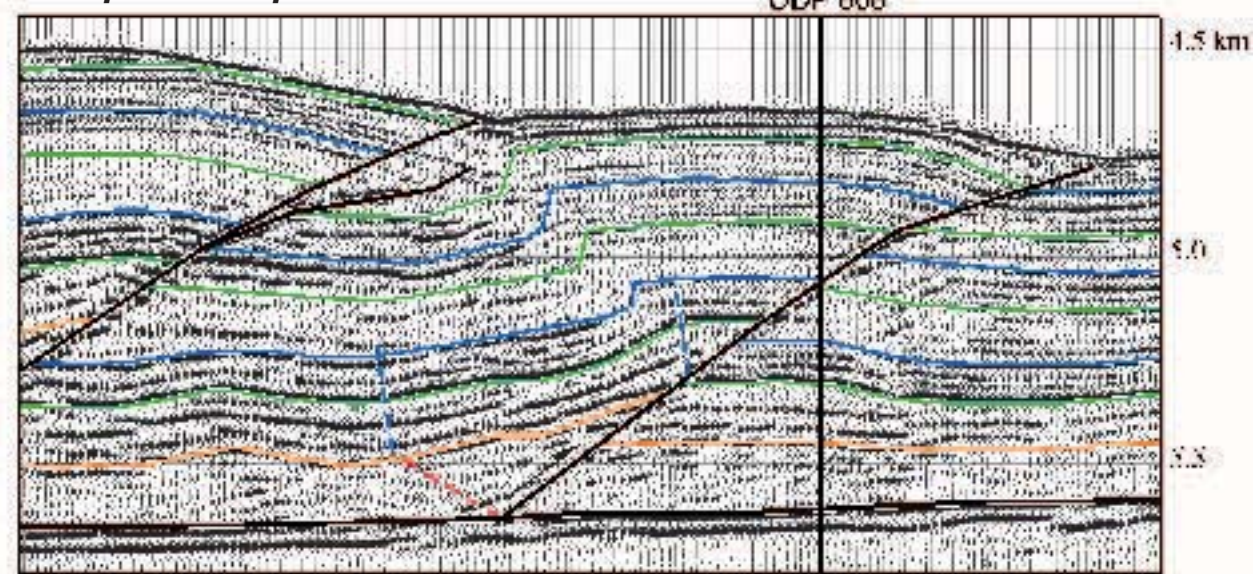-forward* propagation of thrust sheets, by *break-backward* thrusting, or with coeval motion on both deep and shallow faults. In this section, we describe the basic characteristics of imbricate structures, and outline an approach to interpret these structures in seismic profiles using imbricate fault-bend fold theory (Suppe, 1983; Shaw et al., 1999).

Break-forward imbricate   **Break-backward imbricate**

Kinematic Models
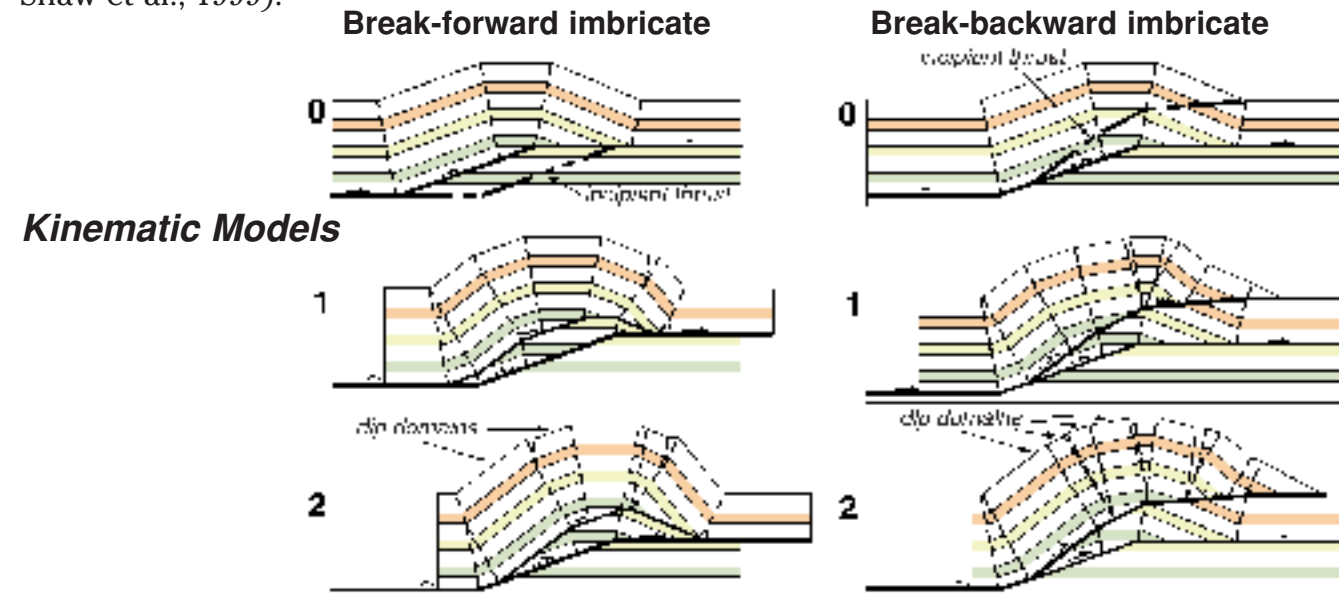
Imbricate structures develop where two or more thrust sheets are stacked vertically. These thrust faults may or may not involve detachments, but imbricate structures are more common in regions with detachments. In the sequential break-forward model (0–2) shown above, slip on the deep thrust fault produces a fault-bend fold that refolds the overlying thrust sheet. In the sequential break-backward model (0–2), a pre-existing fault-bend fold is cut by a shallow, younger thrust ramp.

Common characteristics

Imbricate fault-bend folds typically contain:

1) Two or more vertically stacked thrust ramps;

2) Bedding dips that change across thrust ramps; and

3) Fold limbs at high structural levels with multiple dip domains, reflecting refolding caused by multiple ramps. (Note: multiple dip domains may also be produced by multi-bend fault-bend folds, see section 1B-1).
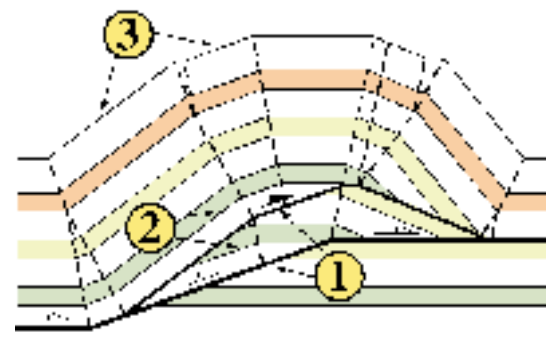
Seismic Example: Alberta Foothills, Canada
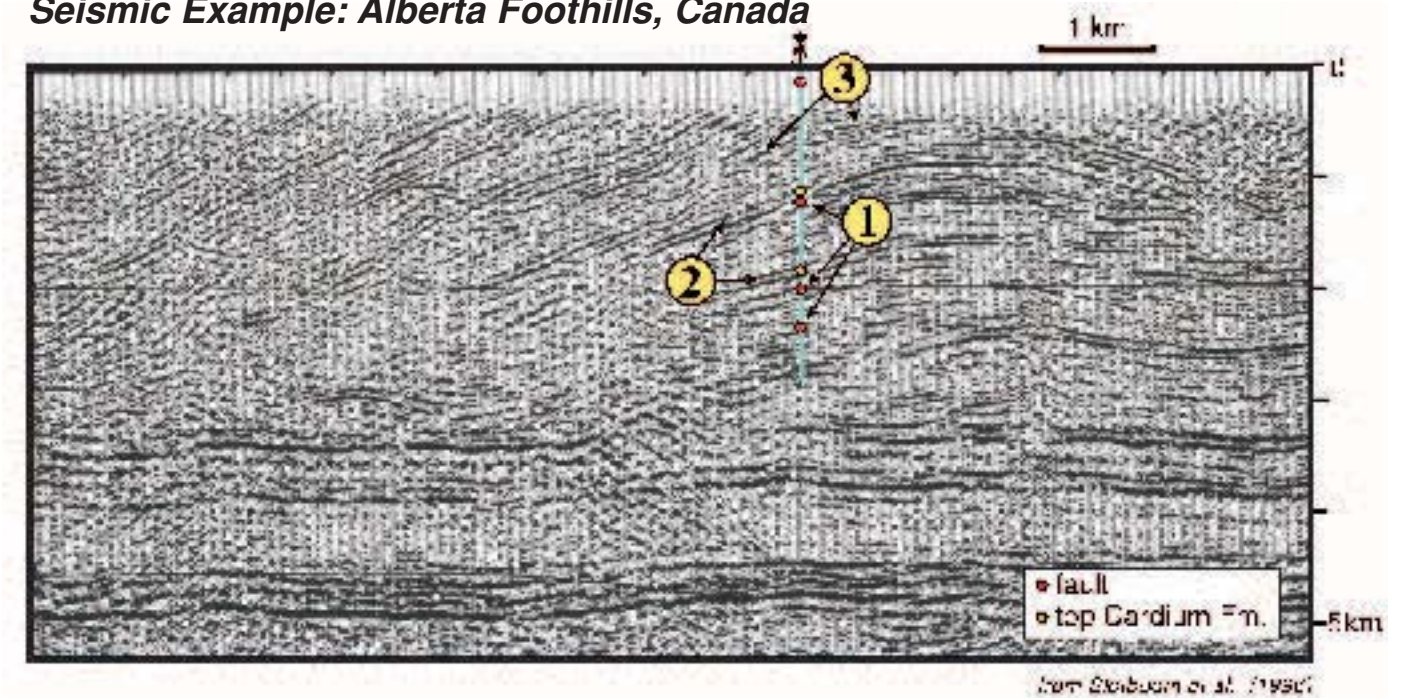
Seismic Example: Niger Delta, Nigeria
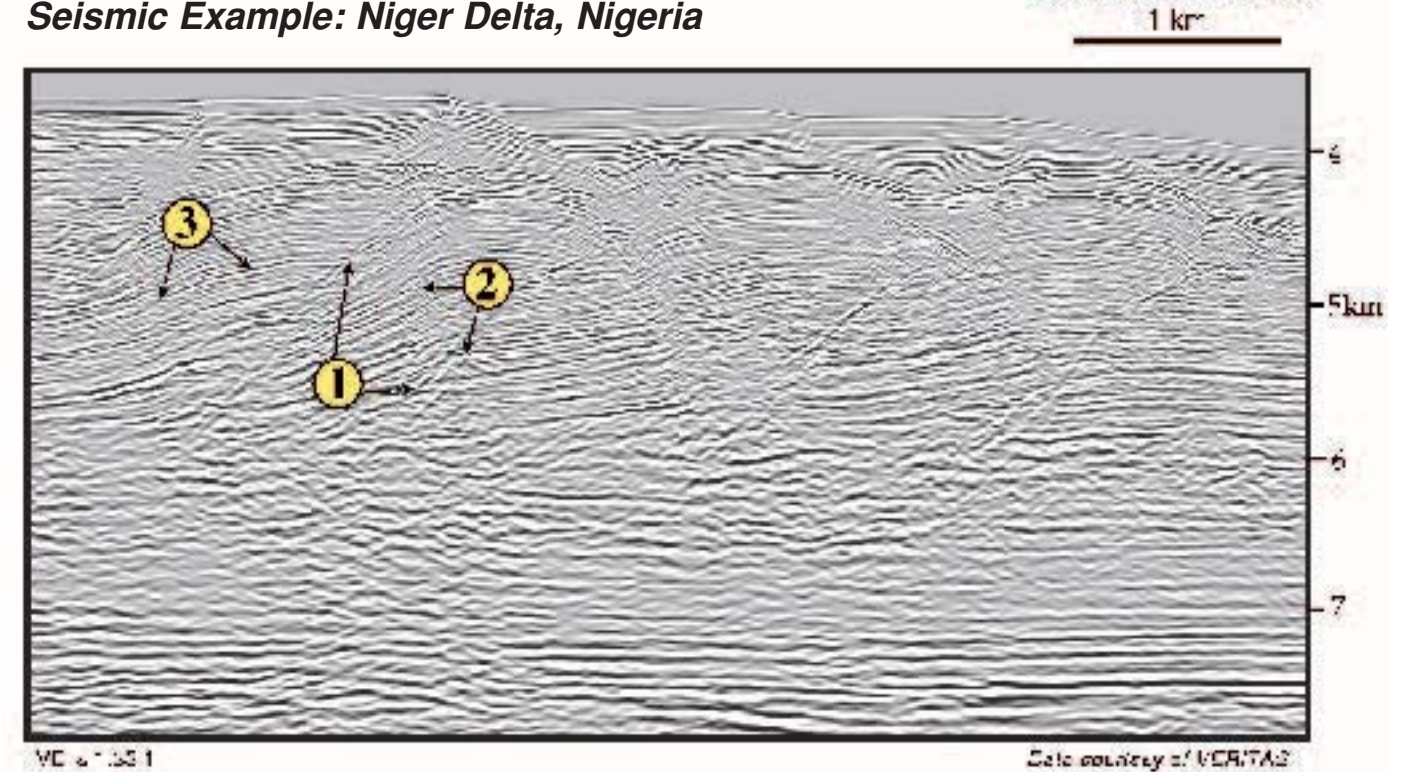
These seismic sections show the three common characteristics described in the model at left, including (1) multiple ramps, (2) changes in bedding dip across ramps, and (3) multiple dip domains in fold limbs

Interpreting break-forward imbricate structures using fault-bend fold theory

Suppe (1983) presents a strategy for interpreting break-forward imbricate structures based on the fact that each lower imbricate increases the dips in the overlying imbricates by fixed or *quantum* amounts that are predictable using fault-bend fold theory. Here we assume that bed-length and thickness are conserved and that all faults step up from a detachment at the same initial step-up angle (ramp dip). This section describes how to implement this approach to interpret imbricate structures imaged in seismic sections.

Theory

Imbricate fault-bend fold theory describes the increases in dip order caused by refolding of shallow thrust sheets by younger and deeper faults. In model 0, with a single thrust ramp A, the forelimb and back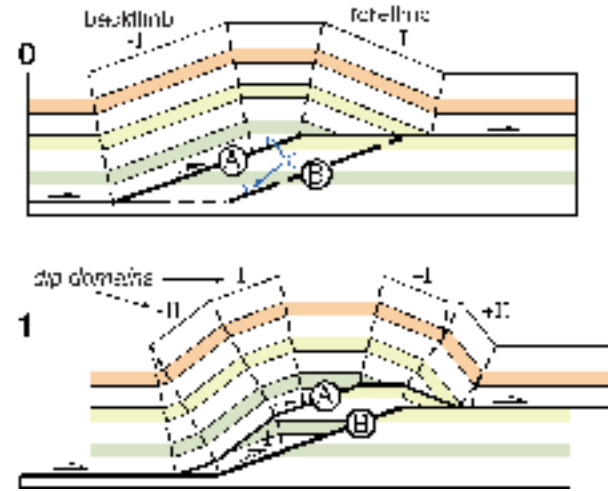limb dip values are first order (-I and +I), because each limb was formed by strata passing over a single fault bend. Incipient thrust B is shown in the footwall of thrust A. In model 1, slip on fault B refolds the shallow thrust sheet, producing second order (-II and +II) dip panels. These second order panels were folded once by thrust A, and again by thrust B. The dips of the forelimb and backlimb panels (-I, +I, -II, and +II) are prescribed by fault-bend fold theory based on the initial cutoff angles (θ).


Forelimb and backlimb dip values are based on the initial cutoff angle (θ) and the number of imbricated thrusts. This table shows the prescribed forelimb and backlimb dips for first- through seventh-order (I-VII) panels based on 8 to 24° fundamental cutoff angles. The order of the dip panel (I-VII) generally corresponds to the number of imbricated faults.

Dip panels are typically measured on seismic sections, and then compared with rows of prescribed values. If a general match between observed and prescribed dip values is obtained, then the structure can be interpreted using this table. If a match is not obtained, it may suggest that the initial cutoff angles of the ramps are not equal, requiring use of values different that those on this table (see Mount et al., 1990). These more complex situations can be interpreted using the folding vector technique presented on the next page.

Dip values measured on seismic profile
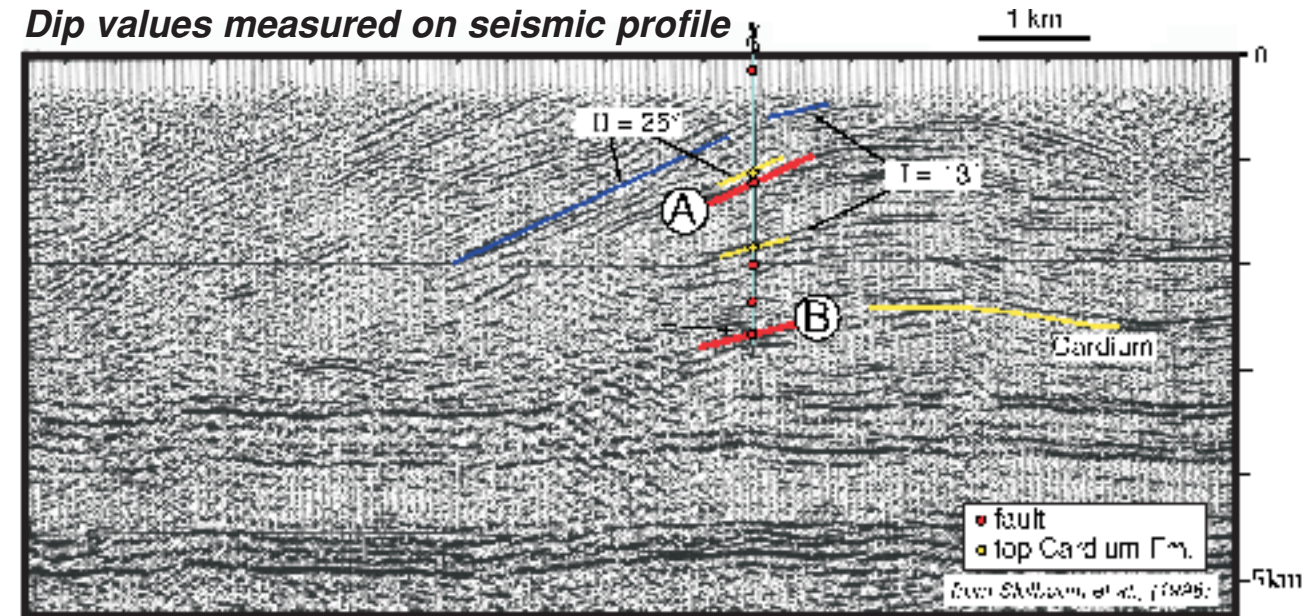
Two backlimb dip values are observed in this seismic section near the well. The lesser value (-I = 13°) occurs between faults A and B, and in the hanging wall of fault A to the right of the well. The steeper value (-II = 25°) is restricted to the hanging wall of fault A. These two backlimb dip values are compared with the values shown in the table at lower left, to determine if they are consistent with imbricate fault-bend fold theory.

Interpreted section
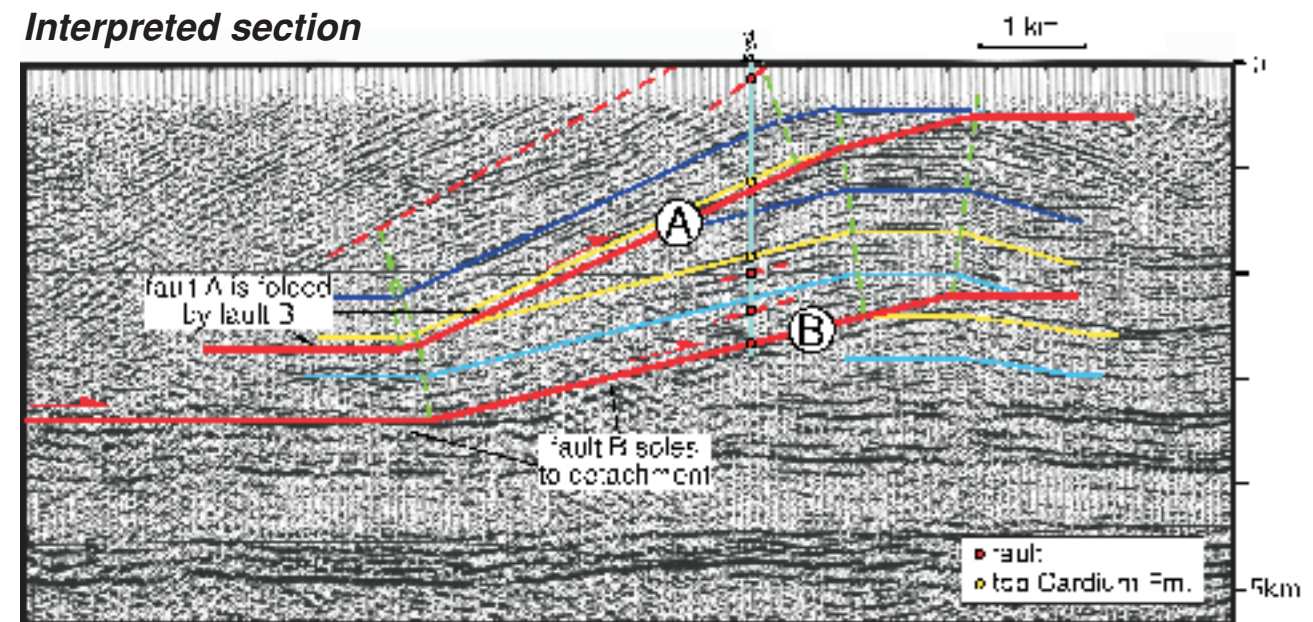
The two backlimb dip values (-I = 13° and -II = 25°) correspond to a 13° initial cutoff angle based on the table at left (see row highlighted in yellow). Thus, the geometries of faults A and B can be interpreted as part of a break-forward thrust sequence. The lower fault (B) dips at 13°, corresponding to the prescribed initial cutoff angle. It shallows to upper and lower detachments based on simple fault-bend fold theory (see section 1B-1) with θ = φ = 13°. The upper fault (A) dips at the second-order value (-II = 25°) where it lies above the backlimb kink band formed by fault B. Where fault A extends beyond the underlying backlimb kink band, it dips at -I = 13°, corresponding to the prescribed initial cutoff angle. The geometries prescribed by the table match the reflection patterns closely. Note, however, that other faults in the section further complicate some aspects of the geometry.

Interpreting break-forward imbricate structures using folding vectors

Here we describe a method of interpreting break-forward imbricate structures using *folding vectors* (Shaw et al., 1999). This method can be applied to a wide range of structures, including imbricate systems where initial cutoff angles of faults vary, bed thickness changes occur, or faults do not sole to detachments. Folding vectors describe the relative displacement of bedding or other surfaces, such as faults, across a fold limb or kink band. Thus, folding vectors can be used to describe the refolding of overlying thrust sheets due to imbrication. In this section, we describe how to determine folding vectors and use them to interpret a break-forward imbricate structure imaged in a seismic section.

Using folding vectors

To describe how folding vectors are used to interpret break-forward imbricate structures, we will consider the case of a shallow thrust sheet (above fault A) being refolded by a deeper thrust (B). In model 1, slip on the deep thrust B has produced a backlimb kink band that must refold the overlying thrust sheet (A). Hence, the orientation of fault A, and beds in its hanging wall, will change as the thrust sheet passes over the underlying kink band. In model 2, the deflection of bedding across the deep kink band is used to determine the folding vector (U). Folding vectors are measured parallel to axial surface orientations. The deflection of thrust A across the deep kink band is described by vector X, which is equal to the folding vector U. This results in shear, and hence line length, being preserved parallel to the axial surface orientation. The orientation of bedding that is refolded in the hanging wall of fault A can be determined using fault-bend fold theory (see section 1B-1), or by using folding vectors as shown in model 3. However, in this (and perhaps many) cases, the axial surface orientation changes between the footwall and hanging wall of fault A because bed dips change. Thus, the new hanging wall axial surface orientation must be used to measure a new folding vector (Y), which is equal to the deflection of fault A. This folding vector, in turn, equals the deflection of bedding in the hanging wall of fault A that is described by vector Z.

This method also applies in cases where axial surfaces do not bisect interlimb angles, and thus bed thickness is not preserved. In all cases, however, proper use of folding vectors results in area-balanced interpretations.

Note: This method can also be used to model the folding of angular unconformities, sedimentary growth wedges, and other cases where bed dips within a kink band are not parallel.
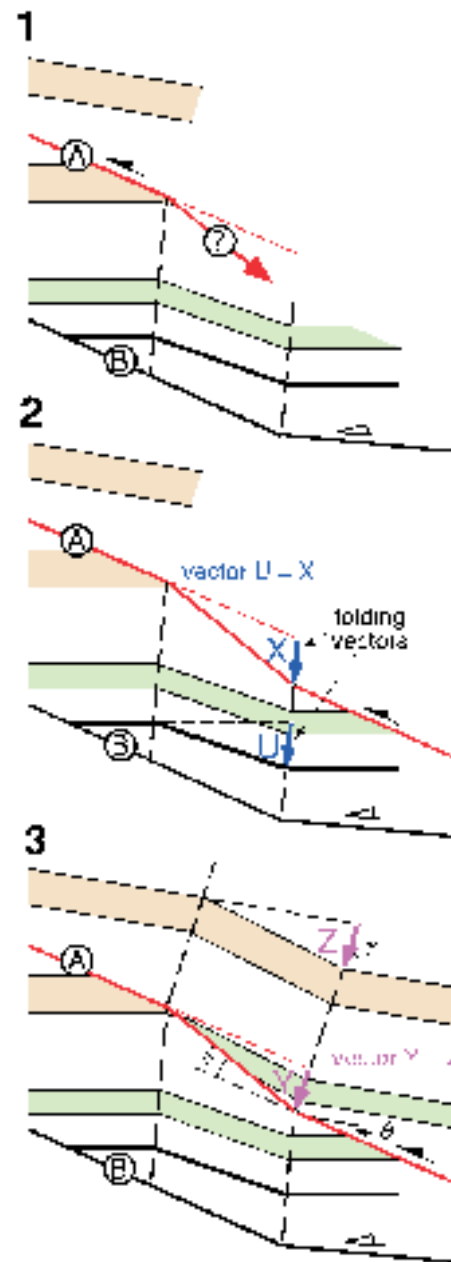
The folding vector method is used to interpret this seismic section, in which fault A is refolded by an underlying kink band bounded by axial surface S′. Fault A enters the left side of the kink band at a dip of 22°. The folding vector U is measured as the deflection of a bed* across axial surface S′ in the footwall of fault A.

*Note that folding vectors must be measured parallel to, but not necessarily along, axial surfaces. In this case, the paired axial surface corresponding to S′ is located off the right side of the section, so the folding vector is measured at an arbitrary point in the direction parallel to axial surface S′.

The folding vector U is then used to predict the deflection of the fault (A) across the kink band (U = X). The predicted fault position is consistent with reflection terminations that appear to represent fault cutoffs. Moreover, the folded fault dips about 30°, roughly parallel to beds in the overlying kink band (T-T′).

Measuring a folding vector
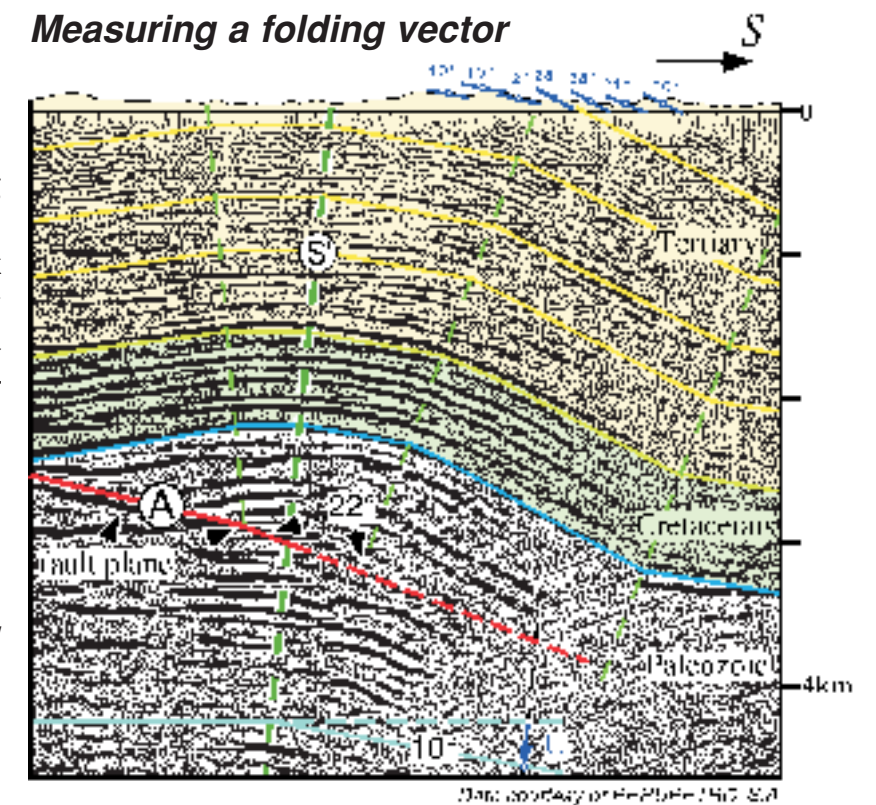
Interpreting a folded thrust

Recognizing break-back thrusting

This section describes fault and fold patterns that are common in break-backward imbricate structures, and shows examples in seismic sections.

Patterns of fault cutting older fold limbs

To describe structural patterns common in break-back imbricate structures, we will consider some simple patterns for a shallow, break-backward thrust ramp (model A1) and detachment (model A2) cutting across a fold limb (S-S') related to an older and deeper thrust. The shallow thrust ramp may cut across and offset a part of the fold limb without changing fault orientation (model B1). Alternatively, the shallow thrust could change its orientation across the fold limb, offsetting and refolding parts of the structure (model C1). In the case of model C1, note that the deep folding vector (U) need not equal the deflection of the break-backward thrust (X), in contrast to the break-forward example described on the previous page. In the case of the detachment, the shallow fault could follow bedding planes across the fold limb (model B2). Based on fault-bend fold theory (Suppe, 1983), slip on this shallow detachment would not modify the fold shape. Alternatively, the shallow detachment could follow bedding across the fold limb but cut up section beyond the fold (model C2). In this case the shallow fault conforms to one axial surface and offsets the other.
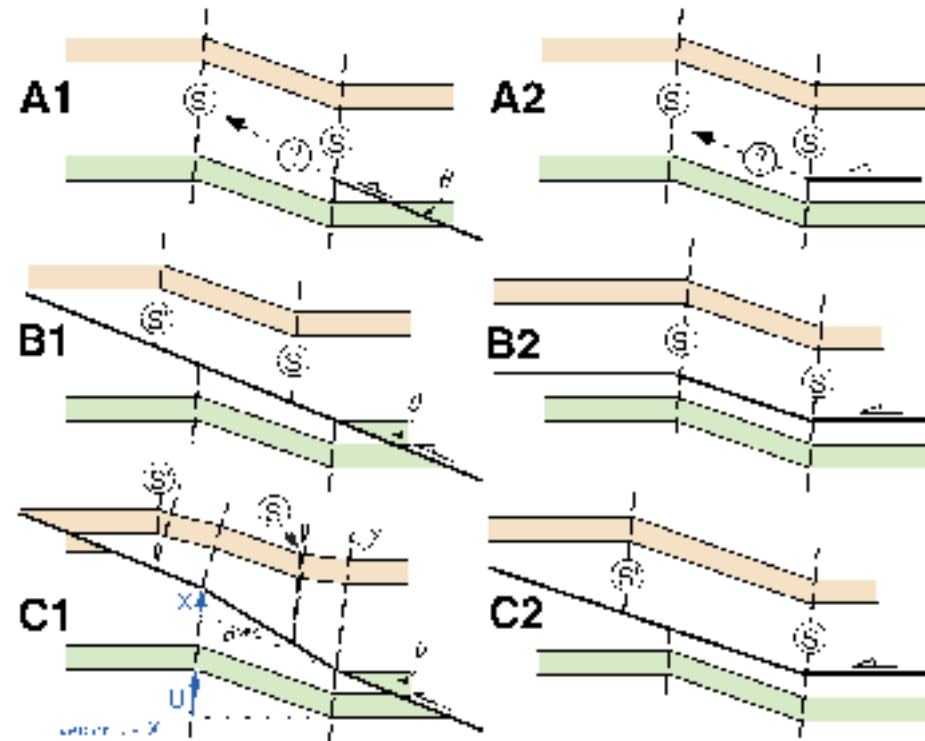
Patterns in models B1 and C1 are generally diagnostic of break-backward imbricate thrusting. However, patterns in models B2 and C2 are more ambiguous. A detachment that conforms to bedding across a fold, as in model B2, can be either a break-backward fault that followed bedding planes or a folded detachment. Similarly, the pattern shown in model C2 reflects break-backward thrusting only if the offset axial surface is considered active (i.e., it is pinned to a bend or tip of the underlying thrust). In contrast, if the offset axial surface is inactive (S'), then the pattern may reflect either break-backward thrusting or coeval motions on the deep and shallow faults. Thus, some patterns are diagnostic of thrusting sequence while others are not. Care should always be taken in interpreting thrusting sequence based on fault and fold shapes.

Patterns of break-backward thrusting in seismic data

These seismic sections show patterns that reflect thrusting sequence. In section A, axial surface S terminates upward into a thrust that is overlain by gently dipping strata. This pattern is comparable to that shown in model B1 (*at left*) and reflects break-back thrusting. In sections B and C, axial surfaces S' are offset by shallow thrust faults. These patterns are comparable to model C2 (*at left*) and are consistent with break-backward or coeval, but not break-forward, thrusting.

A: Permian Basin, Texas, U.S.A.

B: Peruvian Andes

C: La Puna, Argentina
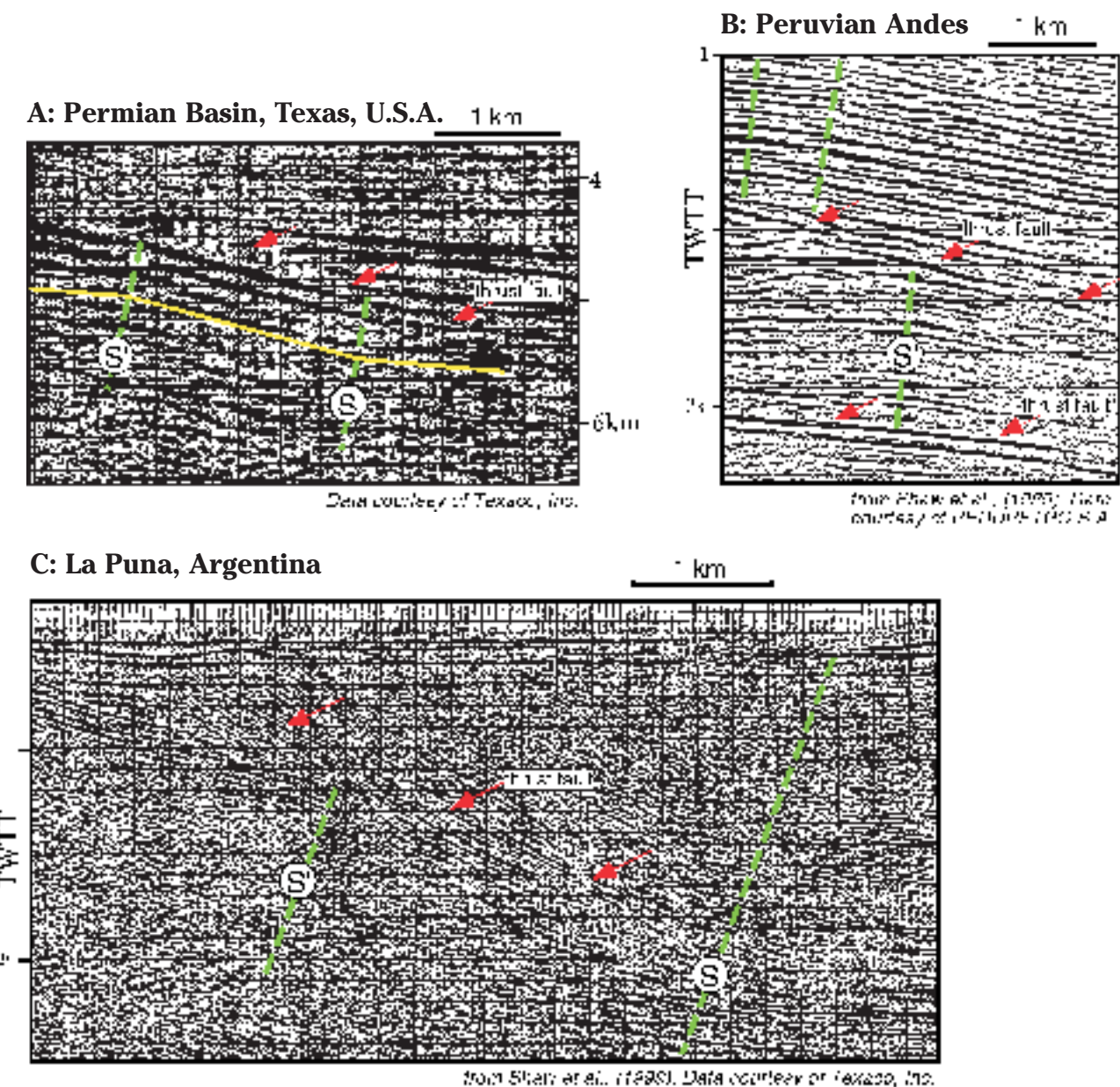
Determining thrusting sequence using growth strata

Growth strata can be used to determine the thrusting sequence in cases where two or more growth structures can be related to separate faults. Associating growth structures with specific faults can be difficult in cases where thrust sheets are everywhere vertically superimposed, but it is straightforward where faults are separated, at least in part, horizontally. This section presents seismic profiles with examples of break-forward and break-back thrust systems interpreted using growth strata.

These seismic sections both image two faults (X and Y) that are separated horizontally at shallow levels, but vertically overlap one another at depth. In section A, the fold associated with fault Y does not deform, and thus pre-dates, the annotated horizon. The fold related to fault X clearly deforms, and thus post-dates this horizon, reflecting a break-forward thrusting sequence. In section B, the fold associated with fault X does not deform, and thus pre-dates, the annotated horizon. The fold related to fault Y clearly deforms, and thus post-dates, this horizon, reflecting a break-backward thrusting sequence. Both seismic images are from the deepwater Niger Delta, Nigeria.
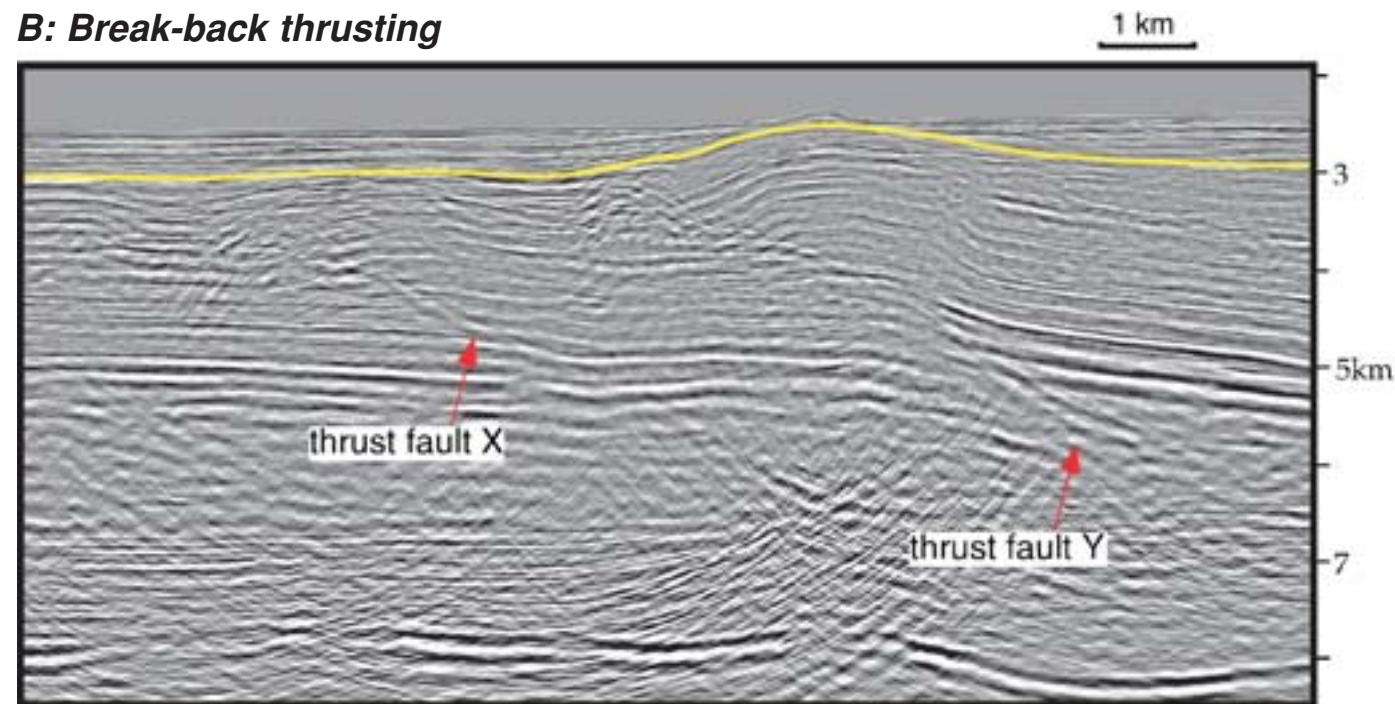
A: Break-forward thrusting

from Corredor et al., (2002). Data courtesy of VERITAS

B: Break-back thrusting
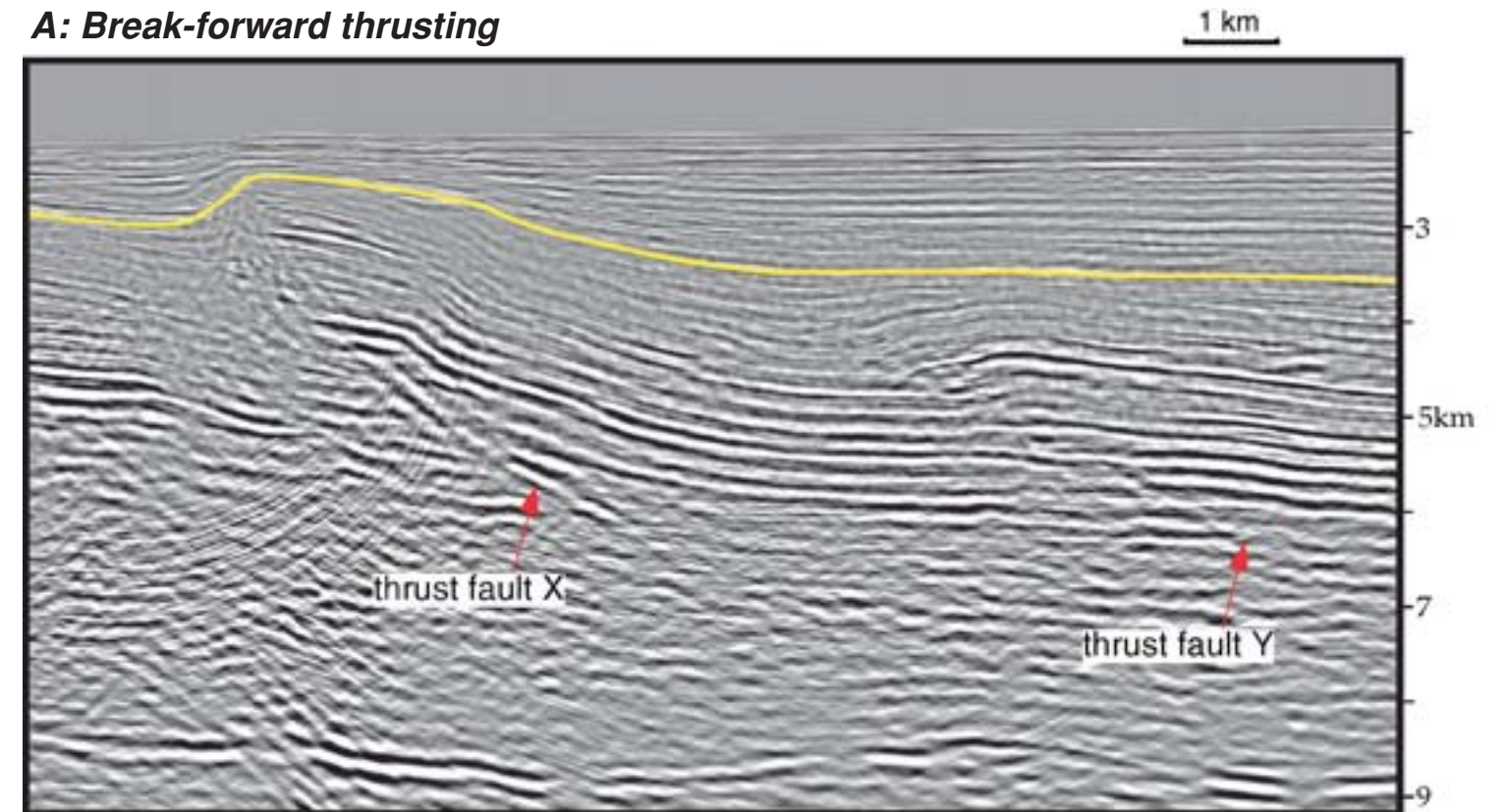
from Corredor et al., (2002). Data courtesy of VERITAS

1B-6: Structural wedges

Basic concept

Structural wedges contain two connected fault segments that bound a triangular, or wedge-shaped fault block. The two fault segments, which typically include two ramps or one ramp and one detachment, merge at the tip of the wedge. Slip on both faults accommodates propagation of the wedge tip and causes folding (Medwedeff, 1989). Wedges occur at a variety of scales. At large scales associated with mountain fronts, wedges are typically referred to as **triangle zones** (Gordy et al., 1975). In this section, we describe common types of wedges and illustrate how these structures are interpreted in seismic sections.

Conjugate faulting theory   Kinematic Model
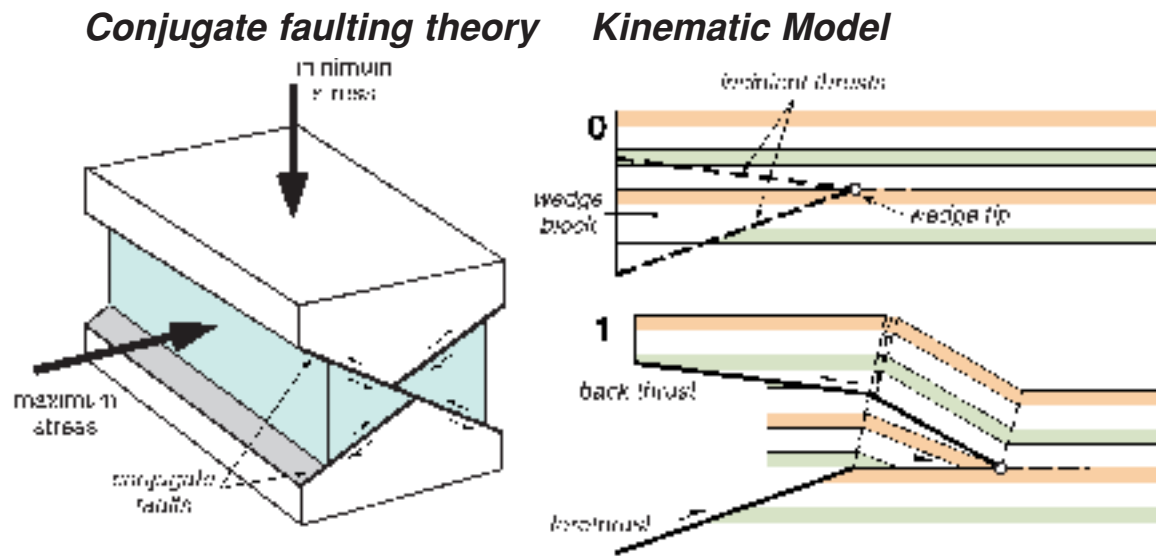

(above left) Brittle failure of rocks in compression commonly leads to the development of two conjugate thrust faults that dip in opposite directions (Anderson, 1942). Planes of weakness, such as bedding, can also lead to the development of detachments. In cross section *(above right)*, two conjugate thrusts bound a wedge-shaped fault block and merge at the wedge tip (model 0). Slip on both bounding faults causing propagation of the wedge (model 1). In this case, the wedge propagates along a detachment, and causes folding of the hanging wall block. The lower thrust is commonly referred to as the *forethrust* or *sole thrust*, and the upper thrust is called the *back thrust* or *roof thrust* (Boyer and Elliot, 1982).

Common characteristics

Wedges exhibit a wide range of geometries. However, several characteristics are common to most wedge structure, including:

1) presence of coeval fore- and back-thrusts;

2) folding localized along an active axial surface pinned to the wedge tip; and

3) folds may exist in the footwall of the back thrust that produce structural relief.
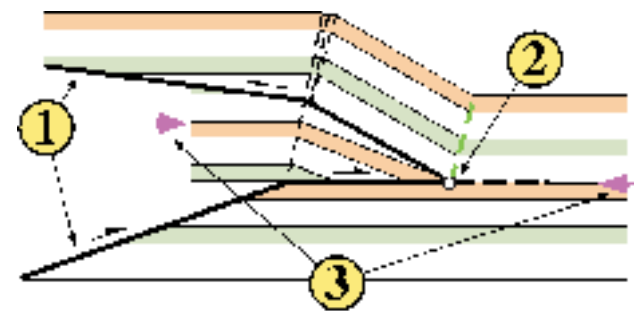
Examples

Field Example

Structural wedge in Carboniferous Rundle Formation, Front Ranges of the Canadian Rockies. Note the highly deformed rocks near the wedge tip. Several smaller wedges are contained within the larger wedge structure. (J. H. Shaw and F. Bilotti)

Seismic Example: Alberta Foothills, Canada
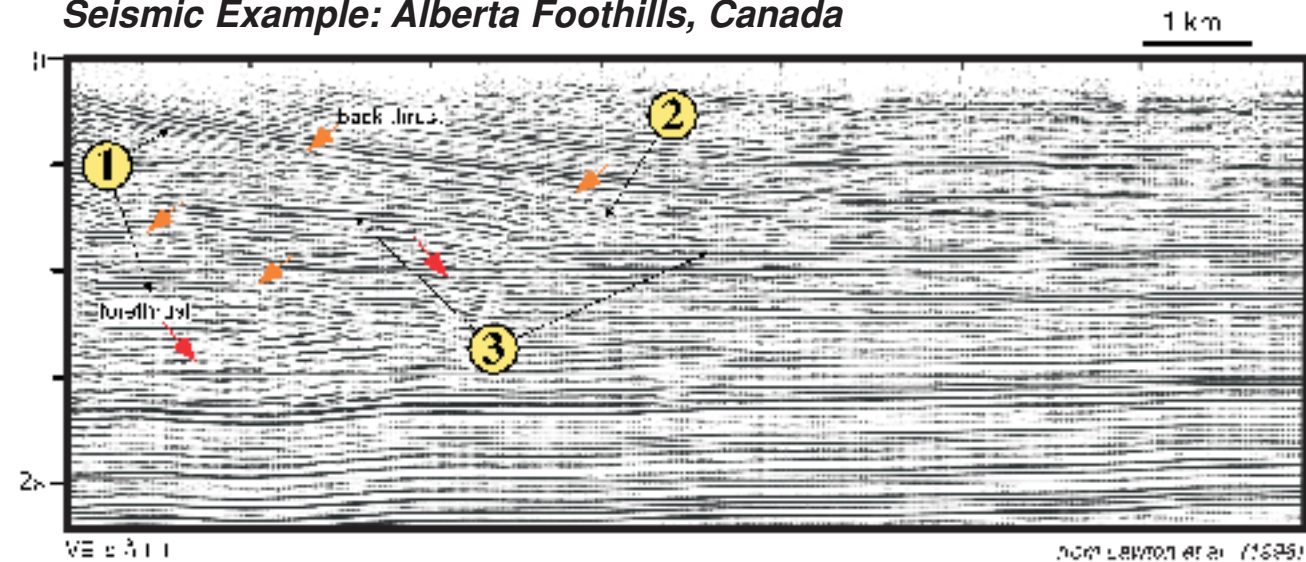
This seismic section images a large structural wedge, or *triangle zone*, at the eastern front of the Canadian Rocky Mountain fold and thrust belt. The common characteristics of structural wedges, (1–3) as described at left, are present in this structure. Note that a second, smaller back thrust is present within the main wedge block.

When the back or roof thrust and its hanging wall are gently tilted or warped, but not deformed to the extent exhibited within the wedge block, the term *passive roof thrust* is sometimes used. Passive roof thrusts are common in triangle zones, as shown in this example.

Wedge models developed using fault-bend fold theory

Structural wedges exhibit a variety of shapes and styles that reflect initial fault geometries, propagation direction, and folding mechanisms. In this section, we present a series of kinematic models that describe basic types of structural wedges governed by fault-bend fold theory (Suppe, 1983; Medwedeff, 1989; see section 1B-1). Models A through C involve detachments, whereas model D does not.

Detachment (decollement) wedges

A0, B0, C0, D0, A1, B1, C1, D1, A2, B2, C2, D2

inactive axial surface
active axial surface
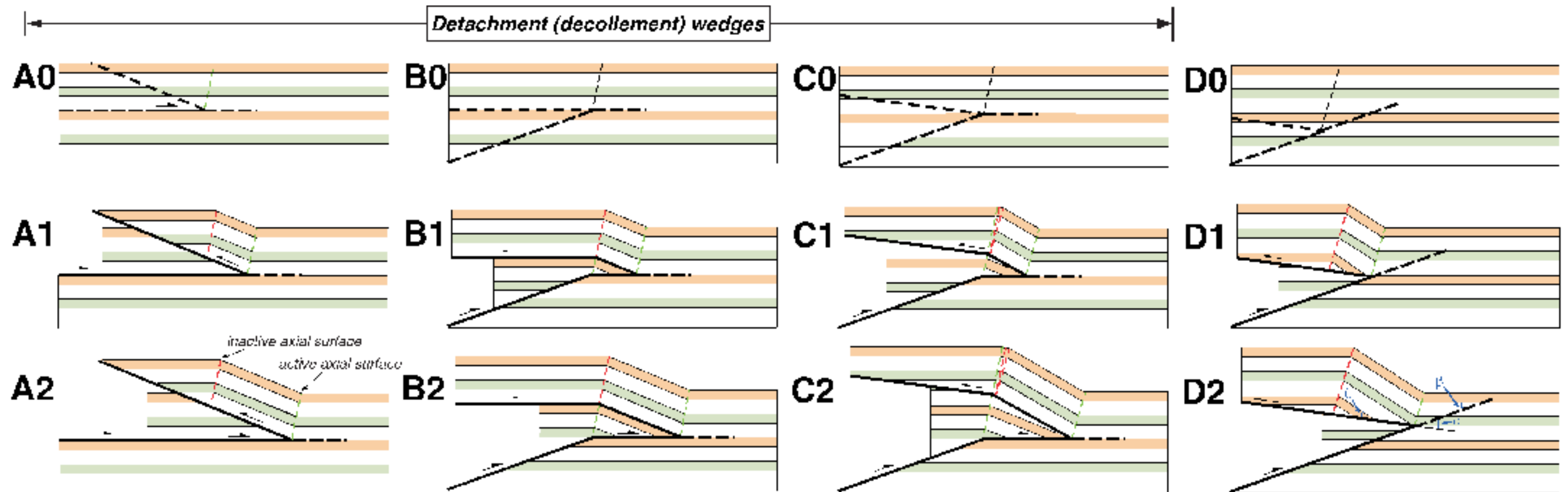
A (0–2): Simple wedge with a detachment and back thrust. Propagation of the wedge tip forms a kink band above the back thrust that is bounded by an active axial surface, which is pinned to the wedge tip. Strata in the kink band are parallel to the back thrust ($\beta = 0$) because the fault rises from a detachment ($\theta = 0$).

Note: green dashed lines are active axial surfaces, red dashed lines are inactive axial surfaces. See section 1B-1 for description.

B (0–2): Wedge with a lower forethrust ramp and an upper detachment that acts as the back thrust. With slip, the wedge tip propagates along the detachment surface. Strata within the wedge are folded in an anticlinal fault-bend fold that deforms the detachment or back thrust. A kink band develops above the back thrust with strata that are parallel to the underlying fault and fault-bend fold. The synclinal axial surface pinned to the wedge tip is active, as is the anticlinal axial surface within the wedge block. The anticlinal axial surface above the back thrust, however, is inactive.

C (0–2): Wedge formed by a dipping forethrust and back thrust. With slip, the wedge tip propagates along a detachment surface. Strata within the wedge are folded in an anticlinal fault-bend fold that deforms the back thrust. A kink band develops above the back thrust with strata that are parallel to the underlying fault, but that dip more steeply than the beds within the wedge block. Both the synclinal axial surface pinned to the wedge tip and the anticlinal axial surface pinned to the fault bends are active. The anticlinal axial surface in the hanging wall of the back thrust is active (in contrast to model B) because a small amount of strata is folded from the crest into limb, thus passing through the axial surface. These kinematics facilitate the conservation of bed length. Alternatively, a small amount of shear or bed-parallel extension could accommodate fault slip without moving strata from the fold crest into the limb.

D (0–2): Wedge formed by a dipping forethrust and back thrust. With slip, the wedge tip propagates along the trajectory of the forethrust. Strata within the wedge are not folded, as they do not pass over a fault bend. A kink band develops above the back thrust with strata that dip more steeply than the fault. The geometry of the kink band (θ) is governed by fault-bend fold theory (see section 1B-1), with ϕ equal to the acute angle between the back thrust and the propagation direction, and β as the hanging wall cutoff angle relative to the propagation direction.
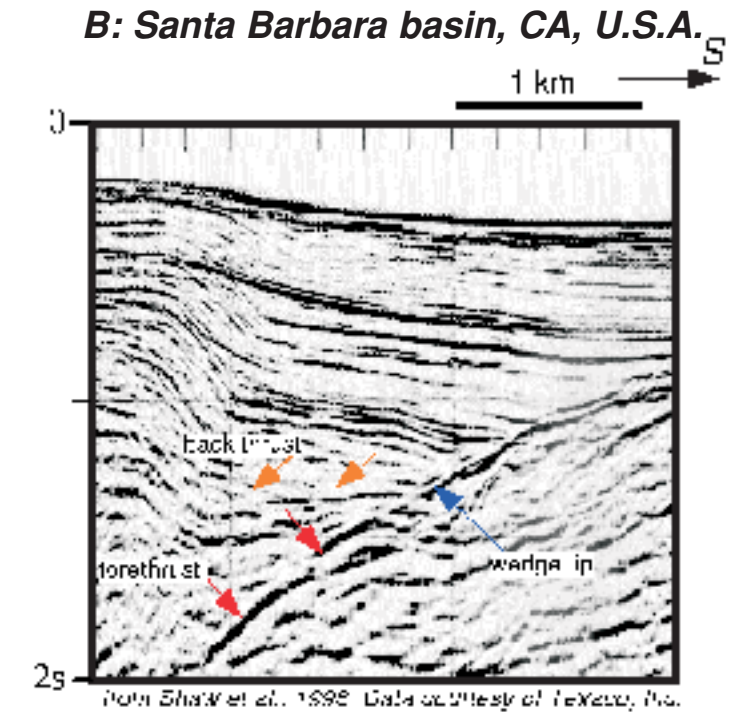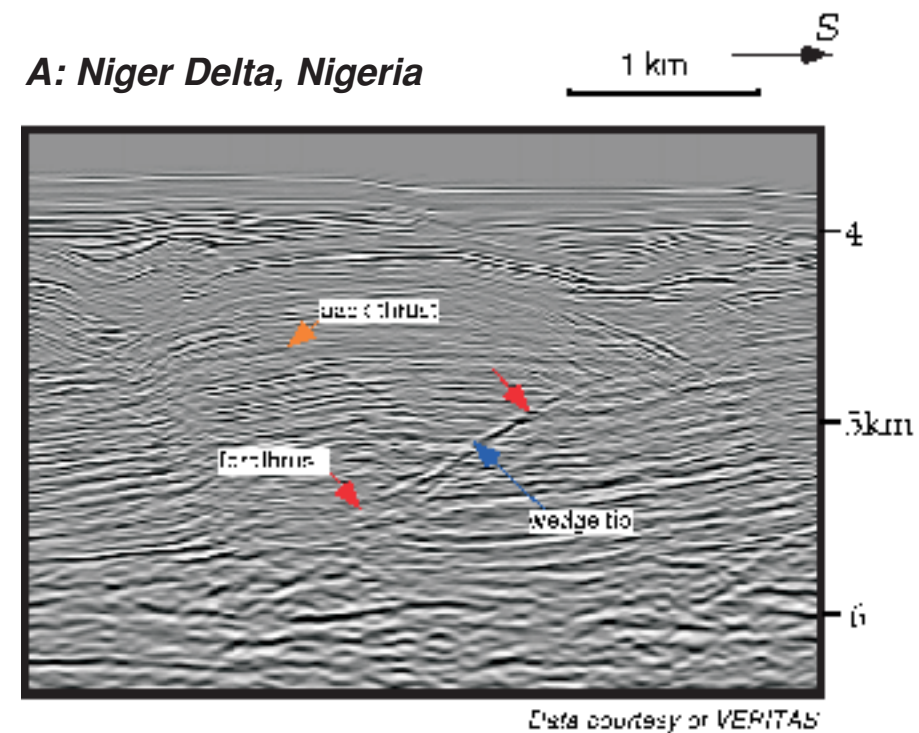
Note that in this wedge the roof thrust locally cuts down the stratigraphic section as it extends upward. This is an unusual relationship for thrust faults, but nevertheless may occur in non-decollement wedges.
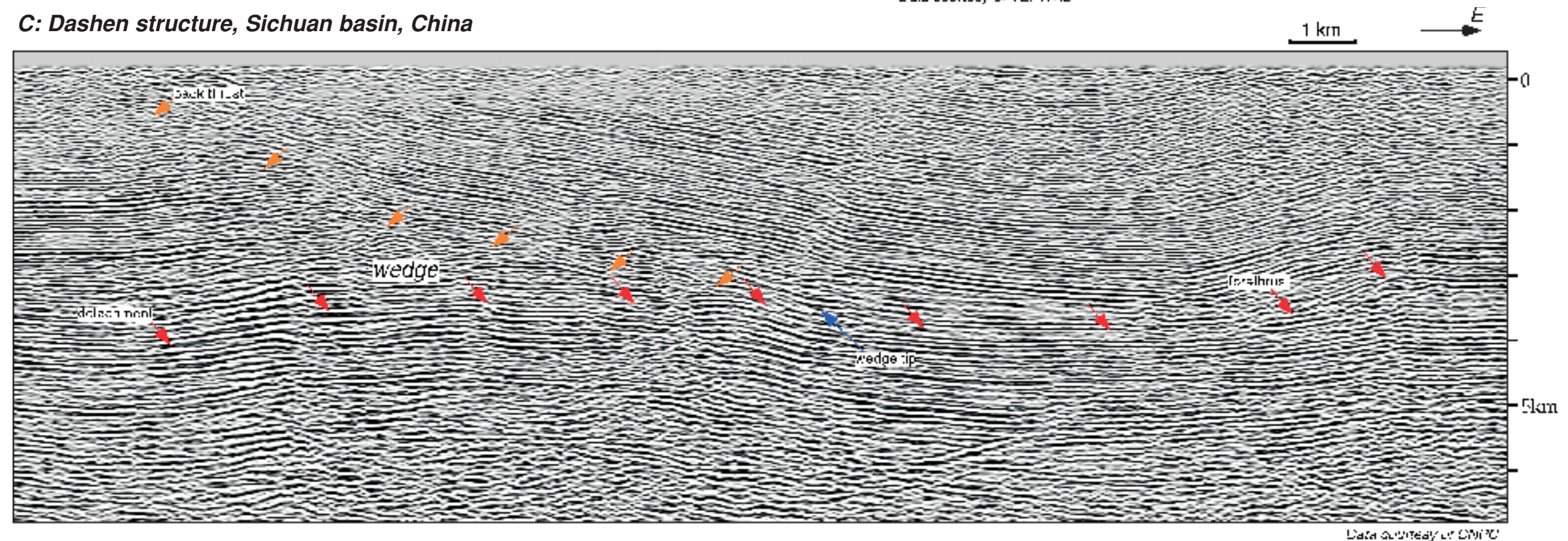
Seismic examples of structural wedges

Here we present examples of structural wedges imaged in seismic reflection data.

Section A images a simple structural wedge that involves a back thrust extending upward from a forethrust ramp. The wedge tip propagation direction is along the path of the forethrust. Note that in this case, the back thrust has very little displacement relative to the forethrust. Section B images a wedge comprised of a gently dipping back thrust that extends from a forethrust ramp. The wedge propagation direction is along the path of the forethrust, which corresponds with an angular unconformity. Folding at the wedge tip is consistent with the pattern displayed in model D on the previous page. Section C images a complex structural wedge comprised of a back thrust extending upward from a folded detachment similar to model A on the previous page. The detachment level is constrained by the discordance of strata and the base of the thrust ramp located east of the wedge tip. The wedge structure, including the detachment, overlies an anticline that is related to a deeper level of faulting.

A: Niger Delta, Nigeria

Data courtesy of VERITAS

B: Santa Barbara basin, CA, U.S.A.

From Shaw et al., 1996. Data courtesy of Texaco, Inc.

C: Dashen structure, Sichuan basin, China

Data courtesy of CNPC

Growth structure in wedges

This section describes growth structures above wedges that are modeled using fault-bend fold theory, after Medwedeff (1989). Growth structures can be very helpful in distinguishing structural wedges from other types of fault-related folds.

Kinematic models
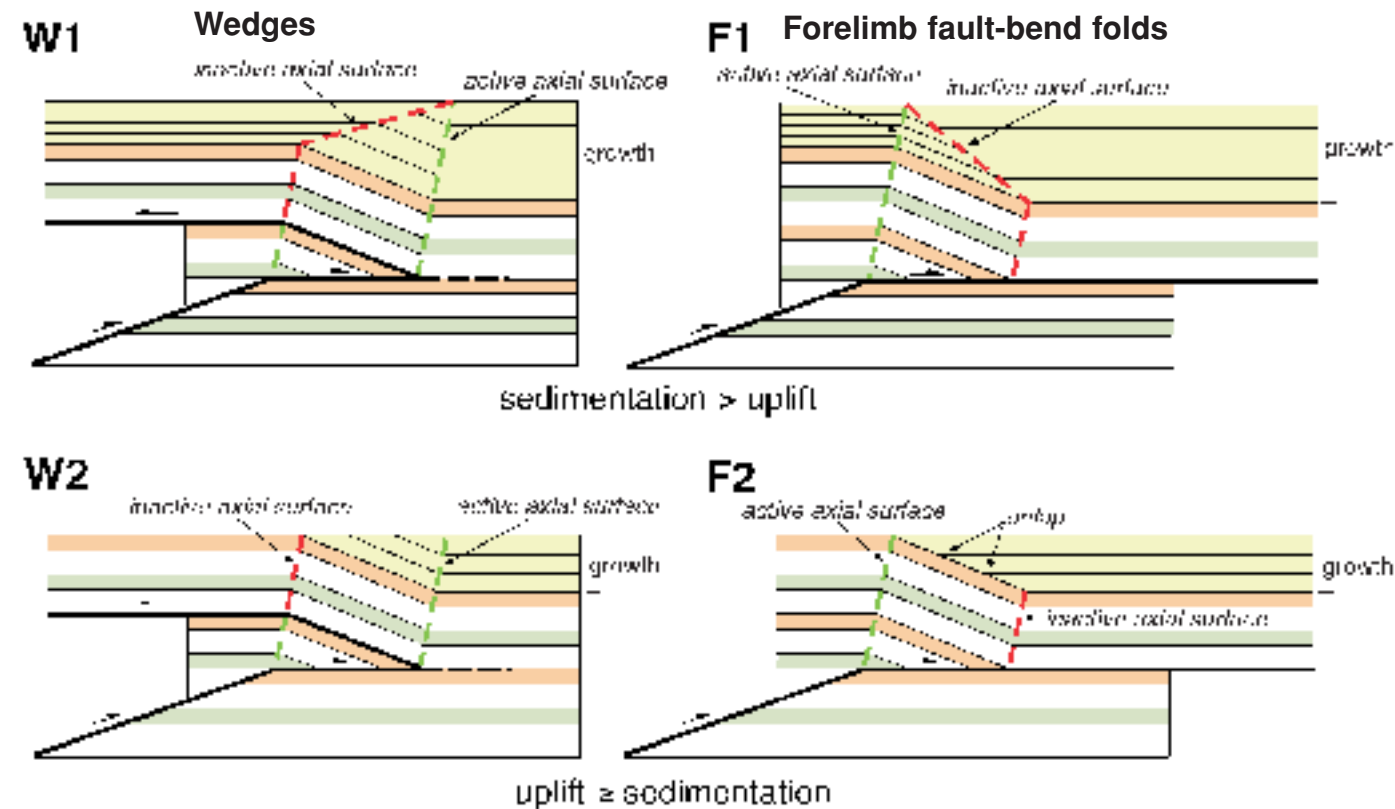
In wedges that are governed by fault-bend fold theory (see section 1B-1), folds grow by kink-band migration. Folding generally occurs along an active axial surface that is pinned to the propagating wedge tip. In cases where sedimentation rate exceeds uplift rate, syntectonic strata form growth triangles above the wedge tip that are bounded by a planar synclinal (active) axial surface and a curved anticlinal (inactive) axial surface (model W1). In contrast, simple forelimb fault-bend folds have growth triangles bound by a curved synclinal (inactive) axial surface and a planar anticlinal (active) axial surface (model F1). In cases where uplift rate exceeds sedimentation rate, the contrast between wedges and simple fault-bend folds is even more distinct. In a structural wedge, growth strata are folded about an active synclinal axial surface and are parallel to the underlying forelimb dip (model W2). In contrast, syntectonic strata are not folded above the forelimb of a simple fault-bend fold (model F2), because they have not passed through an active axial surface. Growth strata, therefore, are horizontal, or maintain a primary sedimentary dip, and onlap the forelimb.

(right) This seismic section images a structure with characteristics of a growth wedge. The structure consists of a forelimb developed above a south-dipping forethrust. Growth strata thin onto the crest of the structure, and are folded above the forelimb. The synclinal axial surface is roughly planar and folds the growth strata. In contrast, the anticlinal axial surface is curved, with an abrupt change in orientation at the contact between pre-growth and growth strata. Based on this growth pattern, which is similar to model W1 above, the structure is interpreted as a wedge. (For more details on this interpretation, see Shaw and Brennan, section 2-23, this volume).

Seismic Example: Sumatra, Indonesia

Interpreted section
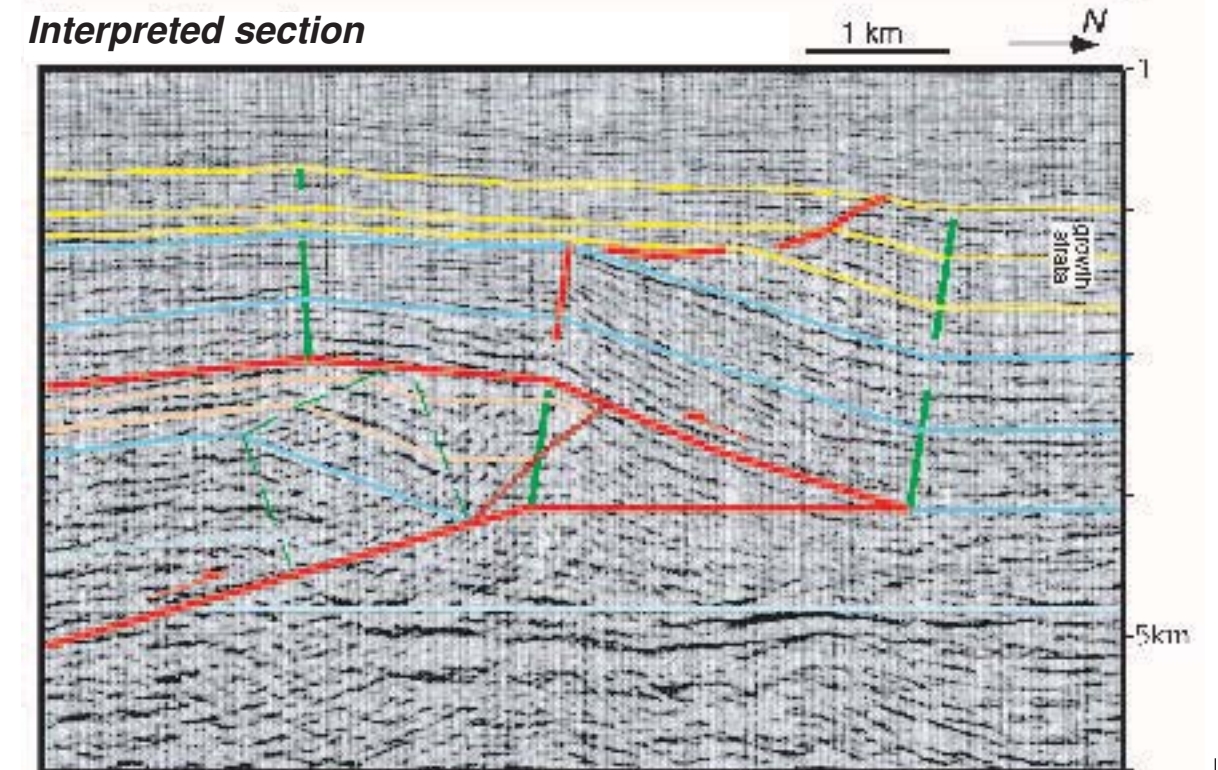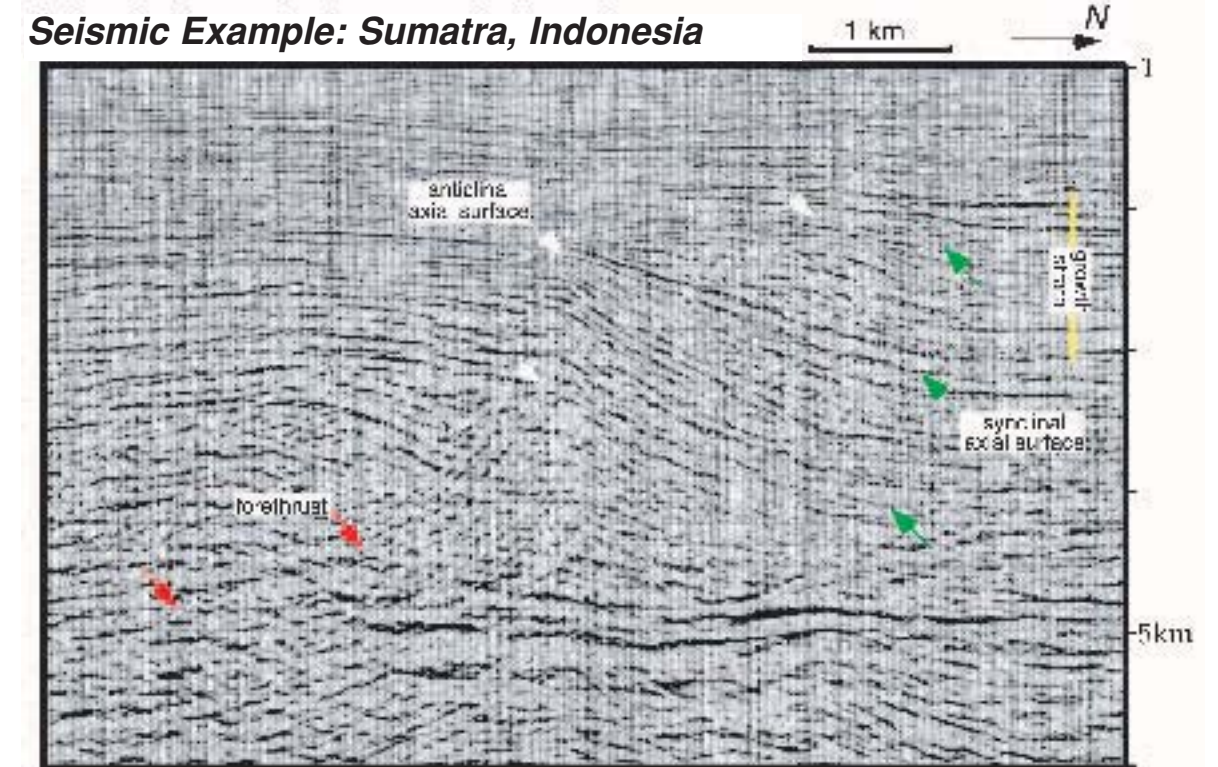
Shaw et al., 1997. Data courtesy of CALTEX

Shear fault-bend fold wedges

Structural wedges can form with non-flexural-slip components of deformation, resulting in fold geometries that differ from those presented on the previous pages. Here, we describe a class of these wedges that form by shear fault-bend folding (Suppe et al., 2004; see section 1B-4), and show an example in a seismic section.

Kinematic models
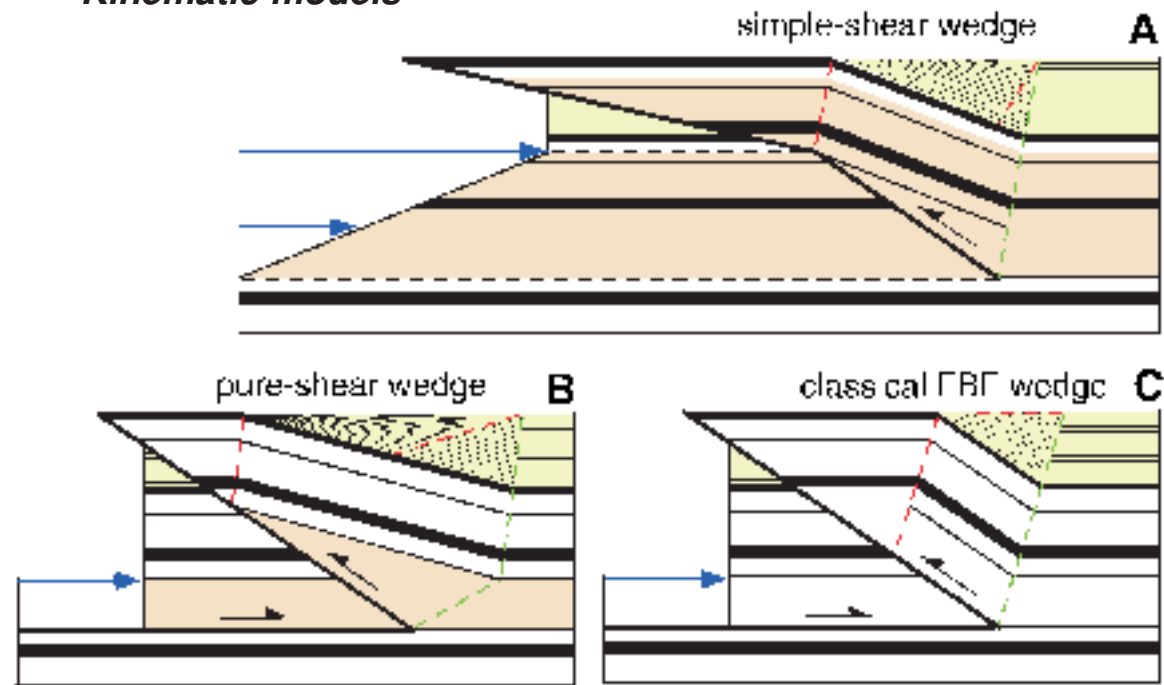
Simple-shear wedges (model A) have shear in the footwall of the back thrust. This shear folds, and induces slip, on the fault, producing a forelimb that is similar to the back-limb fold produced by the forward-thrust, simple-shear fault-bend fold equivalent (see section 1B-4). In this model, growth strata are eroded above the fold crest. Pure-shear wedges (model B) have shear in the hanging wall of the back thrust that occurs as the wedge tip propagates. The back thrust is not folded, and slip produces a forelimb that is similar to the back-limb fold produced by the forward-thrust, pure-shear fault-bend fold equivalent (see section 1B-4). In both shear wedges, the forelimb beds dip less than the underlying back thrust, and the growth structures record folding by a combination of limb rotation and kink-band migration (see section 1A-5). In contrast, classical fault-bend fold wedges (model C) generally have hanging wall beds that are parallel to the back thrust, and growth structures that record folding dominantly by kink-band migration.

Seismic example: Niger Delta, Nigeria

from Corredor et al., (2002). Data courtesy of VERITAS
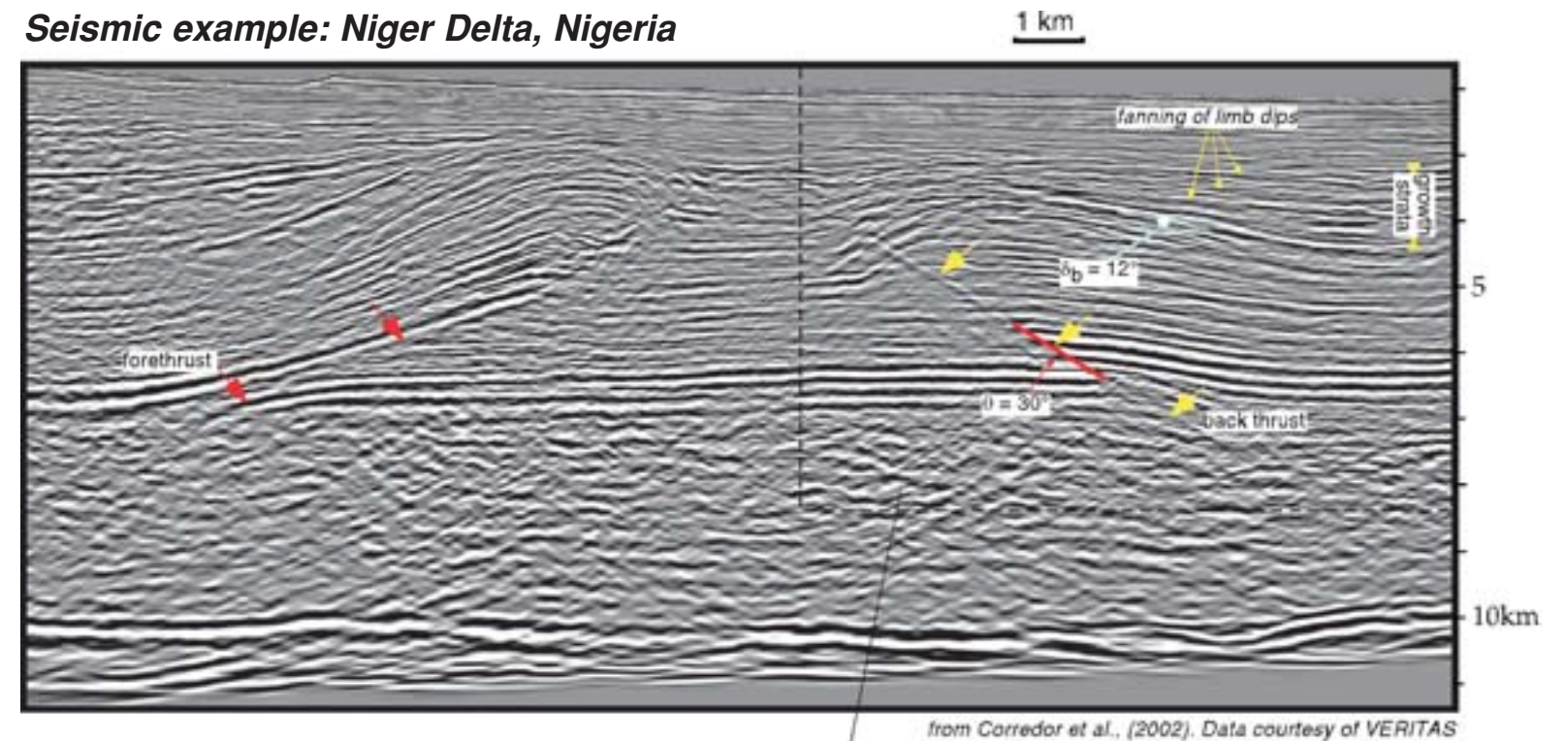
The seismic section shown above images two thrust ramps rising from a detachment. The ramp on the left dips in the same direction as the majority of faults in the region, and thus is considered a forethrust. The ramp on the right is a back thrust. Slip on the back thrust produces a hanging wall structure that has the characteristics of a shear fault-bend fold. However, given that this is a back-thrust above a detachment, the structure is a shear wedge. Based on the fault cut-off angle (θ) and back-limb dip (δ_b), the structure is interpreted as a pure-shear wedge in the section shown at right. Based on shear fault-bend fold theory (Suppe et al., 2004, see section 1B-4), the fault cutoff angle and backlimb dip yield a 27° dip of the synclinal axial surface (ψ) in the basal layer and a shear angle (α) of 67°. Growth strata exhibit a fanning of limb dips that is consistent with the shear wedge interpretation.

Interpreted section
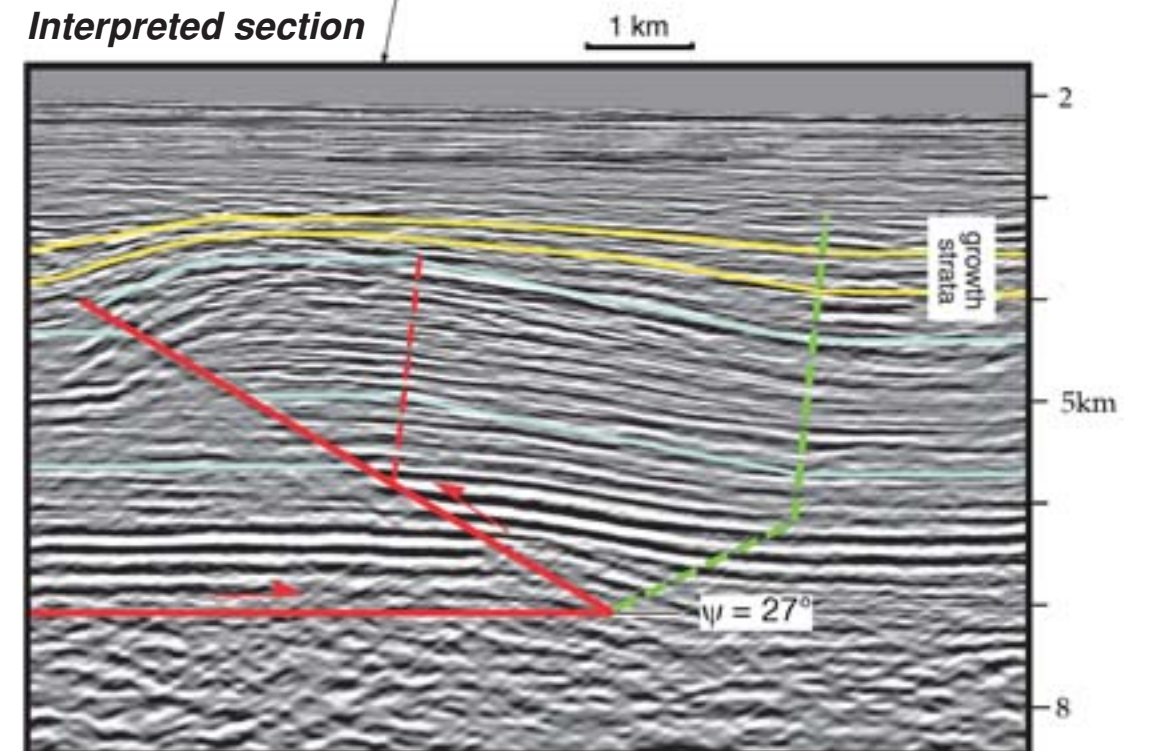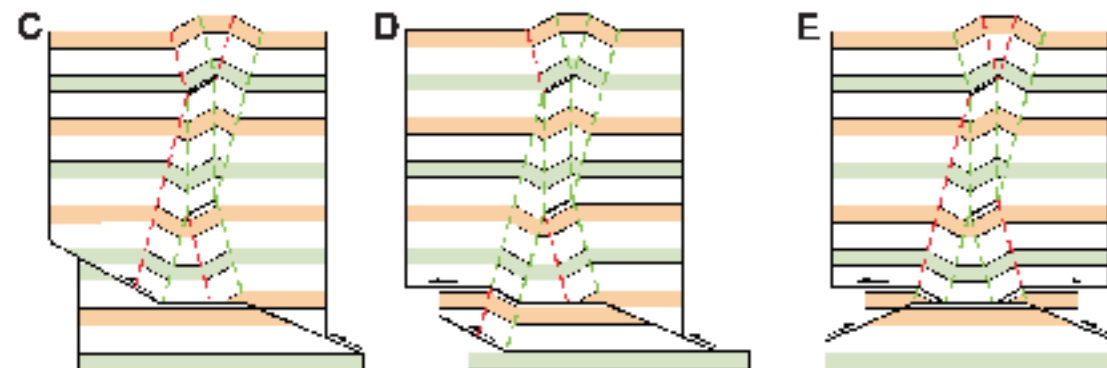
1B-7: Interference structures

Basic concept

Interference structures form when two or more monoclinal kink bands intersect, often yielding distinctive patterns in cross section with anticlines perched above synclines. Interference structures have been documented in the field and laboratory (e.g., Dewey, 1965; Paterson and Weiss, 1966; Stewart and Alvarez, 1991), and have been proposed as the origin of structures imaged in seismic profiles (e.g., Mount, 1989; Novoa et al., 1998; Camerlo et al., section 2-24, this volume). In this section, we describe a simple style of interference structure comprised of two kink bands with opposing dips, and present examples of these structures imaged in seismic sections.

Kinematic Models


Seismic Example: Gulf of Mexico, U.S.A.
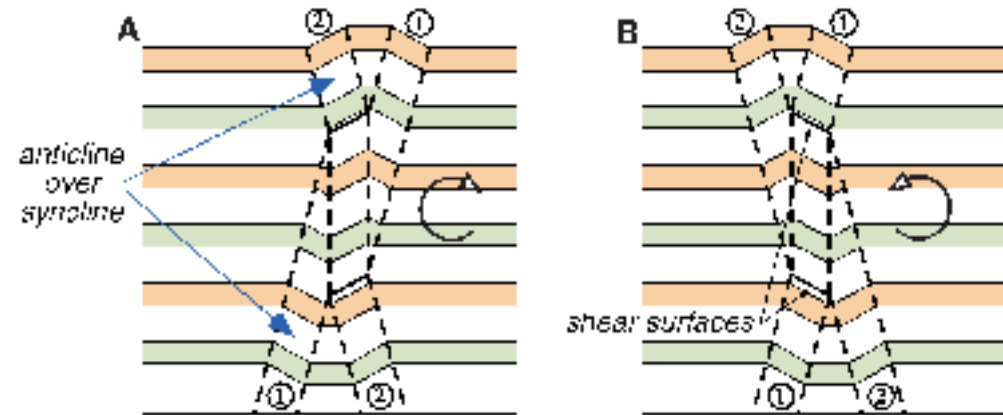
These models (A and B) illustrate interference structures formed by the intersection of two kink bands (1 and 2) that dip in opposite directions. Model A forms by clockwise shear of the through-going kink band (2), whereas model B forms by counter-clockwise shear of the through-going kink band (1). In both models the through-going kink band separates the other kink band into two pieces that are joined along two shear surfaces that are parallel to bedding. As a result, the shear surfaces connect points where the axial surfaces bifurcate. The axial surfaces in these models bisect the interlimb angles (see section 1A-1), and thus bed length and thickness are preserved. The most distinctive aspect of these structures is that they yield anticlines perched above synclines.

Kink-band interference can result from many different structural configurations, involving various types of fault-related folds (Mount, 1989; Medwedeff and Suppe, 1997; Novoa et al., 1998). These three models (C–E) illustrate general structural configurations that can yield kink-band interference. The interfering kink bands are developed: C) above two bends in the same fault; D) by imbrication of two faults; and E) as forelimbs developed above faults that dip in opposite directions. Note that the shallow fold geometries are identical in each of these models. Thus, the geometries of interference folds are not always diagnostic of the underlying fault configurations. The different structural configurations do, however, involve different patterns of active (green) and inactive (red) axial surfaces, which may, in some cases, be distinguished using growth structures (Novoa et al., 1998; see section 1A-3).
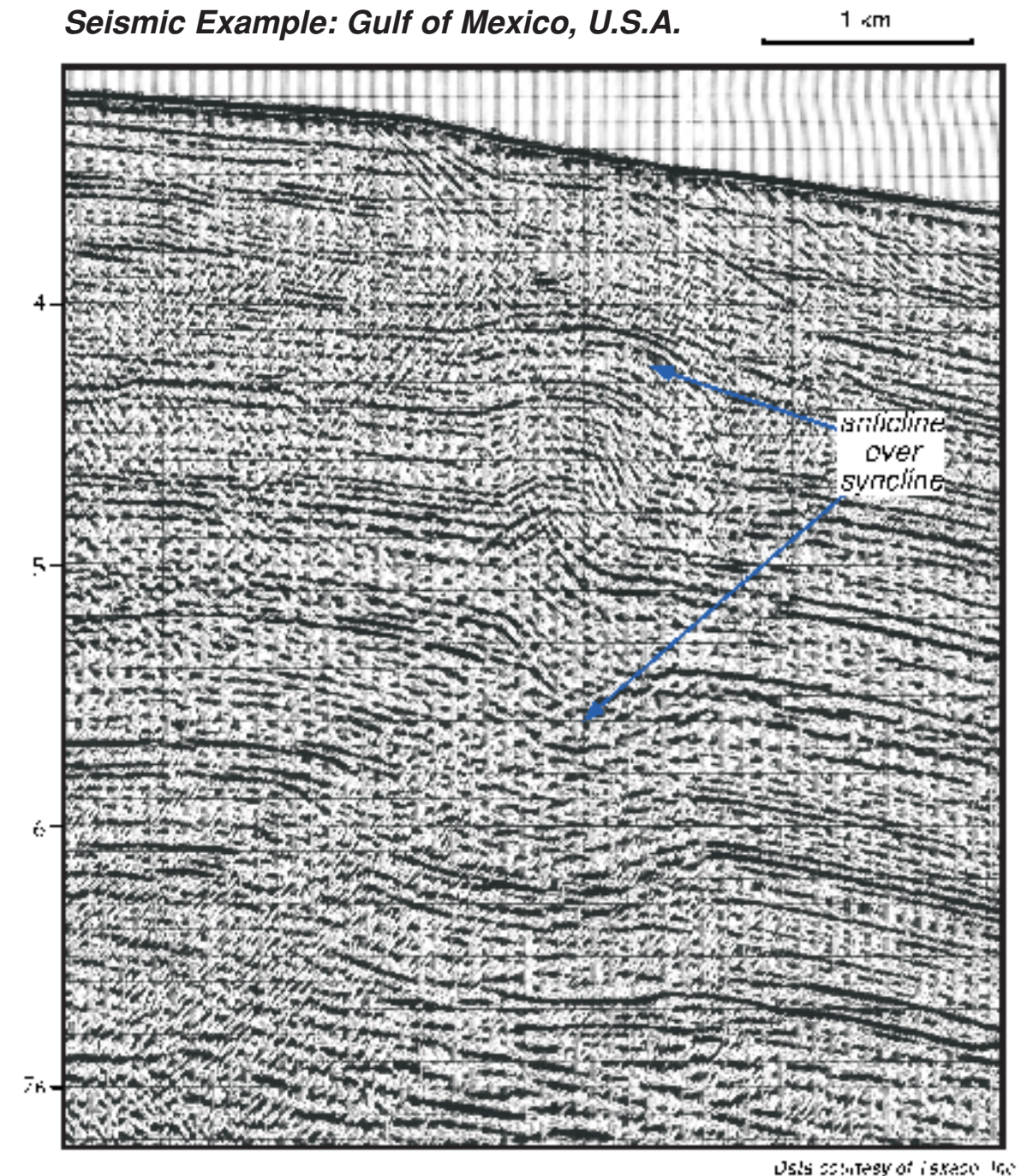
This seismic section images an interference structure from the Perdido fold and thrust belt (after Mount, 1989; Novoa et al., 1998). The structure is comprised of two monoclinal kink bands that intersect at about 5.2 seconds (TWTT). The interfering kink bands produce an anticline that is perched above a syncline, similar to the models shown at left. The sense of shear in the interference structure appears to be counterclockwise, similar to model B. This section is displayed in TWTT, with a V.E. of about 1:1 for a velocity of 2000 m/s, which is representative of the shallow section.

Complex interference structure

Interference structures that are faulted and/or involve more than two kink bands may have very complex geometries. In this section, we describe a complex, faulted interference structure imaged in a seismic section. We use a partial restoration of the structure to document its origins as an interference fold.

The seismic profile shown in panel A images a complex fold from the Sichuan basin, China. The structure exhibits the basic pattern of an anticline perched over a syncline that is characteristic of interference structures. The structures differ from the simple models shown on the previous page, however, in that the core of the fold is cut by a thrust. A narrow monocline appears to be offset by this fault.

In panel B, the section is interpreted with a simple interference fold below the main thrust. Folds in the hanging wall of the thrust are interpreted to be displaced elements of the interference fold that, in part, are refolded by a steepening upward splay of the fault. Panel C shows the same interpretation of the structure without the seismic image. Restoration of slip on the main fault and the associated folding in panel D yields a simple interference structure.

This example is intended to illustrate that interference structure may have complex geometries. Nevertheless, these structures can generally be interpreted using a combination of fault-related folding theories. This interpretation invokes the basic patterns of interference folding with the kink method (section 1A-1) and fault-bend folding (section 1B-1) to describe the hanging wall structure. The hanging wall portion of the offset monocline is refolded using the concept of folding vectors described in section 1B-5.

Interference structures also generally exhibit very distinct patterns in map view and three dimensions. For a description of these patterns, see Novoa et al. (1998) and Camerlo et al. (section 2-24, this volume).

A: Uninterpreted section 0.5 km E

offset monocline?

depth below floating datum   Data courtesy of CNPC

B: Interpreted section 0.5 km

C: Geologic section 0.5 km

D: Partially restored section 0.5 km